City Research Online

City, University of London Institutional Repository

SWIRLING AND NON-SWIRLING FLOW

IN CONICAL DIFFUSERS

————

N.E.A. WIRASINGHE

A thesis presented for the degree of

Doctor of Philosophy of The City University.

Department of Mechanical Engineering,

The City University,

London.   January 1975

ABSTRACT

The performance of conical diffusers with axial and swirling flow has been considered. As a necessary starting point the various criteria used for defining performance have been reviewed and have been extended to swirling flow cases. A new 'AREA-PLOT' method, which unifies presentation of performance information, for plane and conical diffusers has been proposed. An added attraction of this method is that it displays all three geometric variables of the diffusers.

As swirl modifies the boundary layer it was necessary to have some knowledge of the growth of the boundary layer in the axial flow situation. This was achieved by extending the 'ROSS-FRASER' model as a closed form solution requiring only the initial boundary conditions. The predictions compare very well with published experimental results.

The swirling flow case has been considered both mathematically and experimentally, the latter being studied through flow visualisation and measurement. An extensive survey of available literature, on theoretical and experimental work, has been presented with particular emphasis on areas not covered by previous surveys. The mathematical analysis was aimed at identifying the dominant parameters. The solution indicates the preferred coordinate system and the possibility of further extension. It has been shown that it is possible to represent the tangential velocity distribution in the diffuser by a family of exponential curves.

Further analysis indicated that the divergence of the solid-body rotation core was parallel to the wall of the diffuser.

Flow visualisation studies have identified breakdown and non-breakdown areas in turbulent swirling pipe flow. The development of the various modes of breakdown have been recorded. Detailed flow measurement in the 10° diffuser indicates that swirl has a definite effect on eliminating separation tendencies. It was found that swirl modifies the wall static pressure drop in the inlet pipe immediately upstream of the diffuser.

PRINCIPAL NOMENCLATURE.

a   Radius of crank of slider-crank mechanism

A   Constant; cross-sectional area of duct

AR   Area ratio $(= A_2/A_1)$

B,C,k   Constants

C_f Skin friction coefficient

C_p Pressure recovery coefficient

$\bar{C}_p$ Ideal pressure recovery coefficient

$\hat{C}_p$ Coefficient of performance

D   Shape parameter

F   General function

G   Exponent (function of $\mathbb{R}_{\theta_0}$); General function

H   Shape parameter $(= \delta/\theta$)

K   Calibration factor associated with spherical probe

l Mixing length; length of link of slider-crank mechanism

L   Slant length of diffuser

M   Angular momentum

n $= l/a$ as applied to slider crank mechanism

p   Static pressure

$\bar{p}$ Mean static pressure

q   Mean axial kinetic energy

$\dot{q}$ Mass flux through a region in the boundary layer

$\dot{Q}$ Mass flux through a cross-section

r   Radial co-ordinate

R   Radius of duct

$Re,\mathbb{R}$ Reynolds number

S_c Wetted surface area of conical diffuser

SR	Non-dimensional wetted surface area
t	time
u	Axial velocity
$\bar{u}$	Mean axial velocity
$\hat{u}$	Peak value of axial velocity profile
u_*	Friction velocity ($= \sqrt{\tau_w/\rho}$)
v	Tangential velocity
$\tilde{V}$	Total velocity
w	Radial velocity
y	Distance measured radially from wall
Y	Thickness of boundary layer
z	Axial co-ordinate

Greek Symbols

α	Non-dimensional axial length ($= z/R_o$); Angle of yaw
β	Radius ratio ($= r/R$ or $(r/kr_c)^2$ as indicated); Angle of pitch
γ	Functional characteristic ($= u_\theta/u_c$); Angle between velocity vector and a given point on sphere
γ_*	Axial kinetic energy factor
γ_{**}	Axial momentum factor
δ	Dihedral angle; Boundary layer displacement thickness
ϵ	Overall effectiveness; Eddy viscosity
ζ	Velocity ratio ($= \bar{u}/u_{co}$)
η	Nondimensional boundary layer co-ordinate
η_o	Overall energy efficiency
η_e	Energy efficiency
θ	Crank angle; Three dimensional momentum thickness
θ_*	Two dimensional momentum thickness

λ Diffuser loss coefficient

Γ Circulation

μ Core velocity ratio (= u_c/u_{c_0})

υ Kinematic viscosity

ρ Density

τ Shear stress

ϕ Cone angle of diffuser; Probe conical angle

ψ Swirl angle   [$\mathrm{Tan}^{-1}(v/u)$]

$\hat{\psi}$ Projected maximum swirl angle   [$\mathrm{Tan}^{-1}(R\omega/\bar{u})$]

ω Angular velocity

Ω Circulation number (= $R\Gamma/\bar{u}$)

Superscripts

    *   Swirl case

    '   Instantaneous fluctuating components;

    [ ]   Partial differential

Subscripts

    c   Conical diffuser; Value at inviscid core or at "solid-body rotation" core

    CL   Centreline

    d   Based on diameter

    i   General case

    p   Plane diffuser

    w   Value at wall

    θ Based on momentum thickness; Value obtained by extrapolating laminar sub-layer profile to $y = \theta$

    ∞ Inviscid flow outside boundary layer

    o,1   Inlet section

CONTENTS   Page.

LIST OF FIGURES

LIST OF TABLES

CHAPTER I

INTRODUCTION

In fluid mechanics, a duct in which the cross-sectional area increases in the direction of flow is termed a diffuser. In subsonic flows it decelerates the flow with an accompanying increase in static pressure. Which of these is the primary objective is dependent on the particular application; however each of these objectives needs to be achieved with the minimum of losses. Almost any basic contour may be used to achieve this expansion; the conical diffuser however has been used extensively owing to its simple geometry which makes it attractive in practical applications.

Despite the vast amount of research over the years, the basic characteristics of flow in a diffuser are still not clearly understood. Whilst it is desirable to employ an optimum diffuser where possible (i.e. one which yields the highest pressure recovery coefficient), in practice other design considerations preclude this and sometimes it is necessary to employ an other than optimum diffuser. This more immediate requirement of the design engineer has been satisfied by providing performance charts in which the pressure recovery coefficient, defined as

$$C_p = (\bar{p}_2 - \bar{p}_1)/q_1$$

is given as a function of the area ratio and expansion angle (or the axial length).

In major industrial applications even a few percent improvement of efficiency represents a significant financial saving and therefore factors influencing diffuser performance are eagerly sought. Early researchers were of the view that performance was a function only of the geometry of the diffuser. However, recent work has shown that the thickness of the inlet boundary layer and the level of inlet turbulence are also relevent parameters. The adverse pressure gradient associated with flow in the diffuser thickens the boundary layer and can lead to separation. In separated flows the kinetic energy available for conversion to flow work is lost as internal energy.

Over the years various methods have been employed to prevent boundary layer separation. Of these, boundary layer suction in particular has received a great deal of attention. This removal of slow moving fluid from the boundary layer causes high velocity fluid from the core region to replace it. The greater kinetic energy of this fluid enables it to overcome the effects of the pressure gradient thus preventing separation. Ackeret (1958), Furruya, et. al. (1966) and several others have improved performance by this method. Moon (1958) reported that suction was effective only with thin entry boundary layer thickness and that suction was totally ineffective when this was excessively thick.

Several other isolated methods have been used from time to time. Persh and Bailey (1954) increased wall roughness while Nicoll and Ramaprian (1970) used annular secondary injection;

both claim improvements. Improvements have also been claimed for wide angle diffusers by Yang (1965) who suspended an axisymmetric aerofoil centrally inside the diffuser. The effect of screens on performance was investigated by Winternitz and Ramsey (1957) and Moore and Kline (1958). Sprenger (1959), Senoo and Nishi (1974) and several others used vortex generators to improve diffuser performance. These were used only in specific applications and a vast amount of experimentation is required to determine the optimum configuration of vortex generators and to quantify the benefits.

According to Peters (1931), Andres (1909) was the first to suggest that swirl may be used as an efficient means of redistributing energy though the latter did not venture to investigate this any further. Peters himself carried out some preliminary work to investigate this view. As seen from Fig. (1.1), swirl in fact does improve performance. Later, work by Liepe (1960) and Van Dewoestine (1969) further reinforced this view.

The current research programme arose from the view that it may be possible to improve the performance of the fluidic vortex amplifier by attaching a diffuser to its exit. The discharge from a switched vortex amplifier possesses a high degree of swirl and the aim is to generate a higher impedence in the chamber by diffusing the discharge. Following recent work on the performance of fluidic vortex amplifiers by Neve (1971) it was decided to conduct a comprehensive research programme to investigate the character of swirling flow in diffusers and in a pipe (diffuser with zero divergence angle), and also to contribute to the existing knowledge on performance without swirl.
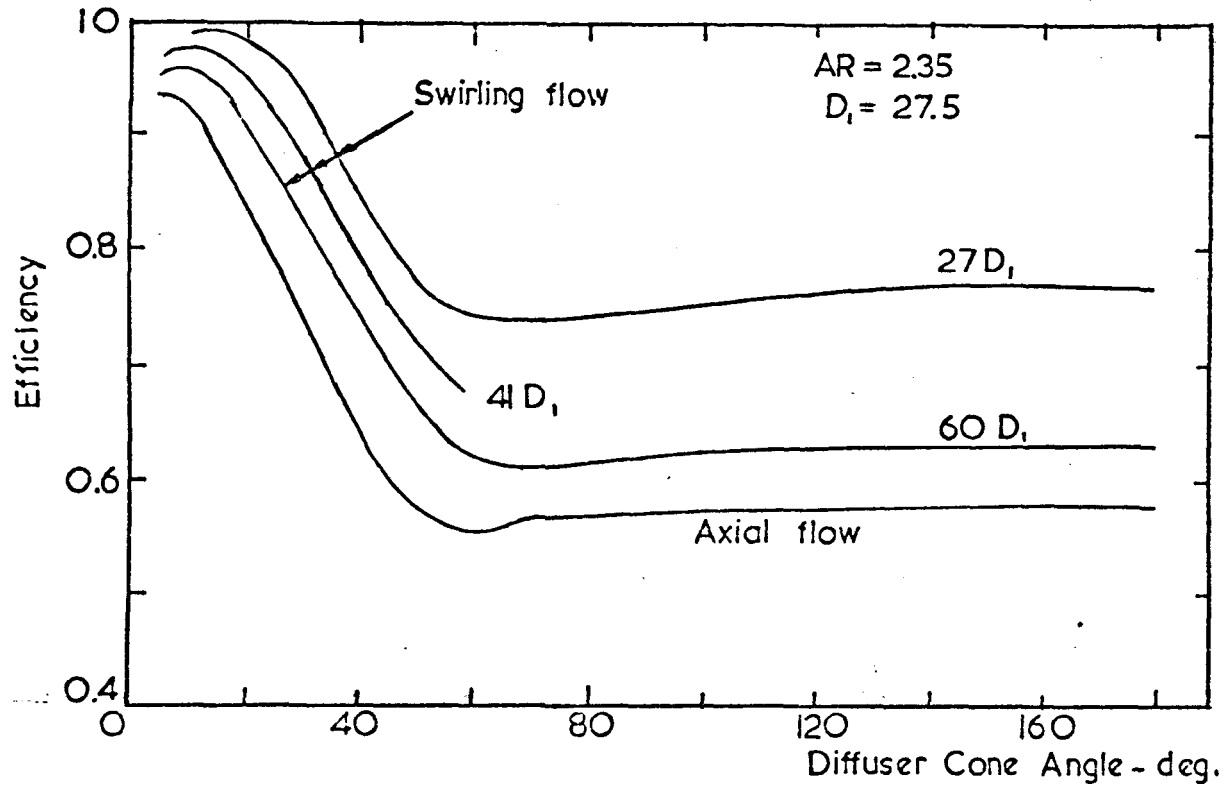
FIG.1.1 DIFFUSER EFFICIENCY; PETERS (1934)

Flow in ducts covers a major portion of the subject of fluid mechanics. As Fig. (1.2) indicates, even when restricted to conical diffusers the subject is extremely wide. It is obviously impossible to build one universal test apparatus to investigate the entire problem. Each individual project, within the main programme, should investigate a few of the parameters at a time thus providing the necessary information to put this subject on a similar footing to that of diffuser performance with axial flow. Owing to the almost non-existent expertise in this field, laying a suitable foundation was seen as an absolute necessity. The present project was seen as one that would make a global assessment of the programme in addition to performing a steering function for future research in this field.

A considerable degree of ambiguity still exists in the manner in which diffuser performance is evaluated. In Chapter Two the various criteria have been developed logically in an attempt to coordinate these. Parallel criteria have also been developed for evaluating performance of diffusers with swirling flow. A new 'AREA-PLOT' method unifying presentation of such information, in two and three dimensional flows, has also been developed. The boundary layer growth in the conical diffuser, with axial flow, is considered analytically, in Chapter Three, by extending the work of previous investigators to obtain a closed form solution. The special numerical techniques developed are also included but the associated computer routines are reported in a separate publication.

FLOW IN DUCTS

DIFFUSERS & PIPES

NOZZLES
(outside scope of present
interest)

With axial flow

(exhaustively investigated
already)

With swirling flow

Effect of fluid properties

Effect of geometry
(Area ratio; length; angle of
diffusion; entry and exit length)

Effect of various
types of entry flow

Relating swirl and geometry
to prevent breakdown.

Defining conical diffuser
geometries and swirl combinations
to obtain maximum efficiency.

Fig. 1.2   FLOW CHART DISPLAYING SCOPE FOR RESEARCH ASSOCIATED

WITH DIFFUSERS.

The characteristics of swirling flow and the associated vortex breakdown phenomenon are introduced in <u>Chapter Four</u>. An extensive survey of relevant previous experimental work is presented. Included is a discussion on the role of swirling flow in jets, pipes, conical diffusers and annular diffusers. Owing to the scarcity of experimental data mathematical analysis of the swirling flow problem has been stunted. Most of the prediction methods proposed have attempted to predict the occurrence of vortex breakdown. Only a few have attempted to study decay of swirl. These methods have been reviewed in <u>Chapter Five</u>. Furthermore the governing equations of motion have been solved to investigate the influence of dominant parameters in laminar swirling flow in conical diffusers.

During the design stages of the test apparatus and instrumentation, it was decided not to limit the scope of the apparatus to this project alone but to endeavour to make it sufficiently flexible to accommodate as much of the forseeable future programme as possible. Consequently convenience had to be sacrificed for greater latitude of experimentation. Design information is reported in detail in <u>Chapter Six</u>. As the five-hole pitot probe used for measurement was the subject of a more detailed analysis, it is discussed separately in <u>Chapter Seven</u>.

<u>Chapter Eight</u> describes the flow visualisation work conducted in water to observe the development of vortex breakdown. The discussion throws light on the difficulties associated with such work. Experimental work associated with flow measurement in air is reported in <u>Chapter Nine</u>.

Diffuser performance information is also included with comparisons, where possible.

The work carried out is reviewed in Chapter Ten, and the results are presented. Possible extensions in the various areas are also discussed.

CHAPTER TWO

ESTIMATION AND PRESENTATION OF DIFFUSER

PERFORMANCE INFORMATION

2.1   INTRODUCTION

As diffusers are concerned with obtaining as much static
pressure as possible from the kinetic energy of the fluid their
functional efficiency must be measured accordingly. Various
definitions for such measurements have been proposed in an attempt
to obtain a convenient method for presenting performance information.
As a result a certain degree of ambiguity has been introduced. In
an attempt to resolve this the various definitions used for
measurement of performance are derived in a logical manner. The
validity of some of the terms used will always remain arguable
though this is of secondary importance. The subsequent discussion
will also concentrate on developing a suitable basis for presenting
such information when the flow at entry to the diffuser possesses
a swirl component of velocity. In addition an improved 'AREA-PLOT'
method has been developed for presenting performance information.

2.2   AXIAL FLOW AT ENTRY

Patterson (1938) suggested that the 'overall energy
efficiency' of a diffuser be defined as the ratio of the power
transformed to the power supplied for transformation.

$$\eta_o = \frac{\int_2 p u \, dA - \int_1 p u \, dA}{\int_1 p/2 \tilde{V}^2 u \, dA - \int_2 p/2 \tilde{V}^2 u \, dA} \qquad (2.2.1)$$

If the flow is axial at inlet and outlet sections

then $\tilde{V} = u$ and, as the uniform pressure is in addition

transmitted through the boundary-layer, the above equation yields

the 'energy efficiency'.

$$\eta_e = (\bar{p}_2 - \bar{p}_1) \bar{u}_1 A_1 \Big/ [\int_1 \rho/2 \, u^3 dA - \int_2 \rho/2 \, u^3 dA] \qquad (2.2.2)$$

Using the kinetic energy (weighting) factor

$$\gamma_* \bar{u}^3 A = \int_A u^3 dA$$

this becomes

$$\eta_e = (\bar{p}_2 - \bar{p}_1) \Big/ q_1 \gamma_{*_1} [1 - AR^{-2} \gamma_{*_2}/\gamma_1] \qquad (2.2.3)$$

where $AR = A_2/A_1$ and $q = \rho \bar{u}^2/2$. If the velocity distribution

is uniform at the initial and final sections then $\gamma_{*_1} = \gamma_{*_2} = 1$

and equation (2.2.3) reduces to the 'coefficient of performance'

$$\hat{C}_p = (\bar{p}_2 - \bar{p}_1) \Big/ q_1 (1 - AR^{-2}) \qquad (2.2.4)$$

In real flows in ducts the presence of the boundary layer

causes a non-uniformity of velocity. As a consequence of its

definition γ_* will always be greater than unity and in the case

of the paraboloid velocity distribution associated with fully

developed laminar flows $\gamma_* = 2$. In the case of a thin inlet

boundary layer γ_* may be assumed to be unity but such an assumption

is invalidated at the exit of a diffuser where the adverse pressure

gradient creates a very thick boundary-layer.

In a typical case using the $1/7^{\text{TH.}}$ power law

$$u/\hat{u} = (1 - r/R)^{1/7}$$

yields $\gamma_* = 1.06$. Peters (1931) suggested the use of a better

approximation to test data given by

$$u/\hat{u} = [1 - (r/R)^m]^{1/7}$$

which for $m = 2$ yields $\gamma_* = 1.045$. Even though γ_{*2} is always greater than γ_{*1}, in diffusers of practical interest AR^{-1} is less than unity and AR^{-2} is very much less than unity. Applying this condition and the assumption that $\gamma_{*1} = 1$ to equation (2.2.3) yields the 'pressure recovery coefficient'

$$C_p = (\bar{p}_2 - \bar{p}_1)/q_1 \qquad (2.2.5)$$

which has been used frequently as it obviates the need to evaluate velocity profile data at exit.

For flow in a diffuser, under uniform conditions, the Bernoulli equation with a loss term Δp is

$$p_1 + q_1 = p_2 + q_2 + \Delta p$$

and in the ideal case this becomes

$$p_1 + q_1 = p_2 + q_2$$

Invoking this ideal condition into equation (2.2.5) leads to the 'ideal pressure recovery coefficient'.

$$\bar{C}_p = 1 - AR^{-2} \qquad (2.2.6.)$$

Almost wholly, diffuser performance has been measured in one or more of the above forms (or a modification of the above forms). Sovran and Klomp (1967) for example, suggested the use of the diffuser "overall effectiveness" defined as

$$\epsilon = C_p / \bar{C}_p$$

Clearly this is identical with the coefficient of performance defined in equation (2.2.4). Cockrell and Markland (1963) proposed the use of the "diffuser loss coefficient".

$$\lambda = 1 - \hat{C}_p$$

Thus it is seen that all the forms are approximations of the "overall energy efficiency" given by equation (2.2.1).

2.3   A UNIFIED METHOD FOR CORRELATING PERFORMANCE DATA OF

PLANE AND CONICAL DIFFUSERS.

2.3.1   Introduction

Systematic studies were carried out at Stanford
University with plane (two dimensional; Fig. (2.1)) diffusers
in an attempt to extend the knowledge gained to conical diffuser
flows. This attempt was greatly hindered by the lack of a suitable
basis for correlating performance information from these two types.

A conical diffuser may be uniquely defined by any two of
the three common geometric paramters; viz. area ratio, divergence
angle and length to inlet diameter ratio. In industrial situations
any one of these may be the constraining parameter. Quite often
the performance itself is the constraining parameter when
equipment downstream of the diffuser requires a prescribed input
pressure. If performance charts are not readily available in
the required form this would cause inconvenience.

2.3.2   Methods Already in Use

The method used by Patterson in his early review is
shown in Fig. (2.2a). A similar method was used by Cockrell and
Markland, Fig. (2.2b). It is useful to note that in both cases
the length parameter has been considered to be the least important.
Recently at Stanford University contour plots were used, with plane
walled diffusers, in which all three parameters were readily
available. The simple geometric relationships of the plane
diffuser have made this possible.

From Fig. (2.1)

Conical Diffuser
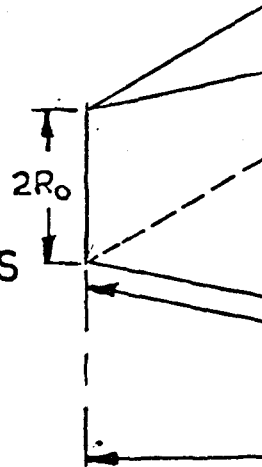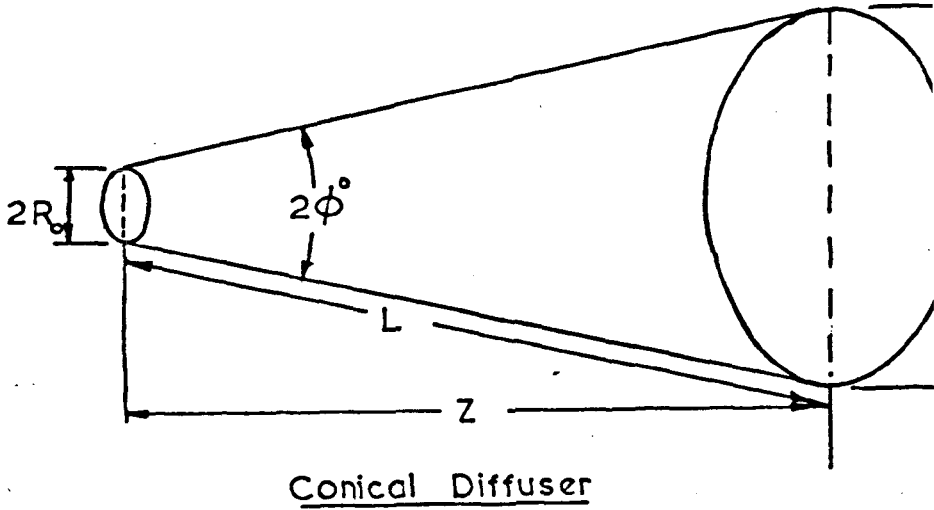
FIG. 2.1 DIFFUSER GEOMETRIES

Plane Diffuser

2R

2R

$2\phi°$

L

Z

b

1

31
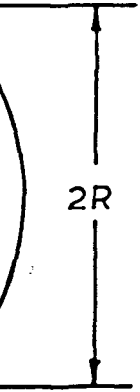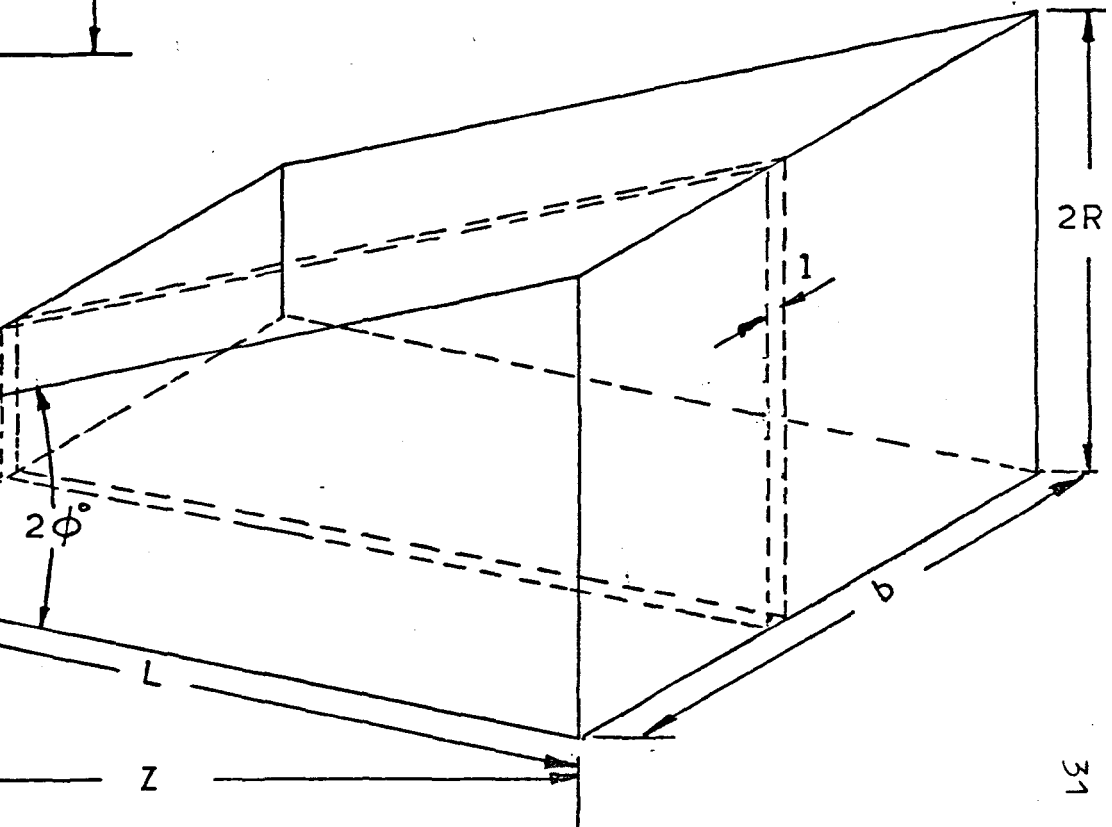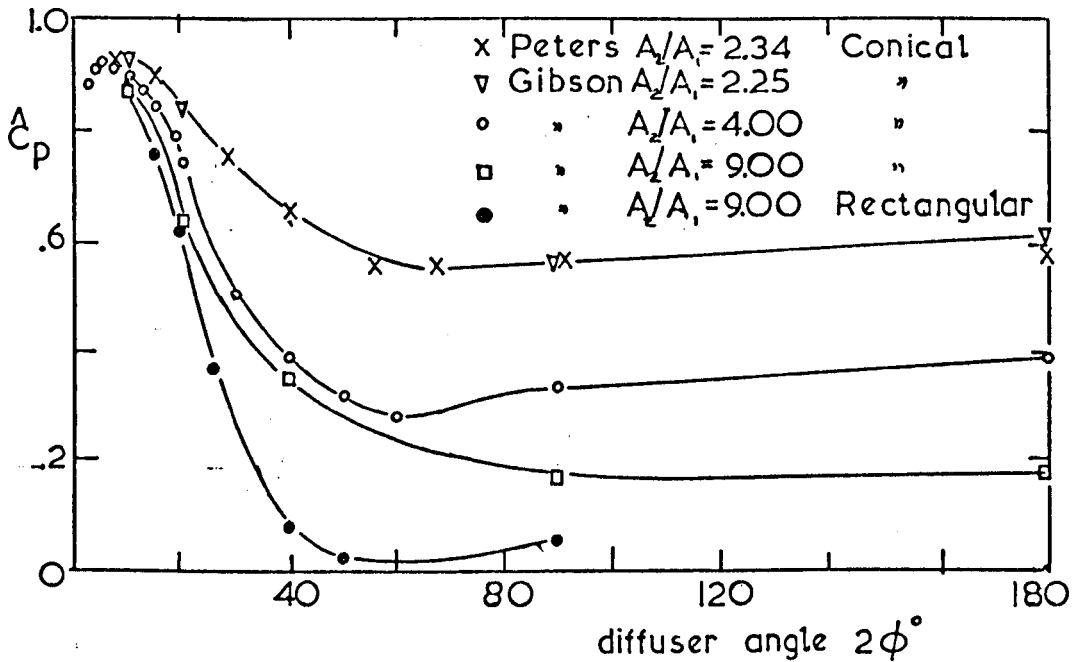
FIG. 2.2a DIFFUSER PERFORMANCE CURVES;
PATTERSON (1938)
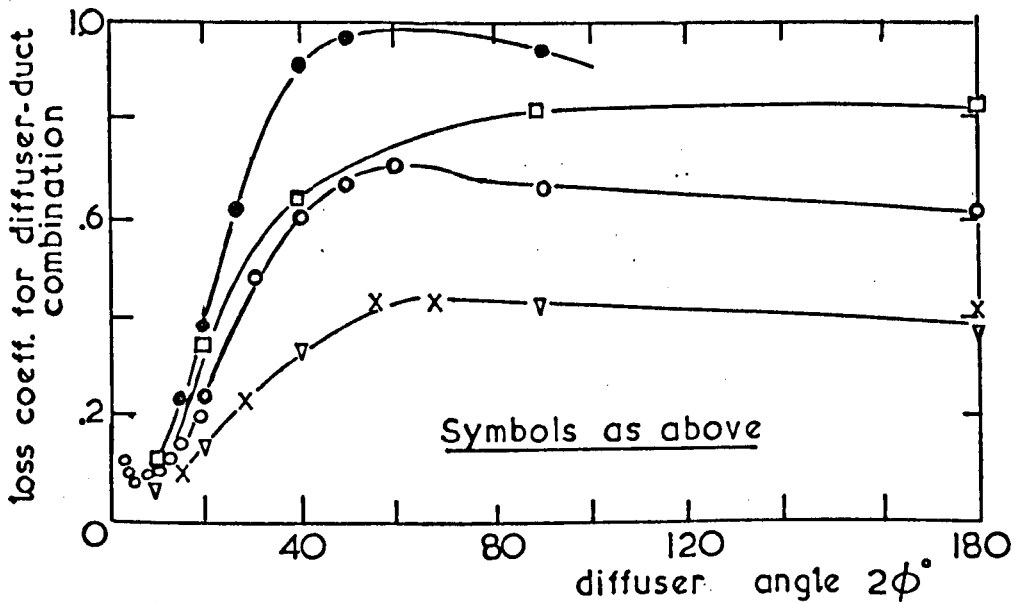
FIG. 2.2b PATTERSON'S CURVES EXPRESSED AS
LOSS COEFFICIENTS; COCKRELL & MARKLAND (1963)

$$R = R_0 + z \tan \phi \qquad (2.3.2.1)$$

For the plane walled diffuser the area ratio is

$$AR_p = R / R_0 = \beta \qquad (2.3.2.2)$$

and substituting this into equation (2.3.2.1) yields

$$AR_p = 1 + (z/R_0) \tan \phi \qquad (2.3.2.3)$$

or $\quad \ln(AR_p - 1) = \ln(z/R_0) + \ln(\tan \phi) \qquad (2.3.2.4)$

The use of logarithmic scales would result in the half angles appearing as a series of parallel straight lines. Furthermore, as the area ratio is always greater than unity, the region of greatest practical interest, which is the region of smaller area ratios, is stretched out by the use of $(AR_p - 1)$ as the ordinate.

On the basis of the limited conical diffuser data available at the time, Kline, Abbot and Fox (1959) postulated that performance data for axisymmetric flows could be correlated on the same basis as the data from two dimensional flows.

For a conical diffuser the area ratio is

$$AR_c = (R/R_0)^2 = \beta^2 \qquad (2.3.2.5)$$

and on substituting for R in equation (2.3.2.1) yields

$$AR_c = 1 + 2(z/R_0) \tan \phi + [(z/R_0) \tan \phi]^2 \qquad (2.3.2.6)$$

This expression would be similar to that given by equation (2.3.2.3) provided the last term is negligible. Fig. (2.3) which has been drawn with and without the last term of equation (2.3.2.6) shows the importance of this term. It follows that while the contour plots provide an opportunity to present all three parameters for plane diffusers they do not permit a similar representation of conical diffuser information. This naturally precludes a proper comparison of information.
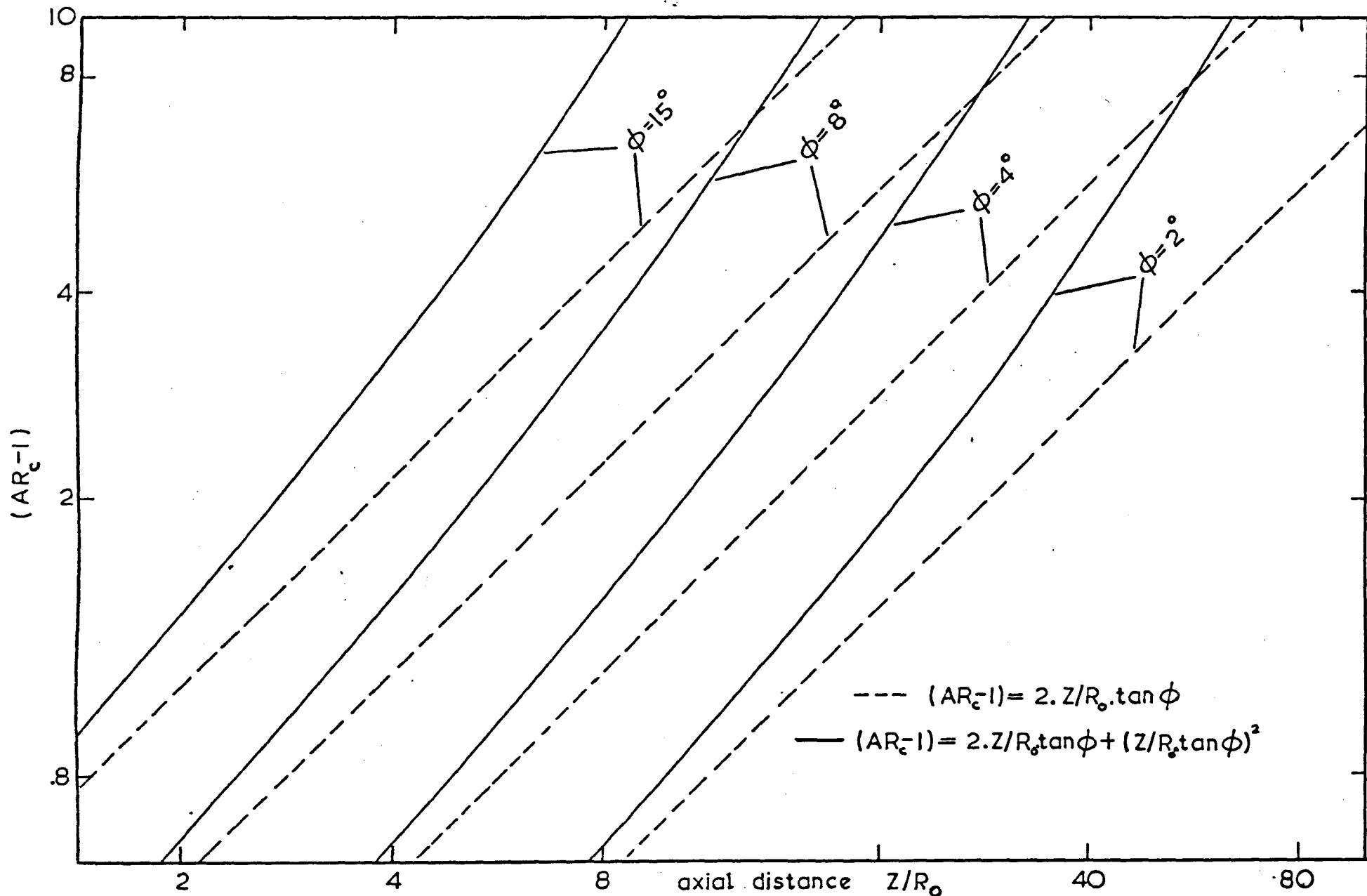
FIG. 2.3 SIGNIFICANCE OF SQUARED TERM IN EQN. (2.3.2.6)

--- $(AR_c-1) = 2 \cdot Z/R_o \cdot \tan\phi$

— $(AR_c-1) = 2 \cdot Z/R_o \tan\phi + (Z/R_o \tan\phi)^2$

axial distance Z/R_o

$\phi = 15°$ $\phi = 8°$ $\phi = 4°$ $\phi = 2°$

34

2.3.3   The 'AREA-PLOT' Method

A new type of 'AREA-PLOT' is suggested as a preferable alternative to the previously discussed contour plots. The ordinate is the flow area ratio and the abscissa is the ratio of wetted surface area to inlet flow area. The introduction of a new parameter, to add to the three already in existence, may at first sight seem an added complication. However it will be shown that this permits the development of identical relationships for both forms of diffuser.

Plane Walled Diffuser

Referring to Fig. (2.1) the slant length is

$$L = (R - R_0) / \sin\phi$$

and

$$L / R_0 = (\beta - 1) / \sin\phi$$

The wetted area per unit width of diffuser is $S = 2L$ and the relevant wetted surface area ratio is defined as

$$SR_p = S_p / 2R_0 = (\beta - 1) / \sin\phi$$

from which

$$\ln(AR_p - 1) = \ln(SR_p) + \ln(\sin\phi) \qquad (2.3.3.1)$$

Conical Diffuser

Considering an element on the conical surface

$$z = L.\cos\phi \quad \text{and} \quad dz = \cos\phi.dL$$

The wetted area is

$$S_c = 2\pi \int_0^L R.dL$$

$$= 2\pi \int_0^z (R_0 + z.\tan\phi) \, dz / \cos\phi$$

integrating and substituting for Z from equation (2.3.2.1)

yields

$$S_c = \pi R^2 (\beta^2 - 1) / \sin\phi$$

Also the flow area ratio is

$$AR_c = (R/R_o)^2 = \beta^2$$

The relevant wetted surface area ratio is defined as

$$SR_c = \mathcal{S}/\pi R_o = (\beta^2 - 1)/\sin \phi$$

from which

$$\ln(AR_c - 1) = \ln(SR_c) + \ln(\sin\phi) \qquad (2.3.3.2)$$

Equations (2.3.3.1) and (2.3.3.2) indicate that it is now possible to correlate plane walled and conical diffuser results. On these 'AREA-PLOTS', lines of constant non-dimensional axial length for the conical diffuser (not applicable to plane walled diffuser) have been drawn as this is the case of greatest practical interest. In addition to this correlation facility all the parameters are now represented in these new plots. In view of the small angles considered in practice it is suggested that $\sin\phi$ be replaced by ϕ (radians); thus

$$\ln(AR - 1) = \ln(SR) + \ln(\phi) \qquad (2.3.3.3)$$

The error, in the geometric relationship of ϕ, AR and SR for a conical diffuser, in assuming $\sin\phi = \phi$ is extremely small. The error in surface area, based on the true value for AR = 6, for a typical range of diffuser angles is as follows:

$2\phi^o$	10	20	30
e %	0.127	0.510	1.152

It should be observed that for the plane walled diffuser the expression obtained by the present method (equation (2.3.3.1)) and that used in the contour plots (equation (2.3.2.4)) are almost equal as in the range of greatest practical interest $\tan\phi \simeq \sin\phi$ Hence for these, contour plots may be used as before with the abscissa read as $SR_p (= L/R_o)$ instead of z/R_o

Figs.(2.4 and 2.5) show the flow regimes for a plane walled

diffuser and a typical performance chart respectively. Figs.

(2.6. and 2.7) show a typical performance chart for conical diffusers

in the earlier and later type of plot.

2.4   SWIRLING FLOW AT ENTRY

It was shown that in the case of a conical diffuser with

axial flow at entry the "pressure coefficient" defined by equation

(2.2.5) may be used to estimate the error. It is arguable whether

the performance of a diffuser should be measured in terms of the

actual dynamic pressure used in the conversion process or in terms

of that which is required at input irrespective of the dynamic

pressure left at exit. The latter has been in common use as it

obviates the need to evaluate velocity profile details at the exit

section.

For the swirling flow case the "overall energy efficiency"

is as defined by equation (2.2.1)

but
$$\tilde{V}^2 = u^2 + v^2$$

and
$$p = p_{c_L} + \rho \tilde{V}^2 / 2$$

The angular momentum flux is

$$\dot{M} = \rho \int_A u \, v \, r \, dA$$

Considering the special case of solid-body rotation, $v = r\omega$,

this becomes

$$\dot{M} = 2\pi\rho\omega \int_0^R u \, r^3 \, dr \tag{2.4.1}$$

Introducing the angular momentum (weighting) factor

$$\dot{M} = \gamma_4 \, \pi\rho\omega \bar{u} R^4 / 2 = 2\pi\rho\omega \int_0^R u \, r^3 \, dr \tag{2.4.2}$$

The flow work term in the numerator of equation (2.2.1)

is
$$\int_A p \, u \, dA = 2\pi \int_0^R p \, u \, r \, dr$$

$$= 2\pi \int_0^R p_{c_L} \, u \, r \, dr + \pi\rho \int_0^R v^2 u \, r \, dr$$
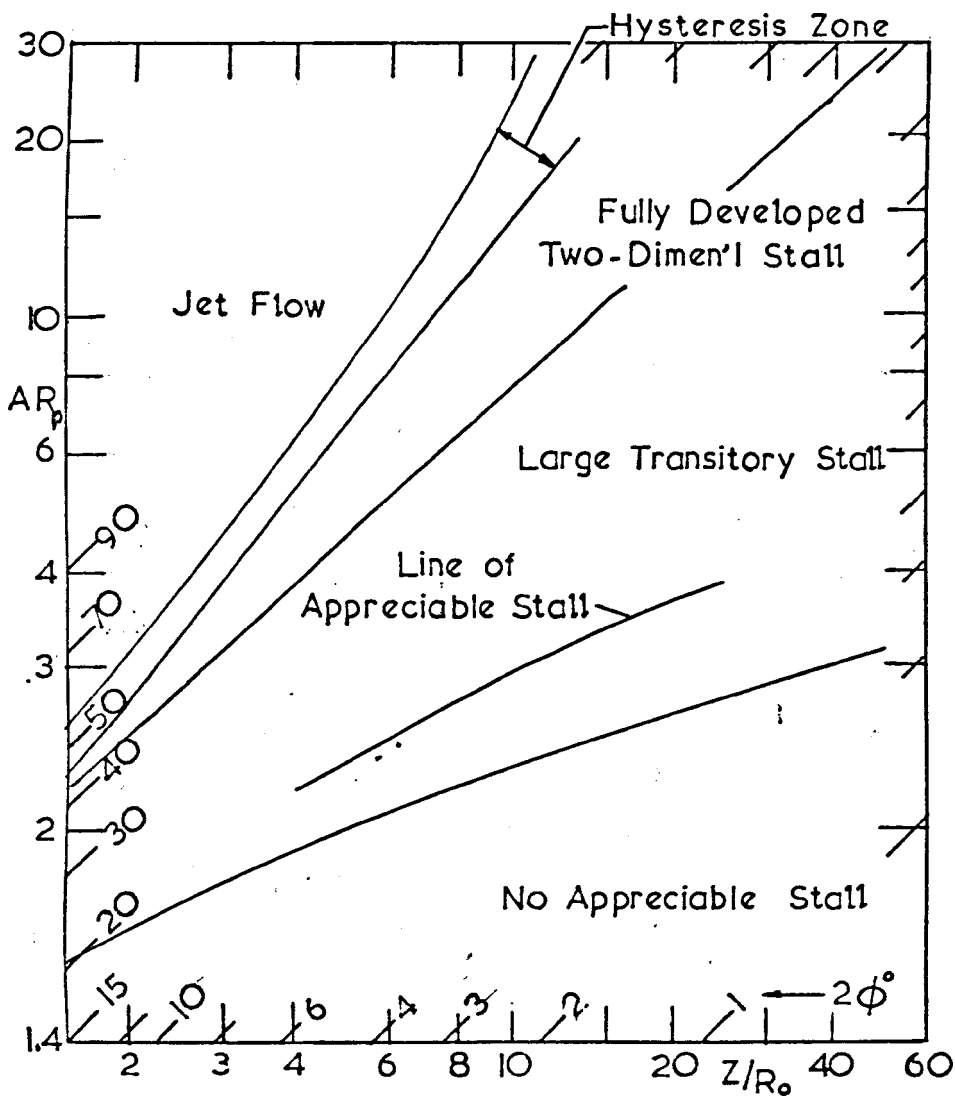
FIG.2.4 FLOW REGIMES IN PLANE
            DIFFUSERS

FOX &
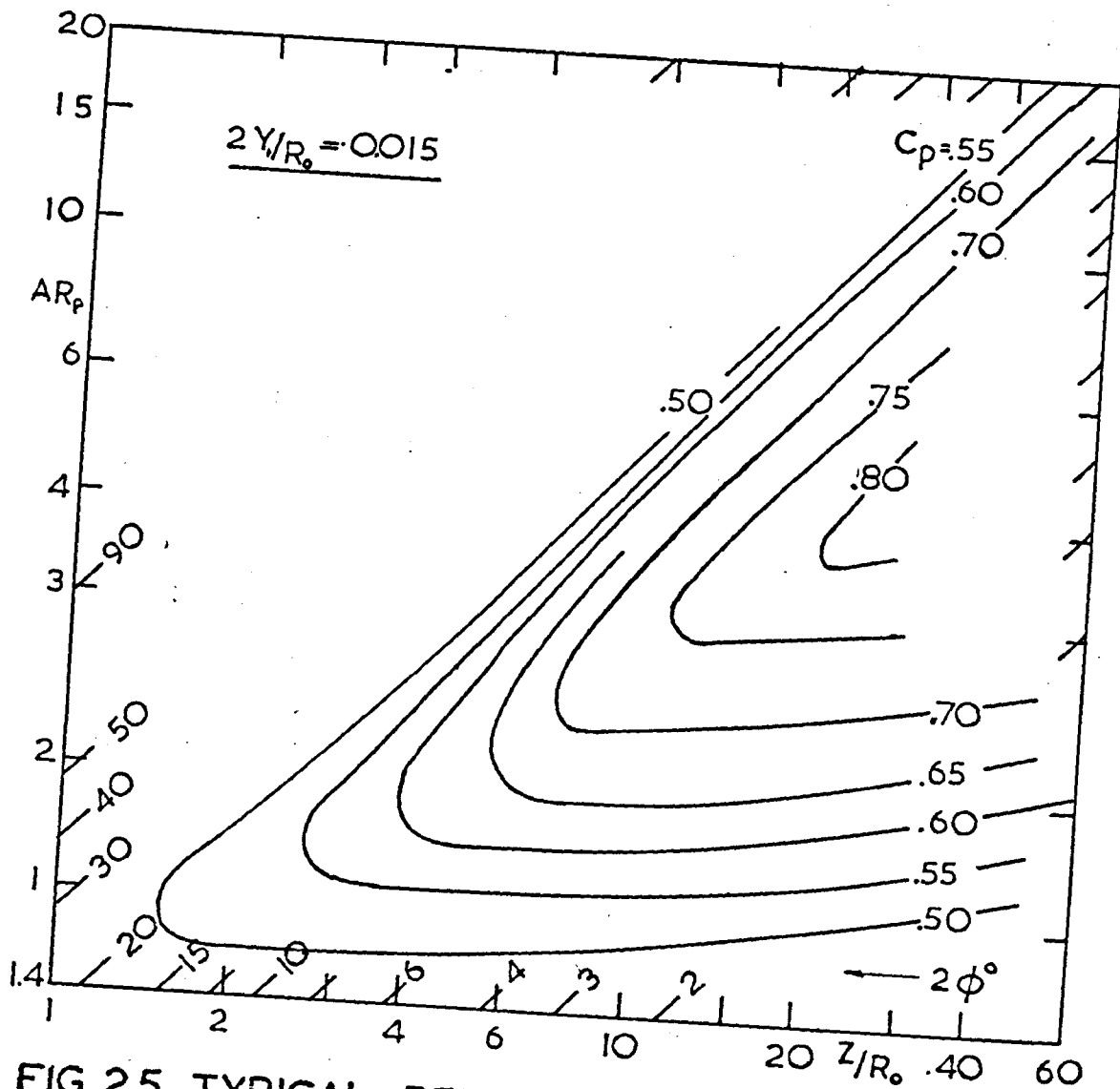
FIG.2.5 TYPICAL PERFOR. CURVES FOR PLANE DIFFUSERS

KLINE (1962)
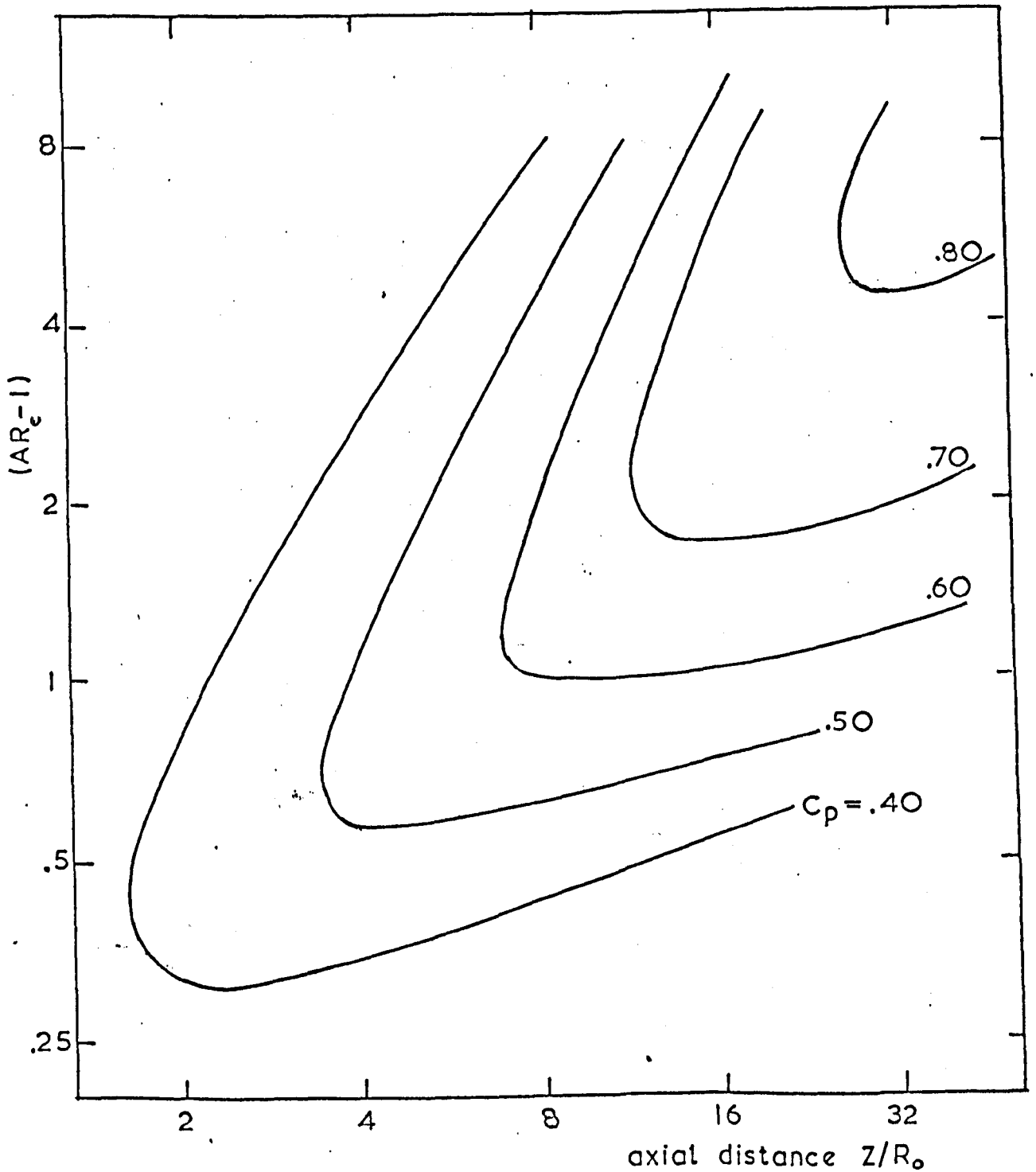
FIG.2.6 CONICAL DIFFUSER PERFOR. WITHOUT SWIRL
MCDONALD & FOX (1966)

which, for the solid-body rotation case reduces to

$$\int_A p u \, dA = \dot{Q}\bar{p}_{c_L}/\rho + \omega \dot{M}/2 \qquad (2.4.3)$$

The kinetic energy term in the denominator of

equation (2.2.1) is

$$\rho/2 \cdot \int_A \tilde{V}^2 u \, dA = \pi\rho\int_0^R (u^2 + v^2) u r \, dr$$

which, for the solid-body rotation case reduces to

$$\rho/2 \int_A \tilde{V}^2 u \, dA = \dot{Q} q \chi_*/\rho + \omega \dot{M}/2 \qquad (2.4.4)$$

Substituting the above expressions into equation (2.2.1)

yields

$$\eta_D^* = \frac{\dot{Q}(\bar{p}_{c_{L2}} - \bar{p}_{c_{L1}})/\rho + (\omega_2 M_2 - \omega_2 M_1)/2}{\dot{Q}(\chi_{*_1} q_1 - \chi_{*_2} q_2)/\rho - (\omega_2 M_2 - \omega_1 M_1)/2} \qquad (2.4.5)$$

If the angular momentum is conserved then

$$\eta = \frac{\dot{Q}(\bar{p}_{c_{L2}} - \bar{p}_{c_{L1}})/\rho + \dot{M}\omega_1(\omega_2/\omega_1 - 1)/2}{\dot{Q}q_1\chi_{*_1}(1 - AR\,\chi_{*_2}/\chi_{*_1})/\rho - \dot{M}\omega_1(\omega_2/\omega_1 - 1)/2} \qquad (2.4.6)$$

If only a very 'mild' swirl is imparted to the fluid

at entry then it may be assumed that the pressure distribution

is uniform across the section. Also if only the kinetic energy

at inlet is used as a reference, as is usually the case, then the

above equation reduces to the 'pressure recovery coefficient'

$$C_p^* = (\bar{p}_2 - \bar{p}_1)/(q_1\chi_{*_1} + \rho\dot{M}\omega_1/2\dot{Q}) \qquad (2.4.7)$$

This equation provides a very convenient basis for

comparison of performance, provided only 'mild' swirl is used,

as it does not require a detailed knowledge of the velocity

profile at exit. The validity of the assumptions made in reducing

equation (2.4.5) to equation (2.4.7) will be verified, in chapter

nine, using typical velocity profiles.

2.5   CONCLUSIONS

It has been shown that some degree of ambiguity exists
in the estimation of diffuser performance; this being more serious
when swirl is present at inlet. An improved 'AREA-PLOT' has been
proposed for the presentation of performance information. Figs.
(2.4) and (2.5) show the flow regimes and a typical performance
chart, respectively, associated with plane diffusers. Fig. (2.6)
shows a typical performance chart for a conical diffuser which
has been redrawn on the new plot on Fig. (2.7). The advantage of
the latter form is the appearance of the cone angles. Fig. (2.8)
shows the flow regimes associated with conical diffusers; this has
been redrawn on the new plot on Fig. (2.9). It is seen that if the
flow regimes in Figs. (2.4) and (2.8) are compared the trends are
not easily apparent. If, however, Fig. (2.4) is compared with Fig.
(2.9) the trends are obvious thus further justifying the use of
these plots. Comparison infact, does   indicate that the lines
of first appreciable stall for plane and conical diffusers do not
correspond to the same geometries. Further analysis is required
to determine whether or not it is possible to correlate performance
data for the two forms of diffuser. In concluding, it is worth
noting that all the previous investigators [Peters (1931), Liepe
(1963) and Van Dewoestine (1969)] omitted the exit velocity profile
details in evaluating performance (for swirling flow cases) owing
to the difficulty of measuring these. The use of angular momentum
flux instead of tangential velocity, in the evaluation of performance
with swirl, eliminates some of the errors associated with
experimental work. This will be discussed in Chapter nine.
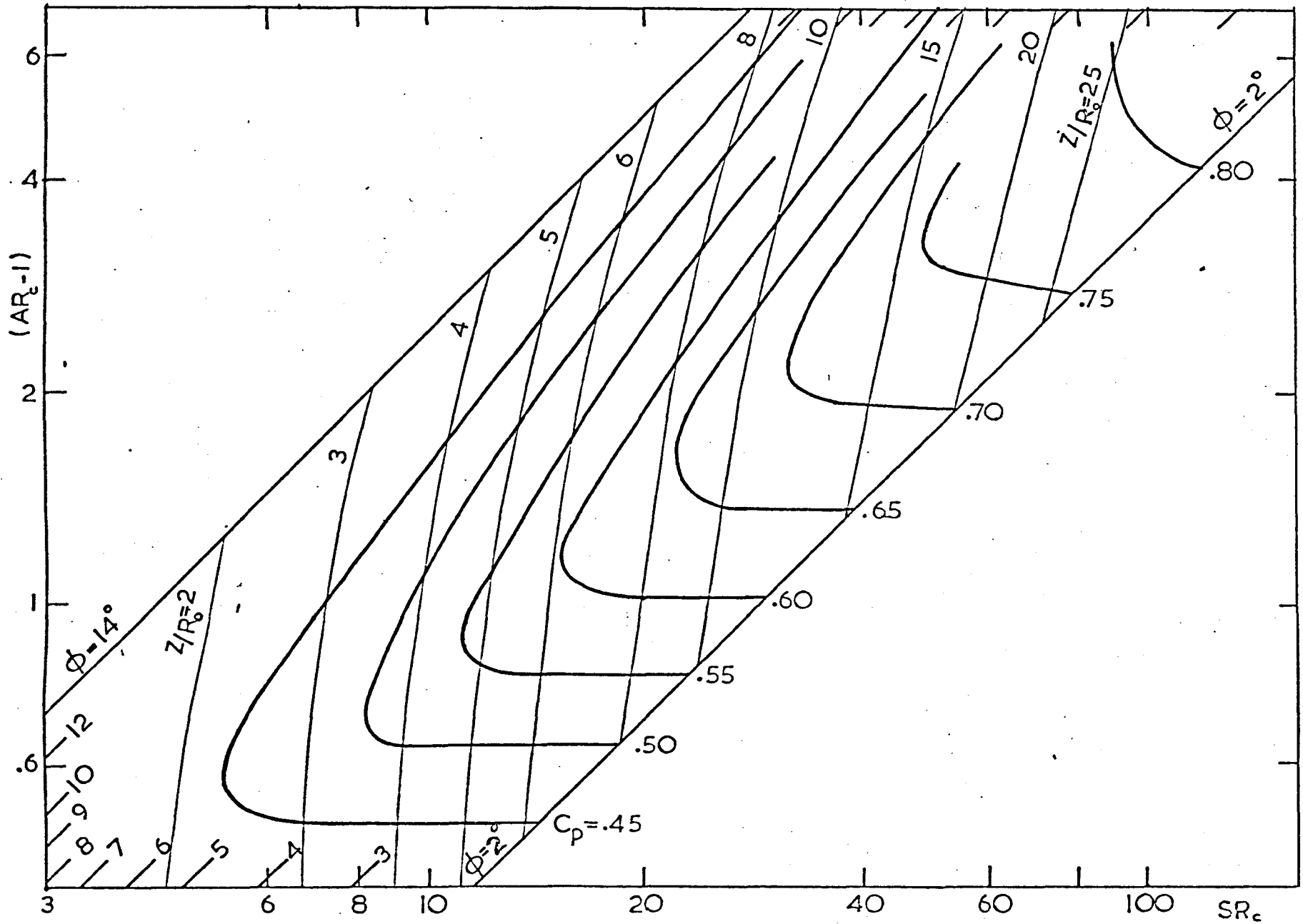
FIG. 2.7 PERFORMANCE OF CONICAL DIFFUSERS – 'AREA PLOT'

42
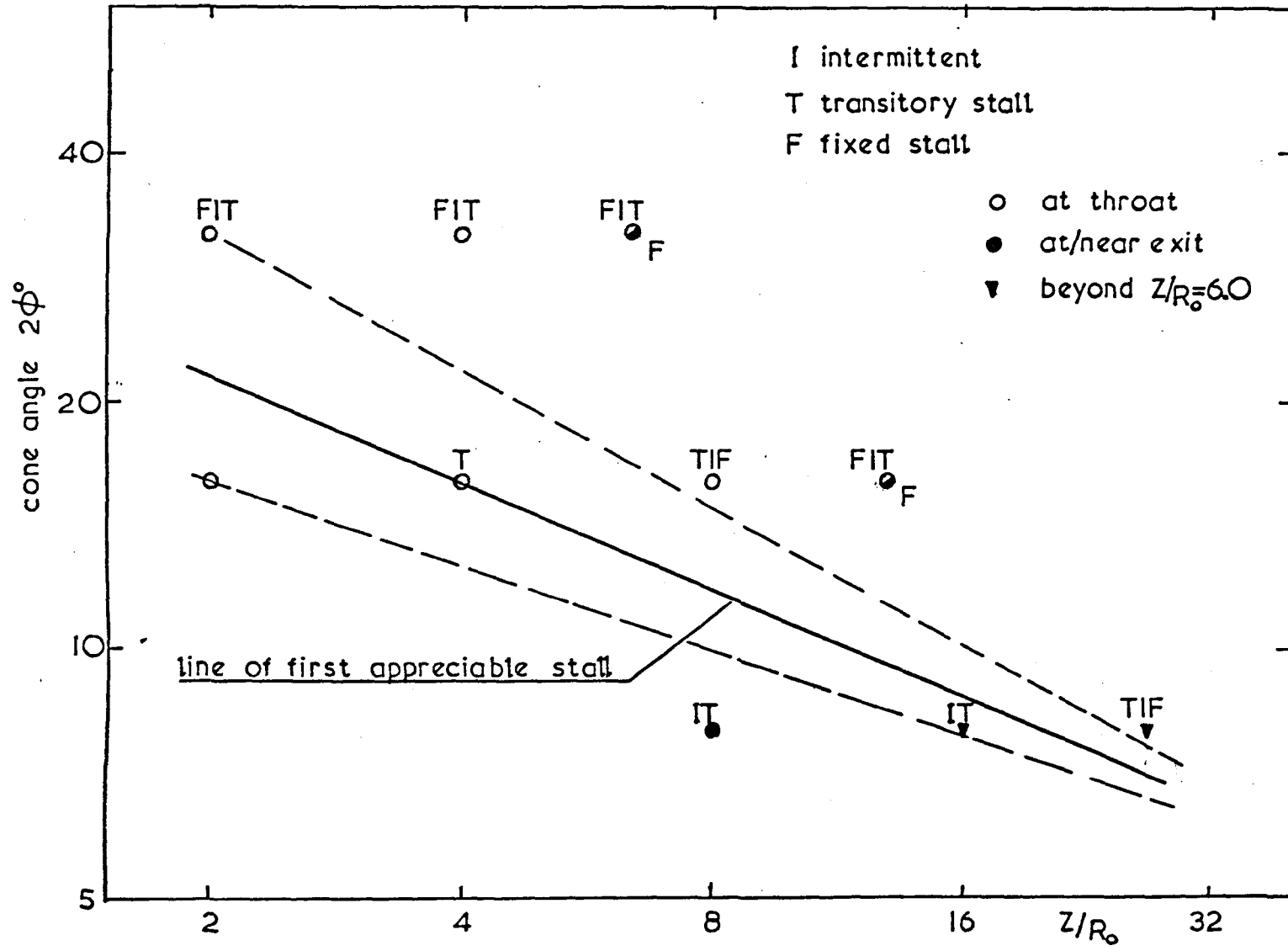
FIG.2.8 FLOW REGIMES IN CONICAL DIFFUSERS: AXIAL FLOW
MACDONALD & FOX (1966)
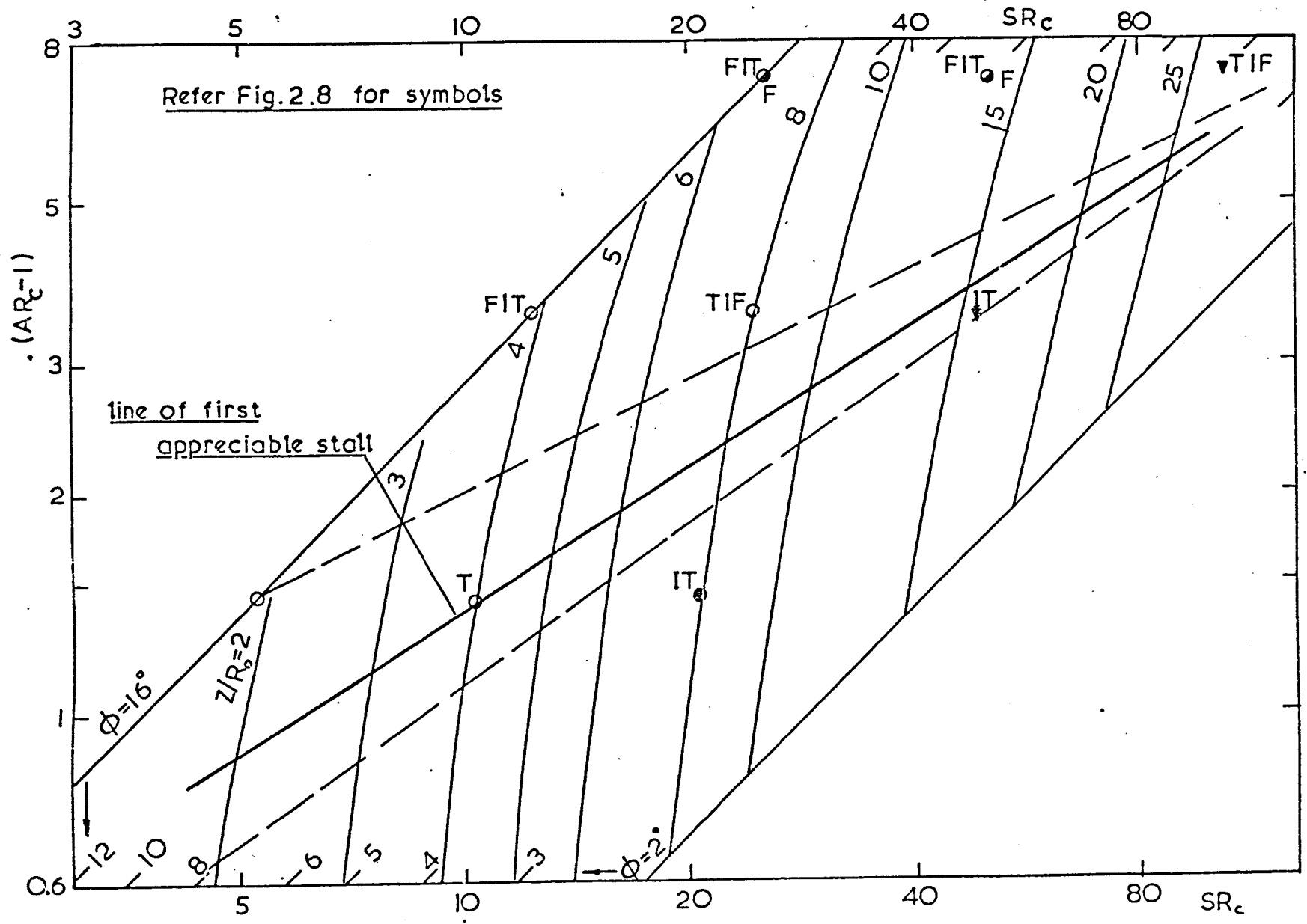
FIG. 2.9 AREA-PLOT PRESENTATION OF FLOW REGIMES IN DIFFUSERS

CHAPTER THREE

BOUNDARY LAYER GROWTH IN A CONICAL DIFFUSER WITH AXIAL FLOW

3.1   INTRODUCTION

The lack of success in the attempts to predict the
flow in a conical diffuser could be attributed to the failure
to solve the governing equations of motion. The Navier-Stokes'
equations have been accepted universally as a basis for the
theoretical analysis of fluid dynamic problems. These were
first developed for laminar flow applications and later Osborne
Reynolds extended these to turbulent flow cases. He replaced
the laminar velocities and mean pressures by their instantaneous
counterparts. The resulting equations, generally known as
Reynolds' equations, had additional terms representing turbulent
transport of momentum known as Reynolds' stresses. The original
laminar equations, being non-linear, have been solved exactly
only for a very few cases. Now with the addition of the
turbulent stress terms such a solution is unimaginable.

Analytical approaches too have had only a limited degree
of success. Where a diffuser is concerned one factor largely
responsible has been the limited knowledge of the growth of the
turbulent boundary-layer in the presence of an adverse pressure
gradient.

This chapter deals with an analytical method for
predicting boundary-layer growth in a conical diffuser. A form

of the model was developed initially during an extensive programme of research on flow in diffusers at the Pennsylvania State University. This has been extended now to obviate the need for information on the core-velocity along the length of the diffuser.

3.2   METHOD OF THE PENNSYLVANIA STATE UNIVERSITY GROUP

A programme of research was initiated in 1945 at the Pennsylvania State University in connection with the design of a high speed water-tunnel. Ross, who was associated with this programme, postulated a new physical approach to the turbulent boundary-layer problems. This, combined with empirical correlations, provided a method for evaluating two-dimensional-turbulent boundary-layer parameters in the presence of an adverse pressure gradient.

Fraser extended this quite successfully to three dimensional flows. Within the range of validity of the method, the predicted values of boundary layer parameters compared very well with their experimental counterparts. Later Robertson and Fraser proposed a method for diffuser design using Fraser's model, based on the occurrence of "separation" as the criterion for determining the geometry of the diffuser. They went further to suggest a method for predicting the performance coefficient.

The method involves using a set of graphs and equations to evaluate the boundary-layer parameters, proceeding downstream in a station-wise manner. It requires prior knowledge of the core velocity outside of the boundary-layer, and it was assumed

that this could be calculated from experimentally obtained
static pressures at each station.

3.3 ROSS'S TWO DIMENSIONAL MODEL

3.3.1 Introduction

The method is based on a new approach to flow in the
boundary-layer. A three-zone division is considered based on
the relative influence of viscosity on flow in the boundary layer.
He analysed a vast amount of experimental data from previous
investigations to obtain correlations between the growth of flow
parameters. As Ross (1956) has already discussed his method in
detail only the basis of his work will be discussed here since
it is the extensions made by Fraser (1958) into three
dimensional flows that are of major interest.

3.3.2 The Turbulent Boundary Layer Profile

Prandtl's mixing length theory for momentum transfer
between various strata in a turbulent flow leads to the following
relationship for the dominant Reynolds stress:

$$\tau = -\rho \overline{u'v'} = \rho l^2 \left| d\bar{u}/dy \right| . d\bar{u}/dy \qquad (3.3.2.1)$$

Amongst others, an assumption of mixing length being
proportional to distance from the wall then leads to the well
known logarithmic velocity profile

$$u/u_* = A \log_e(u_* y/\nu) + B \qquad (3.3.2.2)$$

where A and B have been determined experimentally to be 2.5 and
5.6 respectively. Close to the wall the logarithmic term tends
to an infinitely negative value, but in this region a laminar
sub-layer is known to exist in practice and the concept of the

mixing length tending to zero because of the solidity of the wall accords well with this fact. The three regions involved in this analysis (the laminar sub-layer, logarithmic region and a buffer zone) have known velocity profiles in a turbulent boundary layer up to a height of about $\eta = 0.1$. From $\eta = 0.25$ to $\eta = 1$, equation (3.3.2.2) becomes progressively less satisfactory, largely because the mixing length no longer retains its proportionality to y but attains a constant value of about 0.14Y. Resort is usually then made to the 1/n-power law, where n depends on Reynolds number but is usually taken as 7, or to a "wake" type profile, or to the $\frac{3}{2}$ - power law based on work by Darcy

$$(1 - u/u_\infty) = D.(1 - y/Y)^{3/2}$$ (3.3.2.3)

where D is a shape factor which depends on the past history of the flow.

It seems reasonable, therefore, to divide the boundary layer not into regions which depend on the mixing length being constant, proportional to y, or equal to zero but into regions which are either dependent on past history of the boundary layer and free-stream pressure gradient or influenced by the proximity of the wall and independent of pressure gradient. In any turbulent layer in an adverse pressure gradient, the profile from the wall to about $\eta = 0.1$ is known not to be sensitive to this pressure gradient whereas the profile from $\eta = 0.25$ to $\eta = 1$ is. Ross has therefore suggested that the breakdown shown in Figure (3.1), which includes a blending region, dependent to some extent on pressure gradient and wherein the other two

velocity profiles are made compatible. This latter condition
may often require an inflection, so the equation for this region
would need to be at least a cubic.

Ross states that for the outer turbulent region
(equation 3.3.2.3) an accurate idea of impending boundary layer
separation is given by the condition $D = 1.3 \mp 0.1$. This is
clearly equivalent to the shape factor $H(= \delta/\theta)$ for the $\frac{1}{7}$ - power
law profile tending to a separation value of about 3.5.

The substitution of a constant mixing length into
Prandtl's model leads to

$$D = [2/3][Y/l]\sqrt{\tau_w/\rho u_\infty^2} \qquad (3.3.2.4)$$

and multiplication of both sides by u_∞/u_{∞_0} leads, after
rearrangement, to

$$[Y/D](u_{\infty_0}/u_\infty) = [3l/2] (\tau_w/\rho u_{\infty_0}^2)^{-1/2} \qquad (3.3.2.4)$$

The term on the left-hand side is a function only of
distance downstream from the initial condition (suffix 0) and not
of local wall conditions; experimental results by Schubauer and
Klebanoff (1950) have confirmed this.

3.3.3   Growth of Flow Parameters

The use of the von Karman integral momentum equation

$$d\theta/dz = (2+H).[\theta/\rho u_\xi^2][dp/dz] + C_f/2 \qquad (3.3.3.1)$$

in turbulent flows with adverse pressure gradients has already
resulted in poor approximations. It was originally derived for
use with laminar boundary-layers and has been applied quite
extensively to turbulent flows with some degree of success.
However, it needs to be modified before it can be applied
successfully to turbulent flow.
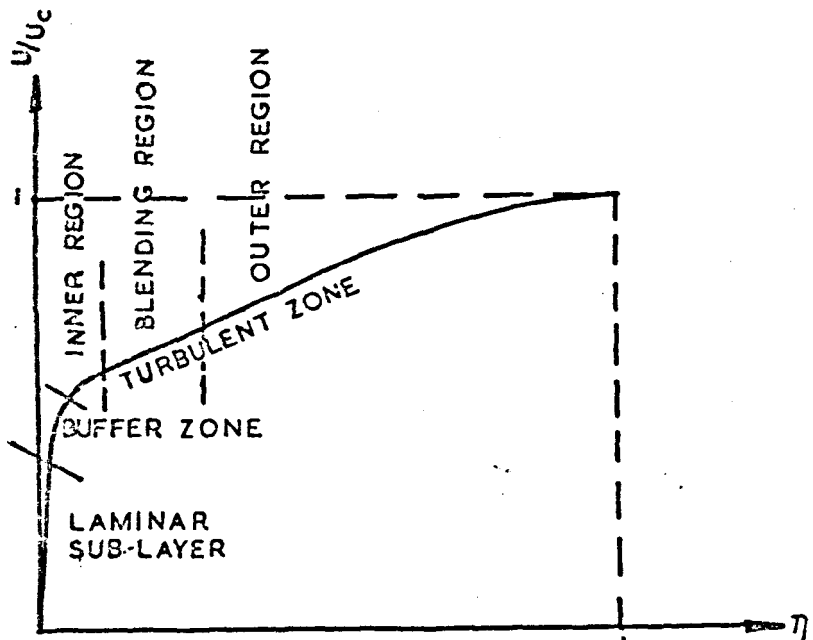
FIG.3.1 ⠂ DIVISION OF VELOCITY
PROFILE IN BOUNDARY LAYER
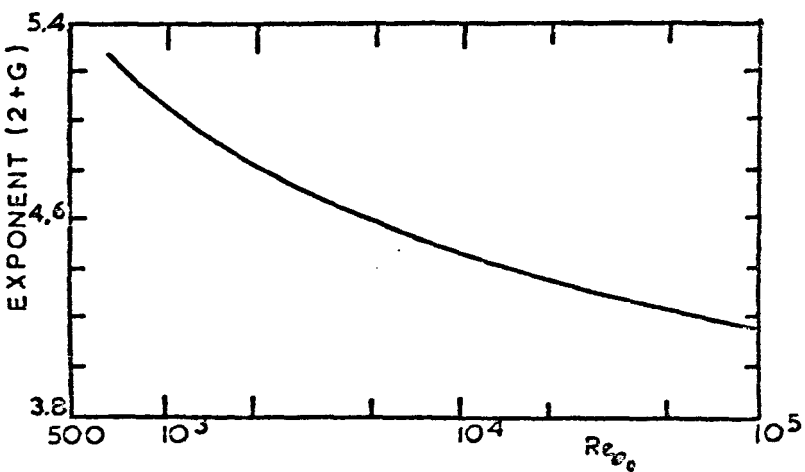
FIG.3.2 VARIATION OF (2+G) WITH Re_{θ_0}

In view of the difficulty in solving such an equation
Ross proposed an empirical relationship for the growth of
momentum thickness,

$$\theta_o/\theta = (u_c/u_{c_o})^{2+G}$$ (3.3.3.2)

where G is a parameter dependent only on the inlet momentum
thickness Reynolds' number. Fig. (3.2) shows the variation of
$(2 + G)$ with R_θ which may be represented by

$$(2+G)=0.0143(\ln R_{\theta_o})^2 - 0.4667 \ln R_{\theta_o}+ 7.554$$ (3.3.3.3)

Furthermore on the basis of the Prandtl momentum-
transfer theory and dimensional analysis, Ross showed the outer
velocity profile parameter D to be governed by,

$$[Y/\theta D][u_c/u_{c_o}] = [(A(z_\sigma-z)/\theta_o)+ Y_o/\theta_o D_o][\theta_o/\theta]$$ (3.3.3.4)

where A is a constant evaluated in the zero-pressure gradient
region ahead of the region of relatively strong pressure gradients.
Ross went on to show that

$$A \simeq 0.025(1+12 C_{f_o})$$ (3.3.3.5)

If the initial velocity profile is known A may be
calculated by determining C_{f_o}. By obtaining $Y/\theta D$, D could
be read off Figure (3.3) which is an experimental curve provided
by Ross from several sets of data. Now the problem is one of
solving a series of algebraic equations with the aid of some
experimental curves.

As pointed out by Ross himself, the most serious
limitation of the method is that, in its algebraic form, it is
applicable only for about fifty inlet boundary layers thicknesses.

3.4   FRASER'S THREE DIMENSIONAL MODEL

3.4.1   Introduction

While the above work did not adequately predict real

flow situations in three dimensions it offered scope for extension into such flows. Fraser made a very useful contribution when he extended Ross's two-dimensional model to three-dimensional flows. There is no justification in discussing this in great detail as it has already been the subject of several publications, (Fraser (1956, 1958)). However, in leading onto the discussion of the present extensions to this method, it is necessary briefly to outline the method with special emphasis on the advantages, limiting factors and the drawbacks.

3.4.2 Modifications to Ross's Equations

The growth of the momentum thickness in three dimensional flow is,

$$\theta R/\theta_o R_o = (u_{c_o}/u_c)^{2+G} \tag{3.4.2.1}$$

furthermore the variation of the shape parameter D is governed by

$$[YR/D][u_{c_o}/u_c] = Az^2 + Y_o R/D_o \tag{3.4.2.2}$$

A, which is a function of the initial shear stress, is given by the empirical relationship

$$A = (\sqrt{C_{f_o}} - 0.038) \tag{3.4.2.3}$$

which provides a reasonable approximation.

A function characteristic γ, related to the inner velocity profile, and the outer law velocity profile shape parameter D are related by the empirical relationship

$$\gamma = 0.9(1 - 0.68D) \tag{3.4.2.4}$$

and it has been shown that the shear stress coefficient now becomes

$$C_f \cong 2\gamma^2/[0.7 + 5 \log_{10}(\gamma R_\theta)]^2 \tag{3.4.2.5}$$

For a solution to be possible one final equation is required, relat-

ing Y/θ and D. Robertson and Fraser (1960) showed that
they were related by

$$Y/\theta D = [2O/D] [\theta/R] + 1.8/D^2 + 3.6/D + .675 D^2 \qquad (3.4.2.6)$$

The shear stress coefficient at inlet may be
evaluated using the relationship

$$C_{f_o} = 2/[6.2 + 5.2 \log_{10}(R_{\theta_o})]^2 \qquad (3.4.2.7)$$

3.4.3   Method of solution

The initial values required for commencement of the
procedure are Y_o, θ_o and U_{co}. It is also assumed that the
core velocity, outside the boundary-layer, could be computed
from a knowledge of the experimental pressure distribution.
The above equations and graphs are sufficient to evaluate the
flow parameters.

In a typical problem, e.g. a diffuser, a marching
technique would have to be adopted. Suitably spaced stations
should be considered. The starting values applicable to any
particular station are obtained from the previous station.

3.4.4.   Limitations and Conclusions

This method is only applicable to flows where a
potential core exists. As Fraser points out, when the flow
approaches a fully-developed state various forces and second
order effects that are neglected in the present analysis might
become important.

Practical application of the method is limited by
the necessity of determining the initial values of D, Y and θ
by experimental methods. It was pointed out by Ross and by
Fraser that a minimum of 15 to 20 points are required on a

profile for the proper determination of D and Y.

For any theoretical model starting values must be provided; the only difference in this case is that evaluating these is cumbersome. This however is not a major disadvantage. One aspect of the method that does not make it very attractive is the need to calculate the core velocity (from the pressure distribution) for each station.

The main aim of the work of the Pennsylvania State Group was to predict the performance of diffusers with a wide variety of geometries and inlet conditions. Development of a method to predict the growth of boundary-layers in an adverse pressure gradient was a necessary contribution towards their main goal.

The performance coefficient of a diffuser is defined as the ratio of the static pressure gain across the diffuser to the inlet dynamic pressure (sometimes the change in dynamic pressure is regarded as the reference value). It follows that if the pressure distribution has to be measured, in order to proceed with the above model to evaluate the boundary-layer parameters and hence compute the performance coefficient, one might as well compute the performance coefficient without recourse to the above model. It must be emphasised, lest the author's comments are misconstrued, that the model itself is very attractive in the analysis of boundary-layer properties though not so, in its present form, for predicting the performance coefficient.

Thus, the logical extension to the Pennsylvania State work would be the development of a method which does not require measured values of static pressure as a pre-requisite.

3.5 EXTENSIONS TO THE 'FRASER-MODEL'

3.5.1 Basis of Extension

The present research programme has extended the invaluable work of the Pennsylvania State Group, thus making it possible to evaluate boundary-layer parameters without recourse to pressure measurement at each station.

The extension involves the introduction of the equation of continuity to the model. However this requires a detailed knowledge of the velocity distribution. Additional equations have been introduced to identify completely the velocity profile. This enables the determination of all the required flow parameters. Another feature is that the initial value of D can be evaluated in a very straight-forward manner by recourse to a subroutine in the main programme.

At the time of the Pennsylvania State programme, computers were not in wide use and graphical techniques were the order of the day. As Ross himself pointed out, it was necessary to develop a method that was easily handled without having to resort to solving differential equations. But with the present wide use of computers there is no reason why the entire process should not be programmed in a manner suitable for the computer. A special programme was developed to handle the the voluminous amount of numerical work required.

As will be seen from the ensuing sub-sections, it would not have
been possible to develop this method without the aid of the
computer. The task of developing the programme was by no means
easy and special numerical techniques had to be developed to
speed up the process.

3.5.2   Velocity Profiles

The shear stress coefficient is

$$C_f = \tau_w/[\rho u_c^2/2]$$

and the friction velocity is

$$u_* = \sqrt{\tau_w/\rho}$$

from which

$$u_*/u_c = \sqrt{C_f/2} = f_* \qquad (3.5.2.1)$$

The following relationships are available for the inner (u_2) and
outer (u_4) regions for $(20\nu/u_*) \leqslant y \leqslant 0.1Y$

$$u_2/u_* = C_1[1 + C_4 \ln(yu_*/\nu)] \qquad (3.5.2.2)$$

and for $.25Y \leqslant y \leqslant Y$

$$u_4/u_c = 1 - D(1 - y/Y)^{3/2} \qquad (3.5.2.3)$$

$$\text{But} \quad yu_*/\nu = [y/Y][Y/\theta][u_*/u_c][\theta u_c/\nu]$$

$$= \eta \, R_\theta f_*[Y/\theta]$$

$$= \eta \, A_c \qquad (3.5.2.4)$$

where $A_c = R_\theta f_*(Y/\theta)$

Also $u_2/u_* = [u_2/u_c][u_c/u_*] = u_2/u_c f_* \qquad (3.5.2.5)$

Using equations (3.5.2., .4, .5) we have

$$u_2/u_c = f_* C_1[1 + C_4 \ln(\eta A_c)] \qquad (3.5.2.6)$$

Very close to the wall in the laminar sub-layer the
inadmissibility of the mixing-length theory makes equation
(3.5.2.6) inapplicable. Furthermore the use of a logarithmic

term precludes its use at the wall where $\eta = 0$. This is overcome by the introduction of a profile governed by a quadratic from the wall to approximately $y u_* / \nu = 20$; thus

$$u/u_c = a_1 \eta + a_2 \eta^2 \qquad (3.5.2.7)$$

valid up to $\eta = 20\nu / u_* Y$

The blending region may be suitably expressed using a cubic equation with four unknowns, thus for $0.1 \leqslant \eta \leqslant 0.25$

$$u_3/u_c = b_0 + b_1 \eta + b_2 \eta^2 + b_3 \eta^3 \qquad (3.5.2.8)$$

We now have a set of equations governing the entire velocity profile. viz.

$$
\begin{aligned}
0 \leqslant \eta \leqslant 20/A_c \; &; \quad u_1/u_c = a_1 \eta + a_2 \eta^2 \\
20/A_c \leqslant \eta \leqslant 0.1 \; &; \quad u_2/u_c = f_* C_1 [1 + C_4 \log_e(\eta A_c)] \\
0.1 \leqslant \eta \leqslant 0.25 \; &; \quad u_3/u_c = b_0 + b_1 \eta + b_2 \eta^2 + b_3 \eta^3 \\
0.25 \leqslant \eta \leqslant 1.0 \; &; \quad u_4/u_c = 1 - D(1 - \eta)^{3/2}
\end{aligned}
\qquad (3.5.2.9)
$$

At any common point between successive segments continuity is satisfied in ordinate and gradient only. For greater accuracy continuity in curvature could have been included though this would have led to more complex equations for the polynomials.

Differentiating the above equations (3.5.2.9) w.r.t. η , yields

$$
\begin{aligned}
(u_1/u_c)' &= a_1 + 2a_2 \eta \\
(u_2/u_c)' &= f_* C_1 C_4 / \eta \\
(u_3/u_c)' &= b_1 + 2b_2 \eta + 3b_3 \eta^2 \\
(u_4/u_c)' &= 3D(1 - \eta)^{1/2}/2
\end{aligned}
\qquad (3.5.2.10)
$$

Solving for a_1, a_2 at $\eta = 20/A_c$ using equations (3.5.2.9)

and (3.5.2.10) yields

$$\begin{bmatrix} 1 & 20/A_c \\ 1 & 40/A_c \end{bmatrix} \begin{bmatrix} a_1 \\ a_2 \end{bmatrix} = \begin{bmatrix} f_*C_1[1 + C_4\ln(20)] A_c/20 \\ f_*C_1 C_4 A_c/20 \end{bmatrix} \qquad (3.5.2.11)$$

Similarly solving for b_0, b_1, b_2, b_3 at $\eta = 0.1$ and $\eta = 0.25$

yields

$$\begin{bmatrix} 1 & 0.1 & 0.01 & 0.001 \\ 0 & 1 & 0.2 & 0.03 \\ 1 & .25 & .0625 & 0.0156 \\ 0 & 1 & 0.5 & 0.1875 \end{bmatrix} \begin{bmatrix} b_1 \\ b_2 \\ b_3 \\ b_4 \end{bmatrix} \begin{bmatrix} f_*C_1[1+C_4\ln(A_c/10)] \\ 10 f_*C_1 C_4 \\ 1 - 3^{3/2}D/8 \\ 3^{3/2}D/4 \end{bmatrix} \qquad (3.5.2.12)$$

At this stage a detailed knowledge of the velocity profiles

is available.

3.5.3   Mass Flux and Core Velocity

From Figure (3.4) $R = r + y$ and $r/Y = R/Y - \eta$

for flow within the boundary-layer

$$\dot{q}_i = 2\pi\rho \int_{r_1}^{r_2} u\, r\, dr$$

$$= 2\pi\rho\, Y^2 u_c \int_{r_1/Y}^{r_2/Y} [u/u_c][r/Y]\, d(r/Y)$$

$$= 2\pi\rho\, Y^2 u_c \int_{R/Y - \eta_1}^{R/Y - \eta_2} [u/u_c][(R/Y) - \eta]\, d[(R/Y) - \eta]$$

or $$\dot{q}_i = 2\pi\rho\, Y^2 u_c \int_{\eta_2}^{\eta_1} [u/u_c][(R/Y) - \eta]\, d\eta \qquad (3.5.3.1)$$

Considering each segment of the profile separately,

(a) Wall region

$$\dot{q}_i = 2\pi\rho Y^2 u_c \int_0^{20/A_c} (a_1\eta + a_2\eta^2)[(R/Y) - \eta]\, d\eta$$

$$2\pi\rho Y^2 u_c [400/A_c^2][(a_1/2)(R/Y) + 20(a_2(R/Y) - a_1)/3A_c - \qquad (3.5.3.2)$$
$$- 100 a_2/A_c^2]$$

(b) Inner region

$$\dot{q}_i = 2\pi\rho Y^2 u_c \int_{20/A_c}^{0.1} f_*C_1[1+C_4\ln(\eta A_c)][(R/Y) - \eta]\, d\eta$$

$$= 2\pi\rho Y^2 u_c f_*C_1 [\eta ((R/Y) - \eta)(1 - C_1 + C_4\ln(\eta A_c)) - \eta/A_c]_{20/A_c}^{0.1} \qquad (3.5.3.3)$$

(c) Blending region

$$\dot{q}_3 = 2\pi \rho Y^2 u_c \int_{0.1}^{0.25} [b_o + b_1\eta + b_2\eta^2 + b_3\eta^3][(R/Y) - \eta]d\eta$$

$$= 2\pi \rho Y^2 u_c [(R/Y)b_o\eta + 0.5((R/Y)b_1 - b_o)\eta^2 + -----]_{0.10}^{0.25}$$

$$= 2\pi \rho Y^2 u_c [\sum_{i=1}^{i=6}((R/Y)h_{i+1} - h_i)\eta^i/i]_{0.10}^{0.25} \qquad (3.5.3.4)$$

where $h_i = b_{i-2}$ and $h_1 = h_6 = 0$

(d) Outer region

$$\dot{q}_4 = 2\pi \rho Y^2 u_c \int_{0.25}^{1.0} [1 - D(1 - \eta)][(R/Y) - \eta]d\eta$$

$$= 2\pi \rho Y^2 u_c [0.75(R/Y) + (9\sqrt{3}((R/Y) - 13/28)/80) - 15/32]_{0.25}^{1.0} \quad (3.5.3.5)$$

(e) In the potential core outside the boundary-layer

$$\dot{q}_5 = 2\pi \rho u_c \int_0^{R-Y} r \, dr$$

$$= \pi \rho u_c (R - Y)^2$$

thus $\dot{q}_5 = 2\pi \rho Y^2 u_c [((R/Y) - 1)^2/2] \qquad (3.5.3.6)$

In general, mass flux through a region in a particular

section is

$$\dot{q}_i = \pi \rho Y^2 u_c \Delta_i \qquad (3.5.3.7)$$

and mass flux through the section is

$$\dot{Q} = \sum_{i=1}^{i=5} \dot{q}_i = \pi \rho Y^2 u_c \sum_{i=1}^{i=5} \Delta_i \qquad (3.5.3.8)$$

where $\Delta_i = \dot{q}_i / \pi \rho Y^2 u_c$

The average velocity is

$$\bar{U}\pi \rho R^2 = 4\rho \int_0^R 2\pi r(u_i/u_c)dr$$

$$= 2\pi \rho Y^2 u_c \int_0^{R/Y} (u_i/u_c)[(R/Y) - \eta]d\eta$$

or $\bar{U}/u_c = (Y/R)^2 \sum_{i=1}^{i=5} \Delta_i$

Let $\zeta = \bar{U}/u_{co}$

then $\zeta = \mu(Y/R)^2 \sum_{i=1}^{i=5} \Delta_i \qquad (3.5.3.9)$

At inlet equation (3.5.3.7) becomes

$$\dot{Q} = \pi \rho Y^2 u_{co} [\sum_{i=1}^{i=5} \Delta_i] \qquad (3.5.3.10)$$

From equations (3.5.3.7) and (3.5.3.10), the core velocity is

$$\mu = [\dot{Q}_0/\dot{Q}_1][(Y_0/R_0)/(\beta Y/R)] \qquad (3.5.3.11)$$

3.5.4 The Axisymmetric Momentum Thickness

The suitability of the functions used to define the velocity profile in the boundary-layer may be verified by comparing the momentum thickness obtained by integrating the profile with that obtained from equation (3.4.2.1). It should be noted that this equation is defined in terms of three dimensional momentum thicknesses and that these differ from the two dimensional thicknesses when the boundary-layer is appreciably thick as at the exit of the diffuser. The axisymmetric momentum thickness may be derived from the velocity profiles as follows.

Consider an axisymmetric duct of radius R, Figure (3.4). The deficit of momentum is

$$\pi\rho[R^2 - (R - \theta)^2]\bar{U}^2 = \int_{R-Y}^{R} 2\pi\rho\, r\, u(\bar{U} - u)\, dr$$

But $\quad R = r + y$

Hence $\quad -\theta^2 + 2R\theta = 2\int_0^1 (u/\bar{U})[1 - (u/\bar{U})](R-y)\,dy$

Introducing $f(\eta) = (u/\bar{U})[1 - (u/\bar{U})]$ and $\quad \eta = y/R \quad$ and simplifying yields

$$(\theta/R_0)^2 - 2\beta(\theta/R_0) + 2\beta(Y/R_0)\int_0^1 f(\eta)[1 - \eta(Y/R_0)/\beta]\,d\eta = 0$$

or $\quad (\theta/R_0)^2 - 2\beta(\theta/R_0) + 2\beta(Y/R_0)F(\eta) = 0 \qquad (3.5.4.1)$

If (θ/R) is small then the above equation approximates to

$$(\theta_*/R_0) = (Y/R_0)F(\eta) \qquad (3.5.4.2)$$

and if (θ/R) is large then

$$(\theta/R_0) = [1 \pm (1 - 2(Y/R_0)F(\eta)/\beta)] \qquad (3.5.4.3)$$

3.5.5 Computation of Boundary-Layer Parameters

A. Computational Procedure

The following information is required as starting values.

1.   Geometric details of the diffuser

      i.e. Throat radius; Area ratio; Cone angle.

2.   Inlet velocity profile.

3.   Kinematic viscosity of fluid.

4.   No. of stations.

      Velocity profiles are divided into segments on the
previously outlined basis.

Entry section

1a.   The momentum thickness Reynolds number is $\mathbb{R}_\theta = u_c \theta / \nu$

      and hence evaluate G using equation (3.3.3.3.)

2a.   The shear stress coefficient at inlet is calculated

      using (3.4.2.7)

3a.   The constant A which is a function of the shear stress

      coefficient is given by equation (3.4.2.8)

4a.   Bairstow's process (Appendix A) is used to solve equation

      (3.4.2.6) to obtain the outer velocity profile parameter D.

5a.   Matrix equations (3.5.2.11) and (3.5.2.12) are solved to

      obtain the constants associated with the velocity profile.

6a.   Equations (3.5.3.7) and (3.5.3.8) yield the flow rate through

      the section under consideration.

      All the required information at the entry section has now
been calculated and the "downstream march" can be commenced.

      Consider the section immediately adjacent to the entry
section.

1b.   Assume a starting value for μ , the core velocity ratio.

      In this case it is assumed, merely for starting computation,

      that the core extends to the wall of the diffuser.

2b.   The momentum thickness is calculated using the non-dimensional

form of equation (3.4.2.1) which is

$$\theta/R = (\theta/R)_o/\beta\mu^{2^{(2+a)}}$$ (3.5.5.1)

3b. Y/RD is evaluated using the non-dimensional form of

equation (3.4.2.2.) which is

$$Y/RD = [Aa^2 + Y/RD)_o]\mu/\beta^2$$ (3.5.5.2)

4b.   Repeat step 4a.

5b.   Calculate the function characteristic γ using equation

(3.4.2.4)

6b.   Obtain C_f using equation (3.4.2.5)

7b.   Repeat step 5a.

8b.   Repeat step 6a.

9b.   Use equation (3.5.3.11) to evaluate the new value of μ

10b.   Using this new value of μ repeat steps 2b - 9b until a

satisfactory value of μ is obtained.

On satisfactory completion of the current section the

calculated value of μ is used as the starting value for the

next section.

It has been attempted to outline the procedure in as

simple a manner as possible. However within this main iterative

procedure are some very complex numerical operations, including

a sub-iterative procedure. The modified 'AITKEN - DELTA' process which

was used in the programme is reported in appendix (3/A).

B.   Solution of Quartic Equation

The solution of equation (3.4.2.6)

$$0.675 \, D^2 + 3.6/D + 1.8/D^2 + 20\,\theta/RD \simeq Y/\theta D$$

proved to be difficult.

It should be noted that at the entry section Y and θ are both known and only D needs evaluating, whence equation (3.4.2.6) becomes

$$0.675 D^4 + [3.6 + 20(\theta/R) - (Y/R)/(\theta/R)]D + 1.8 = 0 \qquad (3.5.5.3)$$

However at any other section it is $\frac{Y}{RD}$ that is known; then the quartic equation takes the form,

$$[(Y/RD)/(\theta/R)]D^2 - [3.6 + 20(\theta/R)D - 0.675 D^4 - 1.8 = 0 \qquad (3.5.5.4)$$

Bairstow's process (Appendix 3/B) is preferred because it does not require a starting value like some other iterative processes. The quartic equation yields four roots which may be real or complex, positive or negative. Observation studies of this particular problem indicated that for the possible range of coefficients, the smallest positive real root was that which was required. This was extracted by first discarding the complex roots and then discarding the negative real roots. The remaining positive roots were set in an ascending order and the first one was accepted.

If this value of D is not acceptable or no positive root is present then a smaller value of μ given by

$$\mu_{i+1} = \mu_i + (\mu_{i+1} - \mu_i)\lambda/2$$

is used and the procedure repeated.

Further information on the procedure is given in appendix (3/C) and in an earlier report (Wirasinghe (1974)).

3.5.6   Discussion and Comparison

As an example of the good agreement between the predictions given by the method detailed in this chapter and experimental results from a 10-deg. diffuser tested by Fraser (1958), Figure (3.5) shows a velocity profile taken at the downstream station $Z/R_o = 4.548$.
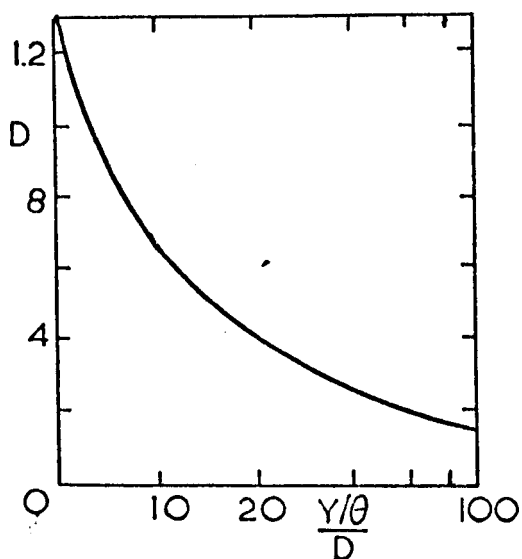
FIG. 3.3 CURVE FOR DET. D
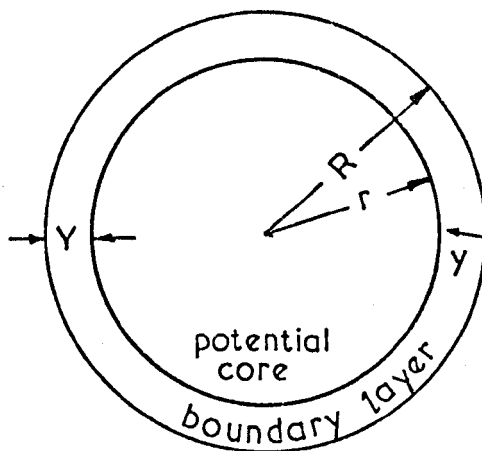
FIG. 3.4
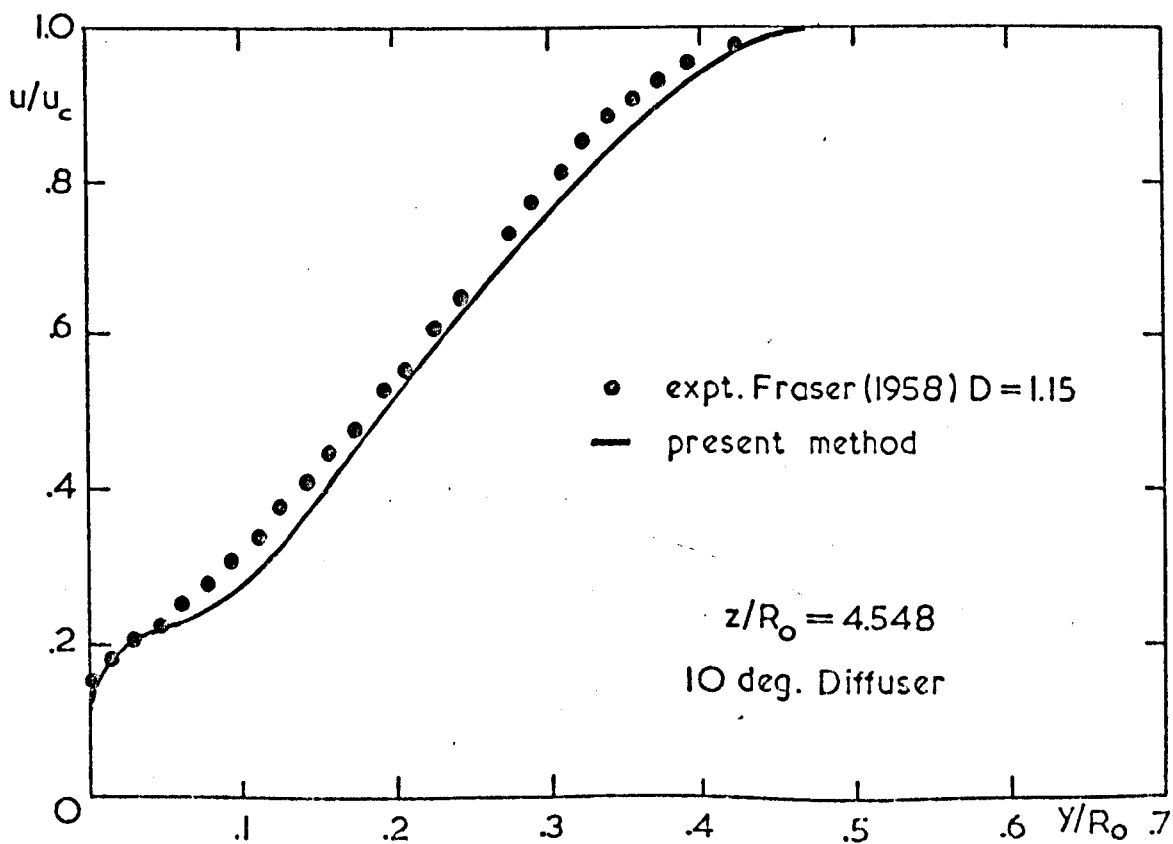
FIG. 3.5 VELOCITY PROFILE IN BOUNDARY-LAYER

The major disagreement between line and points occurs in the blending region but otherwise there is adequate justification for the way Ross split the boundary layer into three distinct regions.

The variation of shape parameter D with downstream distance can be seen in Fig. (3.6), passing from its zero pressure gradient value of about 0.3 to its near-separation value of about 1.3. The importance of the third equation in equations (3.5.2.9) is obvious, the blending region exhibiting the most marked differences between the various profiles.

Figure (3.7) shows the changes in various boundary layer parameters with axial position in the diffuser and agreement between prediction by the present method and Fraser's experimental points is once again seen to be very close. Fraser's prediction for the variation of D, using pressure tappings to give the core velocity u_c, is superimposed in Figure (3.7a) and some improvement is noticed from using the present method. At the downstream end of the diffuser it will be seen that the present prediction continues to rise while Fraser's levels off at D = 1.2. This indicates the difficulty in applying these methods where D is approaching its separation value and where the boundary layer now occupies about 65% of the cross-sectional area. There is a severe lack of knowledge of flow behaviour where boundary layers from opposite walls are about to merge on a diffuser axis and the present model could well be invalidated by the appearance of second-order effects in this region.

The core velocity degradation is shown in Figure (3.7e) where agreement between prediction and experiment is always within

2%, as shown in Table 3/II. Most of the points are within 1% of
the predicted value so agreement is presumably complete within
experimental accuracy. Figure (3.7f) shows, in dimensionless
form, the static pressure recovery in the diffuser, this being
calculated from the velocity in the inviscid core region. The
lowest section of the curve in this figure is shown dotted
because an experimental curve would dip slightly below the origin,
whereas the present method does not allow for the mildly
favourable pressure gradient in the inlet pipe.

All the above comments provide some justification for
extending the Ross model for a turbulent boundary layer into the
field of conical diffuser flows with the proviso that the diffuser
must not be a long one or that the inlet section boundary layer is
not thicker than $\theta/R_o = 0.04$ (Wirasinghe (1974)). These
limitations are essentially a result of replacing the von Karman
momentum integral equation by an algebraic one, this approximation
being valid over only a limited range. Now that a closed-form
solution has been obtained, efforts must be directed towards
extending the method to deal with relatively thicker inlet
boundary layers. Attention should be focussed on extending the
range of validity of the empirical formulae used in the model. In
the case of equation (3.4.2.1) experimental results given by
Cockrell (1964) have shown that a single numerical value of the
exponent can be used only when the diffuser is not too long or
when the boundary-layer at the entry section is not too thick.
In the case of the thin boundary-layer associated with an entry

length of 1.5 pipe diameters, the exponent is constant only up to a value of $\theta R / \theta_o R_o$ of 20 for a 10-deg. diffuser and of about 50 for a 4-deg. one.
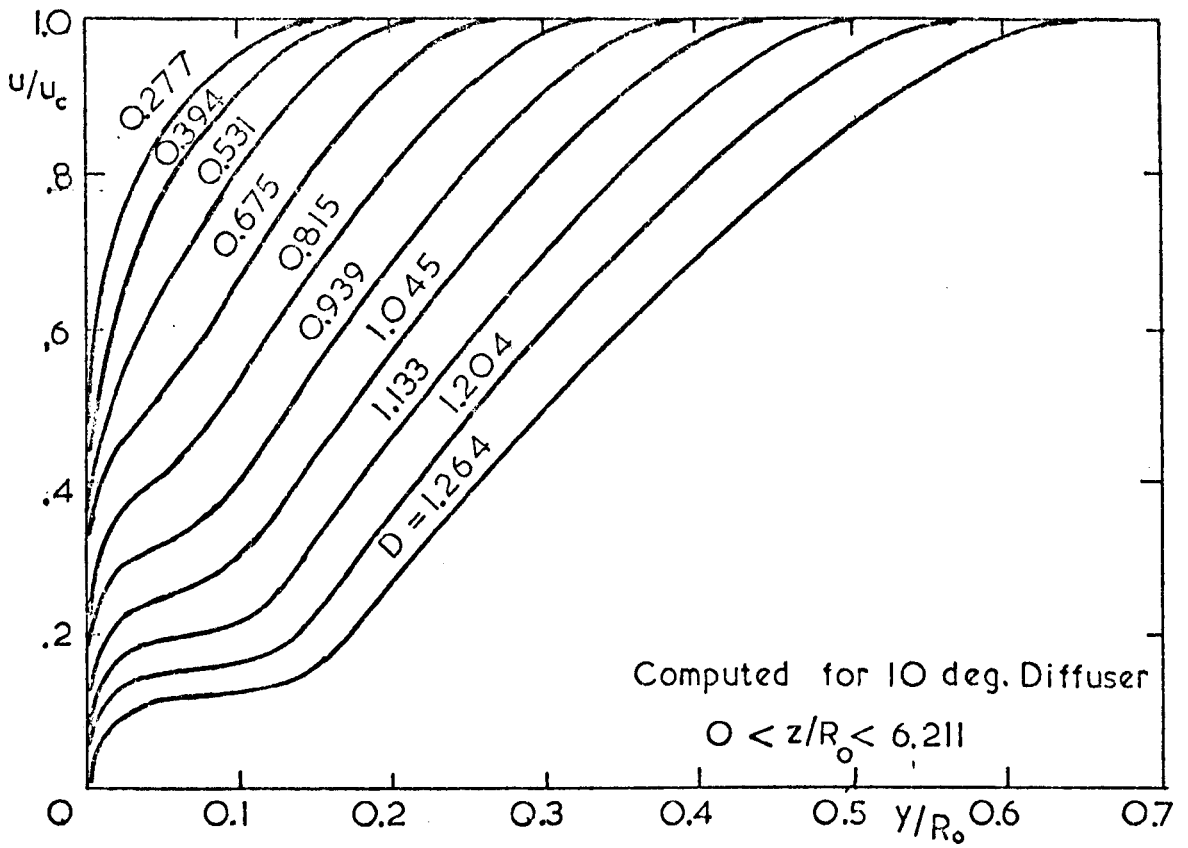
FIG.3.6 VELOCITY DISTRIBUTION IN B'DARY-LAYER
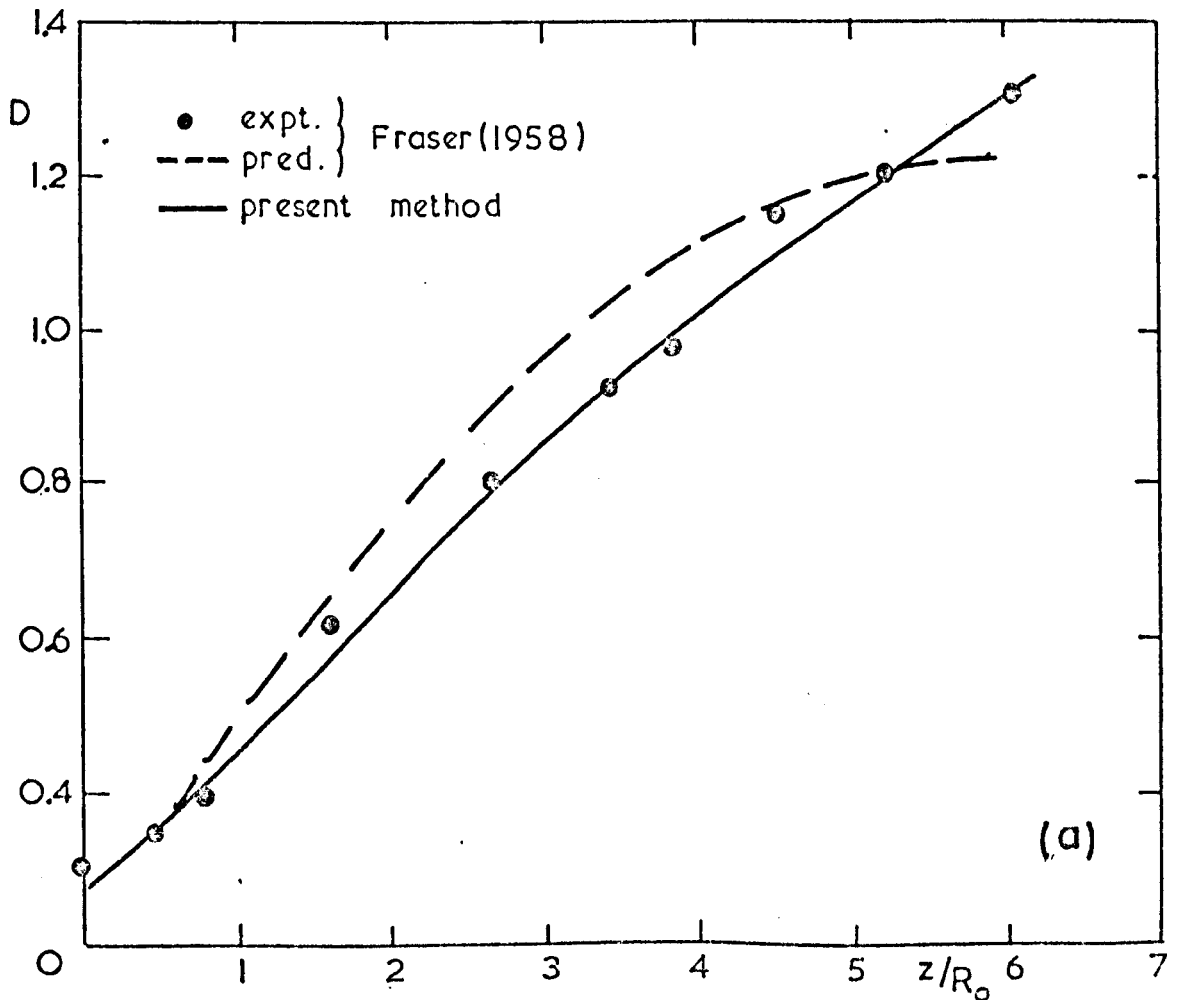
FIG.3.7 COMPARISON WITH DATA FROM FRASER (1958)
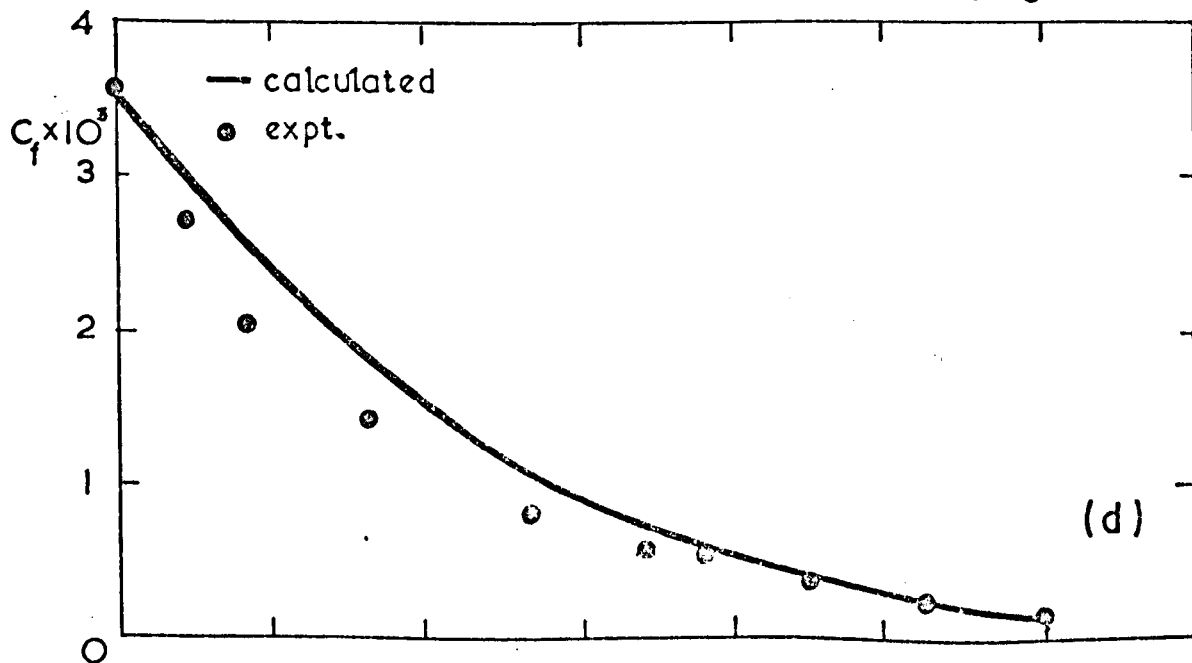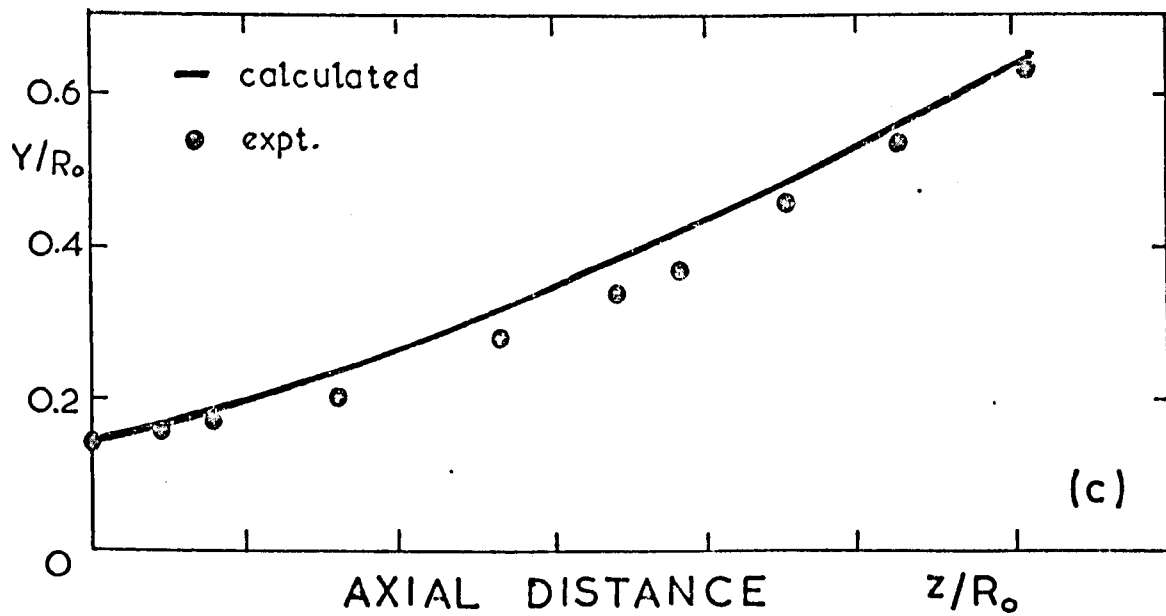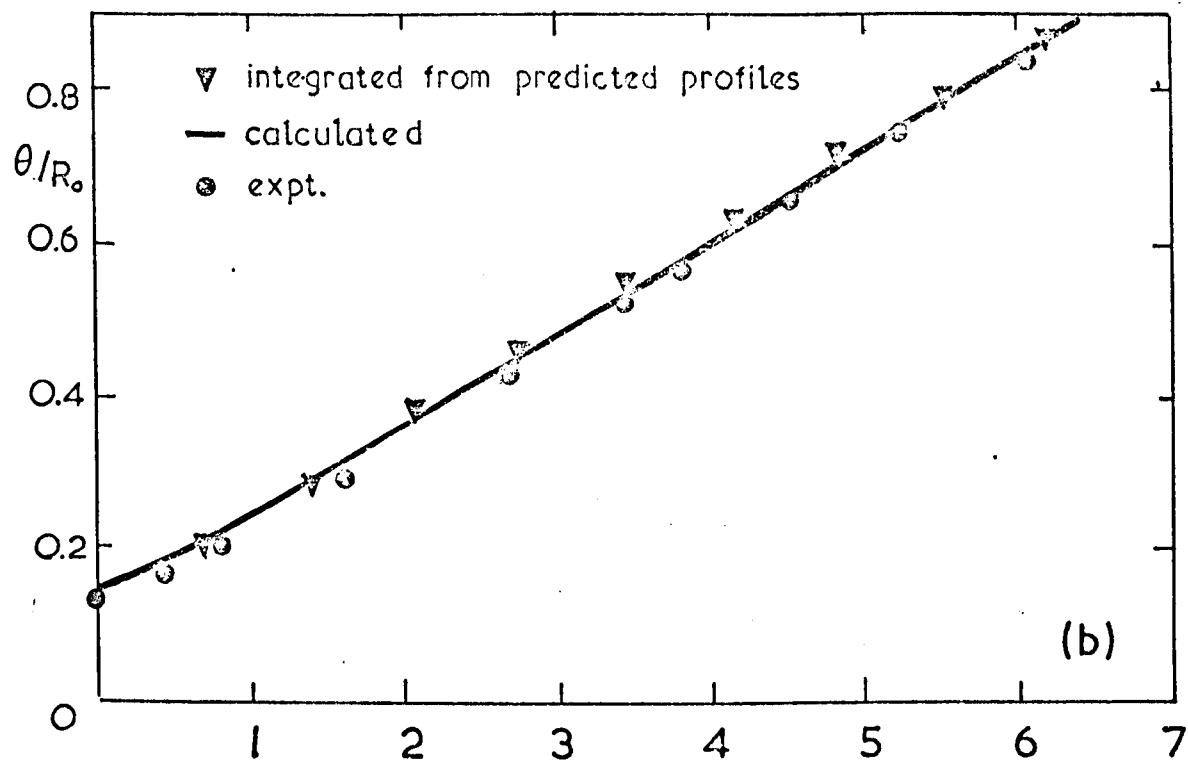
FIG. 3.7 COMPARISON WITH DATA FROM FRASER (1958)
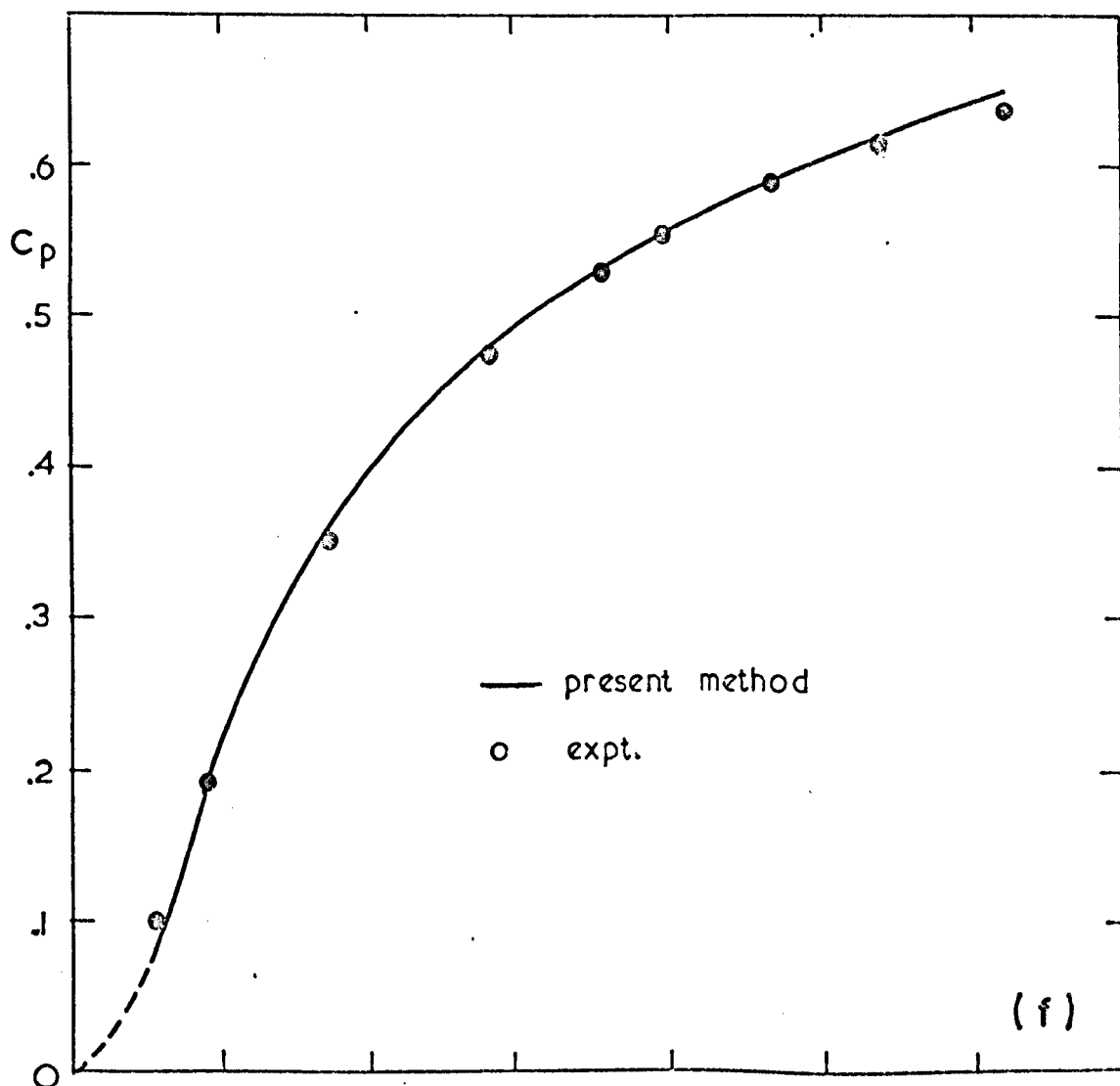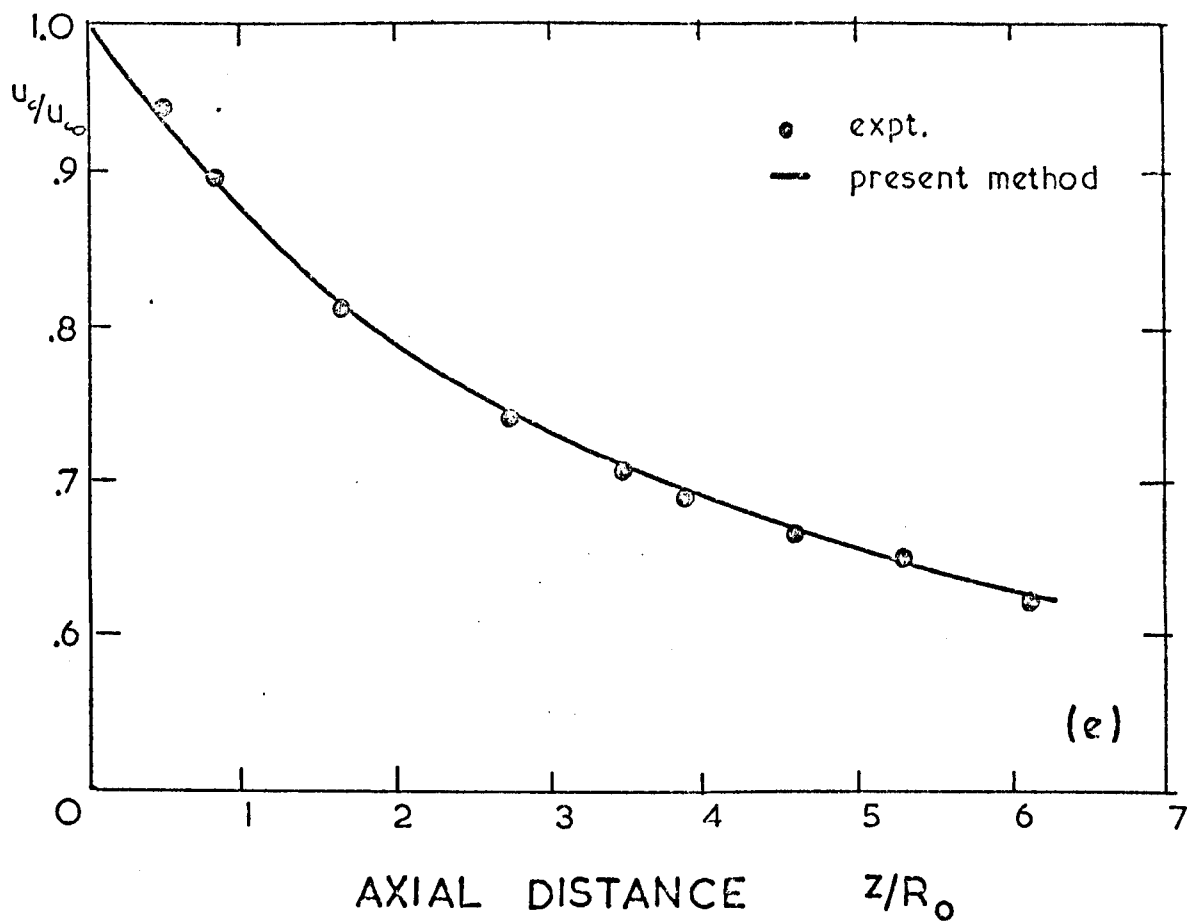
FIG. 3.7 COMPARISON WITH DATA FROM FRASER (1958)
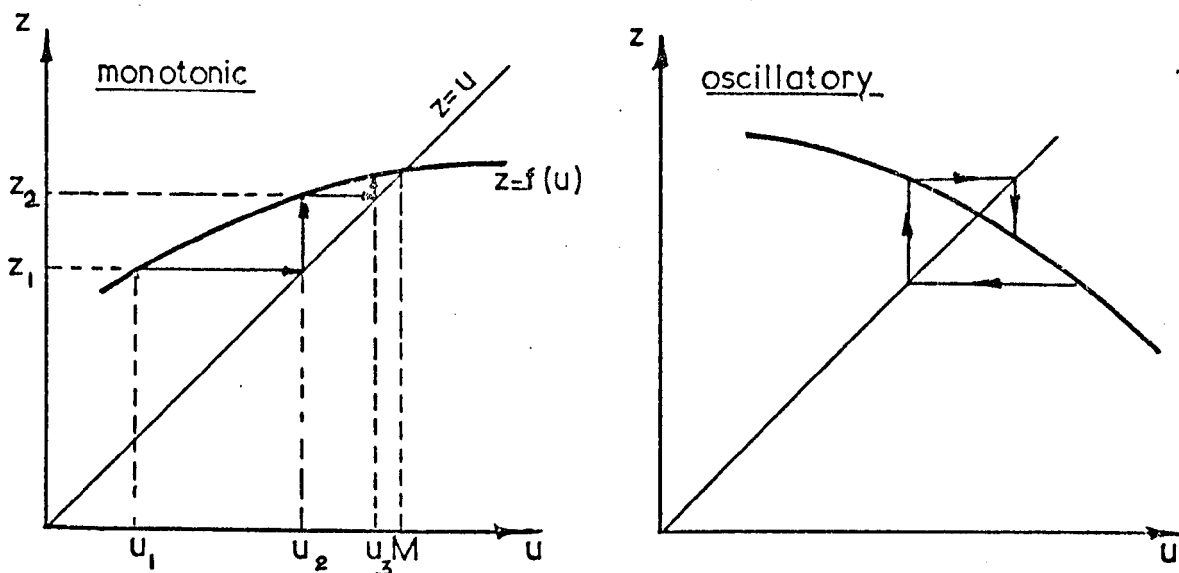
FIG. 3.8 THE TWO MODES OF CONVERGENCE

FLOW DIAGRAM

```
                          ┌─────────┐
                          │  START  │
                          └─────────┘
                               │
                      ┌────────────────┐
                      │  READ DATA     │
                      │  AND CONSTANTS │
                      └────────────────┘
                               │
                      ┌────────────────┐
                      │ CALC. INITIAL  │
                      │ FLOW PARAMETERS│
                      └────────────────┘
                               │
                 ┌───────────────────────────┐
                 │ NEW STATION: MAIN ITER-    │
                 │ ATION FOR CORE-VELY. μ.    │
                 └───────────────────────────┘
```

NEW STATION: MAIN ITER-ATION FOR CORE-VELY. μ.

FINAL STATION DONE   —NO→   —YES→

USE CALC. μ AS STARTING VALUE

CALC. FLOW PROPERTIES

CALC. NEW μ

CALC. D

D SATIS-FACTORY   NO   YES

HAS SEPARATION OCCURRED   YES

NO

STOP

CALC. VELY. PROFILE FLOW & CORE-VELY. CALL SUBROUTINES

CALC. FLOW PROP. AND WRITE.

IS FLOW RATE SATISFACTORY   YES

NO

THREE VALUES OF CALC. μ   NO

APPLY A-D PROCESS

FIG.3.9 SIMPLIFIED FLOW CHART-MASTER 'BLID'

CHAPTER FOUR

SWIRLING FLOWS; INTRODUCTION AND LITERATURE SURVEY

4.1   INTRODUCTION

For a very long time, researchers in various disciplines have been working quite independently with applications involving swirling flows. As a result of the natural interaction between the sciences several problems, common to most applications, have been highlighted. In the late fifties the problem seemed to be the lack of understanding of the structure of the vortex core and the nature and the cause of the rather abrupt breakdown of this core.

Several of the applications with which vortex flows are associated are listed below.

1. HEAT EXCHANGERS

2. THE VORTEX DROP

3. AS A BOUNDARY LAYER CONTROL AGENT

4. VORTICES IN LAMINAR/TURBULENT TRANSITION

5. THE RANQUE-HILSCH TUBE

6. CYCLONE SEPARATORS, BIO-CHEMIST'S CENTRIFUGE

7. VORTEX SHEDDING FROM AIRCRAFT WINGS

8. LIQUID FUEL BURNERS; GAS TURBINE COMBUSTION CHAMBERS

9. THE SWIRL ATOMIZER; AGRICULTURAL SPRAYING MACHINES

10. METEOROLOGICAL DISTURBANCES: TORNADOES; DUST WHIRLS; EARTH'S ROTATIONAL EFFECT ON OCEANOGRAPHY, WHIRLPOOLS

11. PUMPS, TURBINES, TURBOJET/AFTERBURNER COMBINATIONS

12. VORTEX AMPLIFIERS

13. JET PUMPS

In the early sixties this subject was attacked from every conceivable angle. Several authors have reviewed the work lightly in the form of introductions to their own reports. Two very comprehensive reviews have been provided by Gartshore (1962) and Hall (1966). Both reviewers have focussed their attention mainly on the mathematical models and their solutions. Whilst there is no justification for duplicating their work, it is felt that a brief summary should provide a sound introduction, whilst contributing towards building a complete picture of the earlier work. However, emphasis will be placed upon work which has fallen outside the framework of the earlier reviews.

Of the applications mentioned above some require the use of a diffuser which may be treated as a special case of a pipe. Thus previous work associated with swirling flow in pipes warrants a survey and discussion. While in most of the applications swirling flows are an inherent feature, in some cases attempts have been made to improve the efficiency by introducing swirl into the system. In the latter case, however, caution must be exercised in defining efficiency, as the extra energy introduced to produce swirl must be taken into consideration in any efficiency definition.

In the case of the conical diffuser, which is the subject of this research programme, suggestions have been made to indicate that the present form of diffuser might not be the ideal in the presence of swirling flows. Furthermore there exists a view that

the pressure conversion increases with increasing radii, for a given diffuser.

The discussion which follows is an attempt to present relevant information from previous work in an informative manner, and it is hoped that this will form a useful foundation for the work to follow. Unless otherwise stated, 'swirl angle' is defined as the tangent of the ratio of tangential velocity to axial velocity.

4.2   THE VORTEX BREAKDOWN PHENOMENON

In the early fifties Nuttall (1953) observed an instability and a reversal of flow associated with swirling pipe flow. Later in the same decade Peckham and Atkinson (1967) observed a similar phenomenon above aircraft wings at high positive incidences. It was thought that the very same phenomenon may have been responsible for the breakdown in both cases.

Two major areas of research, associated with Vortex breakdown, have emerged since, one being the phenomenon observed above aircraft wings and the other that associated with flow in ducts. Even though this investigation is concerned with the flow in a bounded field, the former phenomenon needs a brief mention, at least, in view of its direct association with the latter.

Above wings, vortex formation manifests itself as two shear-layers which separate from the leading edge and curl upwards and inboard and eventually roll up into a core of high velocity. Under certain circumstances the axial velocity in the core, which is several times the free stream velocity, can be brought to rest

while the entire core expands behind a stagnation point. This
latter behaviour, which has the effect of causing loss of lift
and altering the pitching moment is referred to as vortex break-
down. Jones (1960) proposed that the two cores have opposite
rotation and also that due to the vastly differing boundary
conditions instability in swirling pipe flow was not analogous to
that above wings.

The early sixties saw several investigators studying the
vortex breakdown phenomenon. Harvey (1962) triggered breakdown in
a tube. In the light of his very successful experiments he made
three very important conclusions.

(i)   Breakdown appears to be an intermediate stage between two
        basic types of flow; those that do and those that do not
        exhibit reversal of flow.

(ii)   Transition from one state to the other was orderly and
        under steady conditions very nearly axisymmetric.

(iii)   Changes from one state to the other were reversible.

This type of breakdown is generally referred to as
axisymmetric breakdown and the above conclusions were to be of great
importance in subsequent work.

Lambourne and Bryer (1961) investigated breakdown above
wings very comprehensively. Lambourne (1965) later provided a
detailed description of the types of breakdown. Fig. (4.1a) shows
the axisymmetric breakdown as observed by Harvey. When a critical
swirl number is reached the filament AS swells up to form the
bubble BSB with S as the stagnation point. Under certain conditions

a. Axisymmetric Form
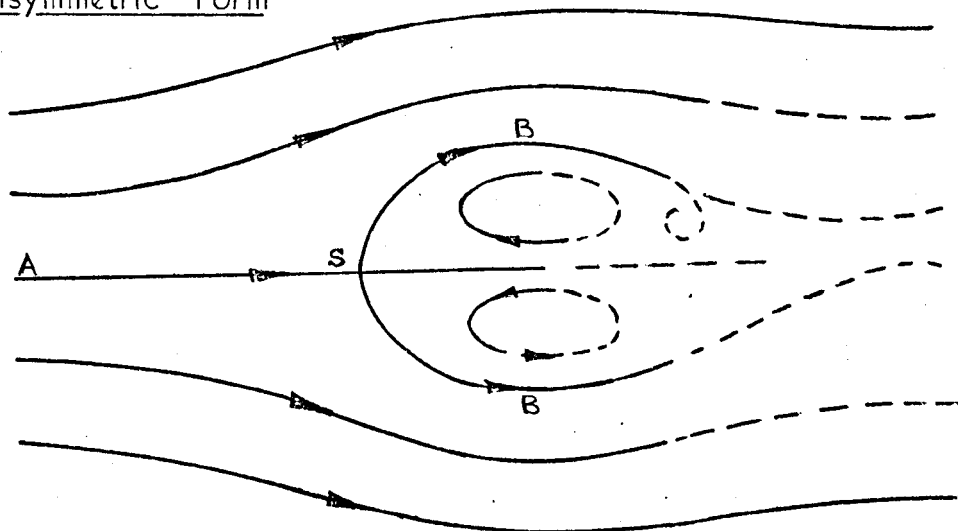
b. Spiral Form
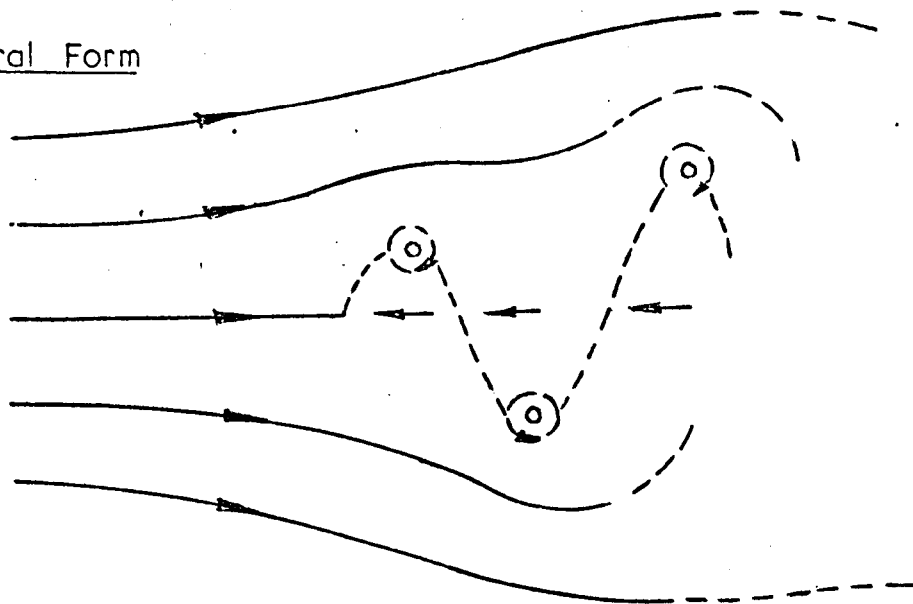
FIG. 4.1

THE TWO FORMS OF VORTEX BREAKDOWN

a second bubble or even a third bubble may form further downstream of the first bubble. Fig. (4.1b) shows the spiral form of breakdown in which the particle S is deflected away from the axis, and rotates in an opposite sense to the primary vortex. Lambourne and Bryer proposed that the spiral form be regarded as arising from instability of the axisymmetric form. Ludwieg (1964) and Jones (1964), however suggest that initially in time the phenomenon manifests itself as a spiralling of the axial filament and that the axisymmetric form is a later development under steady conditions. Fig. (4.2) is unique in that it shows both forms of breakdown occurring simultaneously.

Some of the mathematical models proposed, to provide an explanation to the above observations are discussed in Chapter Five.

4.3   SURVEY OF EXPERIMENTAL WORK.

4.3.1   Swirling Flow in Pipes

Nuttall (1953) and Talbot (1954) made comprehensive investigations of the decay of vortex motion in the laminar range. Instability was observed by the latter using a dye filament and a stable region was defined for combinations of Reynolds and swirl numbers; Fig. (4.3). He related his experimental work to a linearised theory which found good agreement with its prediction. It was suggested that swirl was composed of harmonics and that further downstream the higher harmonics died faster than the first. Menis (1960) investigated the decay of swirl in a pipe with air as the fluid. In calculating the radial pressure gradient, the axial velocity was assumed to be constant, and the former was obtained by
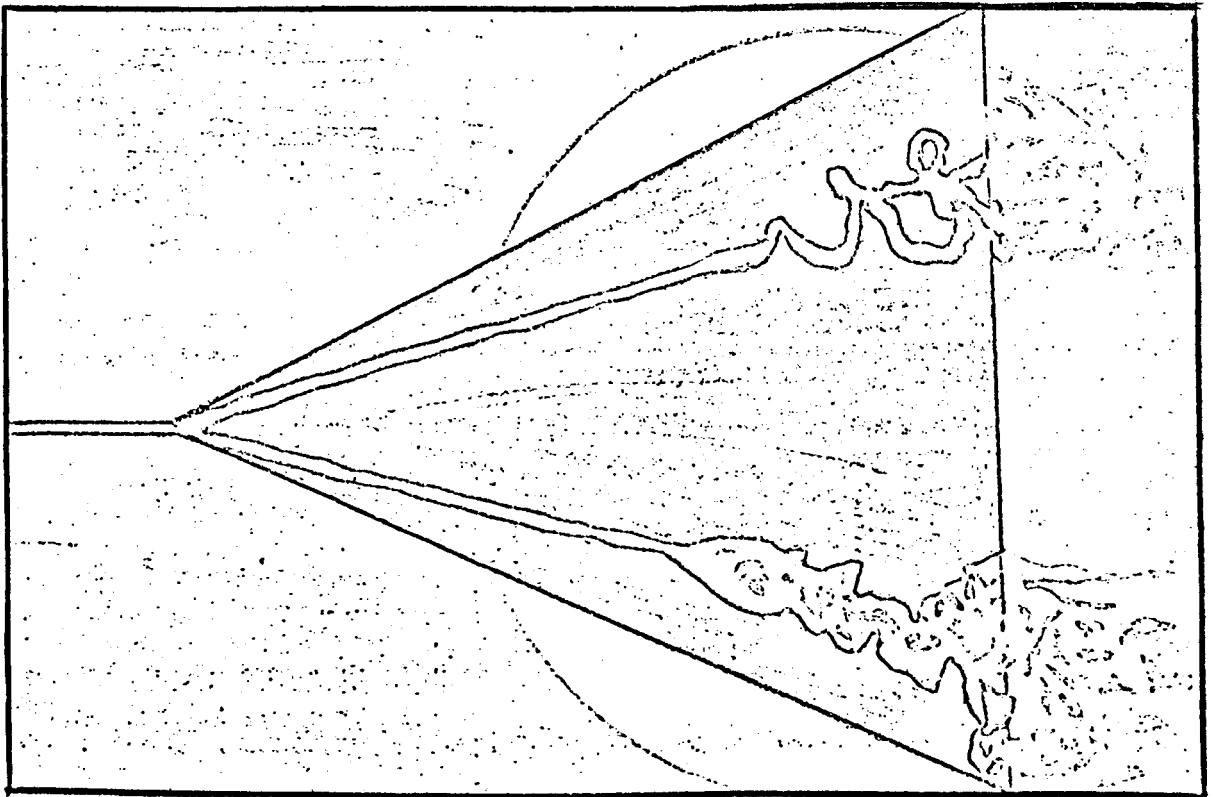
FIG.4.2 THE SPIRAL AND AXISYMMETRIC MODES
OF BREAKDOWN: LAMBOURNE & BRYER (1961)

80
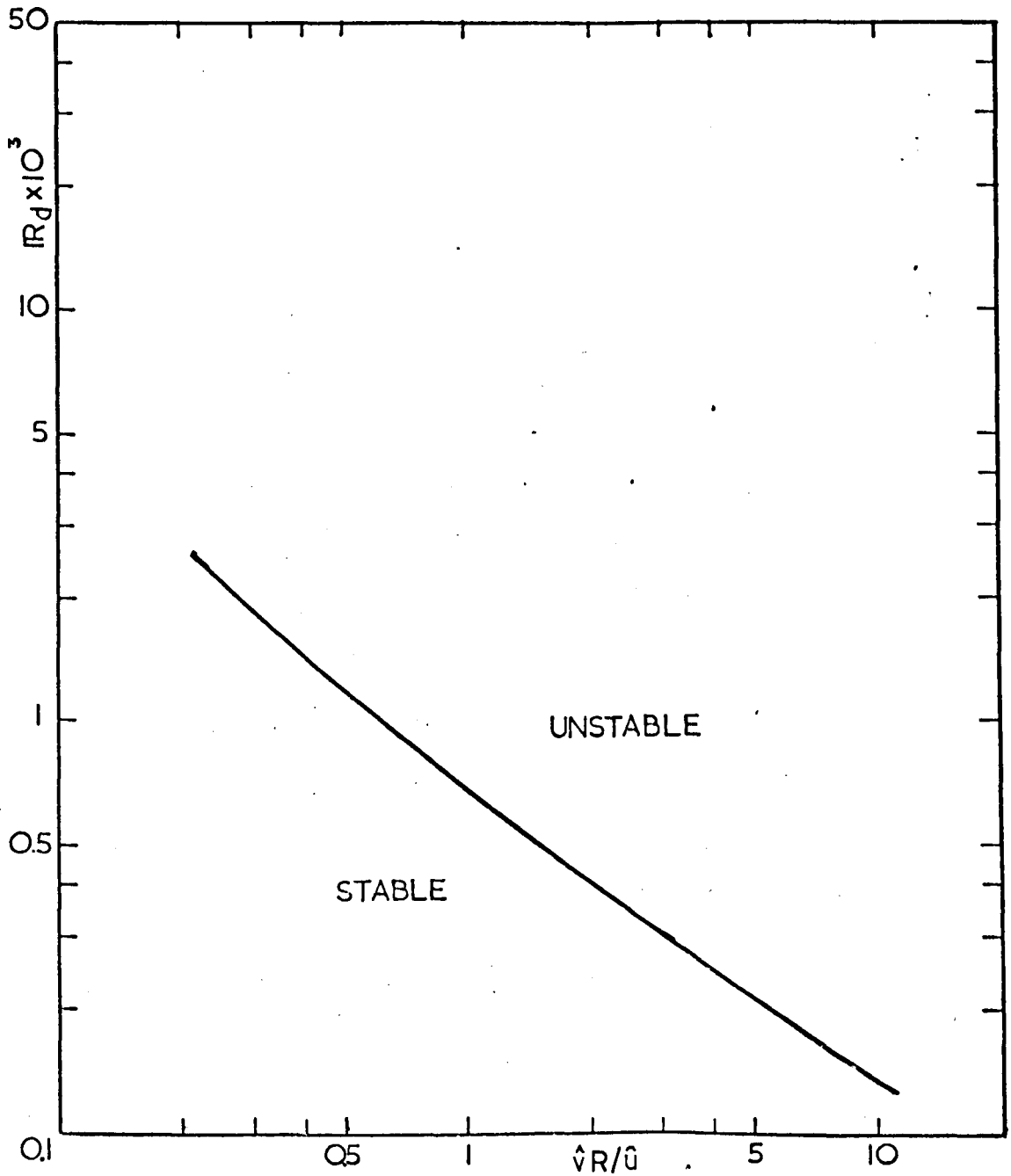
FIG. 4.3 SWIRL INSTABILITY IN LAMINAR PIPE FLOW
FROM TALBOT (1954)

solving the approximate momentum equation

$$[1/\rho].[\partial p/\partial r] = v^2/r$$

Unfortunately information has been provided only at the two extreme stations and hence it is not possible to assess the decay pattern.

Nissan and Bresan (1961) also experimented with swirling pipe flow. Their explanation of flow reversal was as follows;

Where swirl is intense the pressure is low at the centre-line and high near the wall. Downstream, where viscous dissipation has weakened the swirl, pressure is relatively higher at the centre-line and lower at the wall. Thus decay of rotation gives rise to pressure gradients which, if of sufficient magnitude drive secondary back-flows on the axis.

All of the investigators who have been associated with work on swirling flows in pipes until now, while having observed flow reversal, have actually missed the breakdown phenomenon which is believed to be the onset of flow reversal. The first major contribution to swirling flow in pipes was made by Harvey (1962). He was the first to attempt to trigger a breakdown in a tube. His conclusions, more relevant to vortex breakdown, were discussed in the previous section.

Gore and Ranz (1964) studied backflows in rotating fluids associated with free jets and ducts. Rigid body type rotation was imparted to the fluid using a rotating perforated plate. Rotating water in a short tube they observed that when the swirl was increased beyond unity, the region near the axis started to oscillate and when increased beyond a critical value the flow reversed on the axis.

Kirkpatrick (1964), using Harvey's apparatus investigated the pressure gradients associated with breakdown. Pressure and yaw measurements were done using a 0.5 mm pitot probe and with the aid of this he went as close as 0.1" to the vortex axis without disturbing it. He notes that viscous flow plays an important part at low Reynolds numbers and shows that there is loss of total pressure at the centre. He found that when a breakdown was present there were axial pressure gradients fore and aft of it; positive upstream and negative downstream. However, when the breakdown was eliminated by reducing the swirl, the pressure gradients were found to disappear.

An analysis of the flow regimes associated with swirling flows, with a view to studying flow in combustion chambers in gas-turbines, was made by Youssef (1966). The main aim was to attempt to relate the diameter of the flow reversal zone to the flow characteristics. The test section was a 12¼" i.d. x 32' long pipe. Angular momentum was imparted to the fluid by forcing it through a swirler with adjustable vanes. Flow measurement was with the aid of a standard five-hole spherical pressure probe. Measurements were taken as far as 30' downstream of the swirler.

It is claimed, without any further reference, that as the head of the probe may not be a true sphere and also as the holes may not be in exact symmetry, an experimental technique, not sensitive to the above inaccuracies, has been developed for calibration of this probe. His explanation of flow reversal is similar to that of some of the previous investigators. The development of the pressure gradient is as a result of the decay of the tangential velocity owing to wall friction. At any cross-section, the difference between the maximum static pressure and the minimum

static pressure (at the centre) depends on the rate of flow of angular momentum through the cross-section; i.e. this pressure difference decreases as the rate of flow of angular momentum decreases. Thus resulting from the wall friction, the value of the static pressure at the outer radius of the rotating flow decreases in the axial direction, while at the centre, its value increases. Thus the axial pressure gradient at the wall and at the axis have opposite directions which leads to recirculation in the core.

King, Rothfus and Kermode (1969) investigated swirling flow in a 2" diameter tube. Velocity and pressure profiles have been provided. In the light of the information available an order of magnitude analysis was carried out on the turbulent Navier-Stokes' equations. Yet these simplified equations still remain indeterminate.

4.3.2   Swirling Flow in Conical Diffusers

Andres (1909), according to Peters (1934), was the first to suggest that with swirling inflow there is a marked improvement in diffuser performance. However, he did not venture to investigate this further. Peters provided some very interesting experimental data for the swirling inflow case with rigid body type of rotation.

Patterson (1938) quotes Vüllers (1933), as saying that for a free vortex an improvement in efficiency is realised only when the rotation is small and that the present design of diffuser is not efficient when the rotation is large since it does not transform the rotational kinetic energy.

Liepe (1960) studied diffuser performance in the

presence of swirl for a complete range of core angles extending

to a flat plate diffuser. He defined "diffuser efficiency" as

η_D = converted pressure energy/kinetic energy difference

$$\eta_D = \frac{(R_2/R_1)^2\int_0^1(p_2/q_1)(u_2/\bar{u}_1).d(r/R)^2 - \int_0^1(p_1/q_1)(u_1/\bar{u}_1).d(r/R)^2}{\int_0^1(V_1/\bar{u}_1)^2(u_1/\bar{u}_1).d(r/R)^2 - (R_2/R_1)^2\int_0^1(V_2/\bar{u}_1)^2(u_2/\bar{u}_1).d(r/R)^2}$$

However, in presenting experimental information he

neglects the exit terms from the above equation introducing an

"under efficiency", defined as

η_u = recovered pressure energy/inlet kinetic energy

thus

$$\eta_u = \int(p_1/q_1)(u_1/\bar{u}_1)\,d(r/R)^2 / \int(V_1/\bar{u}_1)^2(u_1/\bar{u}_1)\,d(r/R)^2$$

In an universally accepted sense the numerator is the

inlet pressure energy and not the recovered pressure energy. Fig.

(4.4a) shows the performance based on the latter definition. The

curves correspond to solid-body type swirl where the swirl angle is

directly proportional to the radius (F) and to a form of swirl where

the swirl angle is constant (C). Whilst later work cannot be

compared with these results, in their present form, they display the

trends of improvements. It is seen that the most significant

improvement is with diffusers normally stalled in pure axial flow.

Figure (4.4b) is a map of flow regimes, provided by

Liepe (1963), based on wall separation. It is of limited use in

that he does not make any reference to vortex breakdown which is

known to exist.

So (1967) investigated the vortex phenomenon in a 6° cone

angle conical diffuser. On the basis of his experiments he suggests

that there are five regimes of flow characterised by two types of
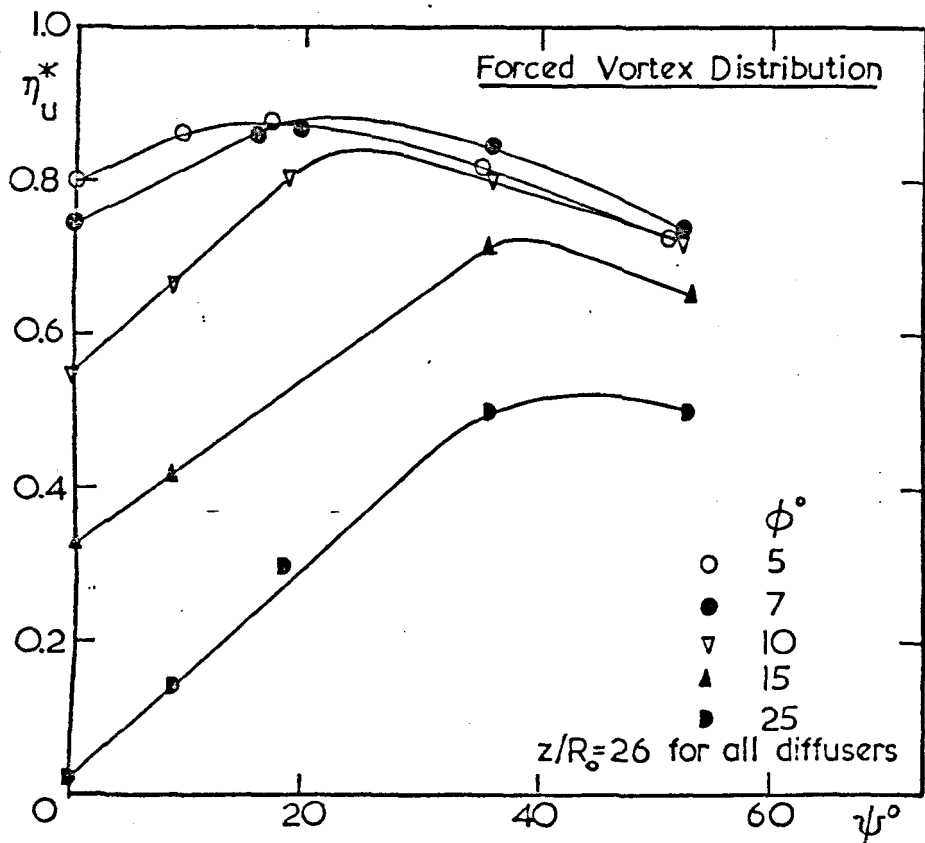
FIG.4.4.a DIFFUSER 'UNDER' EFFY.

FROM
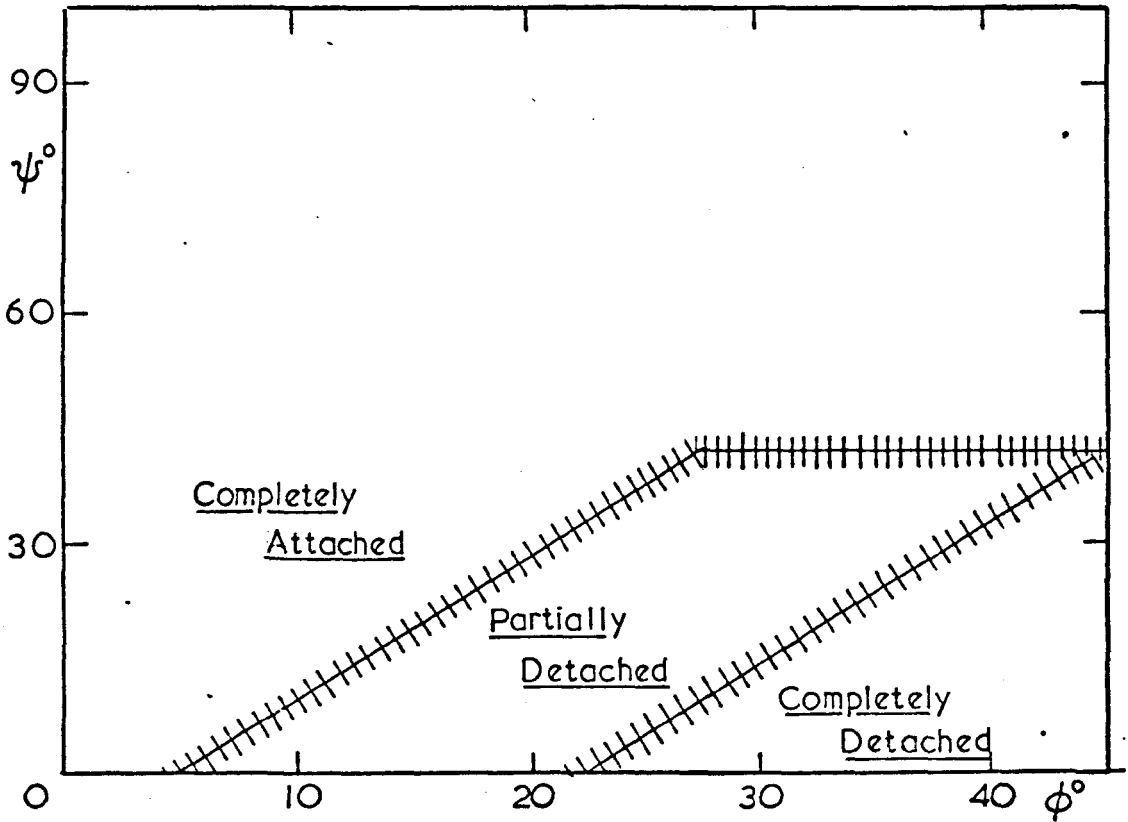
FIG.4.4.b DIFFUSER FLOW REGIMES

LIEPE (1960)

breakdown phenomena.

These are as follows:

Regime 1, flow is a laminar one-celled vortex

Regime 2, represents the transition of a one-celled vortex from
laminar to turbulent flow and is characterised by the
formation of a bubble along the axis.

Regime 3, flow is a turbulent one-celled vortex.

Regime 4, the other transitional phenomenon characterised by the
breakdown of a one-celled vortex to a two-celled vortex.

Regime 5, flow is a turbulent two-celled vortex.

These experiments were based on an exponential type of
vortex distribution produced by guide vanes. It is important
that every effort be made to discuss the effect of swirl on
performance and flow regimes, in isolation, since it is well known
that this parameter is the dominant one, e.g. the effect of swirl
number with low Reynolds number flows and also that with high
Reynolds number flows. So however, has not differentiated between
effects of Reynolds numbers and swirl numbers. According to him,
if either the flow rate or the blade angle or both are large, then
the flow is one possessing strong swirl. The above flow regimes
are for weak, medium and strong swirl in So's sense. In view of
this his conclusions must be interpreted with some caution.

Sarpkaya (1971) performed some very impressive
experiments on swirling flows in a conical diffuser. He used a
38 mm. throat diameter diffuser with a very small (3° total angle)
diffusing angle and furthermore flow was in the laminar range.
Guide vanes were used to generate swirl. Three types of breakdown

have been observed. viz., double helical, spiral and axisymmetric.

In the spiral breakdown, the rotation of the vortex core was of the same sense as the upstream fluid; contrary to the observations of Lambourne and Bryer. The type and shape of the forms depend on the combination of the Reynolds and circulation numbers. The axisymmetric breakdown evolves either from a double helical, or from a spiral or from an axisymmetric swelling of the core. The mode of evolution depends on the particular combination of Reynolds and Circulation numbers. In conclusion he proposes that the vortex breakdown phenomenon is governed by two basic and conceptually different mechanisms. Instability manifests itself more emphatically at low Reynolds numbers and high circulation numbers. The finite-transition-type of behaviour of the axisymmetric breakdown is brought out more clearly in an unsteady swirling flow; such as one created by perturbation of circulation.

In addition to their work on pipes and free jets with swirling flow Gore and Ranz investigated the flow in a diffuser. They summarise their conclusions as follows:

(i)   Axial backflow results from axial pressure gradients created when a rotating fluid moves through an increasing cross-section. When the critical swirl number is exceeded, a pattern of reverse flow replaces these pressure gradients.

(ii)   Backflows could be stopped at a stagnation point on the axis by controlling the distribution of axial velocities and pressure at some cross-section upstream.

The first of these conclusions must be interpreted with caution as it tends to limit flow reversal to expanding cross-sections. It is known that not only does flow reversal occur in diverging and constant cross-section but it does so even in converging cross-sections. This has been shown by Binnie, et al (1957) working with nozzles. He showed that at low swirl the flow was unstable and when the swirl was high enough to establish an air core, the flow stabilised. The reversal of flow does not replace the pressure gradients. As shown by Kirkpatrick (1964) pressure gradients are very much a part of flow reversal and are present even after reversal. It is however, true that it is the pressure gradients that cause flow reversal.

Diffuser research as a whole owes a lot to the school of research at Purdue University in Lafayette. A very comprehensive investigation of the effects of swirling inlet flow on pressure recovery in conical diffusers was conducted by McDonald, Fox and van Dewoestine (1971). No less than twenty-four diffusers with various included angles up to a maximum of 32° were used. The maximum area ratio was 8.27 and the maximum length was 10.65 throat diameters. The swirl generator consisted of a 6" i.d. and 15" long honeycomb driver on its outer periphery. The generator was driven at three fixed speeds of 160, 236 and 410 rev/min giving swirl angles of 9°, 13° and 22° respectively, swirl angle being defined as the ratio of tangential velocity to axial velocity. A nozzle was introduced at the outlet from the generator to accelerate the flow.

Performance maps have been provided to cover the range
of diffusers investigated. It is noted that for cases where there
was no wall separation, the presence of swirl did not improve the
performance. However, if wall separation was present in the absence
of swirl then the introduction of swirl did cause an improvement.
If swirl is increased in magnitude so as to give rise to vortex
breakdown, then the performance is seen to deteriorate.

It should be noted that in contrast to most other work in
this field solid body type rotation has been employed. In referring
to previous work, van Dewoestine makes a very noteworthy comment
regarding the work carried out by Peters. The flow system employed
by Peters consisted of a fixed swirl generator, then a variable
entry length, followed by the diffuser under test. The maximum
swirl was obtained with the shortest entry length. However, the
shortest entry length also produced the thinnest inlet boundary-
layer. Thus it is difficult to determine if the increase in
performance reported by Peters was due to increased swirl or to
decreased inlet boundary layer.

Fig. (4.5a) shows a performance plot for the 9° swirl
angle. The optimum line ɑ-ɑ drawn through points of infinite
gradient is a measure of the shortest diffuser length required,
for a given ratio, to obtain the best performance. The physical
diffuser dimensions required, for a specific swirl strength, to
obtain a given performance (in this case 0.70) is shown in Fig.
(4.5b). Finally Fig. (4.5c) is a comparison of lines of optimum
performance.
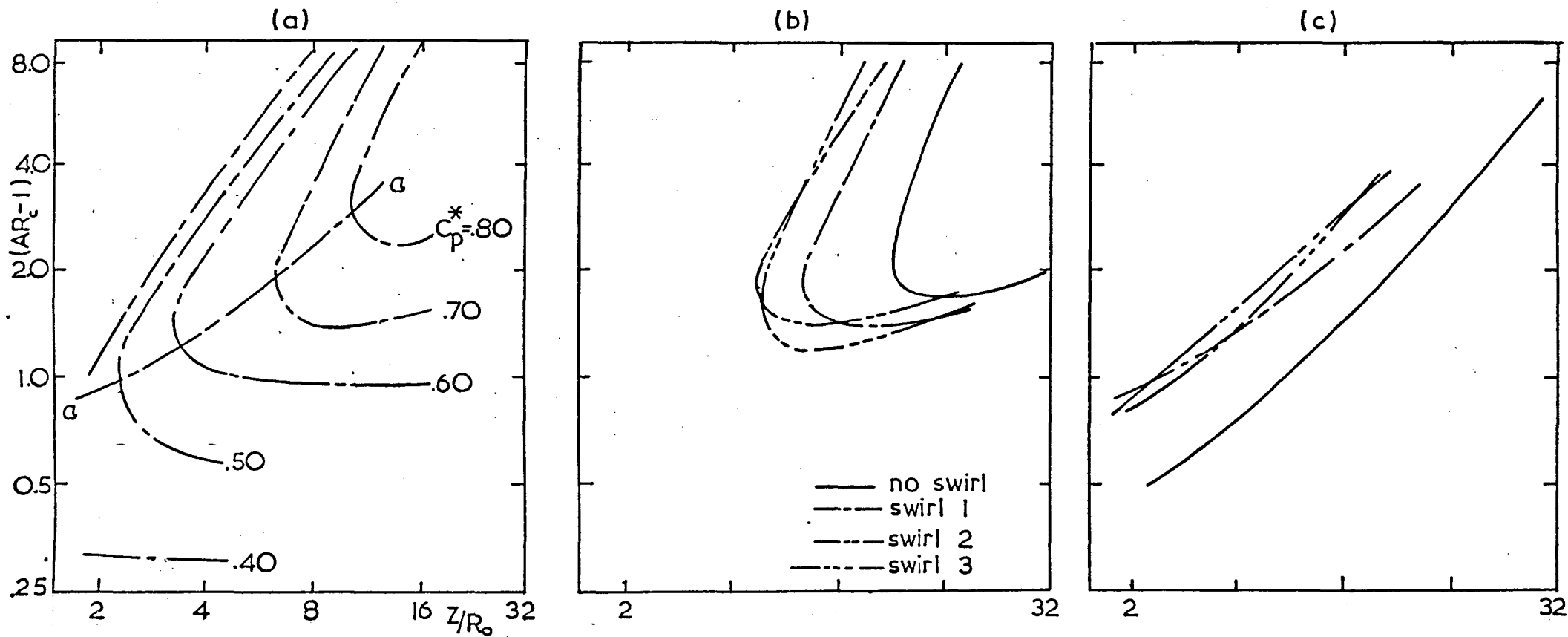
FIG.4.5 EFFECT OF SWIRL ON (a) DIFFUSER PERFORMANCE

(b) CONTOURS OF CONSTANT $c_p^* = 0.70$

(c) LINE OF OPTIMUM PERFORMANCE

FROM VAN DEWOESTINE (1969)

To determine the actual performance, Fig. (4.5a) (or any other similar plot) may be superimposed on Fig. (4.5c). It does seem at first sight that as the lines are extended towards the upper right quadrant (i.e. larger physical dimensions and higher swirl) performance tends to increase. However, it is well known that the triggering of vortex breakdown results in a reduction in performance.

4.3.3. Swirling Flow in Annular Diffusers

A limited amount of work has been done on the investigation of the effects of swirl on the performance of annular diffusers. It was believed at one time that with the use of an annular diffuser it may be possible to eliminate the breakdown in the central core region. Srinath (1968), using an annular diffuser with equal cone angles, has shown that a small amount of swirl does improve the performance. For the case under consideration, the optimum swirl angle was found to be equal to the diffuser cone angle.

In his experiments Hoadley (1970) measured pressures and velocities at a single Reynolds number ($\sim 10^6$) for three inlet swirl conditions. He had a converging section fitted to the exit of his diffuser which tends to inhibit separation and in fact promotes reattachment for already separated flows. For zero swirl occurrence of separation on the outer casing was observed while for higher inlet swirl separation was on the hub. For the largest inlet swirl the region of separation at the hub extends nearly to the diffuser exit.

Flow visualisation has shown that though swirl removes stall from the outer wall, even a small amount of swirl tends to cause stall at the inner wall. At high swirl however, severe backflow results at the inner wall analogous to vortex breakdown. As in the case when swirl is absent, the presence of a downstream tail-piece improves the performance. It is interesting to note that owing to the small width of the annulus, viscous forces tend to dominate, irrespective of the type of inlet vortex.

4.3.4   Swirling Free-Jets

Gore and Ranz (1964) studied swirling free jets as well. They found that, for a rigid body type vortex, a toroidal vortex was observed in the free jet. A balloon of the size of the backflow region was found to come to rest in this region and they claim that a considerable force was required to dislodge it.

Chigier and Chervinsky (1967), carried out a series of experiments in axisymmetric free turbulent jets with degrees of swirl covering weak, moderate and strong ranges, including the case of the onset of flow reversal. Mean velocity and pressure profiles are shown to be effectively similar up to four diameters downstream for weak and moderate swirl. For the case of strong swirl, a vortex is generated in the region close to the orifice resulting in a displacement of the maximum velocity away from the axis. Beyond ten diameters, the influence of the vortex motion becomes small and similarity profiles are described in terms of Gaussian error curves and third-order polynomials. For strong swirl, jet width and rate of entrainment are almost twice those for the non-swirling jet.

Good agreement is found between experimental results for decay of profiles and the values predicted by an approximate theory based on the integration of the Reynolds equation of motion. The tangential inflow and the axial inflow are varied independently to obtain the desired swirl.

The swirl parameter is defined as

$$S = \text{Angular Momentum}/(R \times \text{Axial Momentum})$$

$$= \tfrac{1}{2}\hat{G}/(1 - \tfrac{1}{4}\hat{G}^2)$$

where $\hat{G} = \hat{v} / \hat{u}$ at orifice

Axial momentum $= 2\pi\rho\int_{0}^{R} r(u^2 - v^2/2)\,dr = \dot{Q}\hat{u}(1 - \hat{G}^2/4)$

Angular momentum $= 2\pi\rho\int_{0}^{R} r^2 uv\,dr = \dot{Q}\hat{v}R/2$

4.4   CONCLUSIONS

The above discussion was meant to be informative rather than exhaustive in relation to the present project. A much more comprehensive survey is reported in Wirasinghe (1972).

In the early sixties it was thought that the spiral form developed as a consequence of the perturbation of the axisymmetric form. Later it was suggested that the spiral form manifests itself first and later transforms into the axisymmetric form under steady conditions. In addition to these two forms a double helical form, associated with laminar flow in a diffuser, was also observed. In one experiment the sense of rotation of the core was observed as being the same as, and in another as being opposite to, the rotation of the main flow.

The instability theory was also questioned when it was shown that not only was the phenomenon repeatable but that it was reversible too.

Flow reversal was readily associated with pressure gradients. At an upstream section the pressure is lower at the centre and higher near the wall. Downstream where viscous dissipation has weakened the swirl, pressure is relatively higher at the centre-line and lower at the wall. Thus decay of rotation gives rise to pressure gradients which, if of sufficient magnitude, drive secondary back-flows on the axis. However, this proposition too, as a complete explanation, is questionable as it has been shown that flow reversal exists with converging ducts as well.

It is seen that in conical diffusers, while the presence of swirl eliminates wall separation to improve performance, flow reversal at the centre is detrimental to performance. In annular diffusers separation at the hub has a similar effect.

The above discussion clearly indicates the care needed and the difficulties associated with swirling flow experiments. Various views, ably supported by visual observation and photographs, have been proposed to explain the phenomenon of vortex breakdown. Confusion still exists as to its cause, its form and the conditions under which it prevails.

CHAPTER FIVE

THEORETICAL ANALYSIS OF SWIRLING FLOW

5.1   INTRODUCTION

Within the area of interest, where axial and radial
decay of swirling flow are considered, the work of previous
researchers may be divided into three broad groups. Each group
employs a different physical configuration and consequently has
differing boundary conditions.

These groups are,

1.   Swirling Jets; Unbounded flow-field where excess

     pressures and velocities tend to zero as radius tends

     to infinity.

2.   Swirling Flow in Diffusers; (The pipe being considered

     as the special case of a diffuser with zero divergence

     angle). The existence of a wall boundary layer

     associated with the potential core causes additional

     complications.

3.   Swirling Flow in Annular Ducts; If the annulus is

     small compared with the diameter of the duct the entire

     flow may be considered as being composed of the

     boundary-layer.

The flow in the above groups may be one of three types:
Subcritical, critical or supercritical.

The flow is said to be 'critical' when breakdown occurs.
It must be emphasised that criticality occurs within a band and,
as will be seen from the ensuing discussion, is influenced by
various parameters.

The 'magnetic' appeal of critical flow with its breakdown phenomenon and associated bubble formation has attracted many applied mathematicians. Various theories were proposed to explain the phenomenon in the light of the scant experimental evidence available. Researchers are almost wholly dependent on experimental information to formulate, solve and verify their mathematical models. Interest in swirling flows still being at its infancy, there is a scarcity of experimental information, and in this respect diffuser studies suffer most. As far as the author is aware only Liepe (1963), So (1967) and Van Dewoestine (1969) have provided information on vortex decay in a conical diffuser.

Mathematical models have been formulated and solved to investigate various types of flow situations. Most of these have used numerical or series type solutions. Quite often there is no other alternative but to employ such techniques though they do not offer any intermediate information nor display the relevance of the various parameters. Hence wherever possible attempts must be made to obtain an explicit solution.

In this chapter relevant mathematical models proposed to analyse some of the above combinations are discussed. The governing equations of motion are solved in an attempt to investigate the influence of dominant parameters.

5.2 SURVEY OF PREDICTION METHODS

Most of the prediction methods proposed have attempted to predict the occurrence of vortex breakdown. Only a few have attempted to study decay of swirl, in its own right, in the absence of breakdown.

The problem of the laminar swirling jet was attacked by Loitsianski (1953). It is interesting to note that it was around this time that the breakdown phenomenon was first observed though it seems that he was not aware of it. The Navier-Stokes' equations were solved in conjunction with two integral equations. i.e. for angular momentum

$$2\pi\rho\int_0^\infty vur^2 dr = L_0$$

and for axial momentum

$$2\pi\int_0^\infty (p + \rho u^2) r\, dr = K_0$$

The independent variable $\eta = r/z\sqrt{\nu}$ was introduced. With a view to obtaining the asymptotic expansions of velocities and pressures, the stream-function was sought in the new variable in the form

$$\psi = \nu(\bar{a}z + a_0 + a_1/z + a_2/z^2 + \text{-----})$$

The tangential velocity and pressure were written as,

$$v = b_1/z + b_2/z^2 + \text{-----}$$

and

$$p/\rho = c_1/z + c_2/z^2 + \text{--------}$$

where a, b, c are all unknown functions of η.

The solution technique is standard but tends to be laborious. At one stage appeal is made to experimental data to evaluate a constant associated with the tangential velocity profile. Loitsianski evaluated only the first two terms of the expansion; however additional terms were required to obtain any meaningful results. Later Falkovich (1967) and then Falkovich and Korobko (1969) obtained the next two terms of the expansion.

The expressions obtained are awkward to handle. For example, the axial velocity is given by

$$u = 2a^2/p^2 \cdot 1/z - \beta a^2/2 \cdot (1-3q/4)/p^2 \cdot 1/z^2 + [\gamma/6a^2(5-9q/4)/p +$$
$$+ q/8(1-2q-3q^2/16)/p^4] \cdot 1/z^3 + [-\beta\gamma/8a^2p^4(5-5q-3q^2/16) -$$
$$- \beta^3 a^2/192 p^5(5-73q/4+127q^2/16+13q^3/16 - 12p^3\ln(p)) +$$
$$+ \delta a^2/2 p^3(1-19q/4+12p\ln(p))] \cdot 1/z^4$$

where $p = 1 + a^2\eta^2$ and a, β, γ, δ are related to the constants L_0, K_0 and M_0

Falkovich points out that while at least the first four terms are required to obtain any realistic profiles, at least another two terms are required to investigate the breakdown region. The time lapse, a total of about sixteen years, between the formulation of the problem and the obtaining of any useful results, and the form of the expressions obtained reflect the mammoth task involved.

Squire (1960) considered an inviscid flow model and supposed that the cylindrical vortex has superposed on it a steady disturbance of small amplitude. He showed that very long waves may be present when the critical swirl angle is exceeded. The equation of motion for an axisymmetric flow has been reduced to

$$D^2\Psi = -K(dK/d\Psi) + (r^2/\rho)(dR_0/d\Psi)$$

The total pressure R_0 and the circulation $K/2\pi$ remain constant along any stream tube. The above equation has been solved for three types of tangential velocity distributions and the critical swirl angle obtained in each case. The three

distributions were the ideal forced and free vortex combination, the Rankine vortex and a hyperbolic vortex specially constructed to obtain an explicit solution. The critical swirl angles for the cases were 50.2^O, 45° and 49.3^O respectively.

These predictions of Squire have been the basis for design of most experimental apparatus for the investigation of the vortex breakdown phenomenon.

Benjamin (1962, 1965) proposed that the vortex breakdown phenomenon is a finite transition between two conjugate flows analogous to the "hydraulic jump" phenomenon in open channel flow. Two states of flow are defined, based on $N = \frac{u}{C}$ where C is the speed of longitudinal waves relative to u.

If $N > 1$ flow is said to be supercritical and if $N < 1$ it is said to be subcritical. The existence of these two types is shown most elegantly with the aid of variational calculus. The conservation of stagnation pressure and circulation is shown. The flow force S (or momentum flux) is defined as the sum of total axial momentum and pressure force, and supercritical flow possesses a higher S;

$$S = 2\pi \int_o^R (\rho u^2 + p) r \, dr$$

It is shown from a perturbation analysis that the superposition of an infinitesimal axisymmetric standing wave on a cylindrical vortex causes a reduction of flow force by an amount which is the wave resistance. Benjamin's theory is supported by Harvey's experimental work.

Bossel (1968) using a highly simplified model considered equations of continuity, centrifugal balance and conservation of axial and angular momentum.

He showed that if the initial axial velocity disturbance in the
core of a vortex is decelerating, then further deceleration and
eventual stagnation will result if the maximum swirl parameter

$\hat{v}/\hat{u}$ is greater than $2^{1/2}$, (i.e. $\hat{\psi}_* = 54.8°$).

Lavan, et. al. (1969) developed a linearised analytical
solution valid for small Re_d and swirl number, and extended this
to a wider range of Re_d and swirl numbers by numerically solving
the angular momentum and velocity transport equations. The
combinations of Re_d and swirl numbers for incipient flow reversal
are predicted. Cases of decay and growth of vortex are considered
and in both cases "no-slip" conditions have been applied. Decaying
swirl changes the axial velocity profile from a parabolic curve to
one with zero velocity on the axis; when the swirl vanishes, the
parabolic profile is returned. Decay of swirl is accompanied by an
increase of pressure along the axis and a decrease along the wall.
The stagnation point moves upstream with increasing Re_d. Flow
reversal was also displayed with increasing swirl numbers. The
opposite of the above pressure effect is associated with growing
swirl. Further calculations show that flow reversal is present at
the wall for higher swirl numbers. Solid body type rotation has
been considered in both cases and in the former it is achieved in
only three diameters on the axis downstream.

Chow (1969) studied swirling flow in tubes of non-uniform
cross-sections. He solved the governing equations derived by Long
(1953), so as to study this behaviour. It has been shown that in
contrast with the explanation of Nissan and Bresan, secondary flows
are possible in an inviscid swirling flow.

Bossel (1969) this time reduced the Navier-Stokes equations, for the whole flow field, into three different approximate systems, in four distinct regions of vortex flow having large swirl. His interpretations of the solutions of the equations may be summarised as follows

(a)   Swirl is the primary variable and breakdown will not occur at low swirl.

(b)   An adverse pressure gradient can precipitate a vortex breakdown, which would otherwise not have occurred.

(c)   The phenomenon is basically inviscid and Re_d number effects are almost non-existent.

(d)   Influence of downstream disturbances is pronounced. Upstream decay of disturbances decreases with increasing swirl.

(e)   Rotation inside the bubble may be reversed.

He concludes that vortex breakdown is fully explainable and describable by supercritical solutions to the inviscid equations, to which the Navier-Stokes equations approximate in the breakdown region, and that neither the finite transition theory of Benjamin nor the hydrodynamic instability theory of Jones and later Ludweig (1964) appears to be justified.

Sarpkaya (1971) points out that Bossel's predicted swirl velocities are not comparable with those of either Harvey or his own at the corresponding points. Also in most of the observations made so far, the bubble is not closed completely, while those predicted by Bossel's theory are closed.

Furthermore, the shape of Bossel's bubble remains the same, though the size is variable.

Pedley (1969) investigated the instability of viscous flow in a rapidly rotating pipe. It is interesting to note that for large swirl his flow is unstable if $Re_d > 82.9$. He explains his surprising result by saying that contrary to the wide-spread belief that rotation always has a stabilising effect, in his case it has a destabilising effect. The form of instability found is that of spiral disturbances with a rotation opposite in sense to the bulk flow. His statement and the one made by Bossel are both supported by the observations of Lambourne and Bryer.

Wygnanski (1970) obtained a similarity solution for the complete Navier-Stokes equations describing the flow of an incompressible laminar swirling jet. The solution shows the effect of swirl on the velocity components and is valid at all swirl angles. This non-perturbation type solution shows that the incompressible swirling jet depends on the linear and angular momentum and the wall boundary conditions. This is so because the radial pressure gradient when integrated over the surface contributes to the linear momentum of the jet. William and Hori (1970) studied the formation of hydraulic jumps in Meteorology and Oceanography. They show that in rotating systems, jump cases and non-jump cases are separated by the critical case for which the Froude number is equal to the square of the Rossby number multiplied by a constant.

Further to his previous work Bossel (1971) presents yet another proposition for vortex computation, this time by a method of weighted residuals using exponentials.

The method approximates the axial velocity and circulation profiles to a series of exponentials. Initially, uniform axial flow leading edge and trailing edge vortices are considered. They confirm the existence of two particular critical swirl parameter values: i.e. S_0, which separates vortex flow which decays smoothly from vortex flows which eventually break down and S_1, the first singularity of the quasi-cylindrical system at which point physical vortex breakdown is thought to occur.

So (1967) analysed the decay of a vortex on the basis of a very simple model. An axisymmetric case with negligible radial velocity and boundary layer effects, and constant viscosity has been examined. To be consistent with his experimental results he expressed the velocity profiles as follows:

for $0 < r < r_c$

$$v = F_2 \qquad u = \hat{u} F_1 + u_c(1 - F_1)$$

for $r_c < r < R$

$$v = k/r \qquad u = \hat{u} F_3$$

where

$$F_1(z,r) = (1 - Cos(\pi r/r_c))/2$$

$$F_2(z,r) = k/r_c \cdot Sin(\pi/2 \cdot r/r_c)$$

$$F_3(z,r) = Cos[\pi/2 \cdot (r - r_c)/(R - r_c)]$$

The model contains four unknowns, namely, u, u_c, r_c and p and the choice of equations are continuity, axial momentum, angular momentum and moment of axial momentum. By substituting the expressions into the equations a set of four simultaneous linear differential equations have been obtained, which have been solved using the Runge-Kutta technique of integration. Agreement was found to be unsatisfactory.

The lack of sufficient knowledge of the structure of turbulent flow is offered by him as an explanation for the discrepancy. In the present author's view, another possible reason for the failure is So's assumption that at any one station the peaks of axial and tangential velocities occur at the same radius.

The mathamatical model used by Gore and Ranz (1964) considers an axisymmetric swirling jet having a conical boundary with a constant pressure distribution on the boundary. The usual assumptions are applied once again and viscosity is neglected. Agreement is not satisfactory as a result of the severe approximations made.

Chigier and Chervinski (1967) performed an order of magnitude analysis on the turbulent Navier-Stokes' equations applicable to a swirling jet. They succeeded in getting rid of all the perturbation terms finishing up with two equations which admit the conservation of axial momentum and angular momentum. From this stage they too resorted to experimental decay constants to solve the equations.

The equations governing laminar viscous swirling flow in an annular diffuser were solved numerically by Crane and Burley (1974). Their solution is influenced by the boundary condition at exit of the diffuser. This condition clearly depends on whether the flow exhausts into an infinite still medium, into a cylindrical tail pipe or into any other fluid handling system. Radially directed flow at the exit of the diffuser is considered; the nearest physical analogy to this being claimed to be that of 'free slip' guide vanes at the exit.

The above discussion indicates the complete absence
of an analytical solution of the governing equations of swirling
flow in a diffuser even for laminar flow. In the sections that
follow the governing equations of laminar swirling flow in a
conical diffuser are solved explicitly in an attempt to investigate
the influence of the geometry of the diffuser.

5.3   SOLUTION OF THE EQUATIONS OF MOTION FOR LAMINAR SWIRLING

FLOW IN A CONICAL DIFFUSER

5.3.1   Governing Equations

The Navier-Stokes' equations of motion for an
incompressible fluid with constant viscosity may be written as

$$D\tilde{V}/Dt = -\nabla P/\rho + \nu \nabla^2 \tilde{V} + F \qquad (5.3.1.1)$$

and the continuity equation is

$$\nabla.\tilde{V} = 0 \qquad (5.3.1.2)$$

The following assumptions are made:-

1. Steady flow with no body forces

2. Axisymmetric flow

3. Influence of boundary-layer is negligible.

Furthermore the various parameters are rendered non-dimensional as
follows:-

(a) length parameters are divided by throat radius; e.g.

$$\underline{r} = r/R_T$$

(b) velocities are divided by the bulk mean velocity at
throat; e.g. $\underline{v} = v/\bar{u}_T$

(c) $\underline{p} = p/\rho\bar{u}_T^2$ and $\underline{\nu} = \nu/R_T\bar{u}_T$

The modified forms of equations (5.3.1.1) and (5.3.1.2) are

$$\underline{w}[\underline{v}]_r + \underline{u}[\underline{v}]_z + \underline{w}\underline{v}/r = \nu\left\{[\underline{v}]_{rr} + [\underline{v}]_r + [\underline{v}]_{zz} - \underline{v}/r^2\right\}$$

$$\underline{w}[\underline{w}]_r + \underline{u}[\underline{w}]_z - \underline{v}/r = -[\underline{p}]_r + \nu\left\{[\underline{w}]_{rr} + [\underline{w}]_r/r - \underline{w}/r\right\} \qquad (5.3.1.3)$$

$$\underline{w}[\underline{u}]_r + \underline{u}[\underline{u}]_r = -[\underline{p}]_z + \left\{[\underline{u}]_{rr} + [\underline{u}]_r/r + [\underline{u}]_{zz}\right\}$$

and

$$[\underline{r}\,\underline{w}]_r/r + [\underline{u}]_z = 0 \qquad (5.3.1.4)$$

5.3.2   The Swirl Distribution

The fundamental vortex is of either free or forced type depending on the mode of generation. The existence of the singularity in the model of a free vortex precludes its occurrence in practice while a very good forced vortex may be produced. Whichever type of vortex is generated in a duct$\overset{it}{\wedge}$decays to a form composed of both types, generally referred to as a 'Rankine' vortex.

The mathematical representation of this has been derived from a heat conduction analogy (Prandtl). The exponential form of solution for the heat conduction on a flat plate from a hot body brought into contact for a moment is known. If, in the fluid analogy, the element of rotation is ω then its distribution at time t is

$$\omega = A/t \cdot \exp(-r^2/4\nu t)$$

Invoking Stokes' theorem, which states that the circulation around a circle of radius r is equal to double the surface integral of the element inside the circle, yields

$$\Gamma = 4\pi\int_0^r \omega r\, dr$$

$$= 8\pi\nu A[1 - \exp(-r/4\nu t)]$$

and the tangential velocity is

$$v = \Gamma/2\pi r = B/r.[1 - exp(-r^2/4\upsilon t)]$$ (5.3.2.1)

The decay factor $exp(-r^2/4\upsilon t)]$ is a constant

as long as $r^2/4\upsilon t$ remains constant. If at a given time

a particular radius, say the core radius (i.e. the radius

corresponding to peak tangential velocity) is considered, then

$$exp(-r^2/4\upsilon t) = exp(k)$$

or $r^2/4\upsilon t = 1/k$

Substituting into equation (5.3.2.1) yields

$$v = B/r.[1 - exp(-(r/r_c)^2/k)]$$ (5.3.2.2)

5.3.3   Decay of Swirl Intensity

In the fluid analogy where the flow is continuous,

time in equation (5.3.2.1) is replaced by the axial distance.

To investigate the properties of the linearly decaying vortex,

equation (5.3.2.2) is represented as

$$\underaccent{\sim}{v} = C/2\pi r [1 - exp(-C_2 r^2)]$$ (5.3.3.1)

Only the experimental data of So (1967) and Sarpkaya

(1971) were available to the present author to establish the

suitability of the exponential function for the entire flow.

Sarpkaya who worked in the laminar flow has not provided sufficient

profiles to determine the constants in equation (5.3.3.1). However

if Sarpkaya's tangential velocity profiles are compared with those

of So's, who worked in the turbulent range, it is seen that the

decay pattern in both cases is similar except that the latter

worked with a higher swirl ratio. Hence it was decided to use

So's data for the analysis in spite of the fact that they were

associated with turbulent flows.

The method of analysis and the curve fitting procedure are discussed in appendix (5/A). The suitability of this function for the diffuser and even for a pipe is borne out by Figs. (5.1) and (5.2). In addition to these, various other parameters were evaluated (table 5/I) and the conservation of angular momentum and mass flux are seen from Fig. (5.3).

It was shown in the sections that C_2 may be related to the core radius. Now it remains to investigate the behaviour of the core radius itself. It is seen from Fig. (5.4) that the divergence of the core is identical with the divergence of the diffuser. The variation of the constant C_1, as seen from Fig. (5.5) is within 10% of its mean. The inaccuracy incurred by assuming C_1 to be independent of axial distance seems quite small compared with the major simplifications that follow in the solution of the governing equations. The constant C_2 associated with the exponent shows a much wider variation with axial distance. As seen from Fig. (5.5) C_2 may be related to the core radius as

$$C_2 = 1/(k_1 r_c)^2 \qquad (5.3.3.2)$$

with

$$r_c = \phi z + k_2 \qquad (5.3.3.3)$$

where ϕ is in radians and $k_1 = 0.893$

$$k_2 = 0.260$$

Thus

$$\underline{v} = C_1/2\pi r .[1 - \exp(-(r/k_1 r_c)^2)] \qquad (5.3.3.4)$$

Furthermore conservation of angular momentum and mass flux are displayed in Fig. (5.3) within the accuracy of the data, the method of fit and numerical integration.
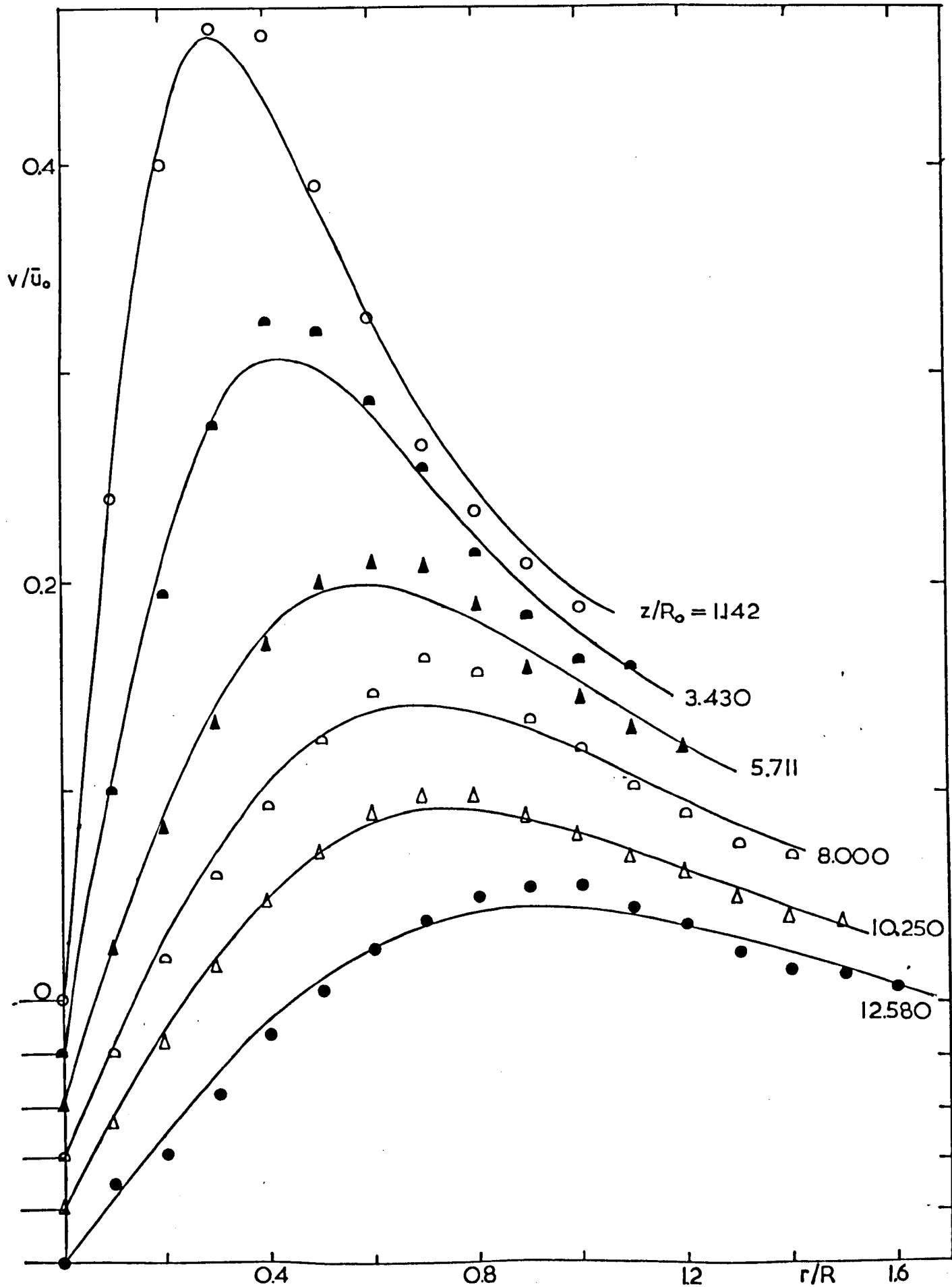
FIG. 5.1 COMPUTER FIT OF EXPONENTIAL FUNCTION
TO DIFFUSER DATA
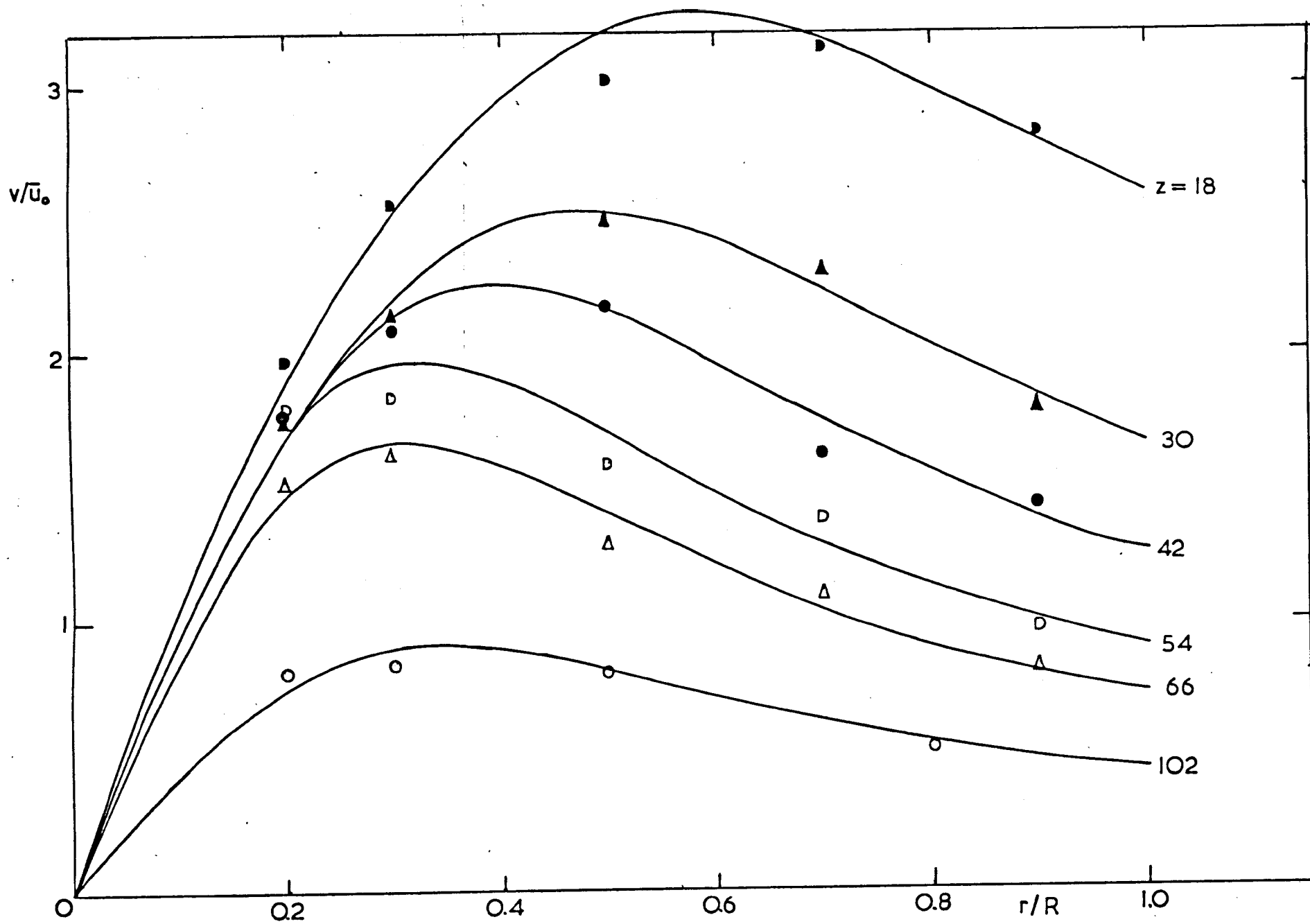
FIG. 5.2 COMPUTER FIT OF EXPONENTIAL FUNCTION TO PIPE DATA
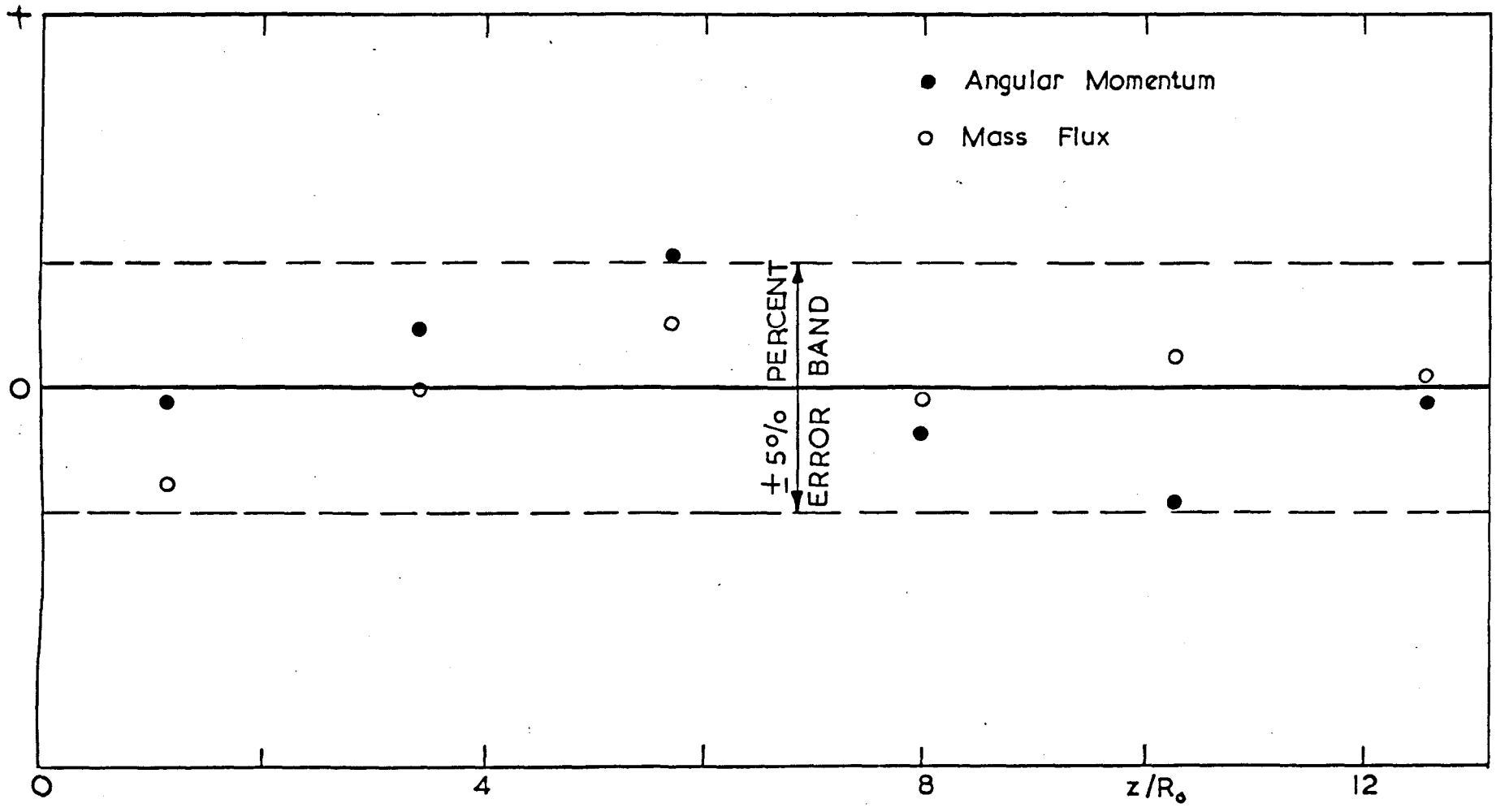
FIG. 5.3   VARIATION   OF   FLOW   PARAMETERS
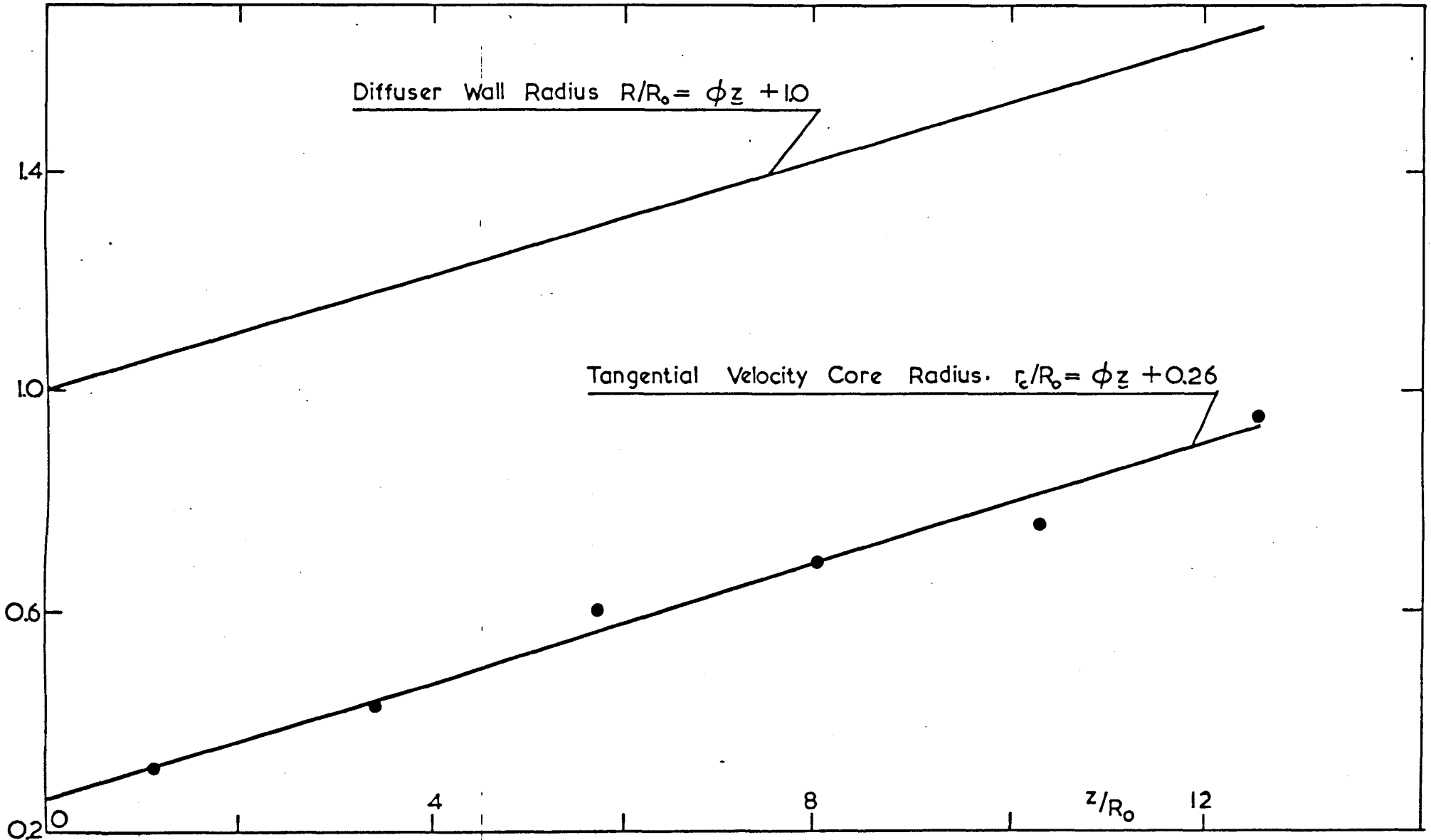
FIG. 5.4   DIVERGENCE   OF   CORE   RADIUS

Diffuser Wall Radius $R/R_o = \phi \underline{z} + 1.0$

Tangential Velocity Core Radius. $r_c/R_o = \phi \underline{z} + 0.26$

z/R_o
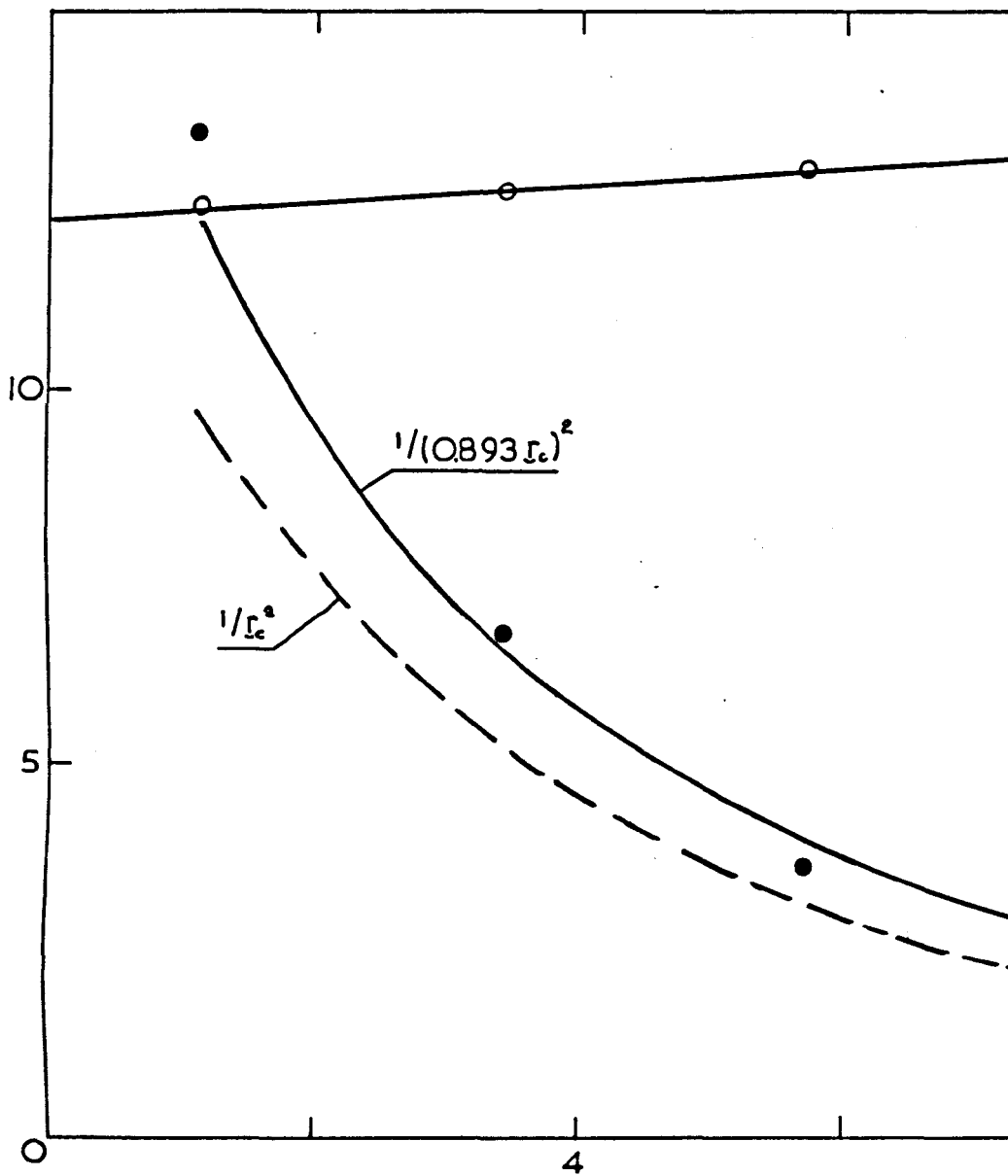
FIG.5.5   CONSTANTS   OF   TANGENTIAL

Constant $C_1 \times 10$
○

Constant C_2
●

z/R_0

8 · 12
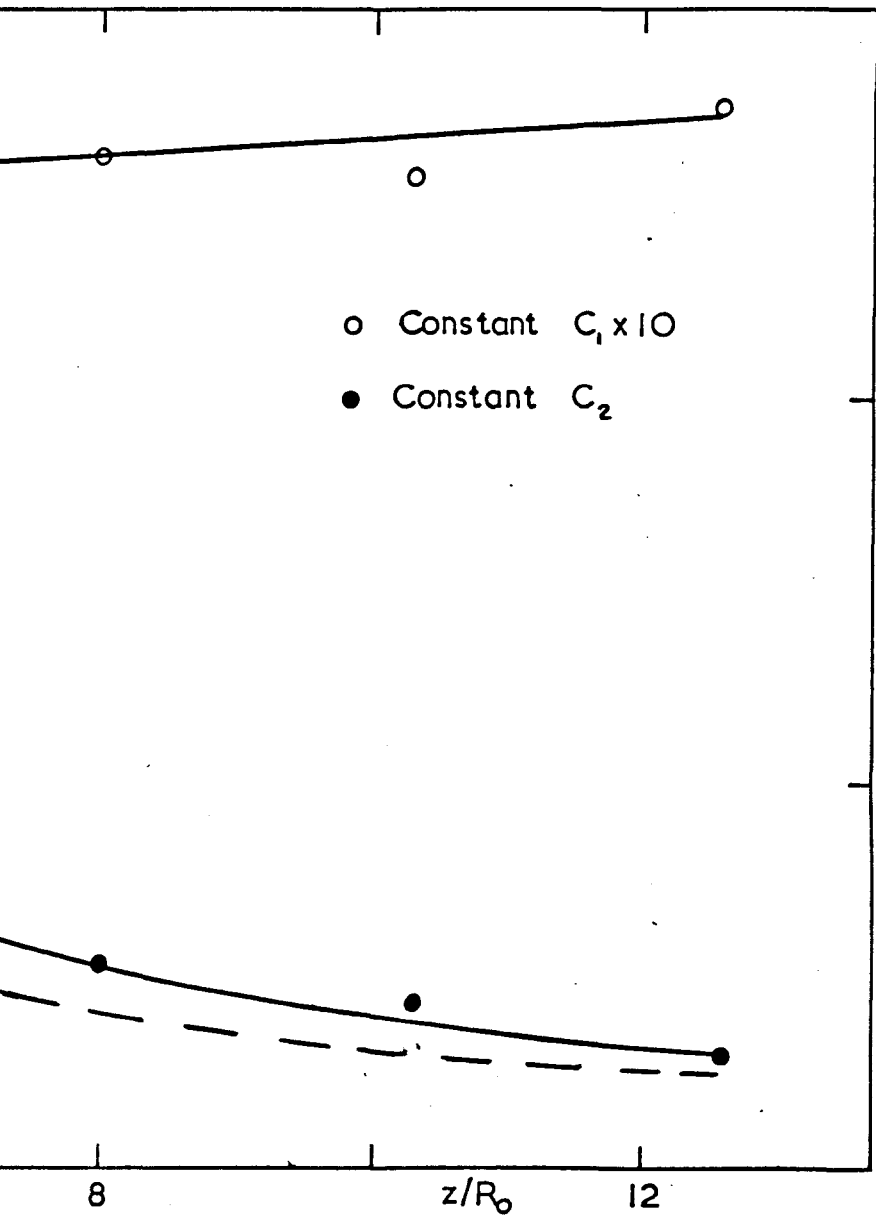
VELOCITY FUNCTION

Thus

$$\frac{\partial}{\partial z} \int_0^{R(z)} u \, v \, r \, dr = 0 \qquad (5.3.3.5)$$

and

$$\frac{\partial}{\partial z} \int_0^{R(z)} u \, r \, dr = 0 \qquad (5.3.3.6)$$

5.3.4   Method of Solution

In this section the 'seat' notation denoting the dimensionless forms will be omitted for convenience. Furthermore some of the more detailed mathematical work has been shifted to appendix (5/B)

Equation (5.3.3.4) may be written as

$$v = (1 - G) \, C_i / 2\pi r \qquad (5.3.4.1)$$

where $G = \exp(-\beta)$ and $\beta = (r/k_i r_c)^2$

and also equation (5.3.1.3a) as

$$p(r,z) w + q(r,z) u = v.\psi(r,z) \qquad (5.3.4.2)$$

where $p(r,z) = v/r + [v]_r$

$q(r,z) = [u]_z$

$\psi(r,z) = [v]_{rr} + [v]_r/r + [v]_{zz} - v/r^2$

Substituting for v from equation (5.3.4.1) into the above functions yields

$$p = C_i \beta G / \pi r^2$$

$$q = -C_i k \phi \beta^{3/2} G / \pi r^2$$

$$\psi = -2C_i k_i^2 \phi^2 \beta^2 G \left\{ \beta - [(3k_i^2 \phi^2 - 2)/2k_i^2 \phi^2] \right\} / \pi r^3$$

Eliminating u from equations (5.3.1.4) and (5.3.4.2) gives

$$[w]_r + L(r,z)[w]_z = M(r,z) + N(r,z)w \qquad (5.3.4.3)$$

where $L(r,z) = 1/k_i \phi \beta^{1/2}$ $N(r,z) = -2/r$

$M(r,z) = 2k_i^2 \phi^2 \beta v (3\beta - k_3)/r^2$

Equation (5.3.4.3) is a quasi-linear partial differential equation of the first order for which the solution is obtained by solving the Lagrangian equation

$$\frac{dr}{1} = \frac{dz}{L(r,z)} = \frac{dw}{M(r,z) + w \cdot N(r,z)} \qquad (5.3.4.4)$$

and obtaining the characteristics.

The characteristic C_{H_1} is given by

$$dr = dz/L(r,z)$$

But
$$L(r,z) = 1/k_1\phi\beta^{1/2} = (\phi z + k_2)/r\phi$$

Thus

$$\frac{dr}{r} = \frac{\phi\,dz}{\phi z + k_2} + C_{H_1}$$

from which

$$C_{H_1} = 0.5.\ln(\beta) \qquad (5.3.4.5)$$

To obtain C_{H_2}, consider

$$dr = dw/[M(r,z) + wN(r,z)] \qquad (5.3.4.6)$$

from which β must be eliminated using equation (5.3.4.5)

Substituting for β from equation (5.3.4.6) yields

$$M = 2k_1^2\phi^2 v.\exp(2C_{H_1})[3.\exp(2C_{H_1}) - k_3]/r^2$$

which when substituted into (5.3.4.6) and rearranged yields

$$[w]_r + 2w/r = 2k_1^2\phi^2 v\exp(2C_{H_1})[3\exp(2C_{H_1}) - k_3]/r^2$$

which is a linear differential equation of the first order and can be solved by using the integrating factor

$$I.F. = \int \exp(-2/r.dr) = r^2$$

Thus the solution is

$$r^2 w = \int M(r,z)r.dr + C_{H_2}$$

which on integrating and with $(\ln\beta)$ replacing $2C_{H_1}$ is

$$w = 2k_1^2\phi^2 v\beta(3\beta - k_3)/r + C_{H_2}/r^2 \qquad (5.3.4.7)$$

The boundary condition $w = 0$ at $r = 0$ yields

Also $[w]_r = 2k_1^2\phi^2 v \beta (9\beta - k_3)/r^2$

Substituting for w and $[w]_r$ in equation (5.3.1.4) yields

$$[u]_z = -4k_1^2\phi^2 v \beta (6\beta - k_3)/r^2$$

which gives

$$u = -4k_1^2\phi^2 v \left[\frac{6r^2}{k_1^4} \frac{dz}{(\phi z + k_2)^4} - \frac{k_3}{k_1^2} \frac{dz}{(\phi z + k_2)^2}\right] + C_4(r)$$

$$u = 4k_1\phi v \beta^{1/2}(2\beta - k_3)/r + C_4(r) \qquad (5.3.4.8)$$

As $z \rightarrow \infty$ the diffuser exit area tends to ∞ and hence

$$u \rightarrow 0 \quad ; \quad \therefore C_4(r) = 0$$

Expressions for all three velocity components are now available and reverting back to the non-dimensional notations, these are

$$\underline{u} = 4k_1\phi v \beta^{1/2}(2\beta - k_3)/\underline{r} \qquad (5.3.4.9a)$$

$$\underline{w} = 2k_1^2\phi^2 v \beta (3\beta - k_3)/\underline{r} \qquad (5.3.4.9b)$$

$$\underline{v} = C_1[1 - \exp(-\beta)]/2\pi\underline{r} \qquad (5.3.4.9c)$$

where

$$\beta = (\underline{r}/k_1\underline{r}_e)^2$$

$$k_3 = (3k_1^2\phi^2 - 2)/2k_1^2\phi^2$$

$$\underline{r}_e = \phi\underline{z} + k_2$$

with $k_1 = 0.893$, $k_2 = 0.260$ and ϕ being in radians.

5.3.5   The Static Pressure Distribution

The static pressure distribution may be calculated using equation (5.3.1.3b). It is seen from inspection that all terms containing $\underline{w}$ and $\underline{u}$ are of magnitude $\underline{v}^2$ and are negligible compared with $\underline{v}^2/\underline{r}$.

Thus the above equation reduces to

$$[p]_r = \underline{v}^2/\underline{r} \qquad (5.3.5.1)$$

On substituting for $\underline{v}$ it will be observed that the resulting equation is not integrable in its present form.

Using the series expansion of the exponent, equation (5.3.5.1) becomes

$$[p]_r = [1 - 2\sum_{n=0}^{\infty}(-1)^n(a\underline{r}^2)^n/n! + \sum_{n=0}^{\infty}(-1)^n(2a\underline{r}^2)^n/n!]C_1/4\pi\underline{r}^3$$

Since at $n = 0$ the first term in each series is unity this becomes

$$[p]_r = C_0\sum_{n=1}^{\infty}(-1)^n a^n \underline{r}^{n(2n-3)}(2^n - 2)/n! \qquad (5.3.5.2)$$

Also since at $n = 1$ the term $(2^n - 2)$ is zero the summation may be commenced from $n = 2$. Integrating equation (5.3.5.2) yields

$$\underline{p}(r,z) = C_5(z) + C_0\sum_{n=2}^{\infty}(-1)^n a^n \underline{r}^{n(2n-2)}(2^n - 2)/(2n-2)n! \qquad (5.3.5.3)$$

using the boundary condition at $\underline{r} = 0$

$$\underline{p}(0,z) = \underline{p}(z) = C_5(z)$$

In the extreme case about seventy terms need to be evaluated before the effect of the later terms may be neglected. In this respect $n!$ should not be evaluated separately as the magnitude of the numbers generated exceed the capacity of the computer. This can be overcome by evaluating $a^n/n!$ for a given n . Fig. (5.6) shows the calculated static pressure distribution.

5.3.6 Discussion of Solution

The validity of the above method cannot be checked immediately as there are no experimental data on laminar swirling flows available to the author.
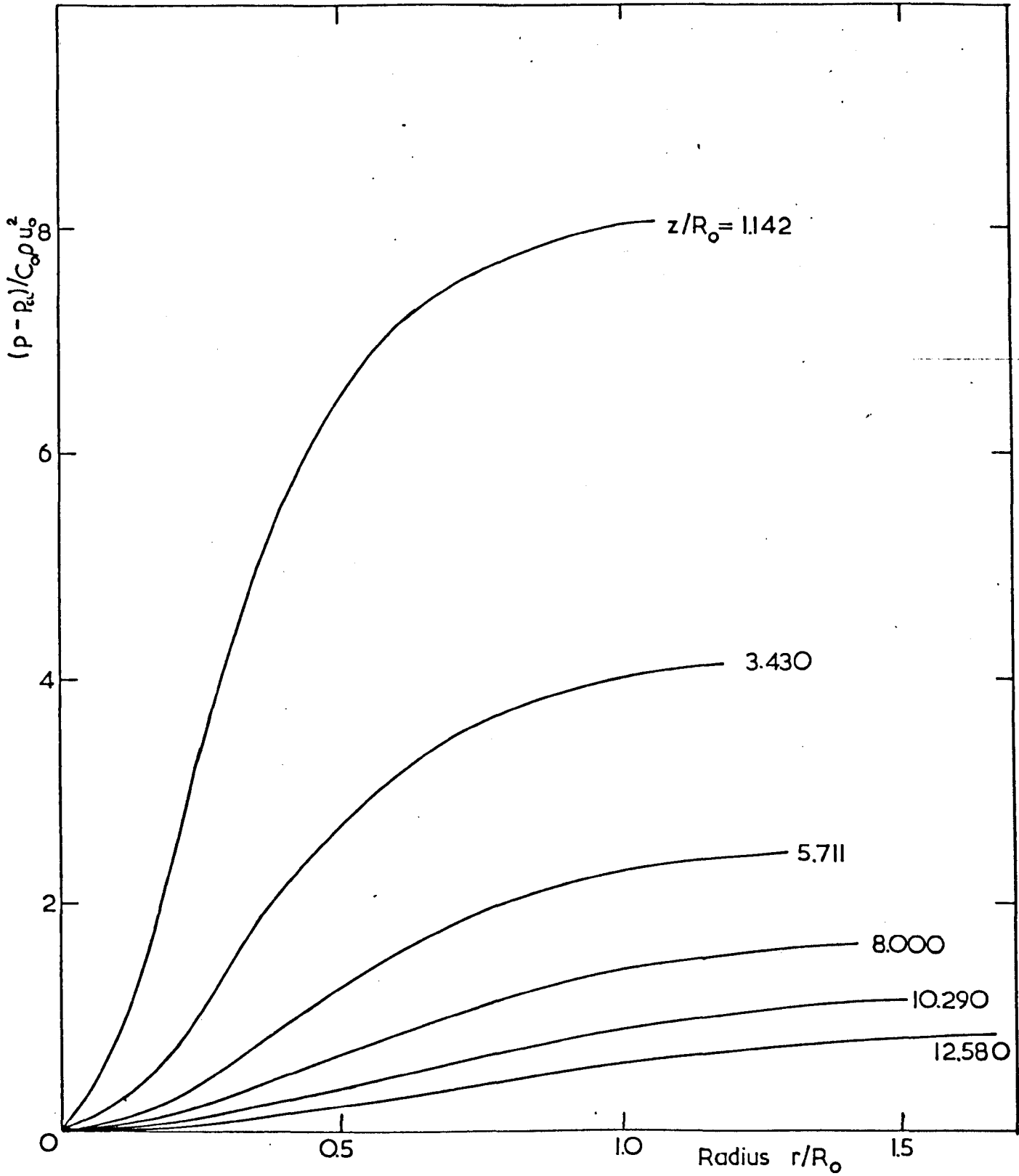
FIG. 5.6 COMPUTED STATIC PRESSURE DISTRIBUTION
IN DIFFUSER

The validity of the method of solution is confirmed by substituting equations (5.3.4.9) into equation (5.3.1.3a). The uniqueness of the solution is established by appealing to the uniqueness theorem which follows from Green's theorem, which states:

"If a function can be found which satisfies the partial differential equation and satisfies all the boundary conditions and does not contain any more arbitrary constants then the function is the only possible solution".

In his analysis of the laminar swirling jet Falkovich used the series expansion of the exponential function used in the present model. The author had hoped that the use of a turbulent velocity profile might obviate the need for the turbulent stress terms in the governing equations. The disagreement between the present laminar results and So's turbulent axial velocity profiles indicate this not to be the case.

5.4   CONCLUSIONS

A semi-empirical solution of the Navier-Stokes' equations applied to laminar swirling flow in a diffuser has been obtained. Resort was made to experimental results for obtaining the two constants which appear in the solution. Unfortunately, the only experimental profiles which were detailed enough for calculating the constants involved were for turbulent flow. However their form was very similar to some laminar-flow profiles, for tangential velocity components, given by Sarpkaya.

The solution for axial velocity u (equation (5.3.4.9)
gives a nearly uniform profile right up to the point where the
boundary layer (which has been ignored) would be present in
practice. This is because, in the bracketed term $(2\beta - k_3)$,
the constant k_3 so dominates the term 2β, which is radius-
dependent, that a plotted u profile appears as a horizontal line.
The present method fails to predict the centre-line dip in u
profile which normally accompanies swirling flow. This is a result
of an adverse pressure gradient situation which shows in Fig. (5.6).
At stations near the diffuser entry, static pressure on the axis
is very low compared with that at the wall whereas at stations near
the exit, the pressure is more uniform. In extreme cases of swirl,
this adverse pressure gradient is severe enough to give reversed
flow and vortex breakdown.

If the present model were extended to turbulent flow by
replacing v in equations (5.3.4.9) with ϵ, the kinematic eddy
viscosity suggested by Boussinesq, (Fig. (5.7)), a centre-line
dip would appear in the u plot because various researchers have
shown that the ratio ϵ/v decreases from a maximum value at the
half-radius position to an indeterminate low value on the axis.

The profiles obtained have been integrated to give mass
flux in the axial direction and angular momentum at each station
and these results have been plotted in Figs. (5.8) and (5.9). The
last three stations give remarkably uniform answers and each point
in the two figures has, therefore, been plotted as a percentage
error from the average value of the last three. Satisfaction of
continuity and constancy of angular momentum is clearly not as
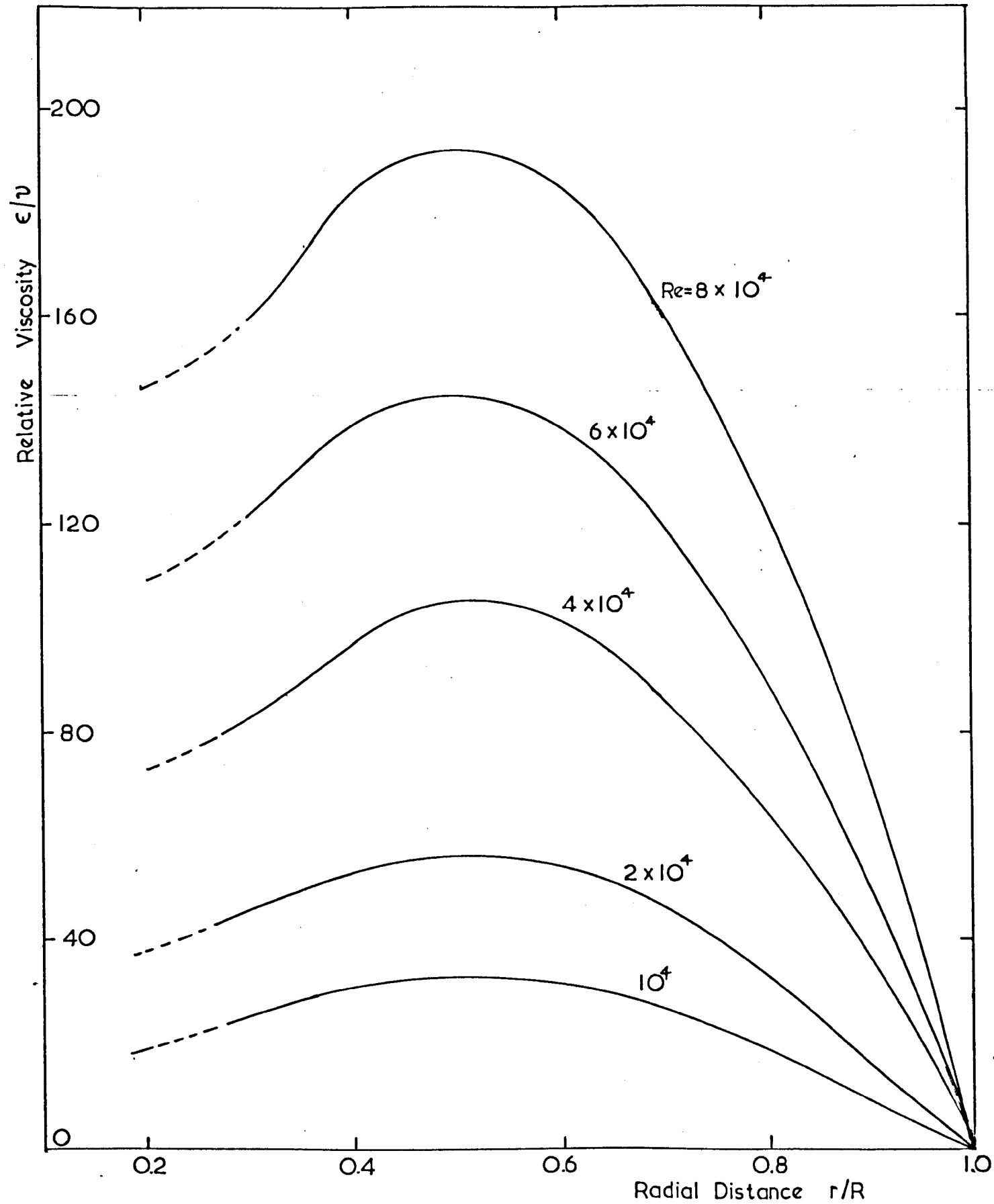
FIG. 5.7 VARIATION OF TURBULENT VISCOSITY IN
PIPE FLOW; SCHLINGER (1953)
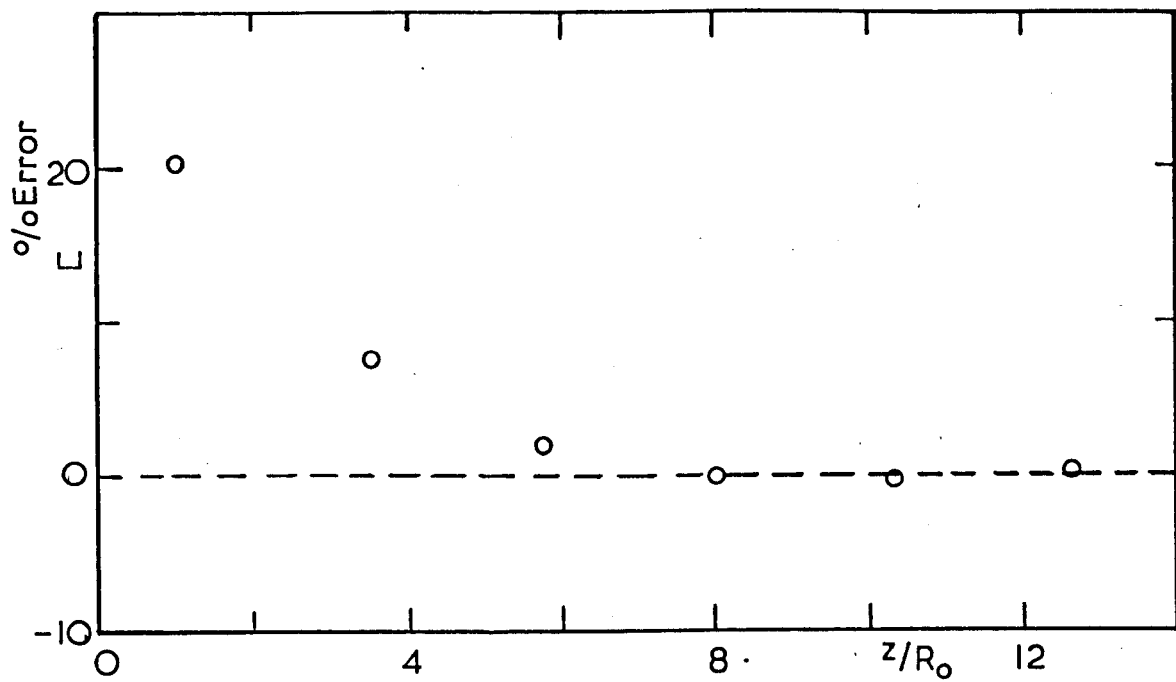
FIG. 5.8 THEORETICAL MASS FLUX
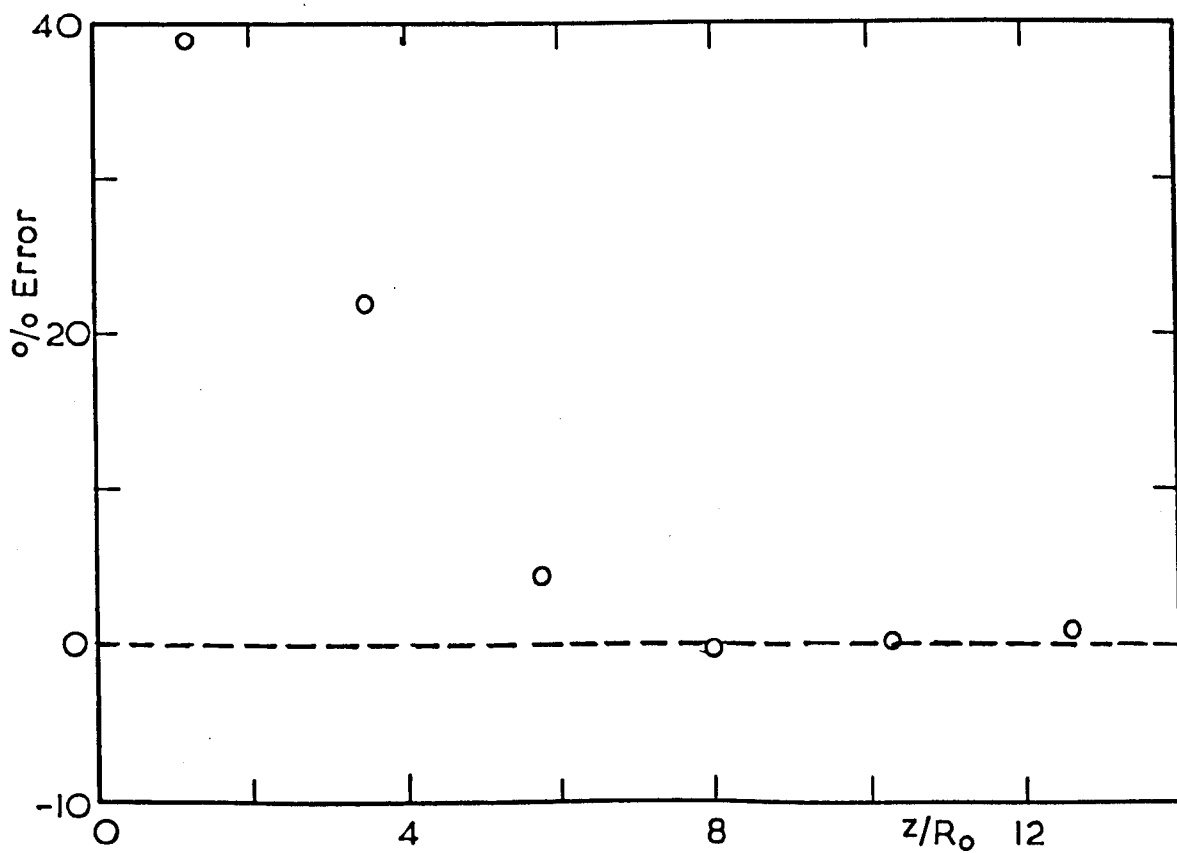
FIG. 5.9 THEORETICAL ANGULAR MOMENTUM

good for the first two stations as were the experimental results of So (Fig. (5.3)) which were used for finding the values of constants involved in the solutions. This almost certainly indicates that the y distribution in the vortex present in So's diffuser had not settled down to exponential form at these initial downstream stations. However, at subsequent stations the exponential form seems to be much more representative of the existing flow situation and satisfaction of the above two criteria is at least as good with the present method as with the experimental results.

The form of characteristic C_{H_1} in equation (5.3.4.5) suggests that some advantage would be gained from using β as a coordinate. This would be equivalent to working in conical coordinates since β is radius-dependent. It will be recalled that Loitsyanski used a radius-dependent variable also $(r/z\sqrt{v})$ and further work here may well prove valuable. It was shown that the vortex core divergence follows the diffuser wall. This needs further verification before it can be extended to other cases.

It is likely that the present method for solving the Navier-Stokes equations for a conical diffuser can be extended to turbulent flows provided sufficient information is available regarding the distribution of Reynolds stresses throughout the diffuser. The problems of accounting for boundary layers and vortex breakdown are more intractable but need to be given serious attention in the future.

CHAPTER SIX

EXPERIMENTAL EQUIPMENT

6.1   DESIGN CONSIDERATIONS

6.1.1.   Basic Requirements

As discussed earlier swirling flow phenomena have very wide
application and this project was seen as one that would lay the
foundation of a major research programme in this field at this
establishment. Thus it was necessary to design the test apparatus
to satisfy a more general requirement as opposed to the requirement
of the present project.

The basic question of which medium was to be used for
studies was influenced by several factors. If flow visualisation was
to be the major interest then water would be preferred. However, if
measurement was of primary interest, then air would be preferable as
liquids tend to be sluggish in response. Use of water would however
create sealing and corrosion problems which in this case were seen
as serious. Air would have been the obvious choice but for the need
to study the performance of diffusers with non-newtonian liquids.
Thus it was necessary to design a test-rig which could handle liquids
as well as air.

6.1.2   Scale and Flexibility of Test-Rig

A small scale test section is ideal from a photographic
point of view. In addition lighting problems are minimised when the
subject of interest is confined to a small area. In his photographic
studies Sarpkaya (1971) worked with a diffuser having a throat
diameter of 50.8 mm.

If it is intended to insert a probe into the flow-field then a much larger scale is necessary to minimise local interference to flow. It is recommended (B.S. 848) that the probe diameter be no more than 1/40 th of the duct diameter. In the light of the above considerations a compromise was arrived at giving a 90 mm. throat diameter and a 180 mm exit diameter.

The degree of flexibility will no doubt add to the complexity of the design. As a consequence of physical limitations flexibility is restricted to the following facilities.

1. The possibility of using air or water.

2. Diffusers with an area ratio of 4, throat diameter 90 mm. and cone angles varying from 0° - 30°, or pipes could be investigated.

3. Swirling and non-swirling studies could be conducted.

4. Flow visualisation and photographic studies are made possible by using a perspex test-section.

5. This also enables the use of a laser - velocimeter.

6. Provision has been made for the use of the five-hole spherical pitot-probe.

7. A probe traverse mechanism was designed to conduct detailed flow measurement.

8. Standard design features permit the use of a DISA anemometer in place of the pitot-probe.

9. Various types of swirl generators may be employed; (Rotating honeycomb, Rotating vanes, Fixed vanes or a Fluidic Vortex Amplifier).

10.   A wide range of Reynolds numbers and Rossby numbers are
      available.

11.   For use with air a separate fan and a bell-mouth entry
      section is available.

12.   The feed-back control system incorporated permits
      continuous increase or decrease of speed.

6.2   TEST-RIG

6.2.1   General Arrangement

A. Layout and Fabrication

The test-rig was built as a recirculating system in view of
the necessity to recover liquids other than water. A two-tier
(Fig. (6.1)) system was adopted as a space saving measure. The top-
tier, which is common to both air and water applications, is the
test-area. The entire test area was mounted on rails which provided
a horizontal reference. In addition each diffuser was dowelled at the
throat to ensure smooth entry. This when used with a thick 'pump'
grease eliminates the need for a gasket which may disturb the flow
at entry. Figs. (6.2, 6.3) show the entire arrangement quite clearly.
The metallic section handling water, which is the lower tier, was
first fabricated and then galvanised to prevent rusting before being
re-assembled. All other metallic areas including the reservoir were
painted on the inside with anti-corrosive paint.

B. Use with Water

In this mode the two tiers are connected by a T-piece with
one limb blanked off. At the discharge end a flexible hose was
connected to the T-piece. The further end of the hose discharges
into a narrow discharge tank which in turn feeds a reservoir-cum-
settling tank.

FIG.6.1 OVERALL DIMENSIONS OF TEST-RIG

discharge to tank

inlet from tank

pump

by-pass

test diffuser

horizontal rail

swirl generator

drive motor

tachogenerator

pump ₵

.28

throttle valve

extension to air intake

motor ₵

.66

1.32

GROUND LEVEL

orifice plate

.49

ALL DIMENSIONS ARE IN METRES
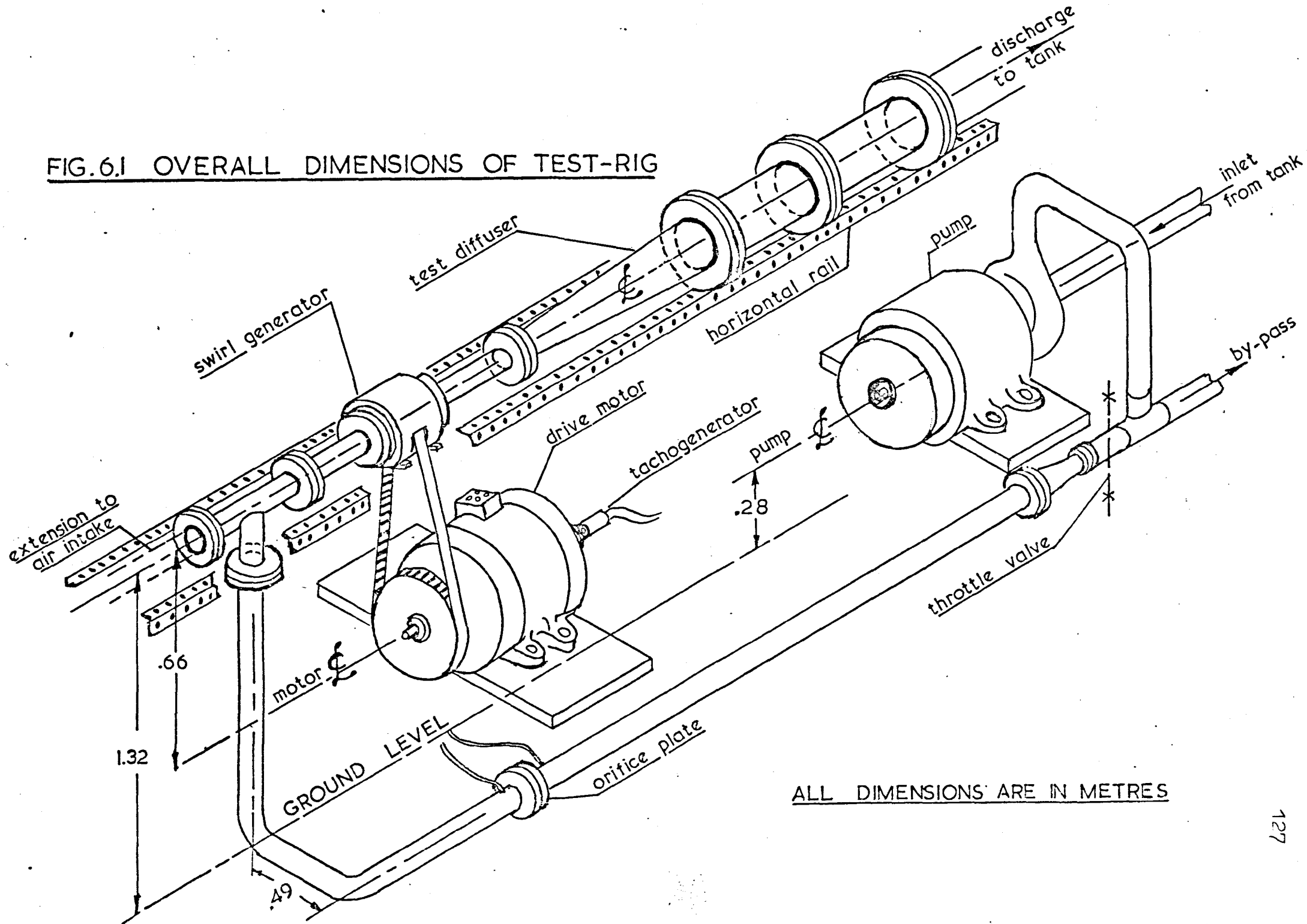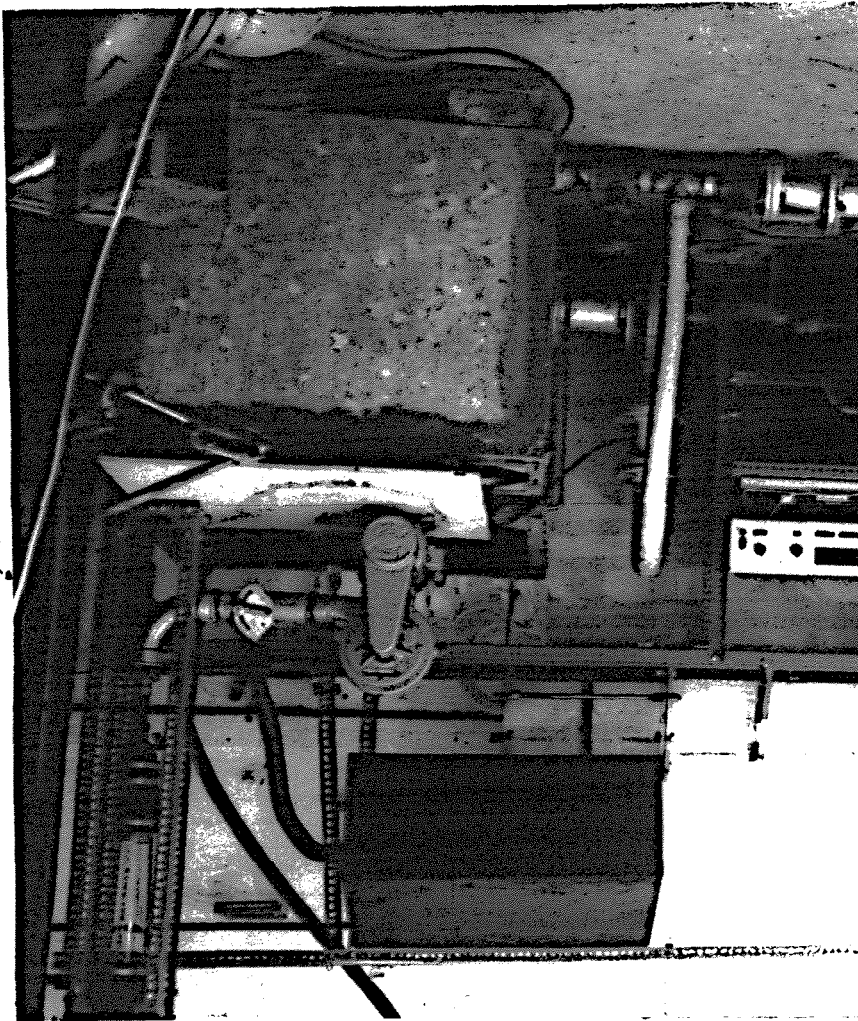
FIG 6.2 LAYOUT OF TEST
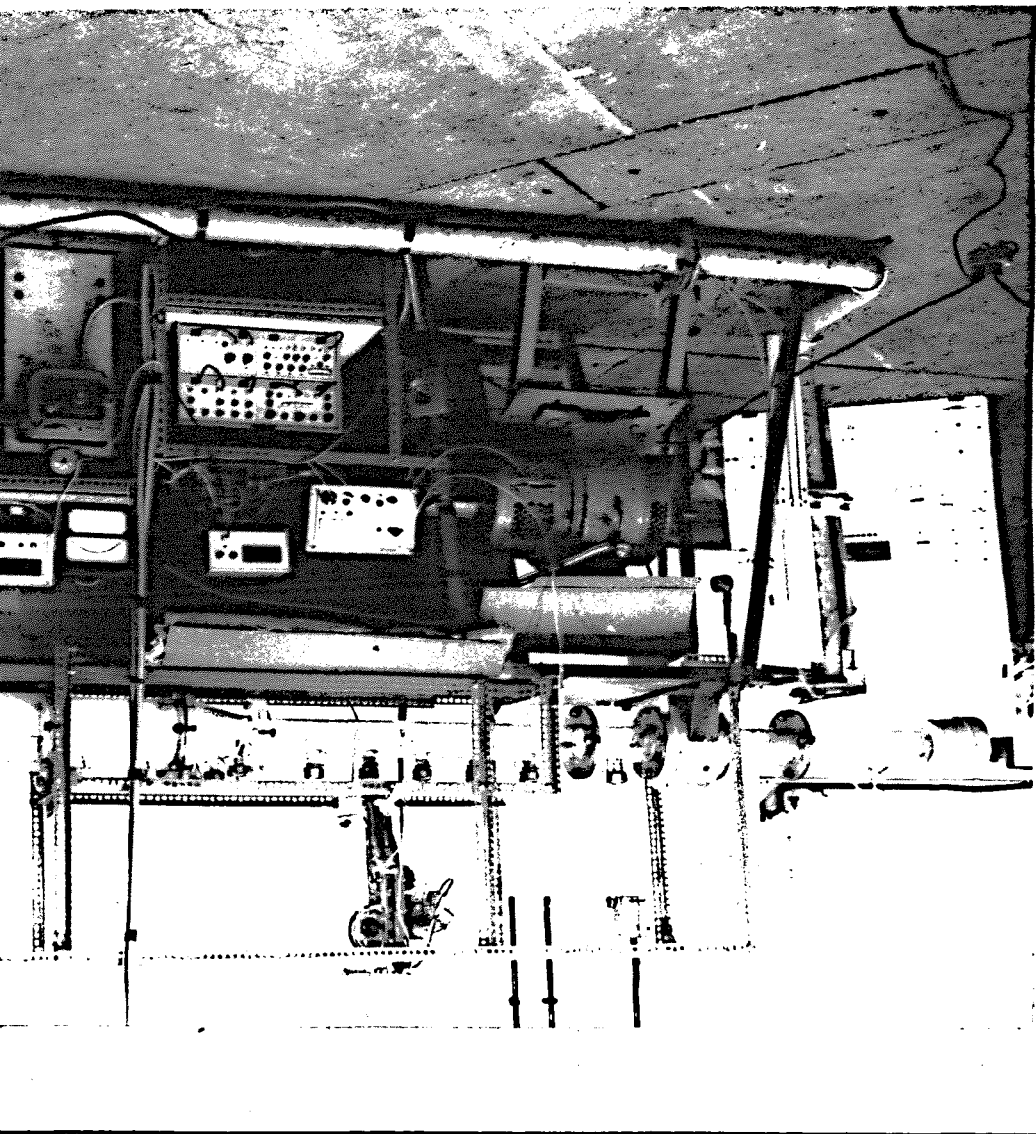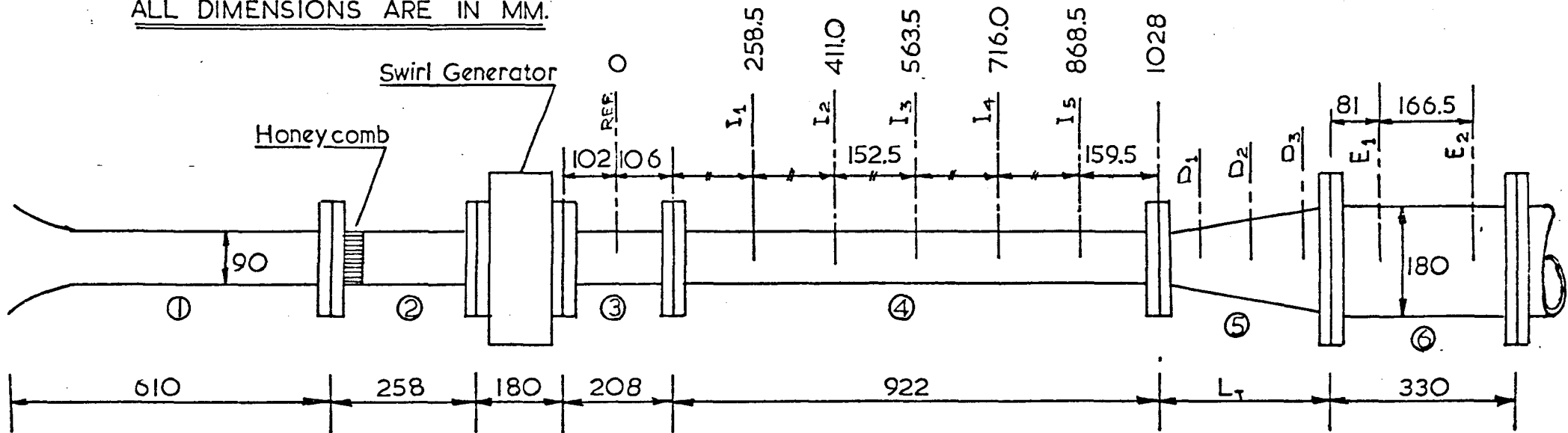
FIG. 6.2a MAIN DIMENSIONS OF TEST AREA

Micromanometer
(output to computing d.v.m.)

Moving-coil Voltmeter
(for Tachogenerator output)

Computing
Digital Voltmeter

DISA Anemo-
meter unit
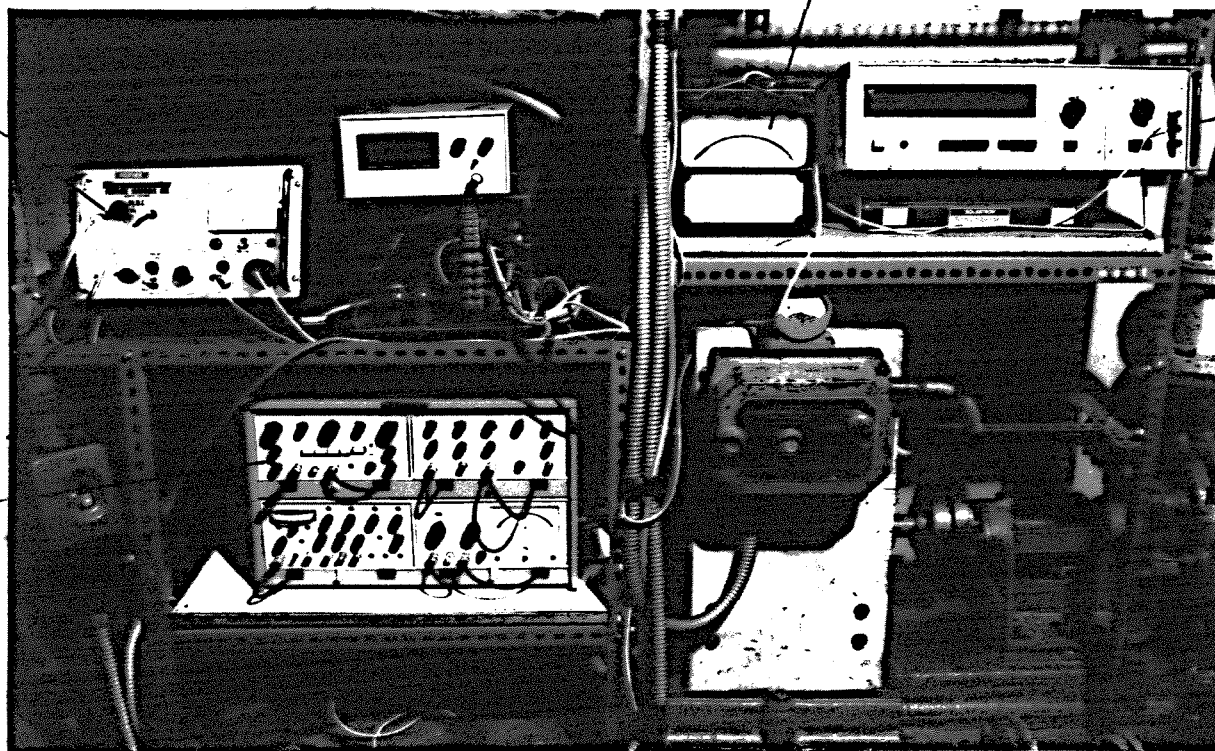
FIG. 6.3 RECORDING INSTRUMENTS USED FOR EXPERIMENTATION

The settling tank was fitted with baffles to break up trapped air and steady the flow at intake. Ideally a large reservoir is necessary to steady the vicious discharge from the main-line and the by-pass but the lack of space precludes such an arrangement. However a very calm state was obtained in the reservoir with the present arrangement and it occupied much less space.

Care must be exercised in judging the amount of water required in the reservoir. With its large intake the pump could empty the reservoir before the discharged water could get from the discharge tank into the reservoir settling area, through the baffles. The system is prone to overflow if too much water is held in the tank, primarily for the same reasons. It is suggested that half of the tank be filled up initially, with the throttle and the by-pass valves open. Now the pump should be started with the throttle valve just 'cracked' open and the discharge and by-pass valves fully open. The throttle valve may now be gradually opened to obtain the desired flow rate while filling the tank as and when required. The maximum static pressure in the system is laid down by the perspex test-sections and should be less than 5×10^5 N/M^2.

PUMP UNIT: GWYNNES CENTRIFUGAL PUMP : (FIG. (6.4)).

CROMPTON-PARKINSON MOTOR

3 Phase, 6 BHP, 1450 rpm.

C. Use with Air

This mode uses only the top-tier, with the upstream T-piece replaced by a bobbin with bell-mouth entry fitted to the up-stream end. At the discharge end, the hose is replaced by a settling chamber. The discharge to atmosphere is via an orifice-plate. The flow-rate is controlled with the aid of a butterfly valve.
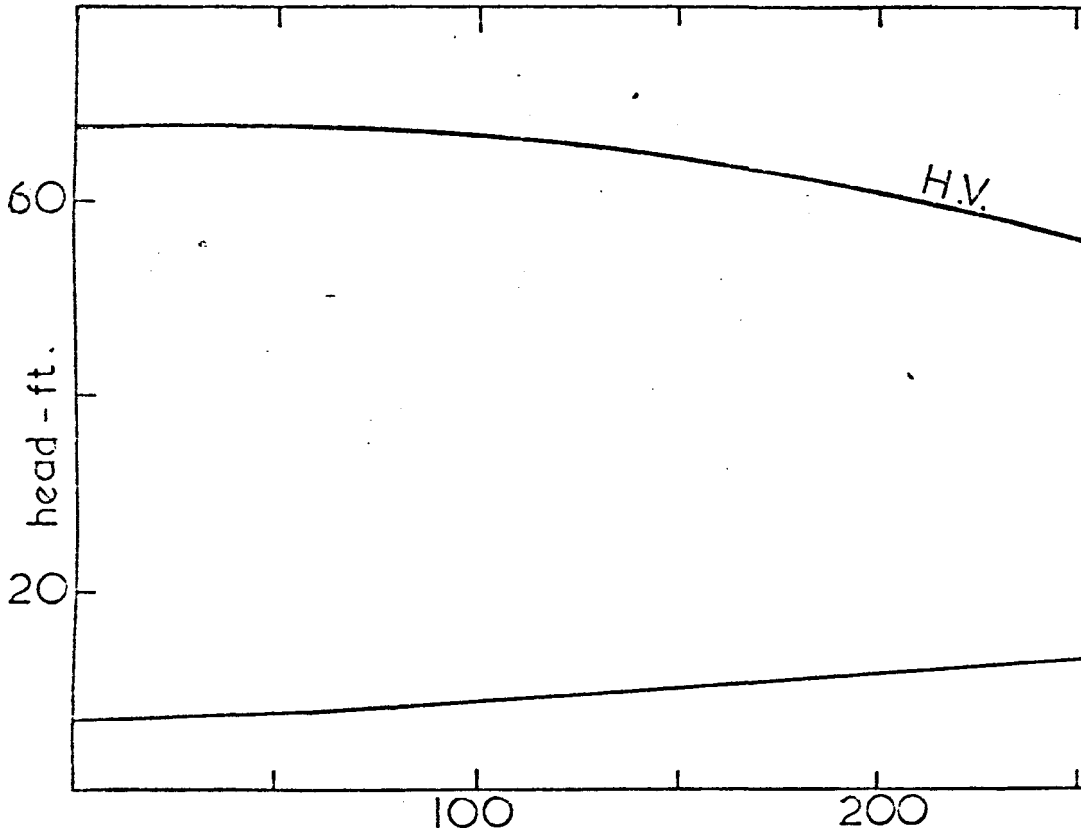
FIG. 6.4   GWYNNES CENTRIFUGAL PUMP
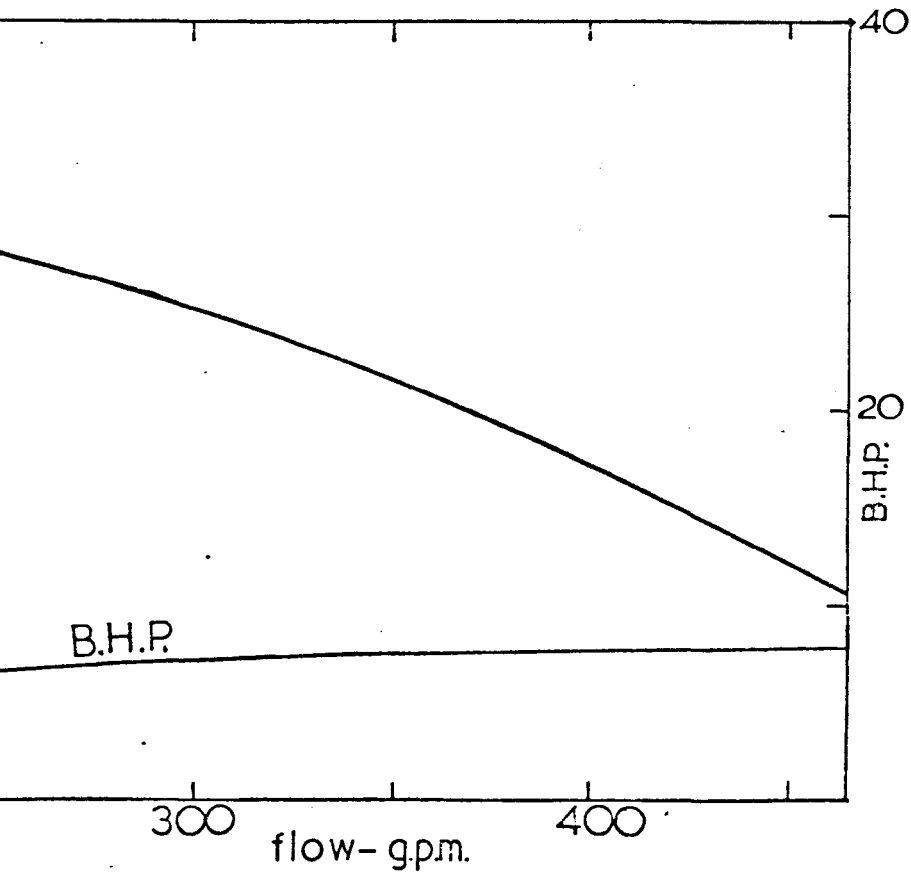
CHARACTERISTICS

FAN UNIT: SECOMACK MODEL 152

SERVICE ELECTRIC CO. MOTOR.

3 Phase, 1.25 HP, 2850 rpm

6.2.2   Swirl Generation

A. Types of Swirl Generators

Swirl may be generated by one of three fundamental methods.

1.   Tangential inlet: A single jet (Fluidic Vortex Amplifier) or a series of jets discharging tangentially, in conjunction with an axial flow to provide swirl.

2.   Fixed guide vanes: Fluid is fed radially through the vanes and enters the test section axially.

3.   Rotating guides: The fluid enters the generator with zero swirl velocity and is carried round by the generator which imparts swirl to the fluid.

As far as the performance of the diffuser is concerned, the type of generator only affects the type of inlet swirl. Fixed guide vanes have been used by Harvey (1962) and Sarpkaya (1971). Liepe (1961) used fixed vanes to produce a constant swirl angle in addition to working with solid body rotation.

Tangential inlet is at present being used at the University of Southampton. A rotating honeycomb was used by Van Dewoestine (1969) though only with air. It was decided to use a rotating honeycomb in this project with a control system to obtain fine control of rotational speed.

B.   Feasibility Study of an 'Isolated' Swirl Generator

Preliminary studies were conducted to investigate the possibility of designing a novel swirl generator. This was to take the form of a honeycomb inserted in the rotor of the motor.

Specialists were consulted and some exploratory calculations made.
It was decided that an induction motor would be required in view
of the stringent speed holding characteristics imposed by
experimental requirements. Calculations indicated that it would
be possible to accommodate such a device provided leakage of
water could be prevented. It was unfortunate that heavy sealing had
to be considered if leakage were not to be risked, which increased
the power requirements significantly. At a conservative estimate
the static friction associated with such sealing is about 5 N-M.

While the actual temperature rise in the water would be
small, in a recirculating system this would soon assume significant
proportions adding another variable parameter to an already
difficult problem. While the use of such a device in the present
arrangement is precluded by temperature considerations, this could
be used if a purely air application is envisaged.

C. 'Honeycomb' Swirl Generator and Drive Unit

The basic unit consists of a honeycomb, (2" long x ¼"
cell diameter) mounted on the same centre-line as the test-section,
driven by an external motor via a tooth belt drive. The rotating
unit of the swirl generator is placed between two stationary pipes
and fluid flows through the entire system. Fig. (6.5) shows the
main features of the generator. With the unit rotating at over
2000 rpm. sealing does become a major problem. This was resolved
by using GACO 'knife-edge type' spiro-seals with special pressure
plates. Owing to the presence of the bearings even a small leak
cannot be tolerated. The excess pressure imposed by the pressure
plates will no doubt reduce the life of the seals, and would require
changing.

Access for dismantling

Housing for bearing and 'GACO' pressure seal

Honeycomb

Driven pulley

Housing for honeycomb
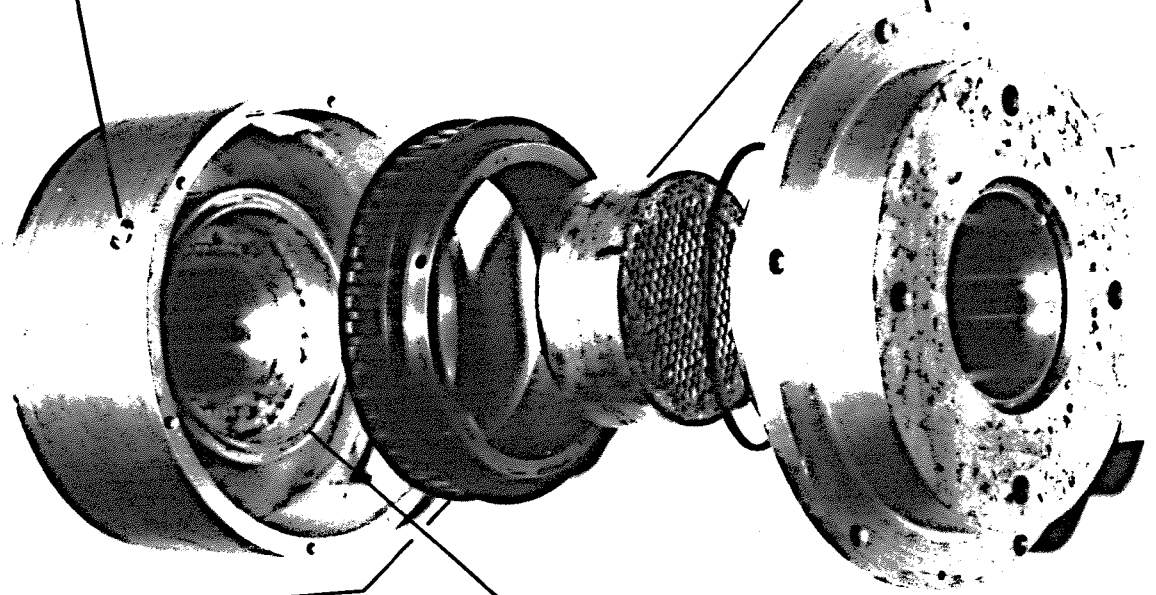
FIG. 6.5 EXPLODED VIEW OF SWIRL GENERATOR

In addition to this it is necessary to be able to have access to the honeycomb for cleaning or replacing. The above considerations and the need to have an external drive necessitated the use of a 'split-system' design particularly since it is not desirable to remove the bearings and the seals too often. Figs. (6.6, 6.7) show the details and the assembly of the swirl generator. The assembly may be dismantled by loosening the socket screws which are accessible through the special openings on the casing.

The drive was provided by a direct current shunt motor. However the speed holding characteristics of such a motor under load are not very good. Furthermore the very fine speed control, during variation, dictated by experimental requirements precluded the use of the conventional manner in which this is achieved, i.e. by controlling the field resistance. In view of these a feed-back control system was provided thus improving speed holding to better than 1% at 1000 rpm and also increasing the speed of the motor.

Such a high degree of control would be of no use if there were to be slip during transmission and furthermore excessive loads (belt tension) on a split-system design could deform the assembly. This discourages the use of friction drives and favours engaging drives which do not require heavy tensioning. This requirement was satisfied by employing a toothed-belt. As with any design work standard products were used wherever possible. However in the case of the driven pulley a special pulley had to be manufactured. The details of this pulley are shown in Fig. (6.7).

The centre distance between the drive motor and the driven generator is governed by the type of pulleys used. In this case two drives are available; one to step down (drive A) and the
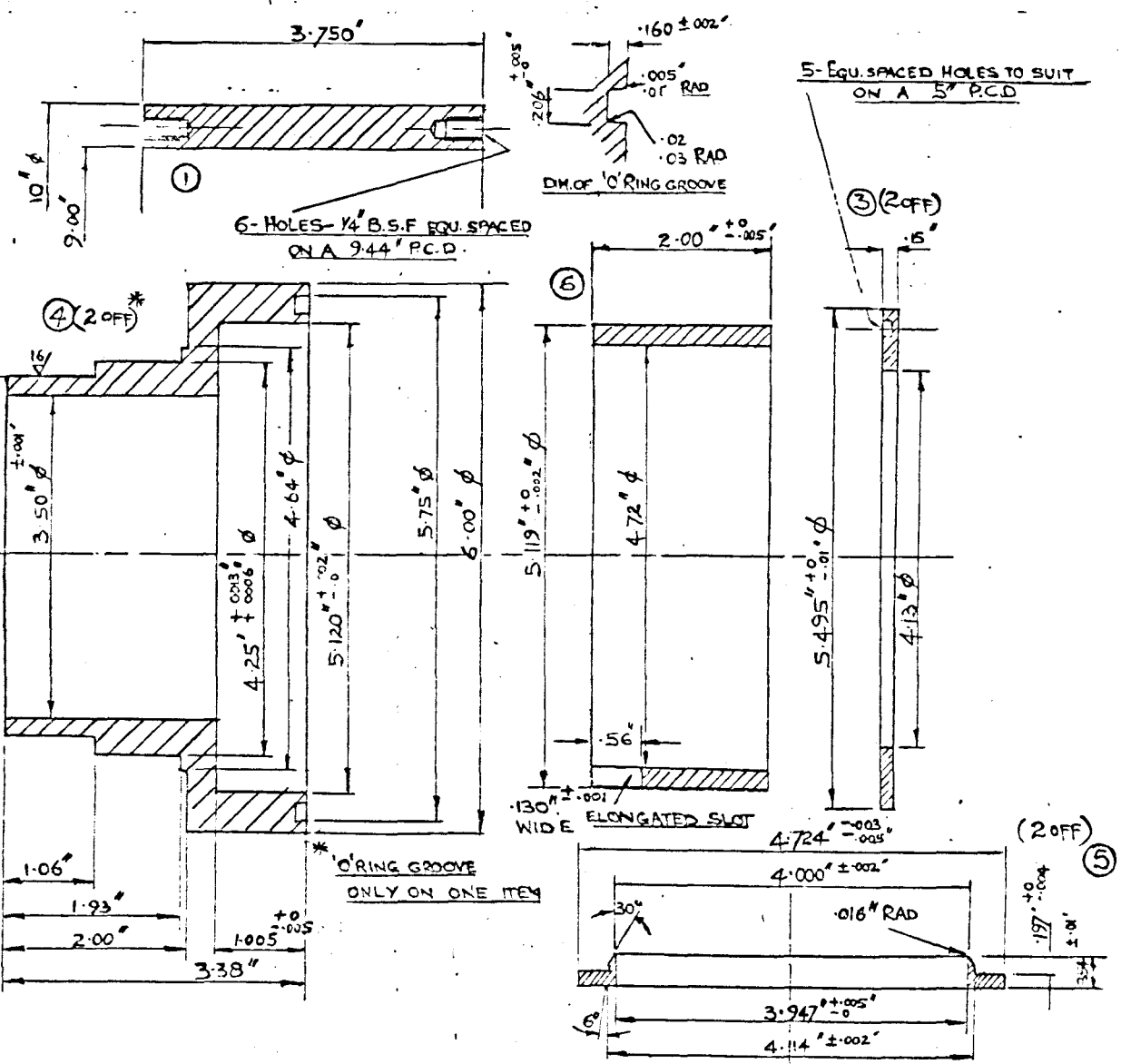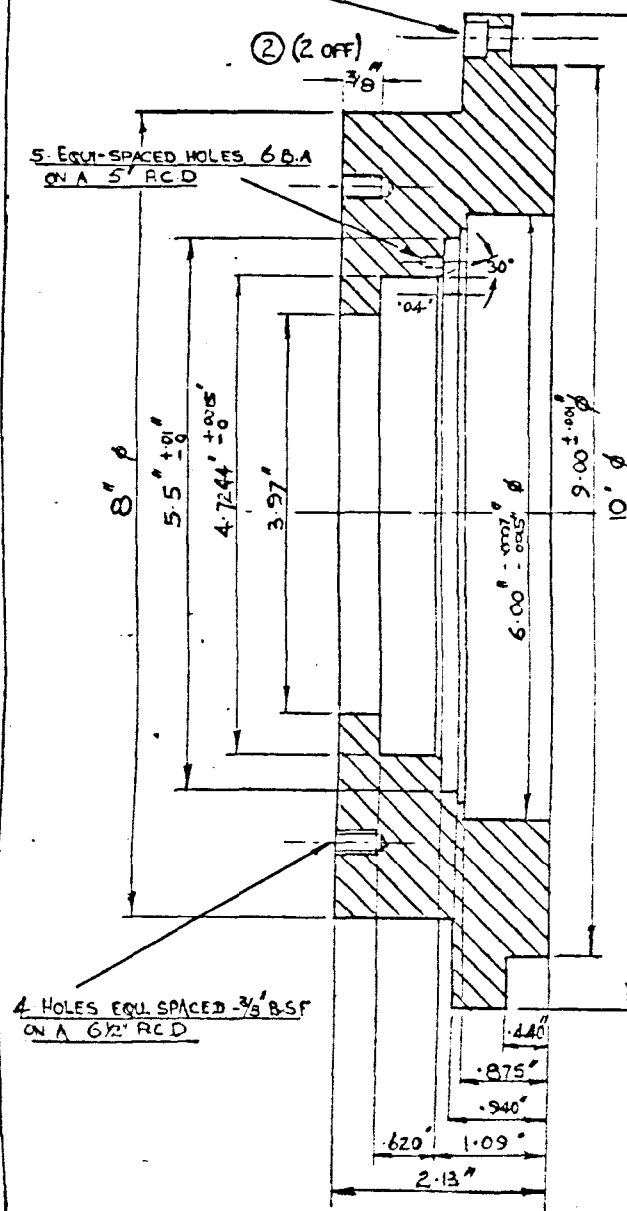
FIG.6.6 HONEY-COMB SWIRL GENERATOR

MAT.^L
ALUMINIUM ALLOY
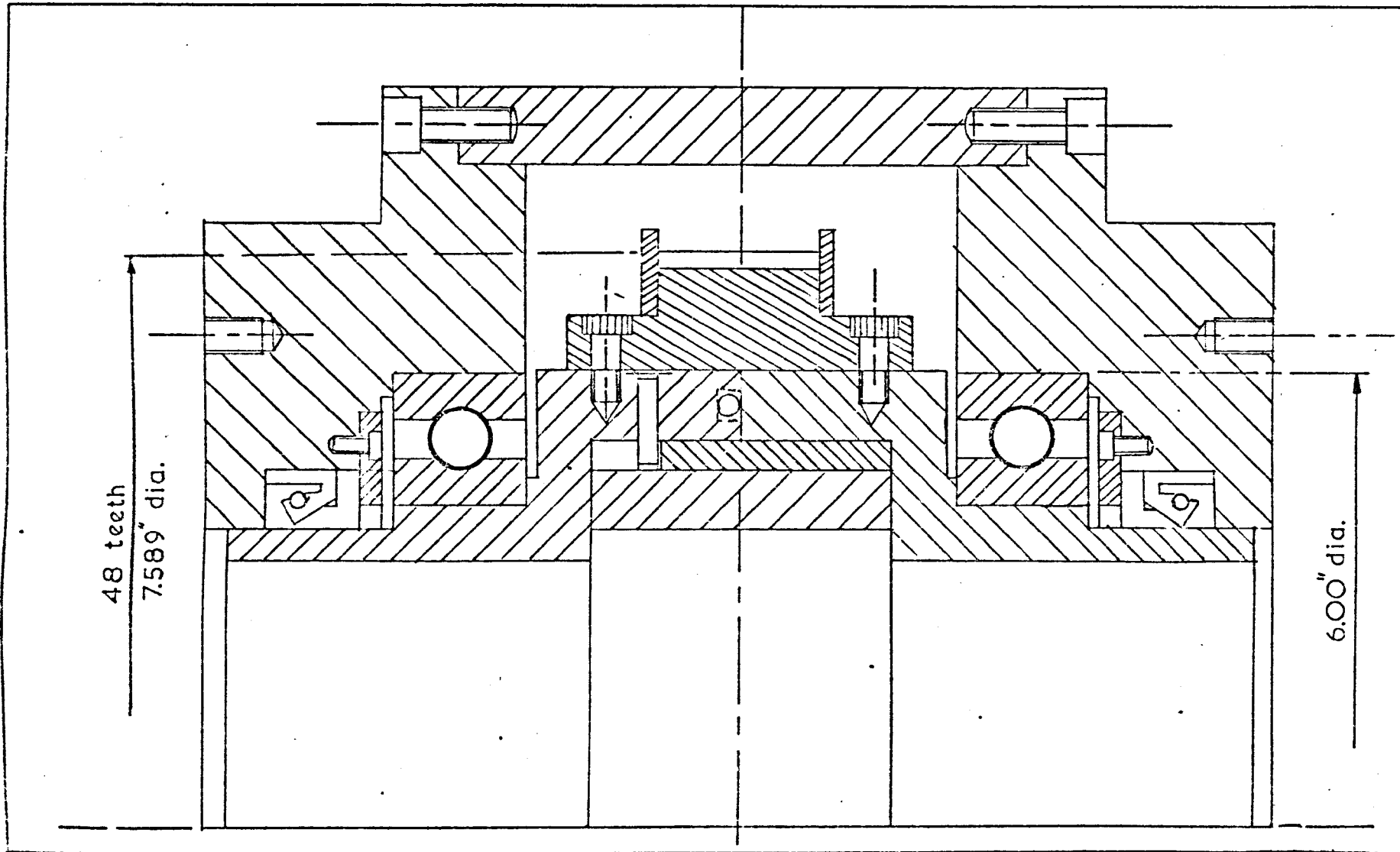
FIG.6.7   SWIRL GENERATOR ASSEMBLY

48 teeth
7.589" dia.

6.00" dia.

other to step-up (drive B) the speed. It should be pointed out here that for each drive there is a high range and a low range available from the control systems. The drives A and B were selected such that the difference between the centre distances were kept to a minimum.

The details of the components used are as follows:

DRIVE MOTOR: THOMPSON HOUSTON D.C. SHUNT MOTOR

                 220 V; 5 HP; 1000 R.P.M.

                 MOTOR SHAFT: 1.375" DIA.

                 KEYWAY: 0.375" x 0.125"

TRANSMISSION: ALL FENNER PRODUCTS

	DRIVE A (STEP DOWN)	DRIVE B (STEP UP)
DRIVE PULLEY	20 H 100; 20T	96 H 100; 96T
DRIVEN PULLEY	48T; SPECIAL	
BELT	700 H	900 H
TAPER-LOCK BUSH	019E0106 (1310)	019M0106 (2517)
CENTRE-LINE DISTANCE	671 mm	679 mm

SEALS: GACO 'SPIROSEAL' DPSM 100 12012

INCLINED TABLE: Inclination 20° to horizontal.

                 Limits of centre distance - 655 mm to 715 mm.

6.2.3.   'Universal' coupling for Probe Carrier

If the radial distribution of velocities and pressure are to be measured then the probe must be mounted on a reference face. Unlike in a circular pipe, in a diffuser the radius at each section is different from the next which makes it necessary to traverse the probe over varying radii within the diffuser.

Furthermore, owing to the limitations of the spherical probe and the peculiarity of the flow system it is necessary to be able to rotate the probe about the centre sensing hole on the spherical cap.

These requirements warranted the design of a 'universal' coupling to facilitate measurement. The coupling is shown on Fig. (6.8). In the interests of economy the brass adaptor is made interchangable so that only the diffuser in use at any one time needs to be provided with these. However owing to the varying angle and radii associated with the diffusers, individual plugs had to be manufactured and contoured to suit. The dimensions were so arranged that a standard 'DISA' type anemometer could be used in place of the pitot probe with only a slight modification. The unit was sealed as it had to be used with liquids. The locking collar and the section above the interface (Fig. (6.8)) is normally attached to the probe carrier.

6.2.4.   Probe Traversing Mechanism

A. General Requirements

The need to traverse the probe linearly and also effect rotation at any point was discussed earlier. Furthermore even with pure axial flow in diffusers a high degree of fluctuation of velocities have been observed and with swirl this problem will no doubt be further magnified. Thus it is necessary to obtain long time-mean observations of velocities and pressure. The (diverging) wall of a conical diffuser, unlike that of a pipe, does not permit it to be used as a reference datum. Thus the axis of the diffuser is regarded as the datum.
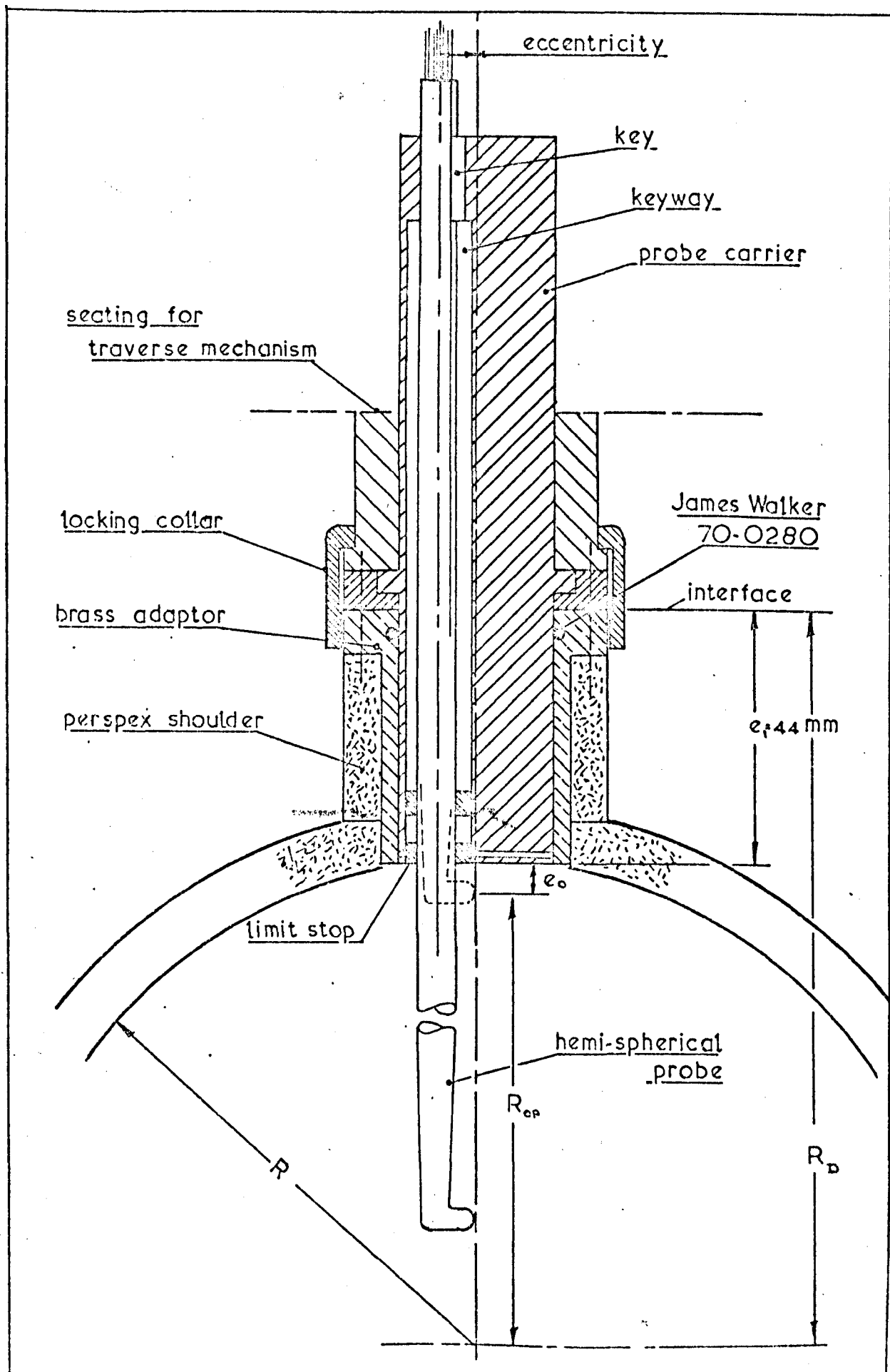
FIG.6.8 `UNIVERSAL` COUPLING FOR PROBE-CARRIER

Furthermore the required radial traverse increases with axial

distance along the diffuser.

In view of the dearth of experimental data associated

with swirling flows a vast amount of measuring needs to be carried

out in the future. An efficient and convenient measurement

technique would ease this problem considerably. Time expended on

developing an automatic or even a semi-automatic system would be

gained certainly in the long term programme.

B. Design Features

The design of the equipment may be considered in two stages.

(i) Mechanical design which includes the linear and rotational

motion.

(ii) Electro-mechanical control of operations and recording of

information.

(i) Mechanical Design

A slider-crank mechanism was employed to execute the

linear motion.
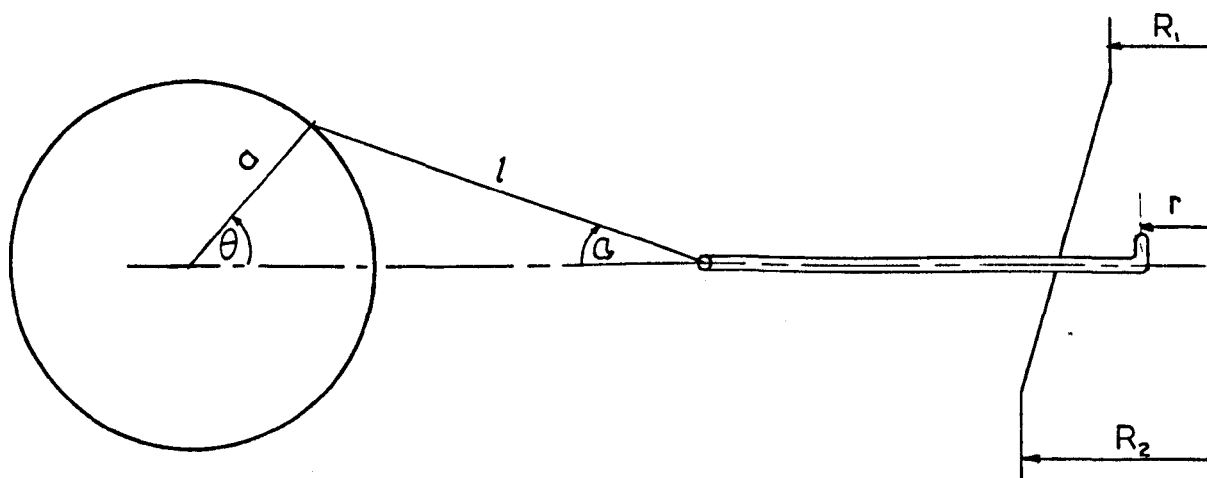
Considering the above sketch,

$$\frac{l}{\sin\theta} = \frac{a}{\sin\alpha}$$

and

$$r = (l + a) - (a\cos\theta + l\cos\alpha)$$

Substituting for $\cos\alpha$ and simplifying yields

$$r/a = (n + 1) - \cos\theta - (n^2 - \sin^2\theta)^{\frac{1}{2}} \qquad (6.2.4.1)$$

where $n = l/a$ and $0 \le r/a \le 2$ as $0 \le \theta \le \pi$

The maximum traverse at any section is $r = R = 2a$ but

there are two maxima (R_1 and R_2) which govern the dimensions l and

a. Each time the crank radius is altered then the length of the arm

l will also change and to estimate the traverse from equation (6.2.4.1)

the new value of n will have to be measured. This is however

inconvenient as it is difficult to estimate the pivots of the arms.

If however ($l - a$) is kept constant then only a knowledge of the

crank radius is required and equation (6.2.4.1) becomes

$$r/a = 2 + p/a - \cos\theta - [(p/a + 1)^2 - \sin^2\theta]^{\frac{1}{2}} \qquad (6.2.4.2)$$

where $p = (l - a) = $ constant.

Fig. (6.9) shows the divisions used for increments of the

traverse. The adjustment of the crank radius is against the fixed

scale. The difficulty of measuring the length of the arm was

overcome by employing an indirect method.

A plot of equation (6.2.4.1) for two typical values of n

is shown on Fig. (6.10). It is seen that the maximum sensitivity

of the curves to n is displayed between approximately 75° and 110°.

If for convenience $\theta = 90^{\circ}$ is chosen as a suitable value for

calculating the length of the arm, then equation (6.2.4.1) becomes

FIG. 6.9 ANGULAR DIVISIONS USED FOR STEPPING MOTION
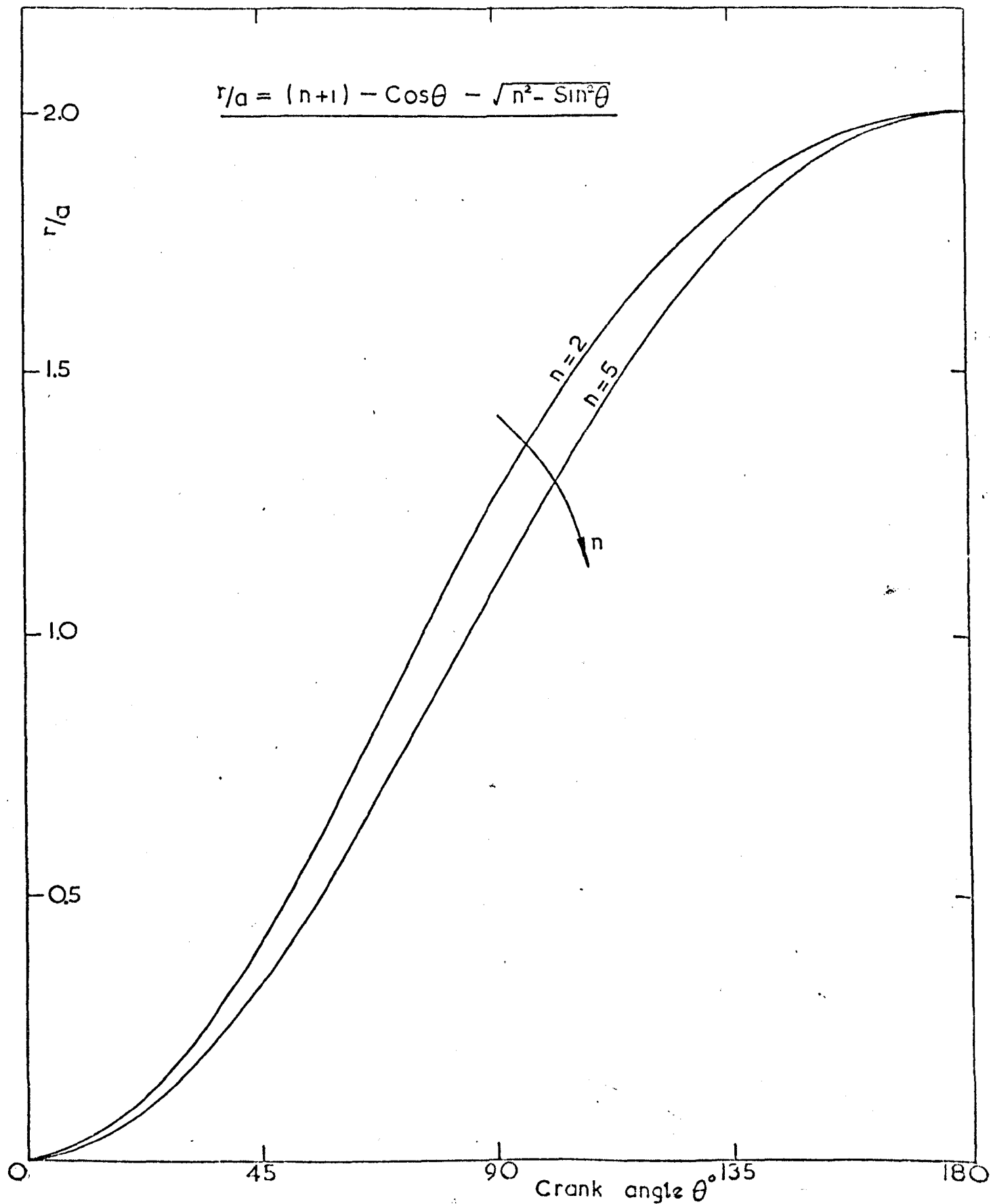
FIG. 6.10 SENSITIVITY OF HARMONIC MOTION TO n

$$r/a = n + 1 - (n^2 - 1)^{\frac{1}{2}}$$

which on simplifying yields

$$n = 0.5 \left[1 + (r/a - 1)^2 \right] / (r/a - 1) \qquad (6.2.4.3.)$$

The length of the arm may be obtained by obtaining a mean value of n from several values of r/a at $\theta = 90°$. Fig. (6.11) shows the complete traversing mechanism. The slots on the radius wheel have been arranged to obtain approximately equal increments of linear traverse. Rotation is effected by a 'Honeywell' (type 362479-2) servo-motor via a worm-wheel. The direction of rotation is governed by the difference in the voltage supplied.

If the system shown in Fig. (6.11) is dismantled then reassembling is likely to cause difficulty owing to the "tight" design limits. To obtain the full range the assembly procedure outlined in Appendix (6/A) must be followed. Owing to physical restrictions it was not possible to measure very near the wall. Since the axis of the diffuser, and not the inside wall, is the reference datum an "operating" radius (a_{op}) for the crank must be calculated as follows.

Referring to Fig. (6.8)

$$a_{op} = [R - e_o] / 2 \qquad (6.2.4.4.)$$

The R values for the ducts used in this project are provided in Fig. (6.12a). Allowing for the backlash of the instrument it was possible to measure the traverse to within 0.5 mm. It should be noted that this figure is more than satisfactory when the limits of manufacture of the perspex tubing and the diameter of the probe head are taken into consideration.
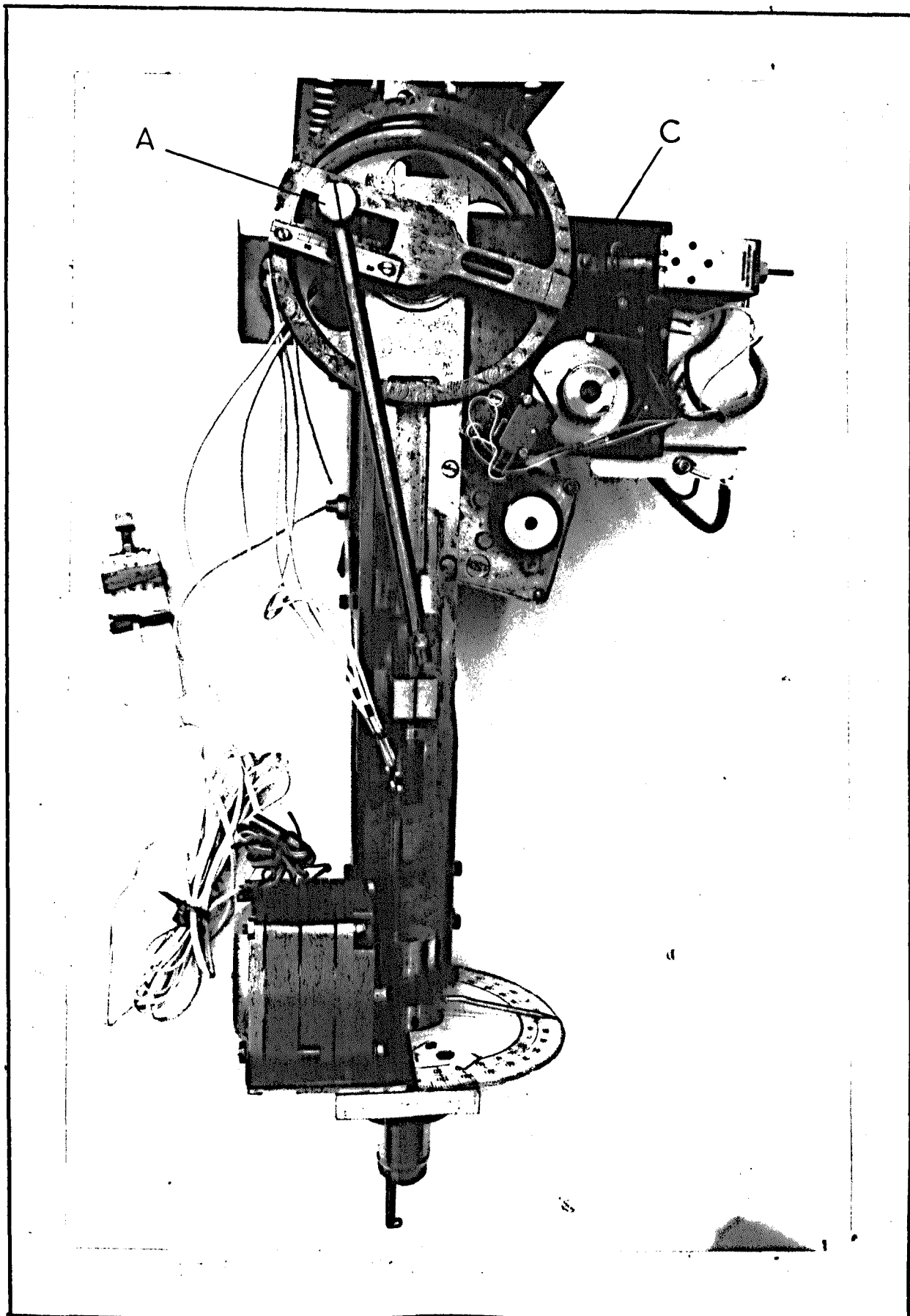
FIG. 6.11 PROBE TRAVERSING MECHANISM
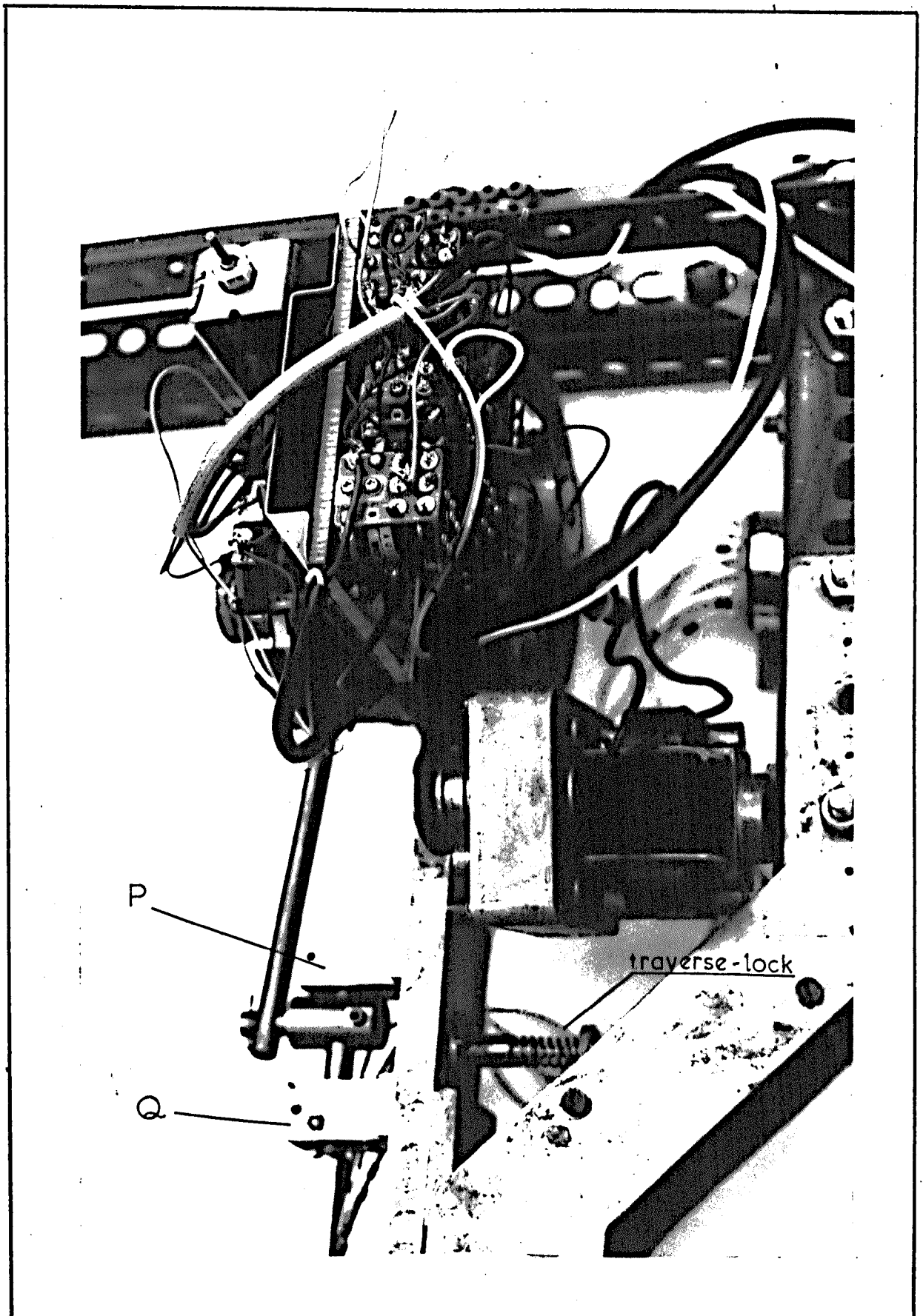
FIG. 6.11a. PROBE TRAVERSING MECHANISM
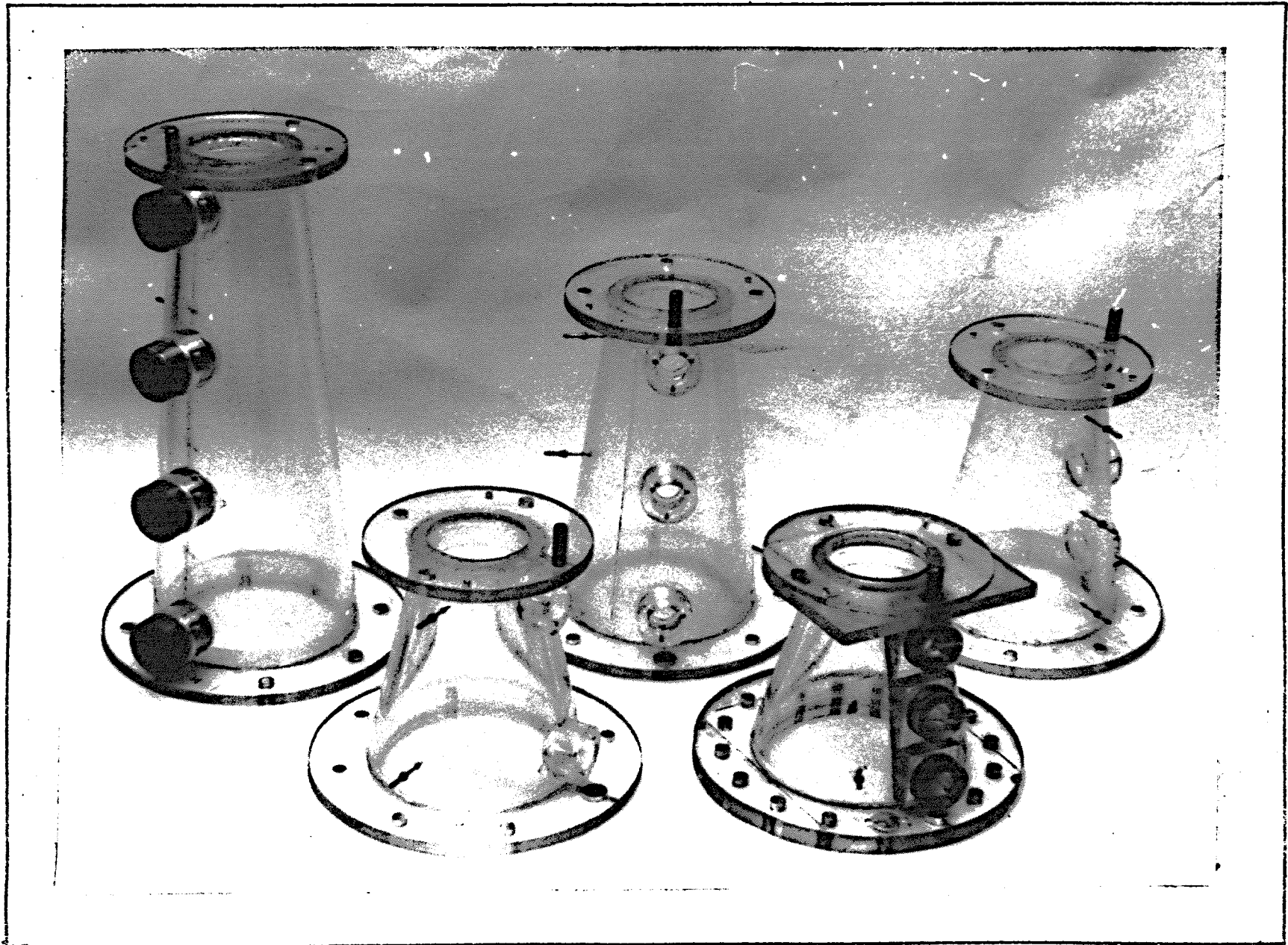
FIG.6.12   DIFFUSERS   USED   IN   EXPERIMENTS
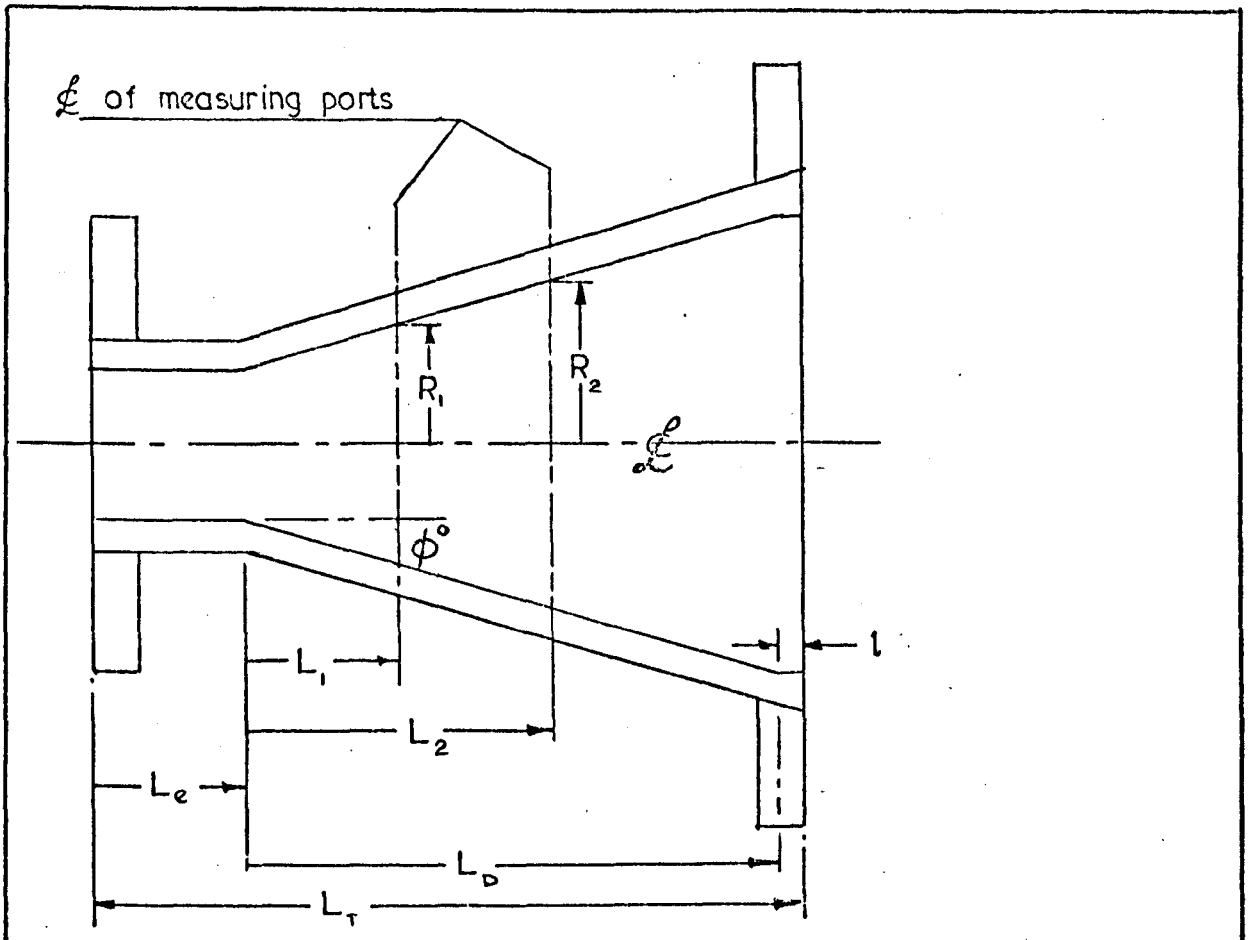
ALL DIMENSIONS ARE IN MM.

2ϕ	$10°$	$15°$	$20°$	$25°$	$30°$
L_T	517	350	291	238	223
L_D	500.3	341.8	245.2	203	168
L_e	10.7	2.2	39.8	28	44.04
l	6	6	6	7	11
R_1 / L_1	48.75 / 42.80	50.50 / 41.80	48.03 / 17.21	48.99 / 18.0	46.33 / 4.96
R_2 / L_2	63.96 / 186.3	67.62 / 171.8	65.49 / 116.2	81.13 / 163	61.94 / 66.96
R_3 / L_3	75.35 / 326.3	84.73 / 301.8	82.95 / 215.2		79.55 / 129
R_4 / L_4	86.74 / 460.3				

FIG. 6.12a DIFFUSERS USED IN EXPERIMENTS

The traverse at any section of the duct is given by

$$r/a_{op} = n + 1 - \cos\theta - (n^2 - \sin^2\theta)^{1/2} + e_0 \qquad (6.2.4.5)$$

For the present assembly the following details apply

$$p = 1 - a = 152.24 \text{ mm.} \qquad e_0 = 4.50 \text{ mm.}$$

Now that the operating radius has been determined it is set on the traverse mechanism as follows:

Set the crank to 180° (i.e. retract probe completely) and lock the system with the 'traverse-lock' (Fig. (6.11)). Loosen the crank at A and adjust the radius using the screw C, against the built in scale. Now clamp the 'arm' to the crank and release slider P; the mechanism is ready for operation.

C. Electro-Mechanical Control and Recording System

The function of this is to index and rotate the probe and record mean observations from all five sensing holes automatically. However at present only automatic indexing has been provided. The mechanical equipment necessary for rotation has been incorporated in the design. The drive for the servo-motor and the equipment necessary for recording on paper tape are also available. The relay circuit on Fig. (6.13) is limited to indexing only but this can easily be extended to accommodate the rest of the system. The pulses at given time intervals necessary to commence and terminate recording can be generated using standard circuitry. The method of operation is described in Appendix (7/B).

If the system stalls it can easily be released by manually retracting the plunger. The peripheral distance between some of the slots being small the manually provided pulse tended to be too long resulting in skipping a slot.

240 volt a.c.

ACTUATOR

C/2

MS/3

start

D/2

E/1

A

D

B

DRIVE MOTOR

A/2

MS/1

MS/2

B/3
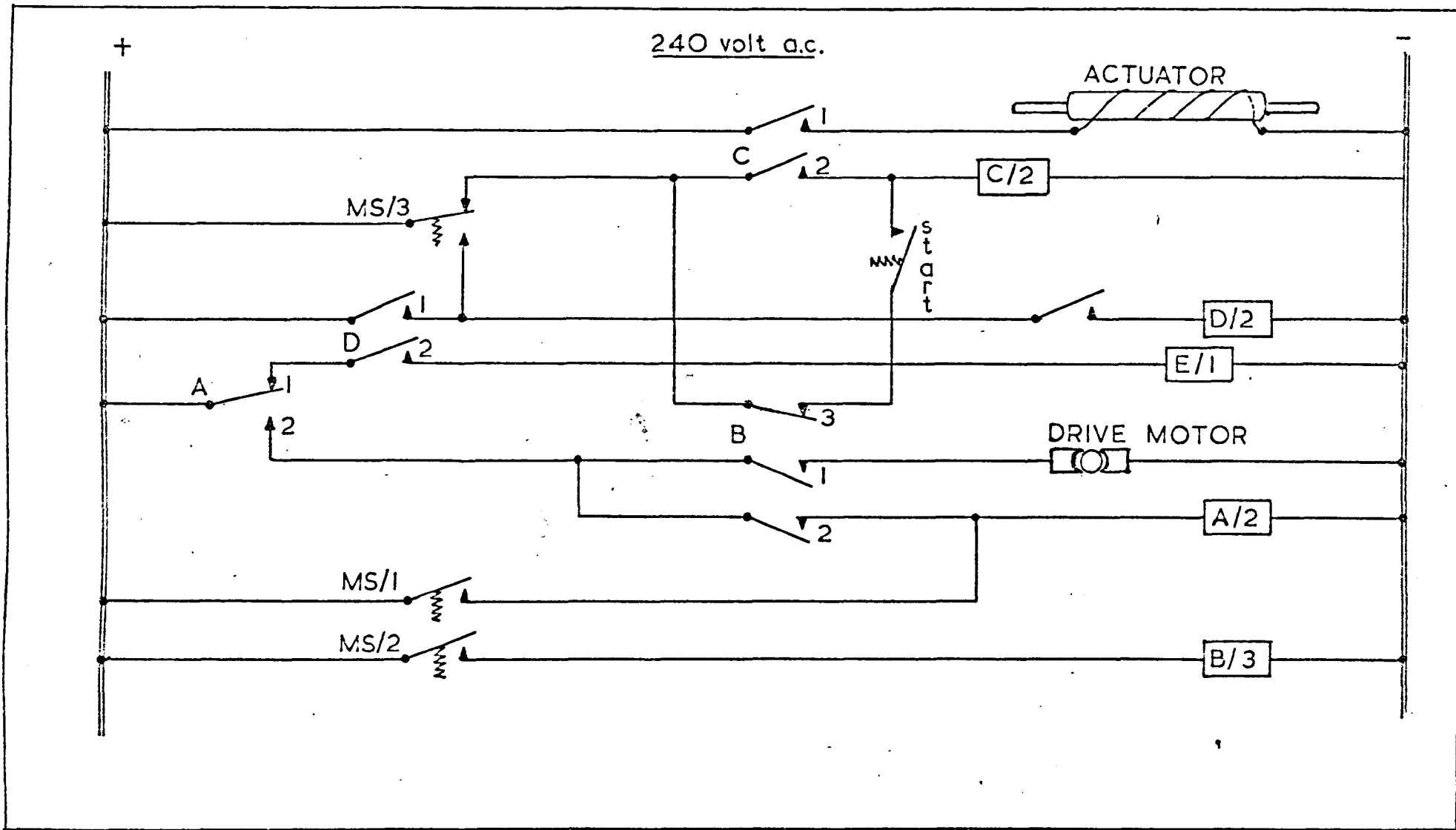
FIG. 6,13 ELECTRO-MECHANICAL CONTROL SYSTEM FOR TRAVERSE MECHANISM

152

This was overcome by modifying the circuit such that the pulse was cut-out automatically from within the circuit. The cams are all independently adjustable and the adjustable torsion spring controls the load on the plunger. The circuit was optimised while in operation as it is dependent on the movement on the plunger and the delays of the switches and relays.

6.3 INSTRUMENTATION AND CALIBRATION

The pitot-probe will be discussed separately in the next chapter in view of the extensive nature of the work carried out.

6.3.1 Measurement of Mean Flow-Rates and Turbulence

A. Water Flow-Rate

Flow-rate of water was measured using an orifice plate with D and D/2 tappings. The orifice plate was designed in accordance with the recommendations made in B.S. 1042, Pt.1; 1964 with a pipe diameter of 76.2 mm. which resulted in an orifice diameter of 38.81 mm. Mercury (for high flow-rates) and Carbon Tetrabromoethane (for low flow-rates) were used as manometric fluids. Flow control was achieved with the aid of a throttle valve and a by-pass valve.

Calibration was carried out using a weighting tank into which water was discharged for a given time. 400 lb of water was measured at times between 150 and 25 secs. The weight was measurable to within 2 lb and the pressure difference could be read to within 0.5 mm. The two calibration curves are shown in Figs. (6.15, 6.16) and can be represented by

$$(\dot{m} \text{ lb/sec})^2 = 0.959 \times \Delta h \quad \text{(cms carbon tet.)} \qquad (6.3.1.1.)$$

$$(\dot{m} \text{ lb/sec})^2 = 6.925 \times \Delta h \quad \text{(cms mercury)} \qquad (6.3.1.2)$$

the gradients being arrived at using regressional analysis.
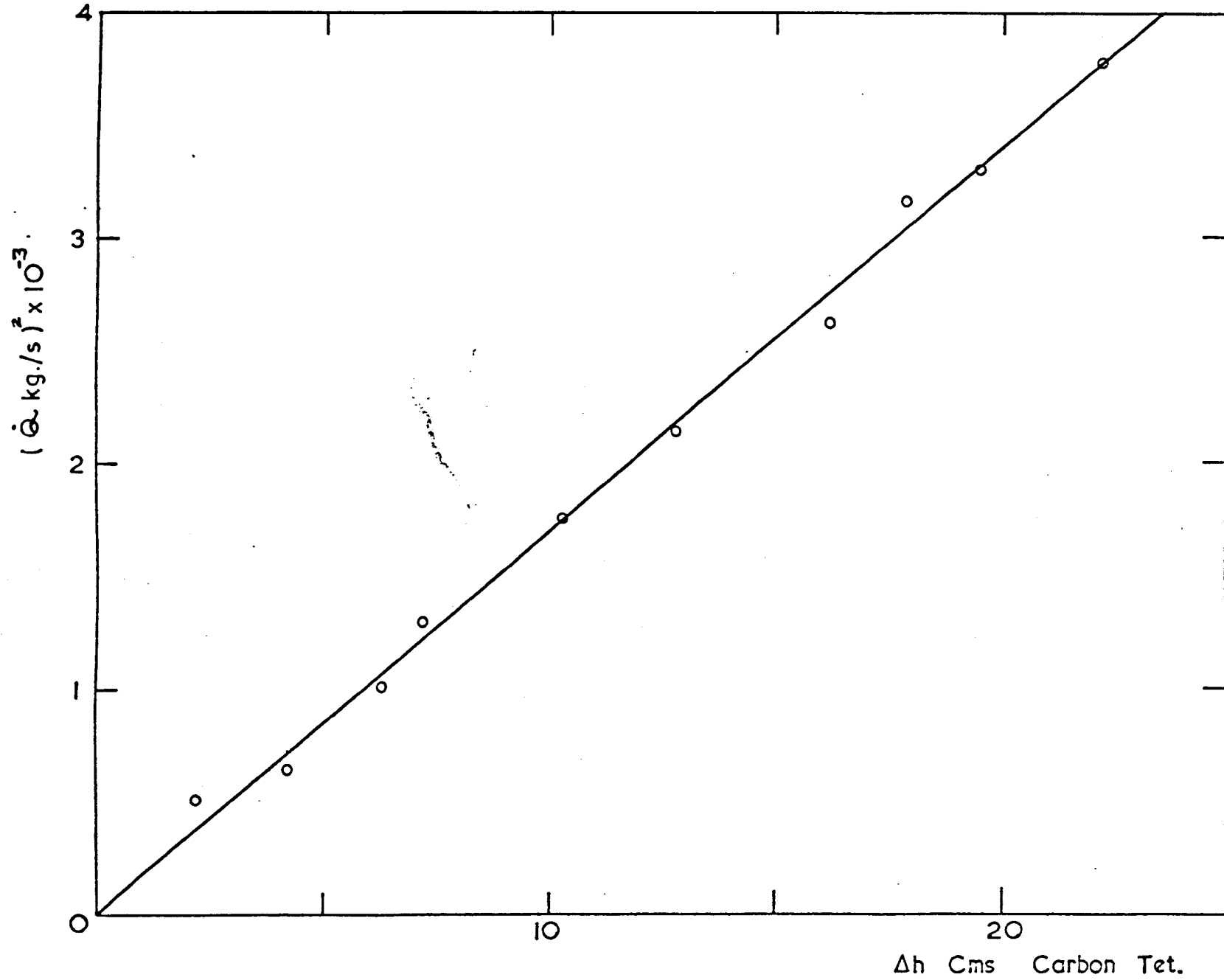
FIG.6.14 ORIFICE PLATE CALIBRATION CURVE — AIR
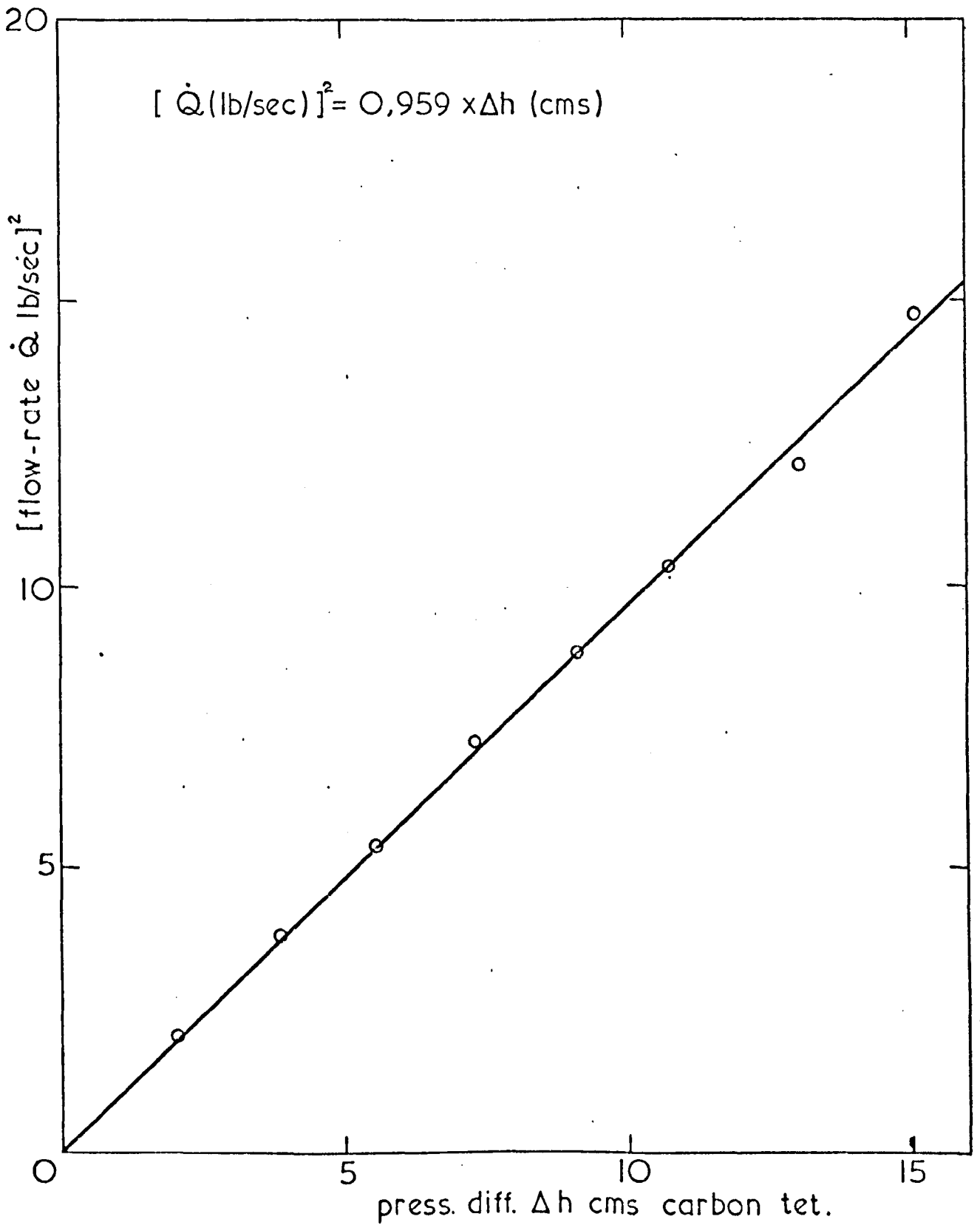
FIG. 6.15 ORIFICE PLATE CALIB. CURVE – WATER

$$[\dot{Q}(\text{lb/sec})]^2 = 6{,}925 \times \Delta h \text{ (cms)}$$
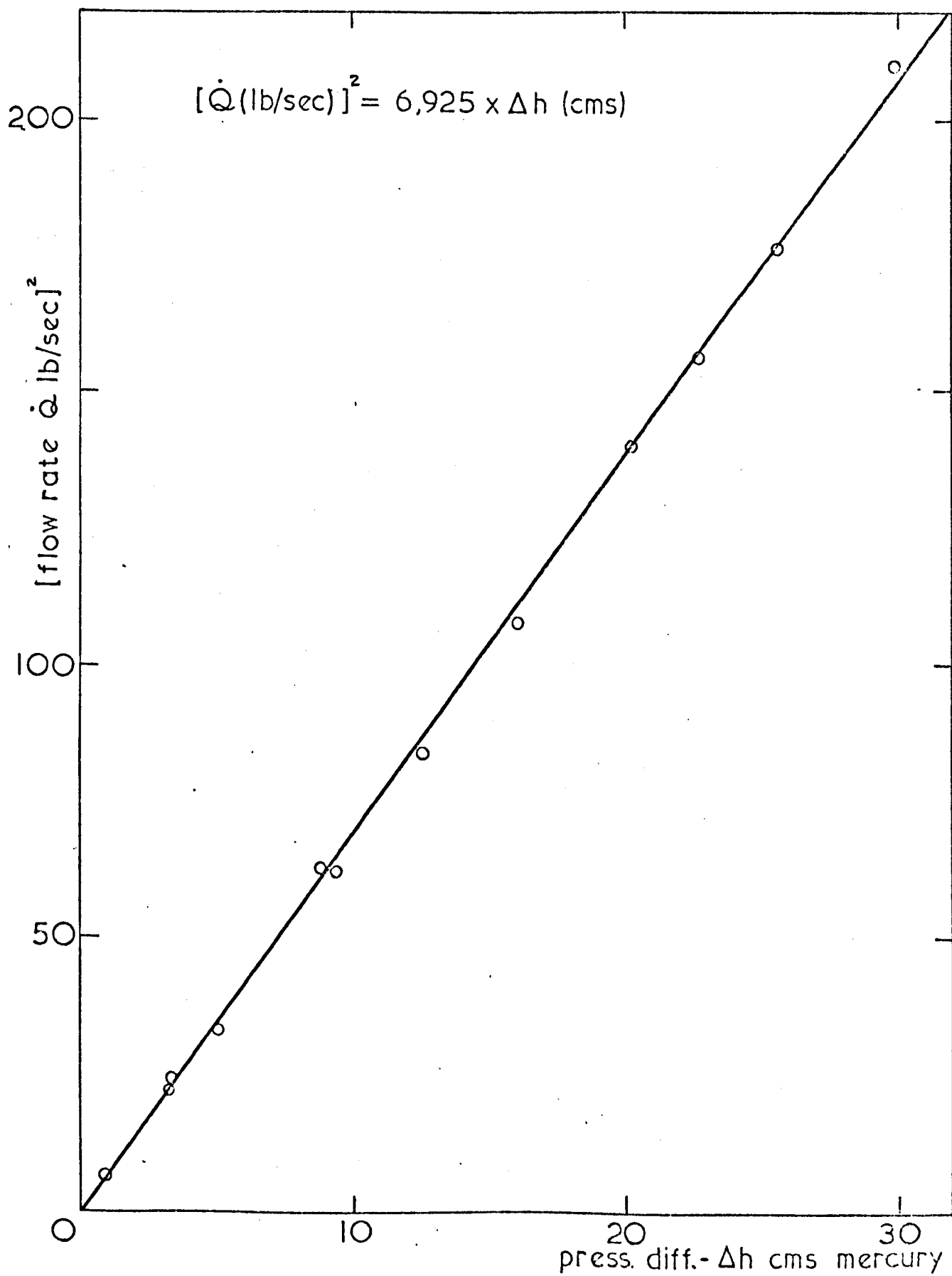
FIG. 6.16 ORIFICE PLATE CALIB. CURVE – WATER

B.   Air Flow-Rate

Air flow rate was measured using an orifice in conjunction
with a butterfly-valve. This was calibrated with the aid of an
anemometer. The anemometer itself was calibrated in a separate
research project and is reported in Perera (1975). The calibration
curve is shown on Fig. (6.14). This also provided an ideal
opportunity for checking the five-hole pitot probe. Flow rates
calculated from velocity profiles thus obtained are also indicated
in the figure.

C.   Turbulence

The mean turbulence level and the calibration of the orifice
plate, for air flow measurement, were achieved using a sub-miniature
hot-wire probe. The following 'DISA' system was employed;

        Anemometer   55 M 10

        Lineariser   55 D 10

        Auxiliary Unit   55 D 25

        R.M.S. Unit   55 D 35

        DVM   JM 1860

6.3.2   Speed control of Swirl Generator Drive Motor

    A.   Characteristics of Motor

The d.c. shunt motor used was already available and had
to be adopted to suit this application. In a direct current
machine

$$E \propto \phi N$$ where E - induced e.m.f.

                          ϕ - flux change

                          N - rotational speed.

If power loss in the armature is neglected then

$$V = E$$ where V - voltage supplied to armature

and the reactive torque is given by

$$T \propto \phi \, I_A \qquad \text{where } I_A - \text{ armature current.}$$

It is seen from above that the speed of the motor may be varied by varying either the armature voltage or the voltage supplied to the field. However the range available by the latter mode of control is very limited while the former would provide the entire range from zero to full speed.

The block diagram associated with the mode of speed control is shown in Fig. (6.17). The armature voltage is varied with the aid of a thyristor which is triggered using an auxilliary firing circuit. At low speeds, under load, the speed is likely to fluctuate and to compensate for this a tachogenerator, coupled to the motor shaft, is used to obtain feed-back.

B.   Control Circuitry

Speed control is achieved using a Thyristor (SCR - Silicon Controlled Rectifier). As the name implies this is a conventional rectifier with the added feature that its 'firing position' could be controlled. It is fired by supplying a pulse to its gate. At this point it commences conducting and does so until the current drops to zero, at which point it effectively switches off. Fig. (6.18) shows the effect of firing on an a.c. input.

The pulse required to trigger the SCR is obtained as follows.

The a.c. mains voltage is rectified to obtain the required d.c. voltage. The 18 volt 'zener diode' chops off voltages in excess of 18 volts giving the "spiked" waveform shown on Fig. (6.19a).
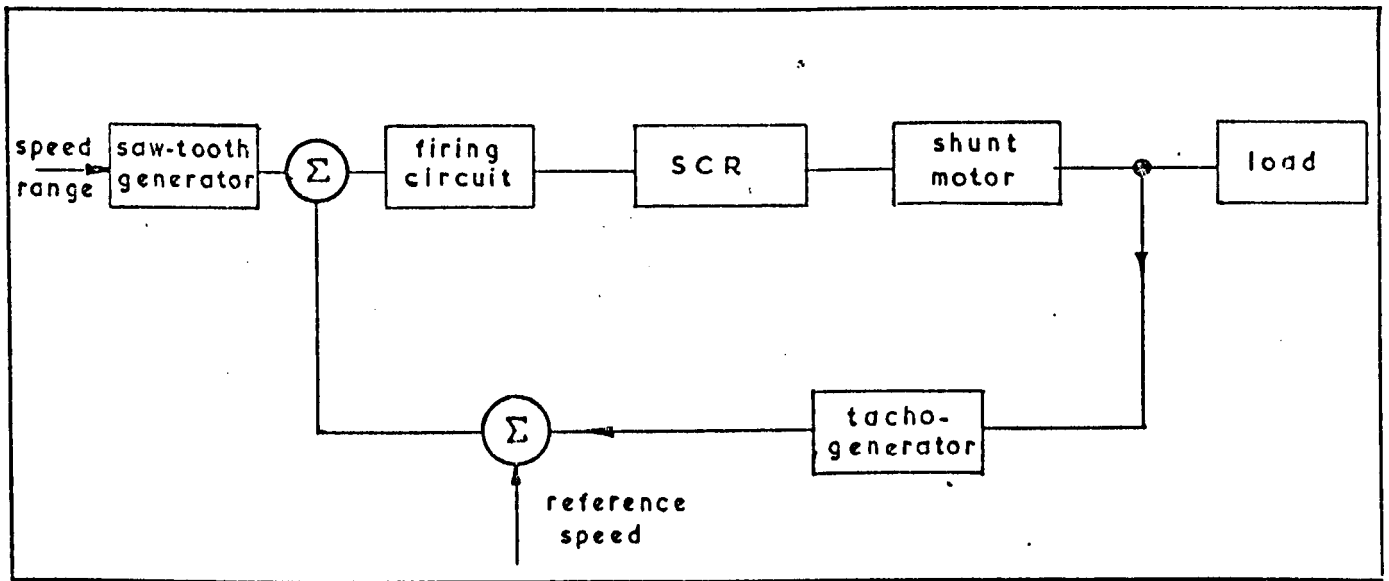
FIG. 6.17   CONTROL SYSTEM FOR SPEED   VARIATION
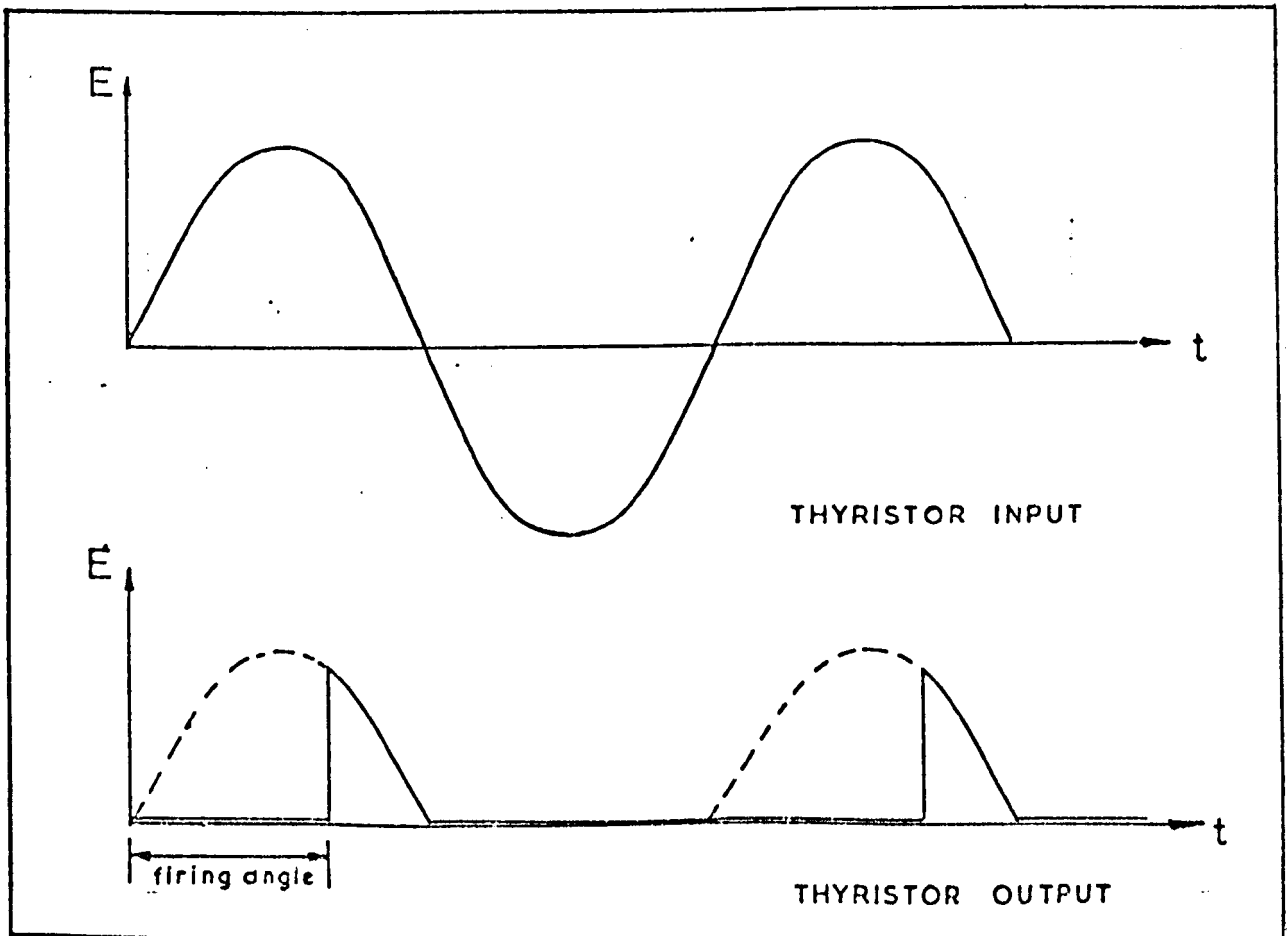
FIG. 6.18   EFFECT OF THYRISTOR ON A.C. INPUT

The capacitor C_4, which is charged via the resistor R_4, is discharged using the spiked waveform to obtain the "saw toothed" waveform shown on Fig. (6.19b). The saw-tooth (which is superimposed on a constant d.c. voltage) is used to fire a Schmitt-trigger. The resulting output which is a square wave (Fig. (6.19c)) is differentiated, using a R - C differentiator circuit to obtain pulses (Fig. (6.19d)). The diode eliminates the negative pulses. Firing of the SCR is via a pulse transformer. The circuit diagram is shown on Fig. (6.20) and the actual layout is shown in Fig. (6.21).

The Schmitt-trigger fires at a certain input voltage determined by R_{12}, R_{13}, R_{14}. The input to the Schmitt-trigger consists of the saw-toothed voltage described above superimposed on a d.c. voltage, the d.c. level, V_L. This d.c. level is the resultant of a d.c. control voltage V_C and the feed-back voltage V_f from the tachogenerator applied in opposition to each other. The 'range of speed' is governed by the magnitude of the controlled voltage which can be altered, using the pre-set potentiometer, to give any desired range. The manner in which speed control is achieved is shown on Fig. (6.22).

The system is initially set to the desired speed range. by setting V_C. To obtain the desired speed the feed-back voltage V_f is set using the potentiometer RP_1. Now the level is $V_L = V_C - V_f$. (Note: V_C is constant for a given speed range). Also $V_f = k\ V_T$ where V_T is the voltage developed by the tachogenerator and k is the fraction of this obtained from the potentiometer.

If the speed of the motor increases, then V_T and hence V_f increases and correspondingly V_L decreases.

(a)
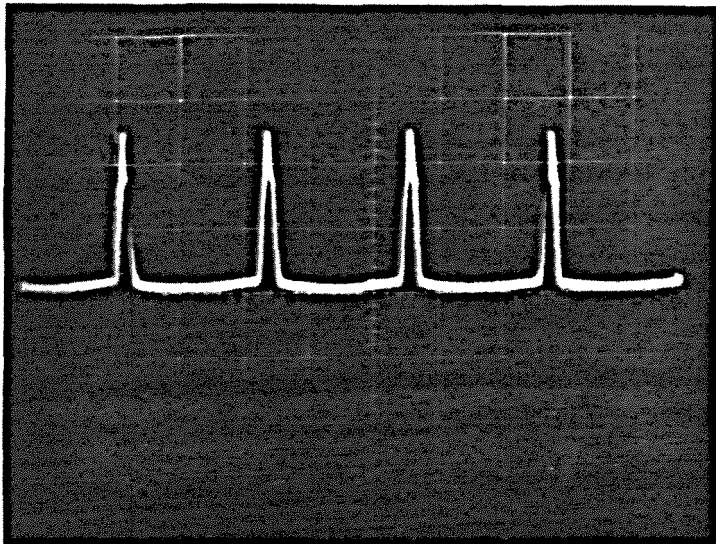
(c)
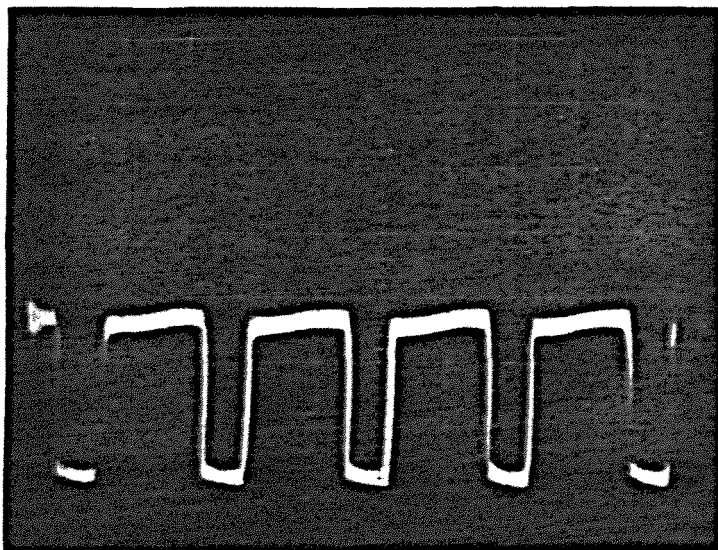
FIG.6.19 METHOD OF OBTAINING

(b)
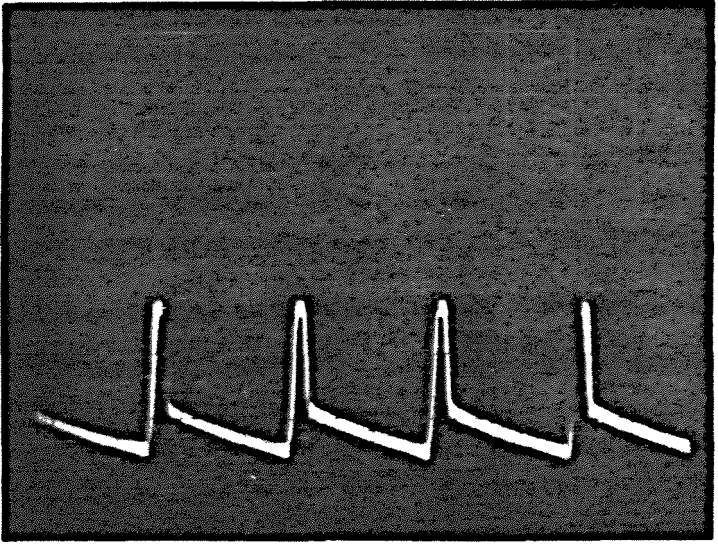
(d)
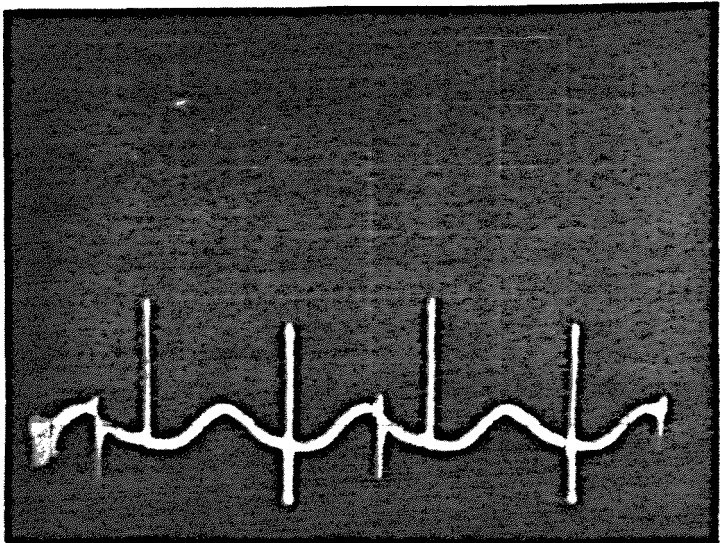
PULSES
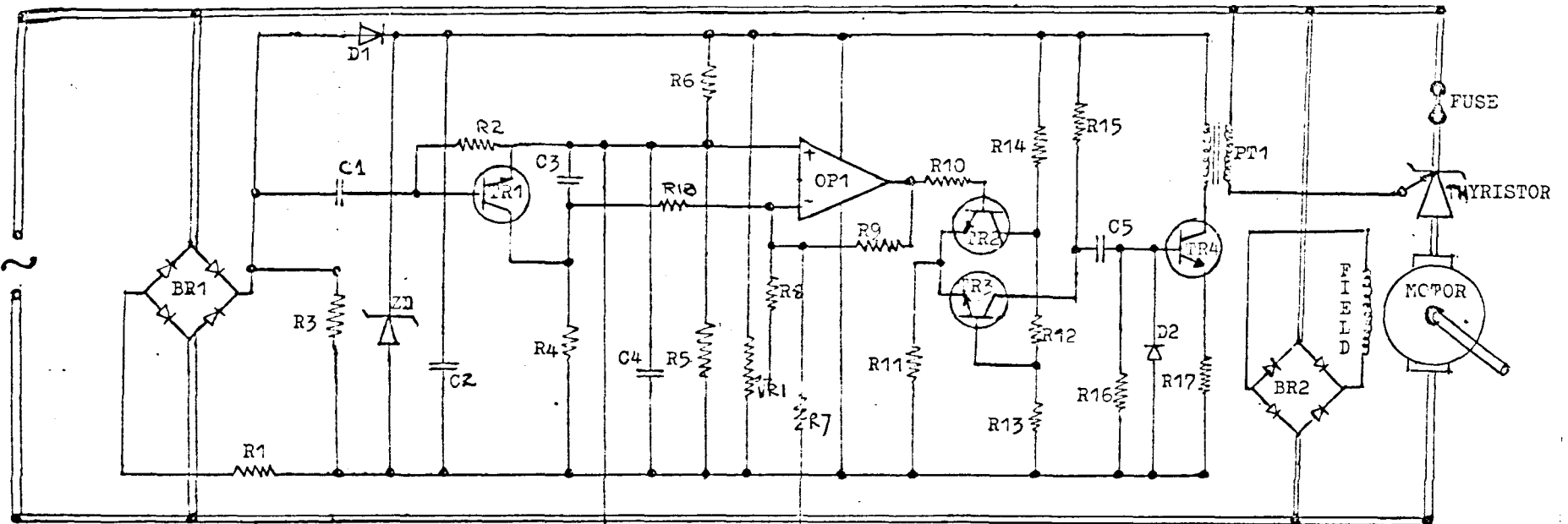
List of Components

R1-15kΩ   C1-0.1 μF
R2-150K   C5-.001
R3-220K   C2,C4-50
R4,R9-100k   C3-.22
R7-10k   C6-10
R8-330k
R10-22k   VR1-100k (PRE-SET)
R11-47k   VR2-5k (POT.)
R12-22k   VR3-10k (POT.)
R13-33k
R14-470k   ZD-18v ZENER DIODE
R15-2.2k   PT1-PULSE TRANSFORMER
R16-68k   TR1-
R17-68   TR2,TR3,TR4-
               OP1-741 OP. AMP.
R5,R6-22k   THYRISTOR-
R18-100k   FUSE-
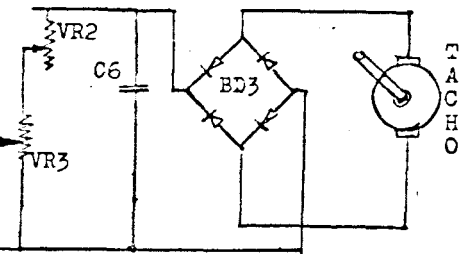
FIG. 6.20 CIRCUIT USED IN SPEED CONTROL SYSTEM

Operational Amplifier

Pulse Transformer

Potentiometer

Zener Diode

Rectifiers
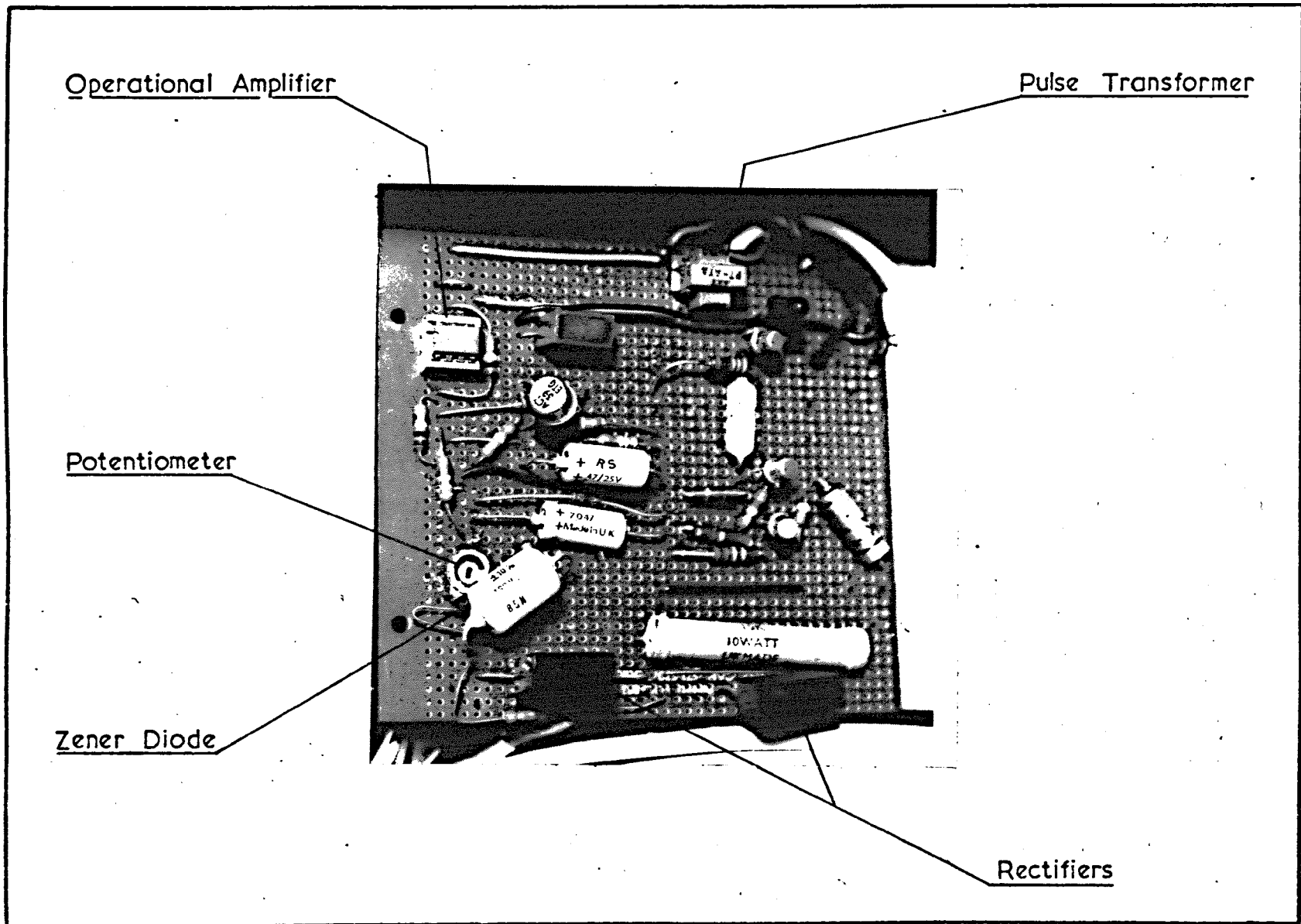
FIG. 6.21. LAYOUT OF ELECTRONIC CIRCUIT
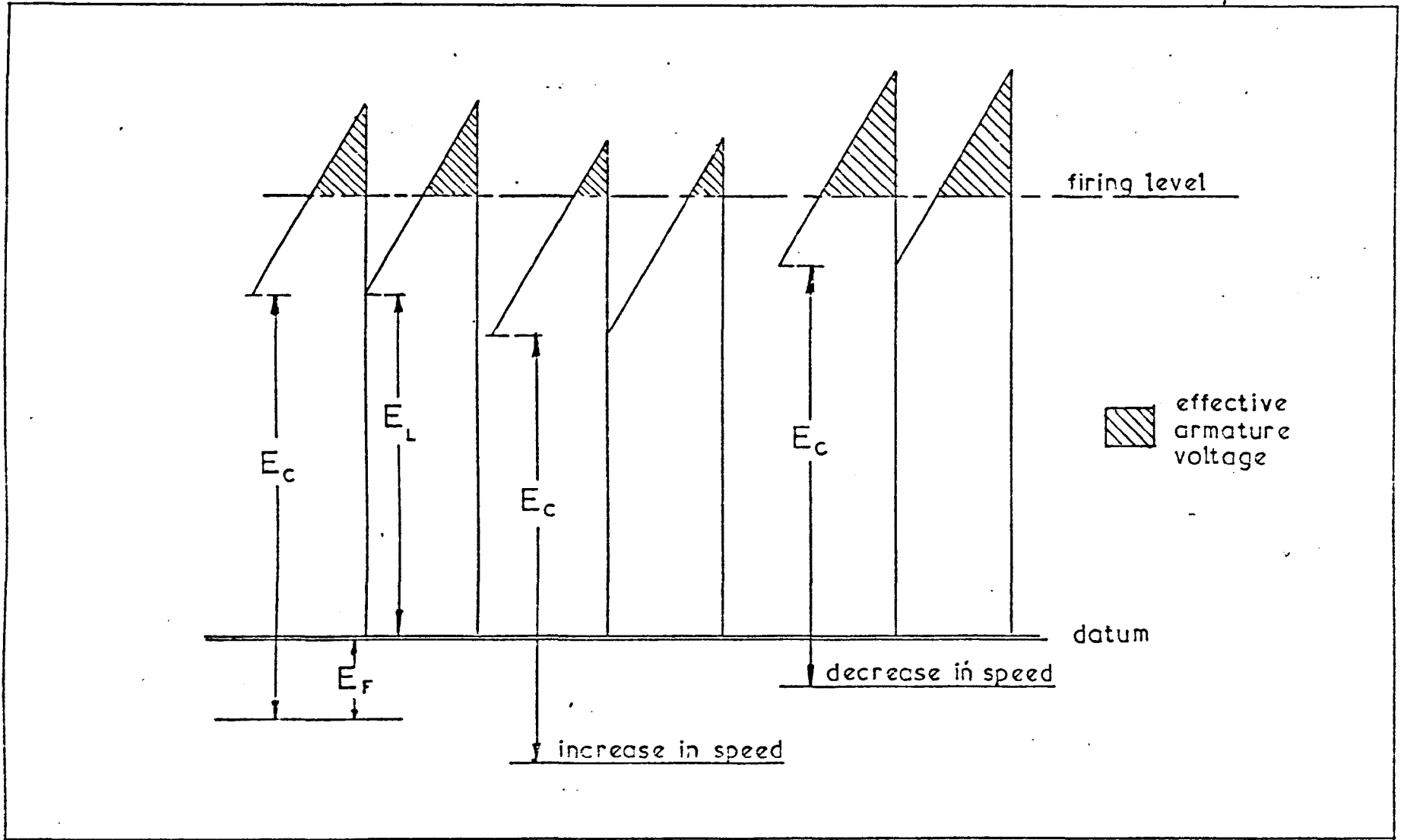
FIG. 6.22 METHOD OF SPEED CONTROL VIA FEED-BACK

When the level decreases the effective voltage supplied to the armature decreases and the effect is to slow down the motor countering the increase. The converse is true in the case of a decrease in speed. The direction of rotation of the motor may be altered by reversing the field connections. The presence of the bridge rectifier ensures that the control system is independent of the sense of rotation of the motor.

C.   Measurement of Swirl - Calibration

The tachogenerator has a linear characteristic over a wide range giving 27 volts/1000 rpm. The output could be measured satisfactorily using a standard moving coil voltmeter. This was simultaneously checked against a digital voltmeter. The speed of the motor was measured using stroboscope. The speed could be held within 1% at 1000 r.p.m. This was seen as a very useful function in view of the need to control and reproduce inlet swirl accurately. Fig. (6.23) shows the calibration curve.

D.   Application

As the system is highly non-liner the control is also non-linear. Two controls (fine and coarse) have been provided. The speed should be kept below that corresponding to 37 volts of tachogenerator feed-back voltage. As the system is not isolated it would be damaged if earthed. From the characteristics discussed earlier it will be seen that if the armature is supplied without supplying the field first the motor would reach speeds beyond its design limitations.

r.p.m. = [1000/27] x volts
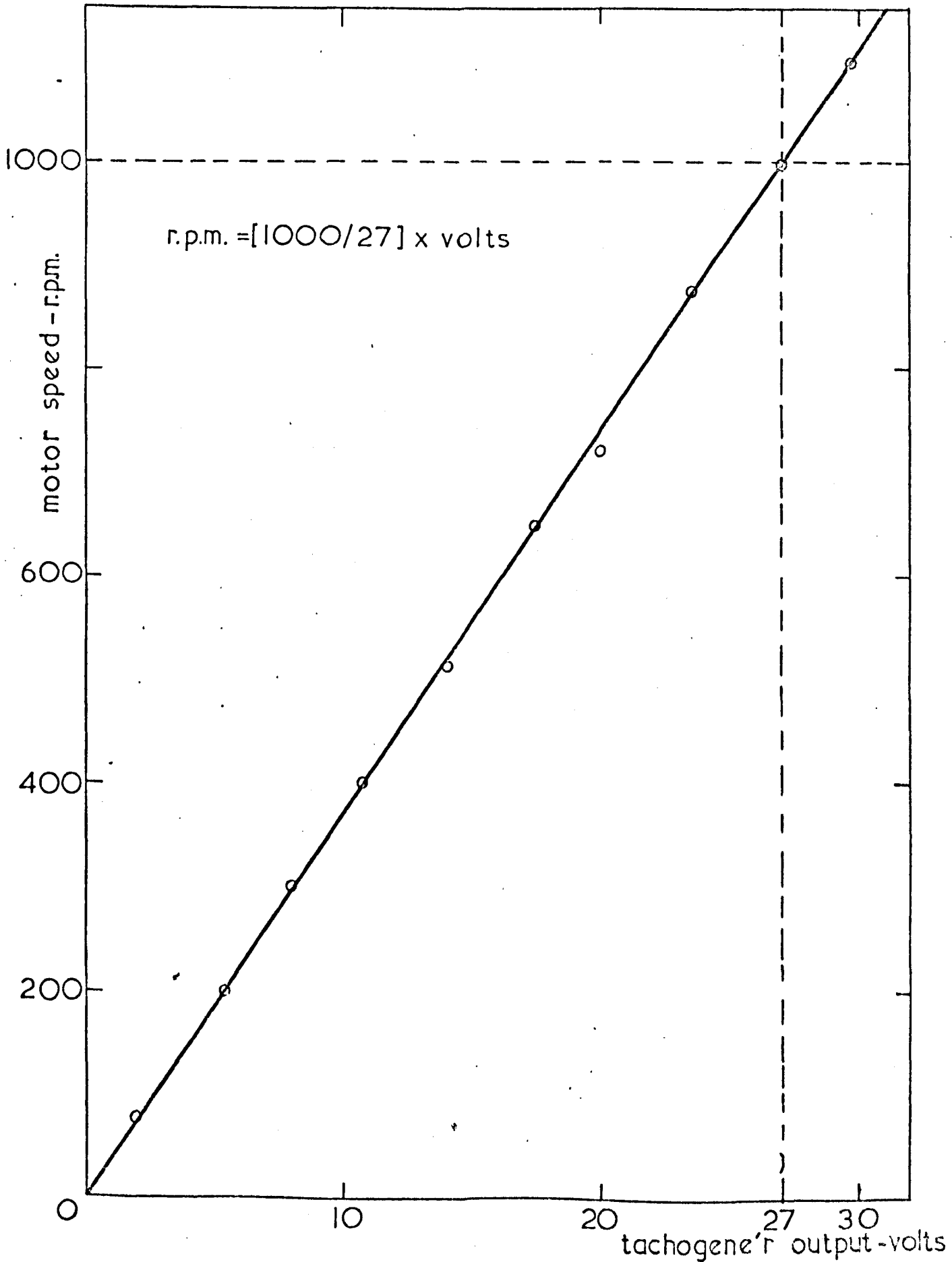
FIG. 6.23 CALIB CURVE; SWIRL GENERATOR DRIVE MOTOR

'PRECAUTIONARY MEASURES'

1. DO NOT EARTH CONTROL SYSTEM.

2. DO NOT SUPPLY ARMATURE WITHOUT FIRST SUPPLYING FIELD.

3. DO NOT INCREASE THE SPEED OF THE MOTOR TOO RAPIDLY.

4. WHEN USING WATER ALWAYS KEEP THE BY-PASS VALVE FULLY
    OPEN.   INTRODUCE WATER GRADUALLY THROUGH THE CONTROL
    VALVE.

CHAPTER SEVEN

THE SPHERICAL PITOT PROBE FOR MEASUREMENT IN SWIRLING FLOWS

7.1   INTRODUCTION

A variety of instruments are available for determining separately the static pressure and the complete velocity vector at a point in a fluid stream. However, only the pitot-static probe, or any other form of it, is capable of determining both these parameters simultaneously. Of the instruments used for velocity measurement some are relatively straightforward whilst others may be quite sophisticated.

Of the three most common types of instrument, the Pitotmeter is undoubtedly the simplest in construction and in use. Current-meters and Laser Velocimeters require sophisticated electronics particularly for signal processing. The choice of a particular instrument will no doubt depend on the nature of the application, information required and economic considerations. In the light of the above, each type is capable of offering a profitable alternative. The Laser Velocimeter is capable of yielding the necessary velocity information in a fluid stream including stream turbulence. Apart from the relatively high initial cost it has an inherent disadvantage in that it cannot be used in opaque ducts. The Hot-wire or Hot-film anemometer suffers from contamination problems, extreme fragility and is very costly to replace. The pitotmeter has the advantage of being relatively cheap to manufacture and is very robust.

Another distinct advantage is that it is the only instrument that may be used in a hostile atmosphere. However, it falls short of the other two in its capabilities.

This chapter deals with the use of a pitotmeter in flow fields where the velocity vector is in yaw and in pitch simultaneously.

7.2   PITOT PROBES IN GENERAL USE

Pitot probes used for the determination of the complete velocity vector and the static pressure simultaneously at a point in a three dimensional flow field (i.e. one in which the velocity vector may be in yaw and in pitch simultaneously) are extensions of the more basic form. Thus factors influencing the deviation of readings from the ideal for the basic form are in general applicable to the extended forms. Effects from several factors contribute to these deviations. These are:

a.   Reynolds number

b.   Turbulence

c.   Pressure gradient

d.   Hole geometry

e.   Local interference

f.   Compressibility (where applicable)

These factors affect readings to varying degrees depending on the type or shape of probe in use. In view of the various combinations of effects possible it has been difficult to account for all of them in any particular situation. However, attempts have been made to isolate and analyse the effect due to each factor separately.

One of the very early review reports on the pitot tube was by Folsom (1956). More recently Bryer and Pankhurst (1971) provided a very comprehensive guide to the manufacture and use of pressure probes.

7.3   PROBES IN YAW AND PITCH MEASUREMENT

Flow measurements in these situations have been carried out using two types of pressure probes; the "spherical or hemispherical five-hole probe" and the "chamfered five-tube probe". The former has been more popular in view of the greater understanding of the flow past a sphere in a fluid stream.

7.3.1   Flow Past a Sphere

The theoretical pressure distribution on the surface of a sphere may be evaluated by considering a three-dimensional doublet in uniform flow, for which

$$p = p_\infty + [\rho u_\infty^2/2][1 - (9/4)\sin^2\gamma]$$ (7.3.1.1)

and $$u/u_\infty = -[3/2]\sin\gamma$$ (7.3.1.2)

where γ , shown in Fig. (7.1), is angle between the velocity vector and the point on the sphere under consideration. When $\gamma = 41^\circ\ 49'$, $u = u_\infty$; the pressure at that point corresponds to the free-stream static pressure.

However, in viscous flow situations there is a slight shift of this optimum theoretical value. Flachsbart (1927) has provided velocity profiles and Tomotika (1935) showed that for $0 < \gamma < 90^\circ$ the former's curve could be represented by

$$u/u_\infty = (1.5 - 0.36402\gamma^2 + 0.024668\gamma^4)\gamma$$ (7.3.1.3)

where γ is in radians. The optimum value for this case occurs when $\gamma = 44^\circ\ 39'$

FIG.7.1 THE FIVE-HOLE SPHERICAL PITOT PROBE
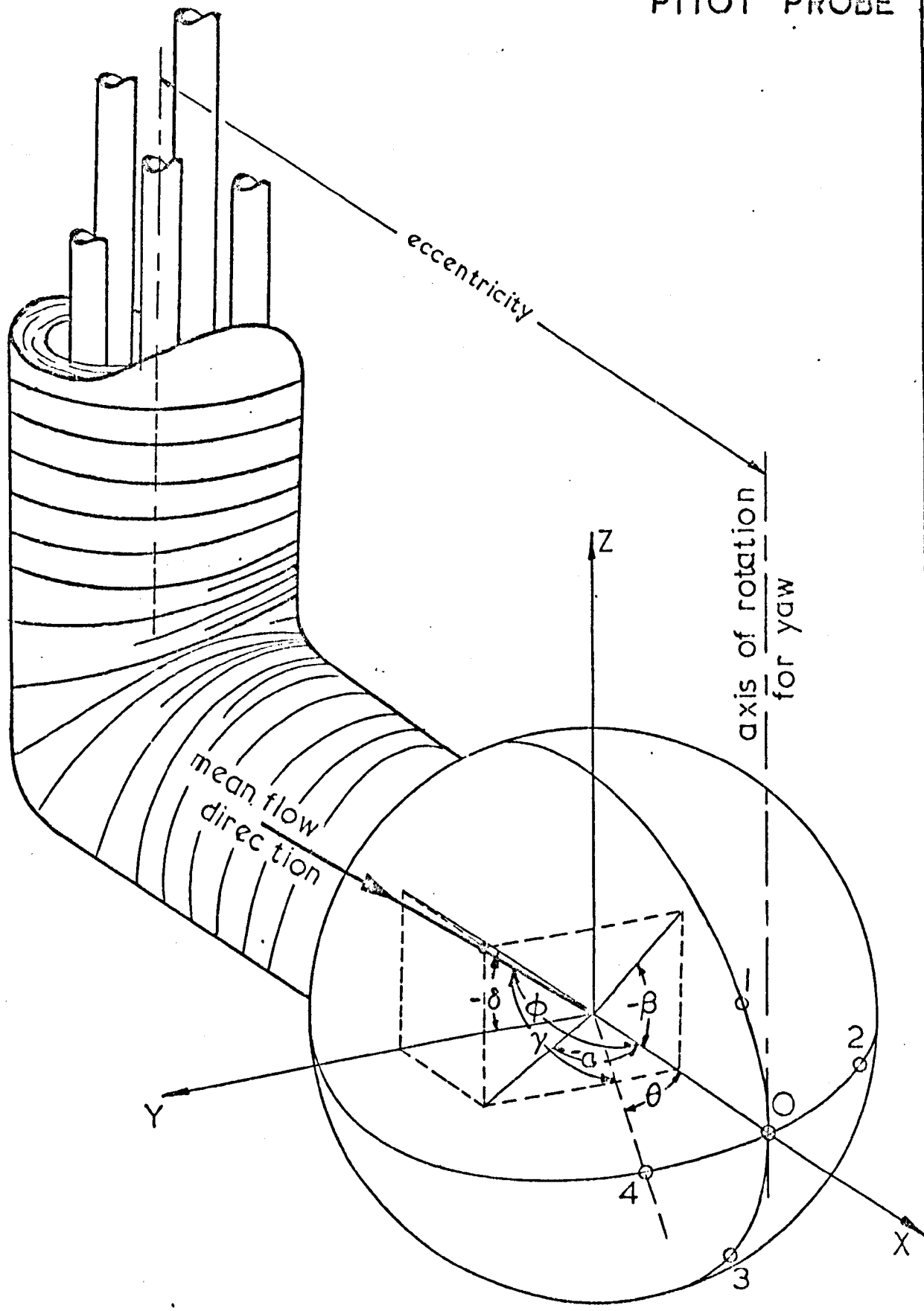
The critical Reynolds number for a sphere is $Re_c = (u_\infty d / \nu)_c$ and lies approximately between $1.2 \times 10^5 < Re_c \leq 3.0 \times 10^5$. Apart from the three usual parameters it is also dependent on such factors as surface roughness, free-stream turbulence and vibrations. The size of the spindle has little effect on pressure and velocity below the critical Reynolds number since the presence of the spindle streamlines the sphere and reduces drag.

7.3.2   Presentation of Calibration Curves

A. Carpet-Plot Methods

Lee and Ash (1956) presented carpet-plots to determine yaw and pitch on the basis of equation (7.3.1.1). Combining the equations for pressure at each of the five holes the following calibration factors were obtained.

$$X(\phi, \delta) = (k_1 - k_3)/(k_0 - k_3) = (p_1 - p_3)/(p_0 - p_3)$$
$$= 2 \sin(2\gamma) . \sin(\delta) . \sin(2\phi)/K$$

$$Y(\phi, \delta) = (k_2 - k_4)/(k_0 - k_3) = (p_2 - p_4)/(p_0 - p_3)$$
$$= 2 \sin(2\gamma) \cos(\delta) \sin(2\phi)/K$$

where $K = 2 \sin^2(\gamma) [\cos^2(\phi) - \sin^2(\delta) \sin^2(\phi)] + \sin(2\gamma)\sin(\delta)\sin(2\phi)$

and $k = 1 - (u/u_\infty)^2 = 1 - (9/4)\sin^2(\gamma)$

Only one octant need be considered in view of symmetry. The magnitude of the velocity vector and the static pressure may be determined from

$$p_0 - p_3 = [\rho \bar{u}^2/2](k_0 - k_3) \qquad (7.3.2.1)$$

$$p_s = p_0 - [\rho \bar{u}^2/2][1 - (9/4)\sin^2(\gamma_0)] \qquad (7.3.2.2)$$

The method is very cumbersome to use as constant reference to the flow map is required.

Care has to be exercised in using the correct forms of X, Y depending on in which octant the velocity vector lay, in order to avoid the occurrence of a zero in the denominator. Lewis (1965) investigated the behaviour of a five hole hemispherical probe employing yaw and pitch factors similar to those already discussed. Similar efforts were made by Nowack (1968) and Dau, et al. (1968).

Chamferred five-tube probes were used by Schaub, Sharp and Basset (1964) with 70° and 90° apex angles. It was possible to measure satisfactorily pure yaw up to about $\pm 15^{\circ}$. Further increase to $\pm 25^{\circ}$ resulted in angular errors of the order of 4% or more. Carpet plots presented were not very different from those of the previous investigators. Since the probes used were of a different type the shapes of the contours were different and as was pointed out by the authors " ---- the plots exhibited considerable irregularity in the contour spacing". Once again the inconvenience associated with carpet plots in application is highlighted.

B. Other Methods

Having recognised the recurring difficulties associated with interpreting calibration curves presented in the form of carpet-plots, investigators sought alternative methods for presentation of calibration curves. The main difficulty was that when a vector was in yaw and pitch simultaneously it was necessary to calibrate it simultaneously as well.

Hale and Norrie (1967) defined an angle factor and a velocity factor,

$$K_{\beta} = (P_3 - P_1)/(2P_0 - P_1 - P_3)$$

and $\qquad K_V = (P_3 - P_1)/[\rho u^2/2]$

respectively, for which the theoretical functions are

$$K_\beta = \sin(\theta).\tan(2\beta)/[1-\cos(2\theta)]$$

and $\qquad K_V = [9/4]\sin(\theta)\sin(2\beta)$

The deviations from these ideal functions were accounted for on the basis of a perturbation analysis. The same factors are applicable whether in yaw or in pitch up to about $\pm 15^{\circ}$ without any significant errors. However, beyond this value the error in angle measurement could be as high as 10%.

Wright (1970) translated the yaw/pitch (α, β) system to the conical/dihedral (ϕ, δ) system (Fig. (7.1)) and defined a conical angle factor which was only a very weak function of the dihedral angle. This permitted the evaluation of the conical angle explicitly. From this point onwards the rest of the parameters could be evaluated without much difficulty. The relevant factors are as follows.

Conical angle factor,

$$K_\phi = \left[1 - [\sum_{i=1}^{4}(P_0 - P_i)]/2[\sum_{i=1}^{4}(P_0 - P_i)^2]^{1/2} \right]^{1/2} \qquad (7.3.2.3)$$

Dihedral angle factor,

$$K_\delta = \tan^{-1}[((P_2 - P_4)/(P_1 - P_3)] \qquad (7.3.2.4)$$

Velocity factor,

$$K_V = \left[[\rho u^2/2]/[\sum_{i=1}^{4}(P_0 - P_i)^2]^{1/2} \right]^{1/2} \qquad (7.3.2.5)$$

Pressure factor,

$$K_p = 2(P_0 - P_w)/\rho u^2 \qquad (7.3.2.6)$$

Corresponding to Fig. (7.1), the relationships

between γ, ϕ and δ (derived in Appendix 7/A) are as follows.

$$\cos \gamma_0 = \cos \phi$$

$$\cos \gamma_1 = \cos\phi\cos\theta + \sin\phi.\sin\theta.\cos\delta$$

$$\cos \gamma_2 = \cos\phi\cos\theta - \sin\phi.\sin\theta.\sin\delta$$

$$\cos \gamma_3 = \cos\phi\cos\theta - \sin\phi.\sin\theta.\cos\delta \qquad (7.3.2.7)$$

$$\cos \gamma_4 = \cos\phi\cos\theta + \sin\phi.\sin\theta.\sin\delta$$

Also the relationship between the angles in the spherical

and cartesian coordinate system (derived in Appendix 7/B) is

$$\tan^2 \phi = \tan^2 \alpha + \tan^2 \beta$$

$$\tan^2 \delta = \tan \beta/\tan \alpha \qquad (7.3.2.8)$$

Introducing equation (7.3.2.7) into equation (7.3.1.1)

and using the resulting equations in equations (7.3.2.3, 4, 5, 6)

it is possible to obtain the theoretical calibration curves. These

theoretical curves provide a useful guide towards calibration.

However, as could be seen from Wright's work, individual calibration

curves are required in practice. Wright's curves are quite

satisfactory except for the velocity factor which behaves eratically.

C. Further Investigation of Wright's Work

The hydrodynamic relationship on which Wright's method

was based assumes a perfectly manufactured sphere with its sensing

holes exactly positioned and hole size approaching zero, placed

in an inviscid flow-field. The varying degree to which these

criteria are satisfied and the effects of the factors discussed

earlier warrant calibration of each probe in situ.

Prive communication with Wright and Witton (National

Coal Board) and Lowes (International Flame Research Foundation)

all of whom have worked extensively in this field, reinforced the view that individual calibration was necessary. Furthermore Wright expressed the view that in the light of the little experience gained with this method of analysis it would be useful to investigate this further. Calibration curves presented by him were obtained with the probe in a jet-stream with the stem in the wake of the sphere; however in applications associated with ducted flow situations, stem effects may well prove critical.

7.3.3   Coordinate System

Owing to inherent practical difficulties associated with probe orientation and the theoretical relationship for the pressure distribution on a sphere, it is convenient to use two separate coordinate systems. When measuring in the duct (probe through side-wall) freedom of movement exists in the yaw direction only, hence cartesian coordinates are used. The pressure distribution on the sphere however, is conveniently expressed in terms of spherical coordinates.

In the conventional cartesian coordinate system, angles are measured relative to the axes in accordance with the cork-screw rule. However, in flow studies it is customary to refer to yaw and pitch with respect to longitudinal axis of the duct; thus there exists an obvious dichotomy. In resolving this it was decided to adhere to the latter. The sign of the conical angle is affected only when flow reversal occurs. The dihedral angle assumes the same sign as the pitch angle and is greater or less than $\pi/2$ depending on whether the yaw angle is positive or negative respectively.

This convention is shown on Fig. (7.1). It is worth noting that during calibration the velocity vector moves in a direction opposite in sense to the movement of the probe. The above convention is necessary only when calibrating, as in application the relevant octant is obtained by considering the relative magnitudes of the pressures sensed by the four side tappings.

7.4   CALIBRATION EQUIPMENT

7.4.1   Design Considerations

Pressure probes for this type of application take one of two standard forms; i.e. right angled or cranked. Rotation of the probe must be effected with the centre sensing hole on the sphere as the centre of rotation. If the cranked form is used rotation is about the stem, the centre line of which passes through the centre-hole on the sphere. This type has the advantage that local interference is minimised, but the larger the crank the greater is the restriction to measurement near the wall. If the duct is small then measurements may be made at the opposite wall, but if the duct is large (e.g. exit end of a diffuser), then this requires an intolerably long stem which will be subject to vibration in addition to increased interference. If the right-angled form is used (Fig. (7.1)) the stem should rotate on a circle whose centre-line passes through the centre-hole. Whilst this form does not suffer from the spatial restrictions imposed by the other, it requires a relatively long foot to avoid local interference. This being much less than that required in the cranked form to avoid "kinking" of the inner tubing during bending.

If the foot is unduly long then the radius of rotation becomes intolerable giving rise to sealing problems and unacceptably large measuring ports.

In the light of the above considerations, since it was necessary to measure near the wall, employing a right-angled probe was mandatory and a compromise of the various problems had to be accepted.

Wright's theoretical considerations indicated that the optimum probe conical angle was approximately 40°. Furthermore he found that a slight deviation from this was not detrimental to the calibration curves. However it was decided to increase this to 45° which, being almost equal to the critical angle (44° 39'), would yield the static pressure. In addition, from a manufacturing standpoint, drilling a number of very small holes on a spherical top is by no means a simple task and the use of a 45° angle instead of a 40° angle alleviates aligning problems. The stem dimensions were arranged so that a standard DISA type anemometer may be used in place of the pitot-probe.

7.4.2 Probes Used and Calibration Tunnel

Two probes, one with a spherical head and the other with a hemi-spherical head were constructed. This was to verify Wright's proposition that latter had an overall advantage over the former. The method of manufacture was as follows; a solid form of the probe head was made first. A female-jig was made in two pieces as on Fig. (7.2). The back plate was dowelled to allow location in any quadrant. The centre hole and one side hole was drilled on the block and on the back plate.
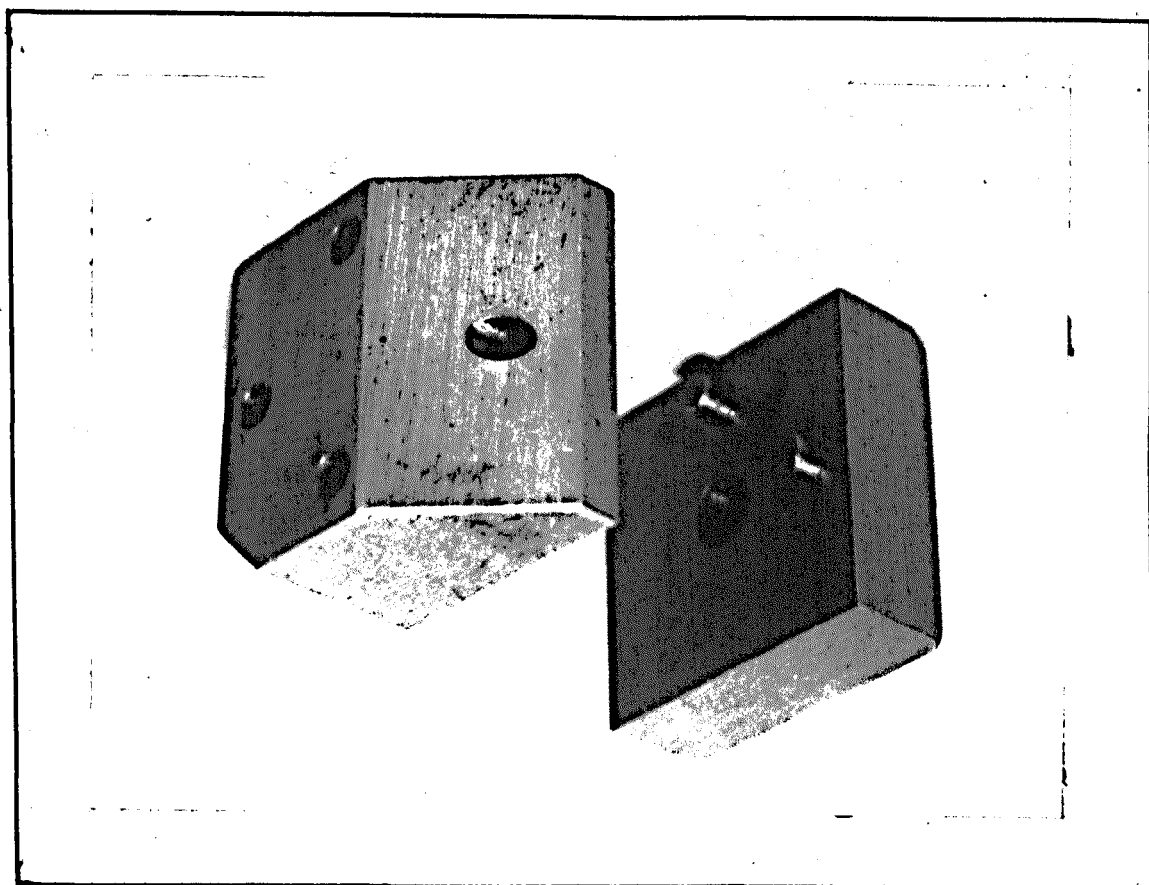
FIG.7.2 DRILL-JIG FOR HEMI-SPH'CAL PROBE H'D
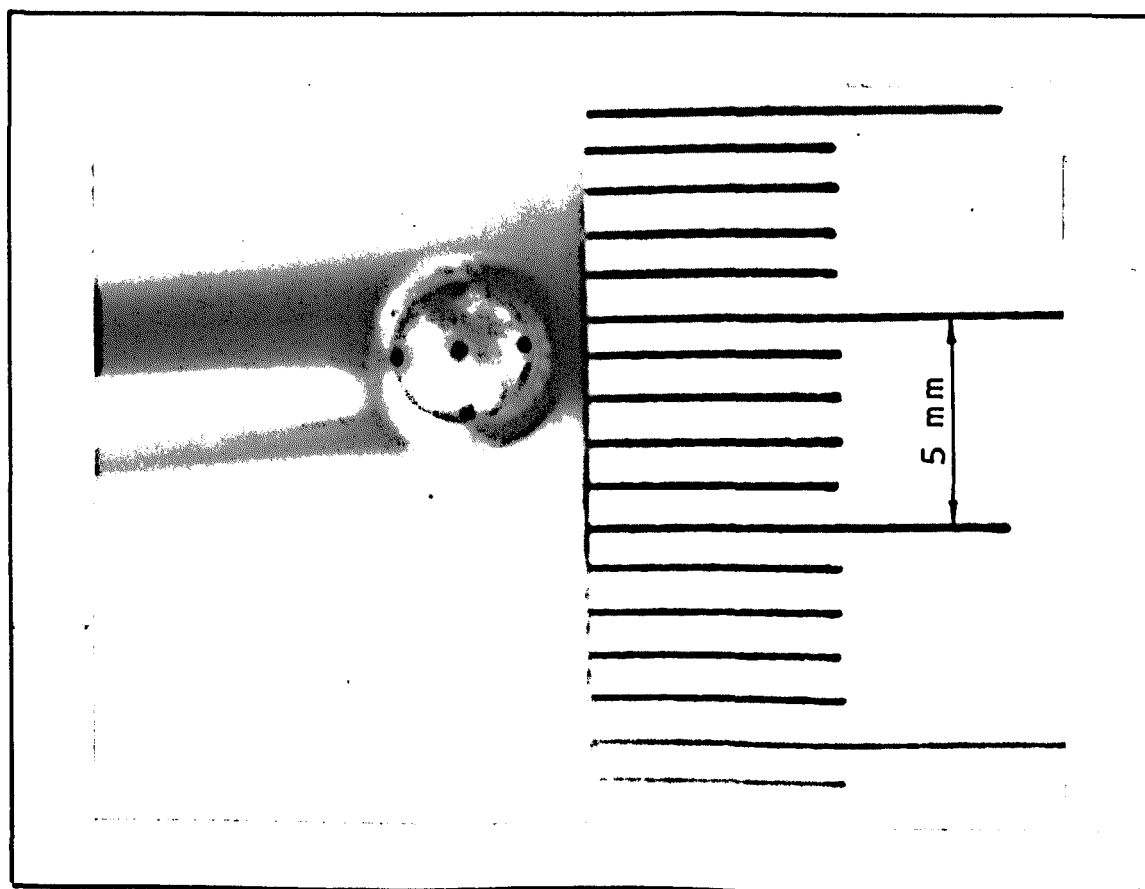
FIG.7.2a THE HEMI-SPHERICAL PROBE

The probe-head was inserted in the block, then the backplate pushed into place and the probe head clamped to the latter. The holes were drilled in turn rotating the backplate on each occasion. The most difficult part during construction was fixing of the head to the stem. The foot (part containing the head) had to be attached at right angles to the stem and the centre-hole and the two pitch sensing holes had to be lined up with the stem.

The manufacturing precision was checked as follows. (Only details of the hemispherical probe are reported as the spherical probe was rejected following early calibration).

(a) Using a shadowgraphic enlarger with a magnification of 100 the probe contour was plotted. The profile error was estimated to be within 1.6% of radius.

(b) The 'SIP UNIVERSAL' (a multipurpose measuring instrument) used with the Goniometer Head to measure the angles between the four side holes showed the error to be less than 1.5°.

(c) The relevant probe dimensions are as follows:

Radius of hemi-sphere   -   2.5 mm.

Eccentricity of probe   -   6.7 mm.

Hypodermic tubing   -   0.8 mm o.d. x 0.1 mm wall

Diameter of sensing hole -   0.33 mm; each hole occupying 7.5° of spherical cap.

Calibration had to be carried out in situ. To do this a special calibration tunnel with facilities for yaw and pitch measurements were designed.Fig.(7.3) shows the details of this along with the probe.
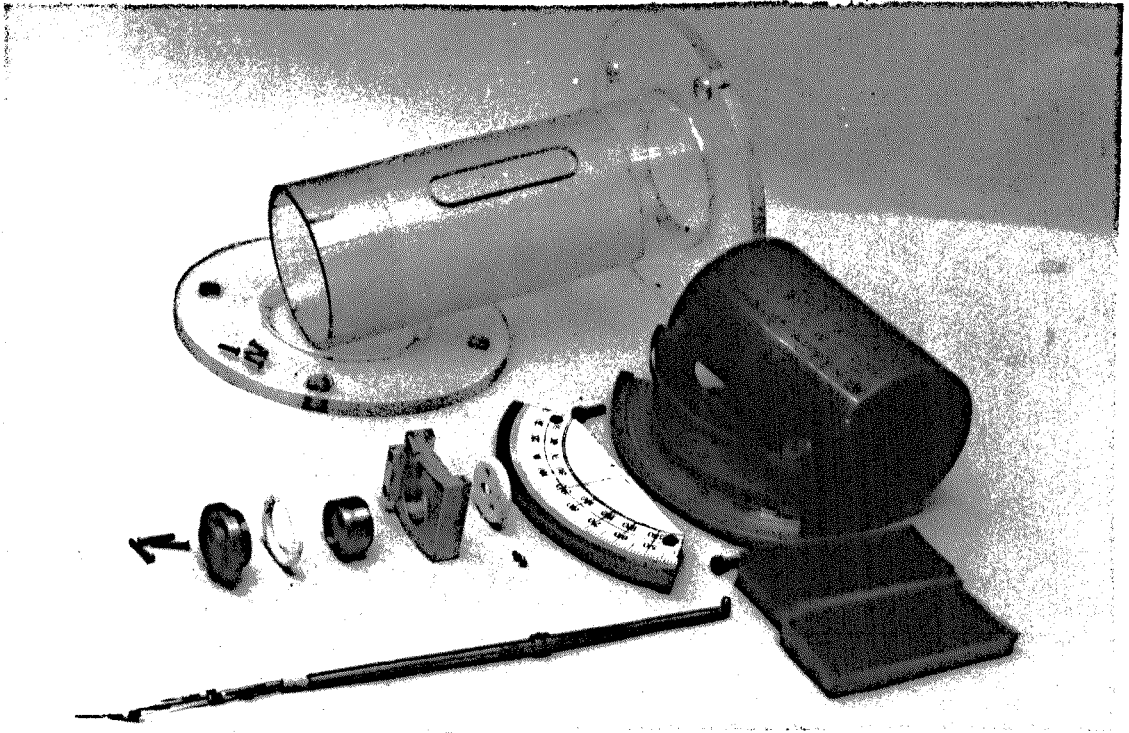
FIG. 7.3   THE CALIBRATION TUNNEL
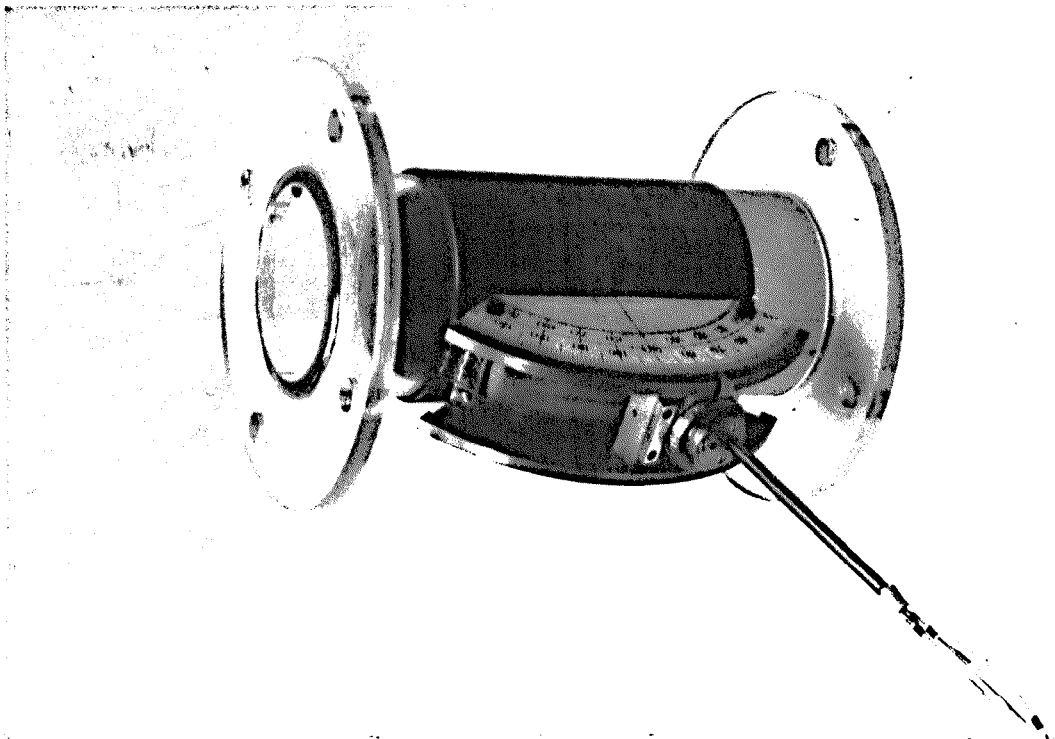
Pressure measurements were carried out using a 'Furness Control MDC type' micromanometer. This uses a differential capacitance transducer with a highly stable bridge network and is capable of measuring pressure differences down to $\pm$ 0.0001 mm. wg. The accuracy in any range is within 1% of full scale deflection. Fluctuating readings were integrated in the time domain using a 'Solartron JM 1776' computing voltmeter. At any instance the voltmeter displays the time mean of the input,

7.5   CALIBRATION AND ANALYSIS

The range investigated was restricted by design limitations to $\pm$ 30° in yaw and in pitch. Using 5° intervals this gives a total of 169 points of measurement and at each point readings of the five sensing holes were obtained. This was repeated for three not very different Reynolds numbers, not to investigate the effects of Reynolds number but, to obtain separate samples of the same population assuming that this parameter has no significance. Thus the calibration curves are the result of more than 2500 pressure readings. Initially each measuring point required about 10 minutes to obtain a steady value owing to fluctuations in readings. This unacceptably long procedure was later reduced by over half by using the computing voltmeter to obtain an approximate mean value and smoothing the results subsequently. Even with these improvements calibration consumed about 100 man-hours.

The raw probe characteristic curves are shown on Fig. (7.4). Close examination (e.g. Fig. 7.4a)) will reveal that the

FIG.7.4 CHARACTERISTICS OF
HEMI-SPHERICAL
PITOT PROBE
FROM TABLE 7-I

$k \times (P_o - P_r)$

250

240

-20   -10   O   pitch $\beta°$ 10   20

yaw a° 0

-20   -10   10   20

(a)

(b)

$k \times (\rho - \rho_r)$

100

50

-20

-10 pitch

0

10

184

$\frac{kx}{(P_2 P_r)}$

100

50

20

10

0 pitch

-10

-20

(c)

185
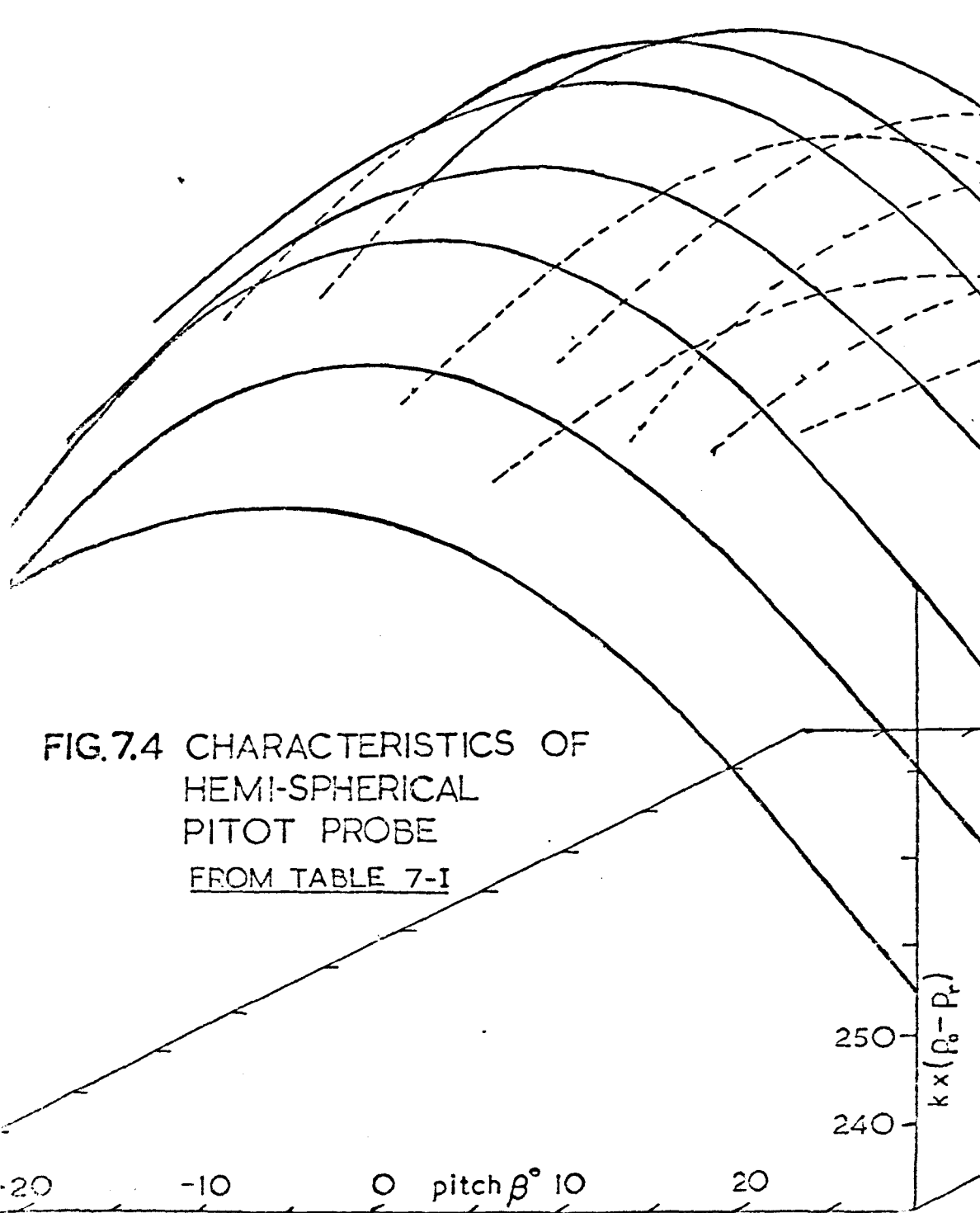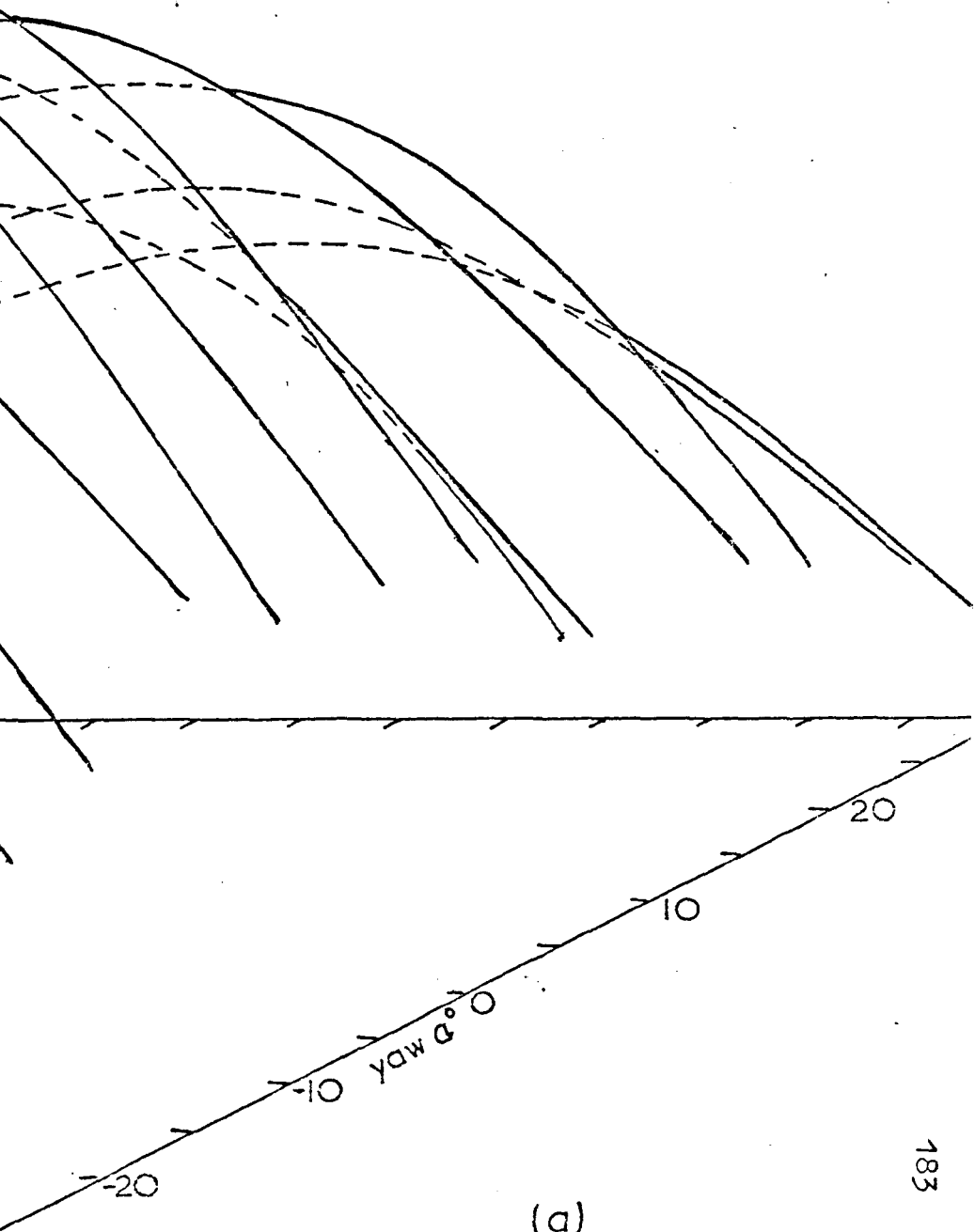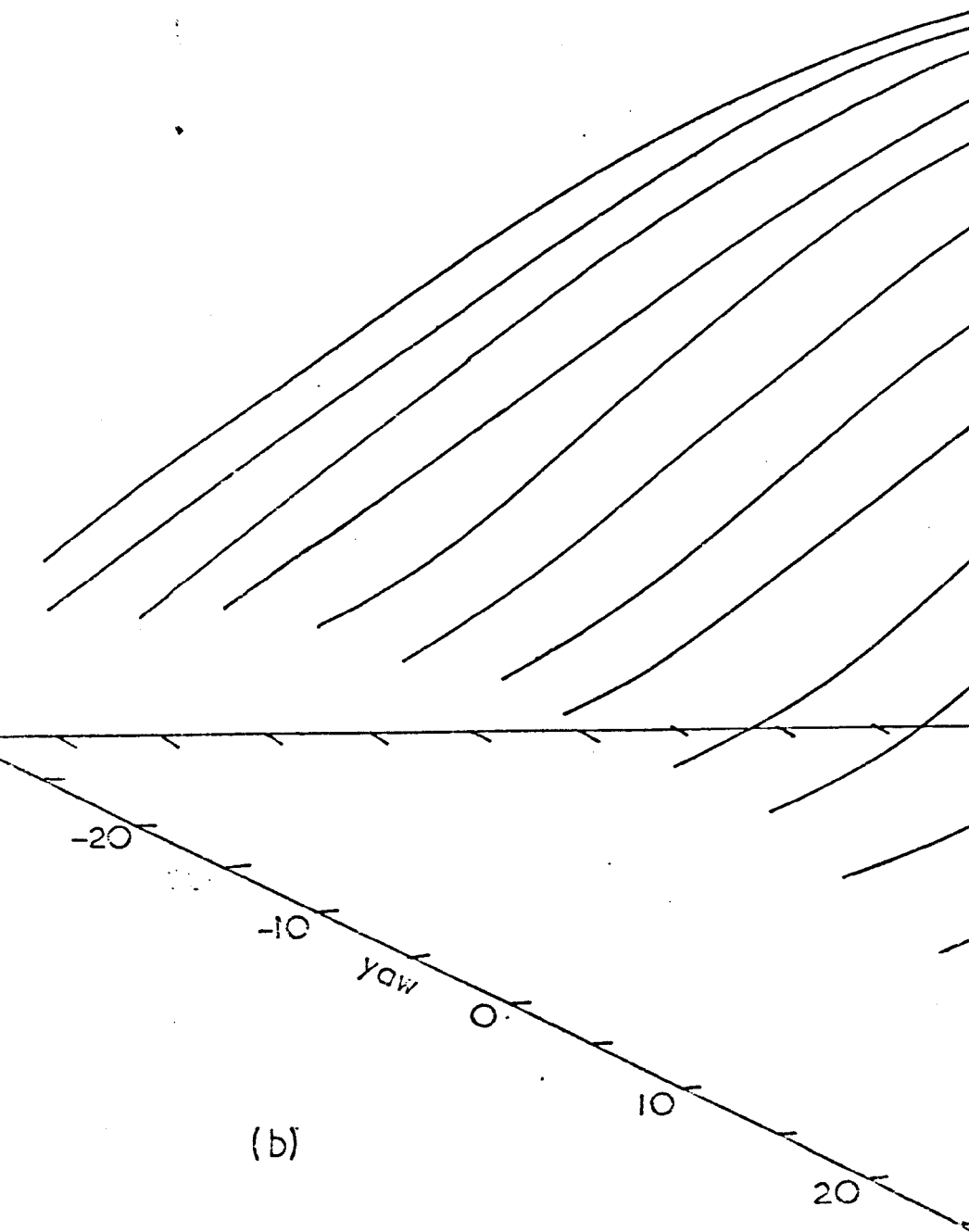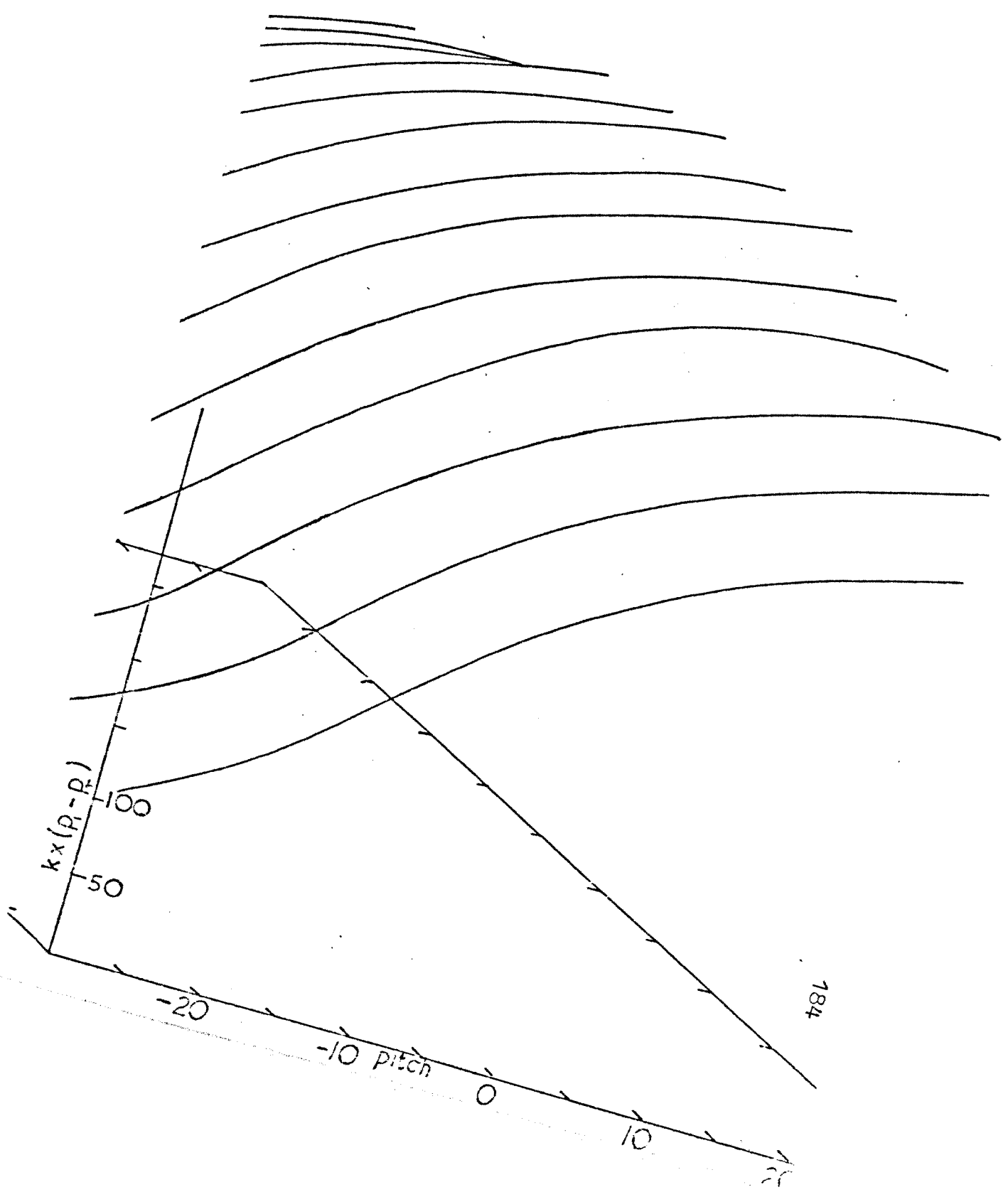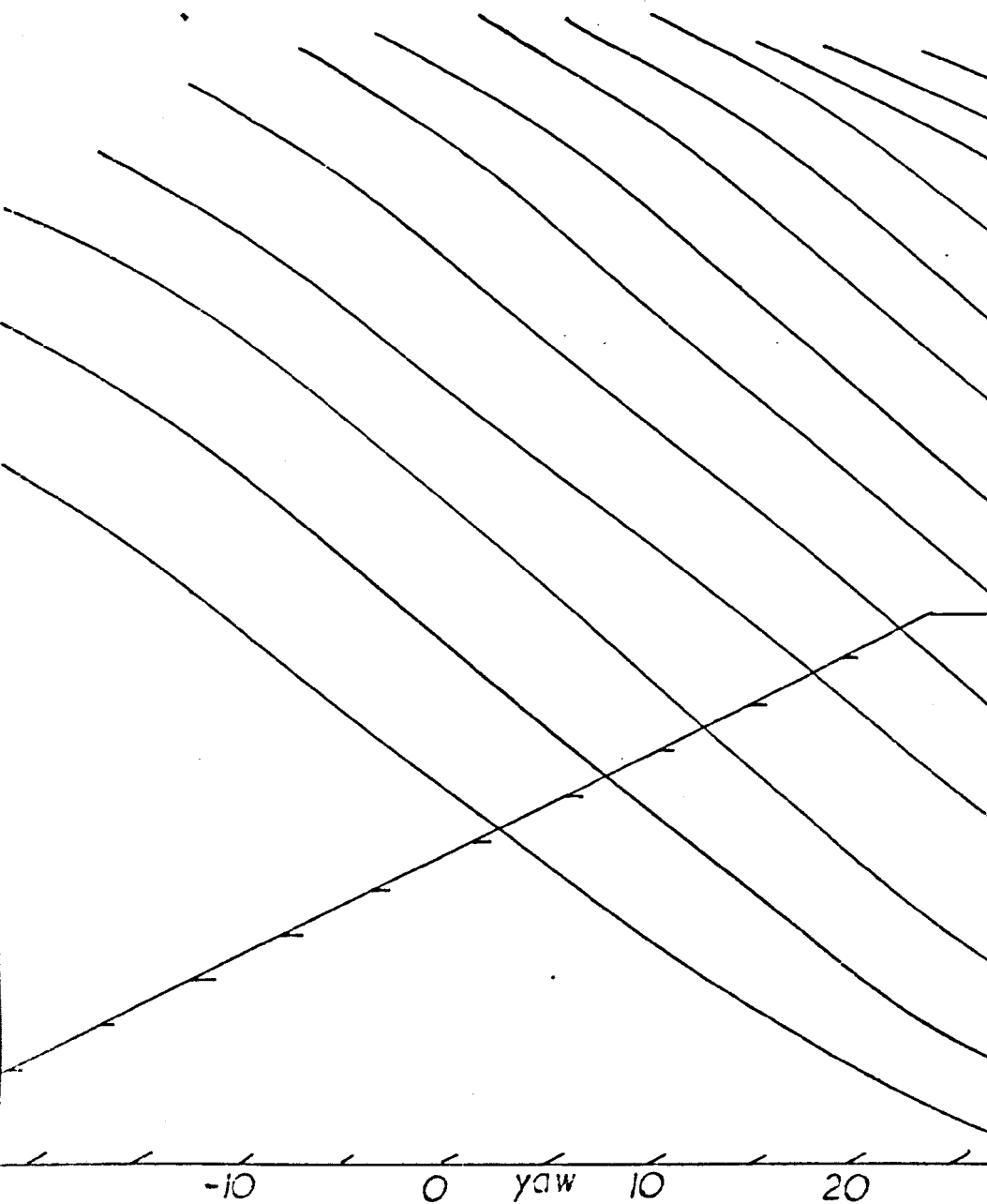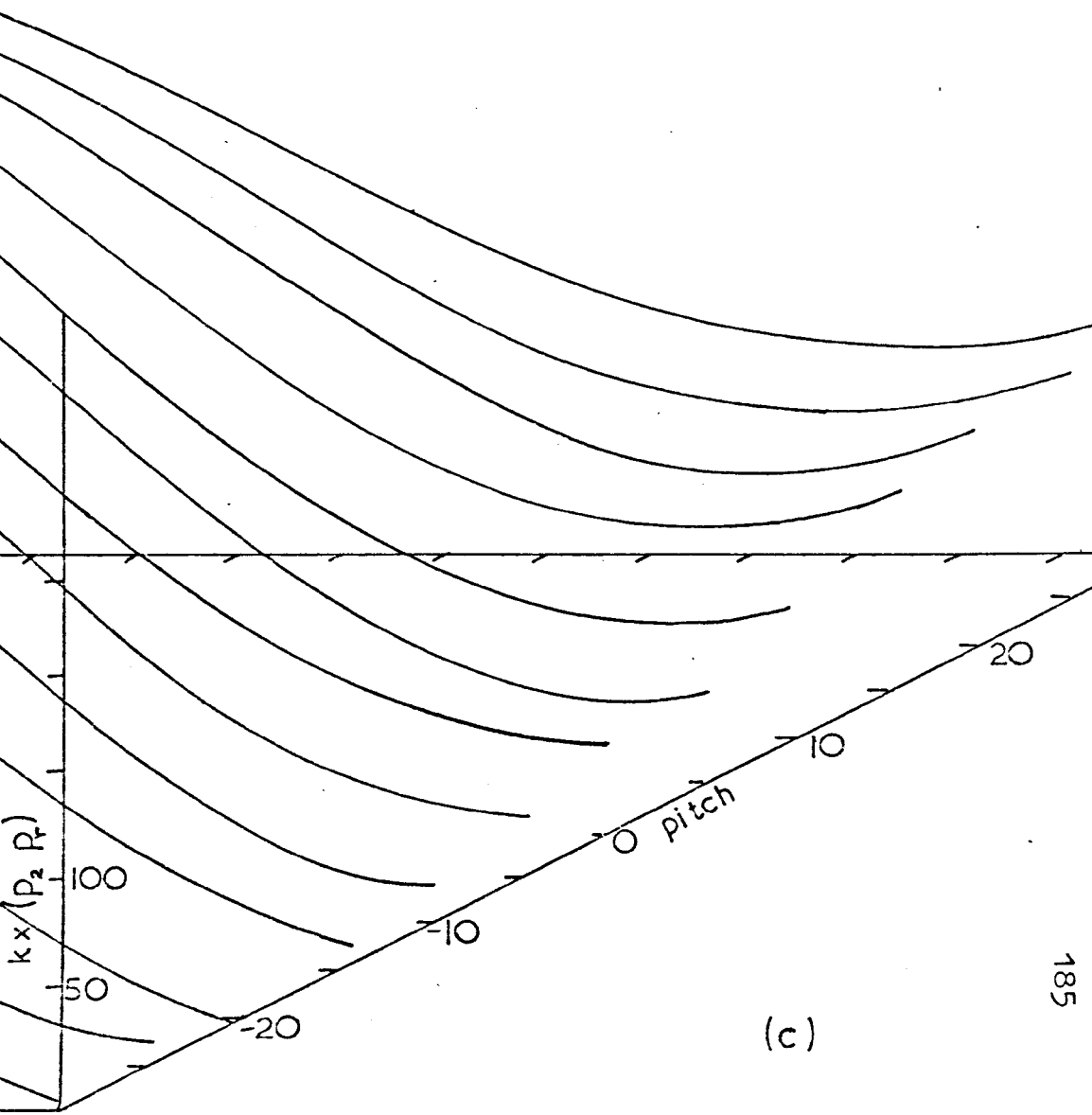
surface defined by the curves is uneven. The standard least squares method for obtaining the best fit is not suitable in this case as simultaneous smoothing in two planes (pitch and yaw) is required. Such a technique (useful in many applications) which is capable of identifying and replacing unacceptable 'rogue' points was developed and is reported in Appendix (7/C).

The suitability of the method of analysis proposed by Wright was investigated. As seen from Fig. (7.5) the conical angle factor (K_ϕ) was satisfactory. However it was not possible to obtain a suitable curve for the dihedral angle factor (K_δ). The various attempts made to see if the effect of the stem could be eliminated proved unsuccessful and as a result Wright's method had to be abandoned. Further close investigation would be required to correct this non-linear effect of the stem. If the swirl angles are less than about 30° it is possible to use the method of Hale and Norrie. This provided an estimate of the radial velocity which was negligible. It was much simpler to yaw the probe to obtain a null reading on the two side holes. Balance could be achieved and the angle read (off a scale) to better than one degree in steady flow conditions. Fig. (7.6) shows the suitability of the characteristics to obtain this balance. The suitability of this method for static pressure measurement was verified and the results are seen clearly from Fig. (7.7). The centre sensing hole is insensitive to about 3° when aligned in the flow direction. Thus velocity measurements are free from errors due to small misalignments and the neglecting of the radial velocity.
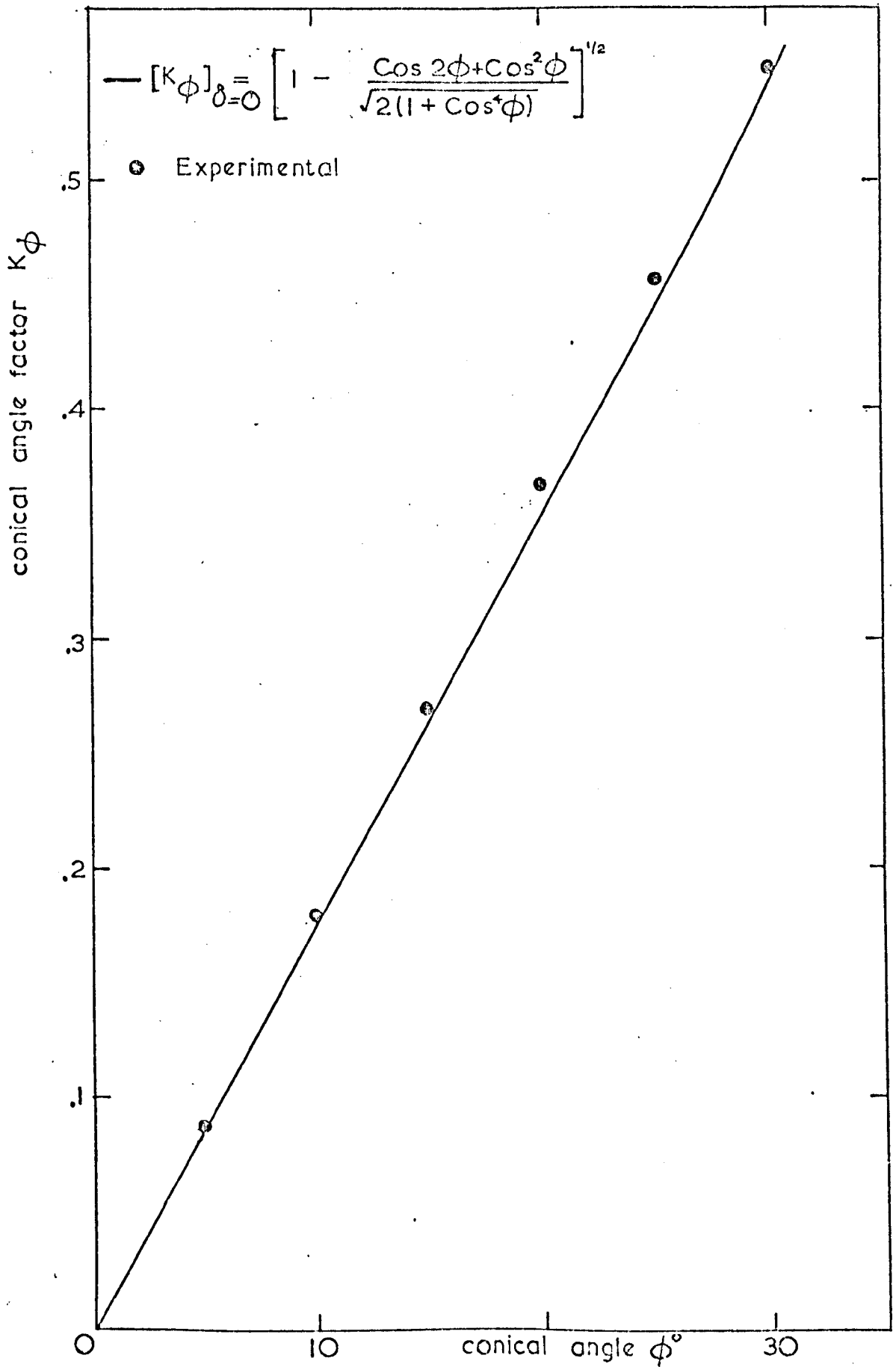
FIG. 7.5 CALIB. CURVE FOR HEMI-SPHERICAL PROBE

FIG. 7.6 CURVES SHOWING SUITABILITY OF p_2 AND p_4 FOR BALANCING PROBE

$(P_2 - P_r)$

$(P_4 - P_r)$

k × press — N/m²

angle of yaw $a°$

-20   -10   10   20

300

200

189
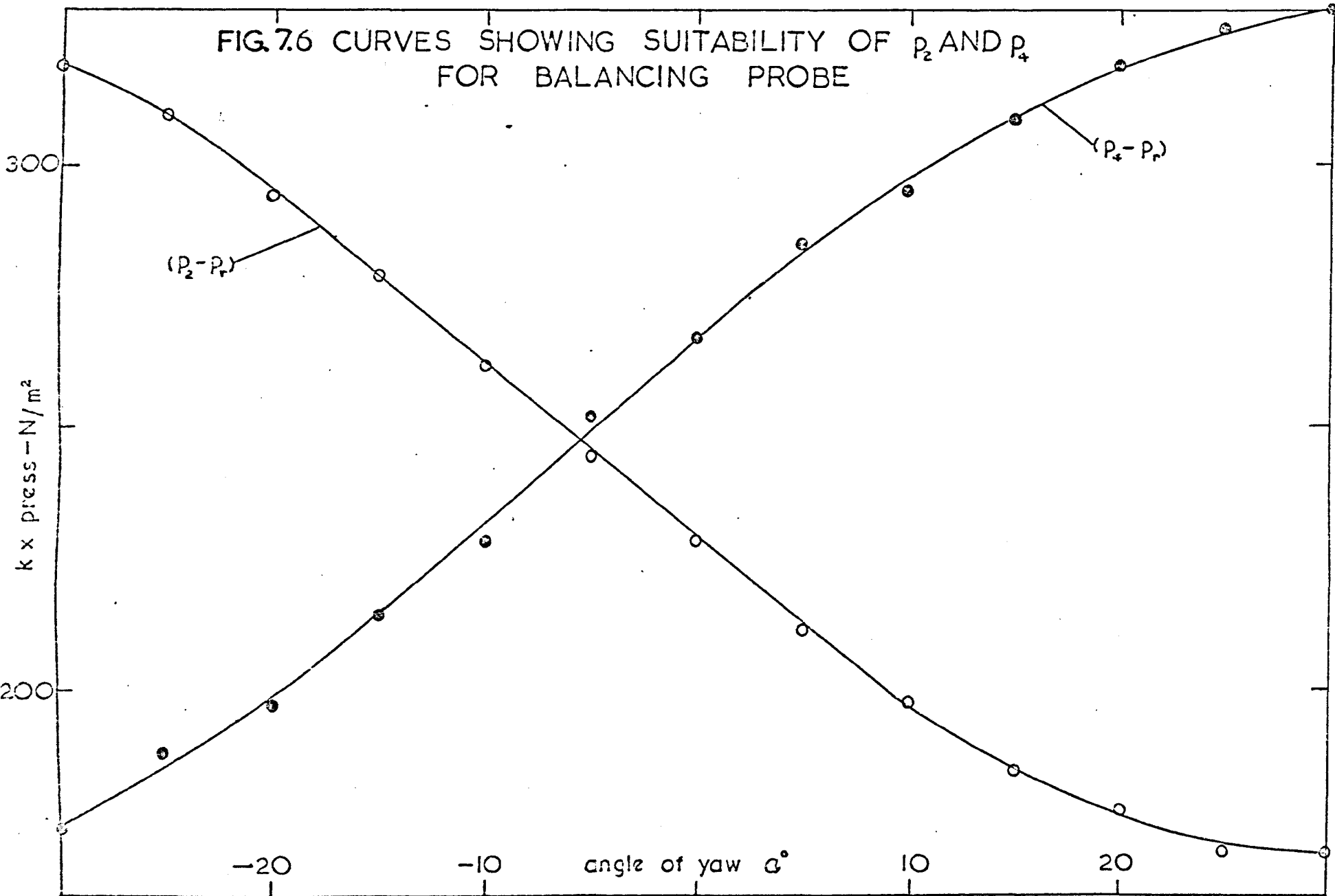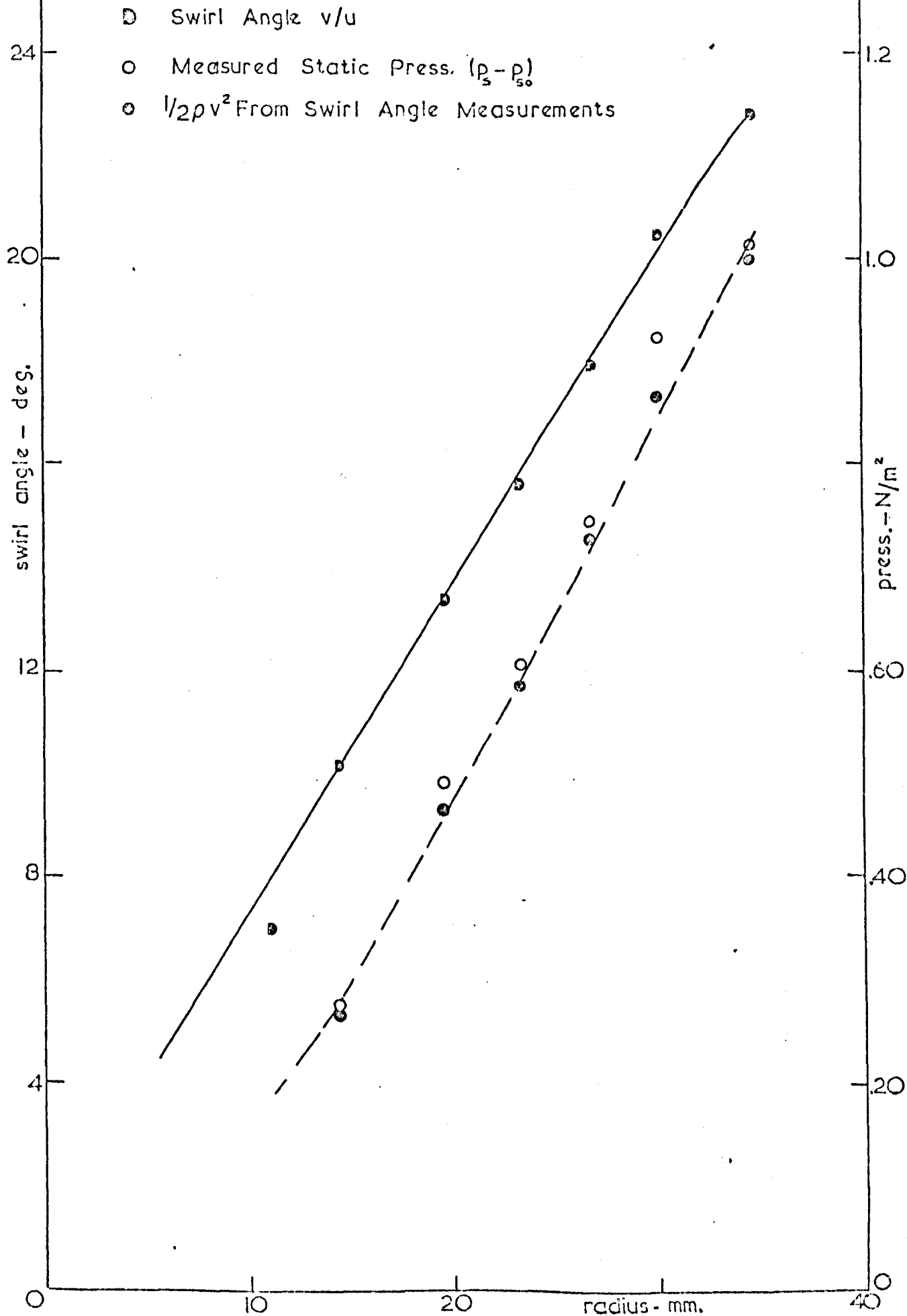
FIG.7.7 SWIRL ANGLE AND STATIC PRESS. MEASUREMENT
USING HEMI-SPHERICAL PROBE

7.6 CONCLUSIONS

The analysis carried out indicated that it is not possible to use the method proposed by Wright, owing to stem effects, without further analysis. In the present investigation the swirl angle is measured by obtaining a null-reading of two diagonally opposite sensing holes. The static pressure is obtained directly from the side sensing holes.

CHAPTER EIGHT

FLOW VISUALISATION STUDIES IN WATER

8.1   INTRODUCTION

        The main purpose in building the test-section in perspex

was to observe the occurrence of the classical vortex breakdown

phenomenon and the events leading up to and following it. Recording

techniques such as measurement, photography, etc., lend themselves

quite well to postmortem analysis and comparison of results. Before

any recording technique could be profitably employed it is

necessary to obtain a reasonable assessment of the situation through

observation. However the major disadvantage associated with

observation studies is that it can only provide an instantaneous

assessment of the behaviour and neither after-study nor close

scrutiny is possible and furthermore it is subject to human error.

The essential details of a survey of techniques of flow visualisation

is included for completness.

        A comprehensive review of the work associated with vortex

breakdown was provided in Chapter 4. As the purpose behind each

programme was different so were the experimentation and the governing

boundary conditions. Hence it is not possible to make a direct

comparison between any of them. Of these only Harvey (1962) and

Sarpkaya (1971, 1971a) studied breakdown in a bounded flow field.

It is worth recalling that Harvey experimented with air and used

Titanium Tetrachloride to study the breakdown in a tube .

Sarpkaya, however, using a diffuser, conducted his studies with water or more appropriately in water as his entire test apparatus was immersed in water. Both investigators used guidevanes to generate 'exponential' type vortex and confined their experiments to laminar flow. Stability in a 'rigid body' type vortex was studied by Talbot (1954). He too confined his work to the laminar range and used a rotating pipe section to produce swirl. Talbot did point out that his rotating section was too short to produce a proper 'rigid body' type vortex.

As far as the author is aware, the present project is the only one to attempt to investigate and photograph the breakdown phenomenon in turbulent flow.

To gain a broader understanding of the phenomenon it was necessary to investigate initially the development of vortex breakdown in a pipe (i.e. a diffuser with zero divergence angle) and then extend the investigation to study the effect of an adverse pressure gradient on this. Owing to several difficulties, discussed in the ensuing sections, it was only possible to observe and photograph the events in a pipe. Observation of the phenomenon inside the diffuser was unsuccessful. In the main, deductions were made purely from observations and wherever possible photographs are provided to supplement the discussions.

8.2.   FLOW VISUALISATION AND TRACER AGENTS

Most cases of flow visualisation, other than those associated with imaging techniques, essentially consist of the introduction of a tracer agent into the flow field and observation of the resulting behaviour of the agent.

Over the years a wide variety of techniques have been developed and used for flow visualisation studies. The techniques used may be classified under two groups: viz., Static Methods and Kinetic Methods, within which several sub-groups exist.

The static method basically consists of treating of the boundary of the flow field with an agent which is sensitive to the flow and studying the effects of the flow on it. This sensitivity may either be a reaction between the agent and the fluid or even etching of the treated surface by fluid friction. They are rather limited in their usefulness in that they are only capable of yielding information in the boundary layer region. In general they are a useful supplement to kinetic methods. As pointed out by Clayton and Massey (1967) in their review, static methods are only suitable for systems in which at least reasonably steady flow conditions prevail.

Kinetic methods (tracer-agents that move with the fluid) however may yield a wealth of information, depending on the degree of sophistication of the technique employed. In the present research programme only kinetic methods were considered. Tracer-agents may be gaseous, liquid, or even solid. The necessary features of a good tɡracer-agent are

1.   It must be immiscible in the main fluid.

2.   It must not alter the properties of the main fluid.

3.   It must not cause any resistance to flow.

4.   If not recoverable it must be of relatively low cost.

Obviously it is impossible to obtain an agent satisfying every condition; the degree of tolerance exercised in the choice of a

particular agent depends entirely on the application at hand. The
first of the requirements stated may be over-looked provided the main
fluid is not used in a ring-main or if observations are made in short
intervals, between which the polluted fluid is discharged and the
system replenished with fresh fluid.

When the main fluid is water, hydrogen bubbles or air
bubbles may be used successfully. In the present study the natural
low pressure regions at the centre of the vortex attracted any
entrained air towards the axis. This was very convenient as it
eliminated the unnecessary complication of setting up an apparatus
to generate hydrogen bubbles. In addition to the use of air, a liquid
agent namely nitrobenzene and olive oil (mixed to give a relative
density of 1.0) and a solid agent, polystyrene particles, were used.
As will be seen from the ensuing discussions, each had a useful
function to perform.

Use of particles as tracer agents is also quite common
practice. Some of the more popular agents are lycopodium, aluminium
powder and more recently, polystyrene waste.

Before the availability of polystyrene, aluminium powder
was widely used. It is generally coated with wax to reduce the
compound density to that of the main fluid. This undoubtedly is a
tiresome process. Clayton and Massey point out that an aqueous
suspension may be made from small spherical particles of aluminium
which must first be wetted in alcohol and then vigourously shaken in
a bottle. A drawback to the prolonged use of aluminium particles is
that they soon became tarnished by an oxide film.

Polystyrene "waste" is now almost exclusively used in preference to aluminium. It has the advantage that it is cheap, and has a relative density in the range 0.98 - 1.02. Werle (1953) points out that the density of polystyrene could be sufficiently reduced by treating it with acetone.

The major disadvantage of tracer particles is that they are not suitable for use in a ring-main unless it can be separated at discharge and reintroduced just upstream of the test section. This is because they tend to block pressure tappings, flow into manometer lines, clog valves and get into the pump.

A very useful and comprehensive review of flow visualisation in water is provided by Clayton and Massey about which they say "... it is intended to be useful rather than exhaustive."

8.3.   EXPERIMENTAL APPARATUS

Details of the apparatus were provided in Chapter 6. Here it suffices to report the particular arrangements used in each experiment. The development of vortex breakdown was investigated with sections 3 and 6 (Fig. (6.2a)) on either side of the 30° diffuser. The upstream movement of the initial core was investigated with sections 3, 4, 5 and 6. This was to provide sufficient length for the core to travel.

Mean flow rate was measured using an orifice-plate with a mercury manometer, Fig. (6.16). The 'step-down' ratio was used in the swirl generator drive. Most of the photography was conducted on standard 35 mm (50 ASA) film but in some cases a much faster (125 ASA) film had to be used.

8.4   EXPERIMENTAL WORK

As pointed out earlier, the fact that the test apparatus
was not purpose built for a particular investigation, but for an
entire range, undoubtedly caused some difficulties. This was
foreseen before the designs left the drawing board, but it was
decided to tolerate a degree of inconvenience for greater latitude
of investigation.

For the purpose of studying the effect of increasing swirl
a fixed flow rate was maintained. No less than three tracer agents
were used for flow visualisation. Whenever possible air was preferred
for visualisation as it was the least troublesome. A controlled supply
of air was maintained with the aid of a needle valve positioned upstream
of the swirl generator. Judicious positioning of the valve ensured
that air was sucked into the system. Polystyrene particles proved to
be a very useful agent under certain conditions. These were obtained
from commercially available 'polystyrene waste'. They were sieved to
obtain an average size between 300 $\textit{\&}$ 500 microns. Fig. (8.1) shows the
size distribution of a few such samples whose specific gravity is 1.025.

To study the effect of swirl the swirl-rate was increased
in discreet increments. On each occasion the flow was allowed to
settle down and all three tracer agents were introduced in turn.
Much time was spent exploring the various developments in an effort
to determine the axial flow rate most suitable for the range of the
swirl generator. In addition the length of ducting upstream and
downstream were also altered during the exploratory stage. Three
diffusers (10°, 20° and 30°) were also used initially. It soon
became apparent that in addition to its dependence on swirl-rate, the
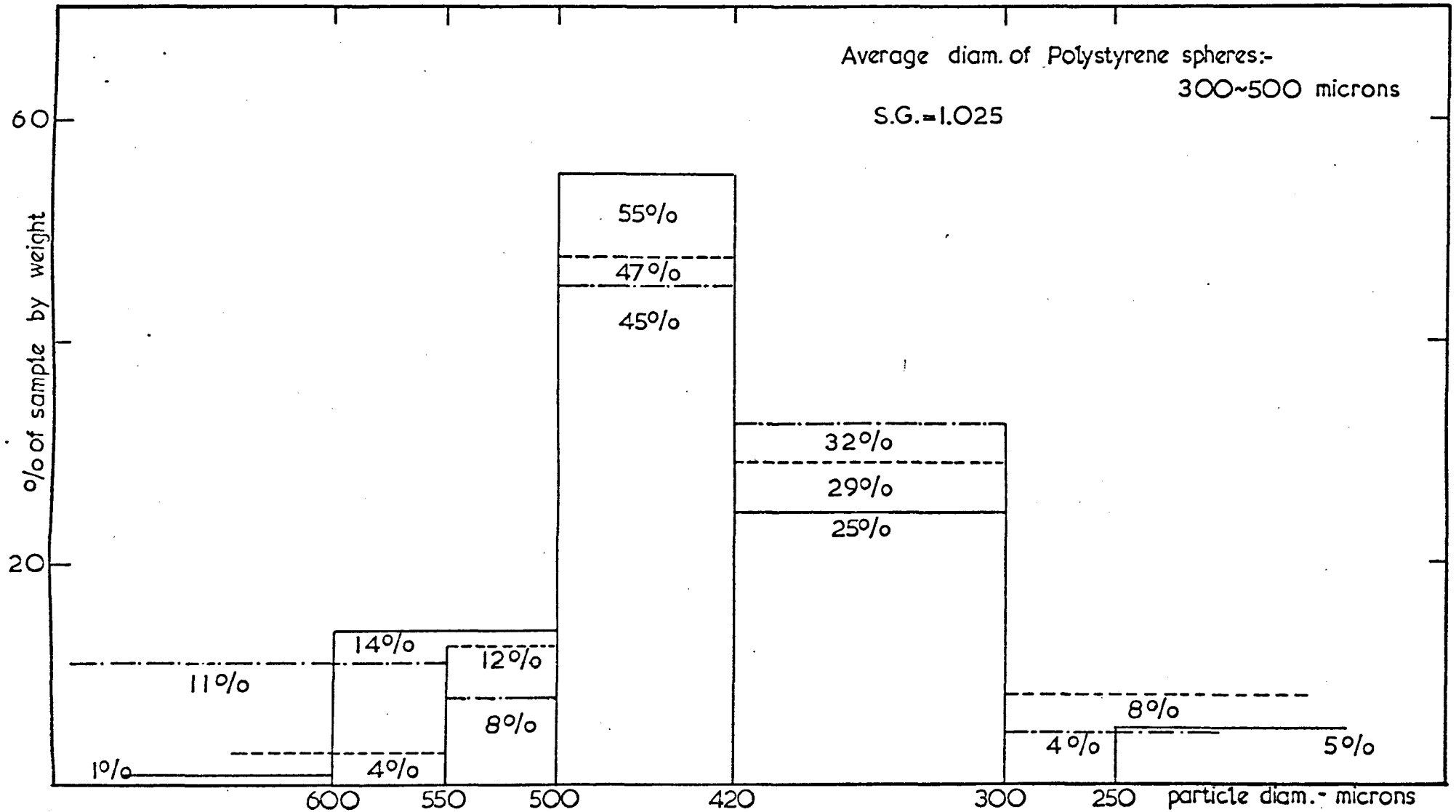
FIG.8.1 SIZE DISTRIBUTION OF POLYSTYRENE 'WASTE'

breakdown phenomena were dependent on the geometry of the diffuser, the lengths of ducting upstream and downstream of the diffuser and the axial flow rate. It was decided to reduce the number of variables by employing a fixed geometry and a fixed mass flow rate.

Observations made were subject to random human error. A close study of the development of the various forms was required and in a case such as this, where patterns execute a variety of antics, relating them to a particular sequence was an arduous task. Long hours had to be spent training the eye to pick up as much detail as possible and recording them each time. The rotational speed at which any particular phenomenon appeared was noted as accurately as possible. This appeared to vary from one period to another. This was attributed to human error as in observing an irregular occurrence and comparing it with a similar occurrence in the past a loss of a certain degree of accuracy is inevitable. However with a trained eye and a prior knowledge of the sequence the task did seem less difficult. The ideal solution would have been to record on cine-film the behaviour for each discrete increase of speed. This too would have caused problems as the phenomena are time-variant. The cost of this would be prohibitive and furthermore analysing such a large quantity of film would not have been an easy task.

The test-rig could not be run for more than two hours at a time as the water became appreciably warm. In addition very fine bubbles collected on the walls of the test-section thus obscuring the view.

The problem of heating up of the water was overcome by adding ice regularly. A very small amount of detergent (washing-up liquid) was added to arrest the bubble formation. This improved the situation but by no means eliminated it. It should be mentioned that these very same bubbles were necessary for flow visualisation and if removed completely the original purpose would have been destroyed. However with these improvements a continuous running-time of about four hours was possible. About 25 points were considered for increase of speed between 0 - 40 volts of the tacho-generator. They were not at fixed intervals as some ranges were not critical. About two hours were taken for the entire range which was immediately repeated. This was conducted for about a month with a day's break in between because of the hypnotic effect that developed when the same behaviour was observed continuously. With 4 - 6 points at each speed setting it was possible to eliminate some of the errors associated with observation studies. Photographic work too required quite a lot of effort owing to the faintness of the subject. Fig. (8.2) shows the arrangement used for photography. Over 100 photographs were taken to obtain a photographic record of the breakdown phenomena in their various modes.

8.5   OBSERVATIONS

8.5.1   The Development of Vortex Breakdown

To investigate the effect of increasing swirl a fixed axial flow rate was maintained. To aid flow visualisation air was allowed to enter the test area at a controlled rate.

At zero swirl the entrained air passed through the stationary swirl generator, floated to the top of the test section and travelled downstream towards the discharge.
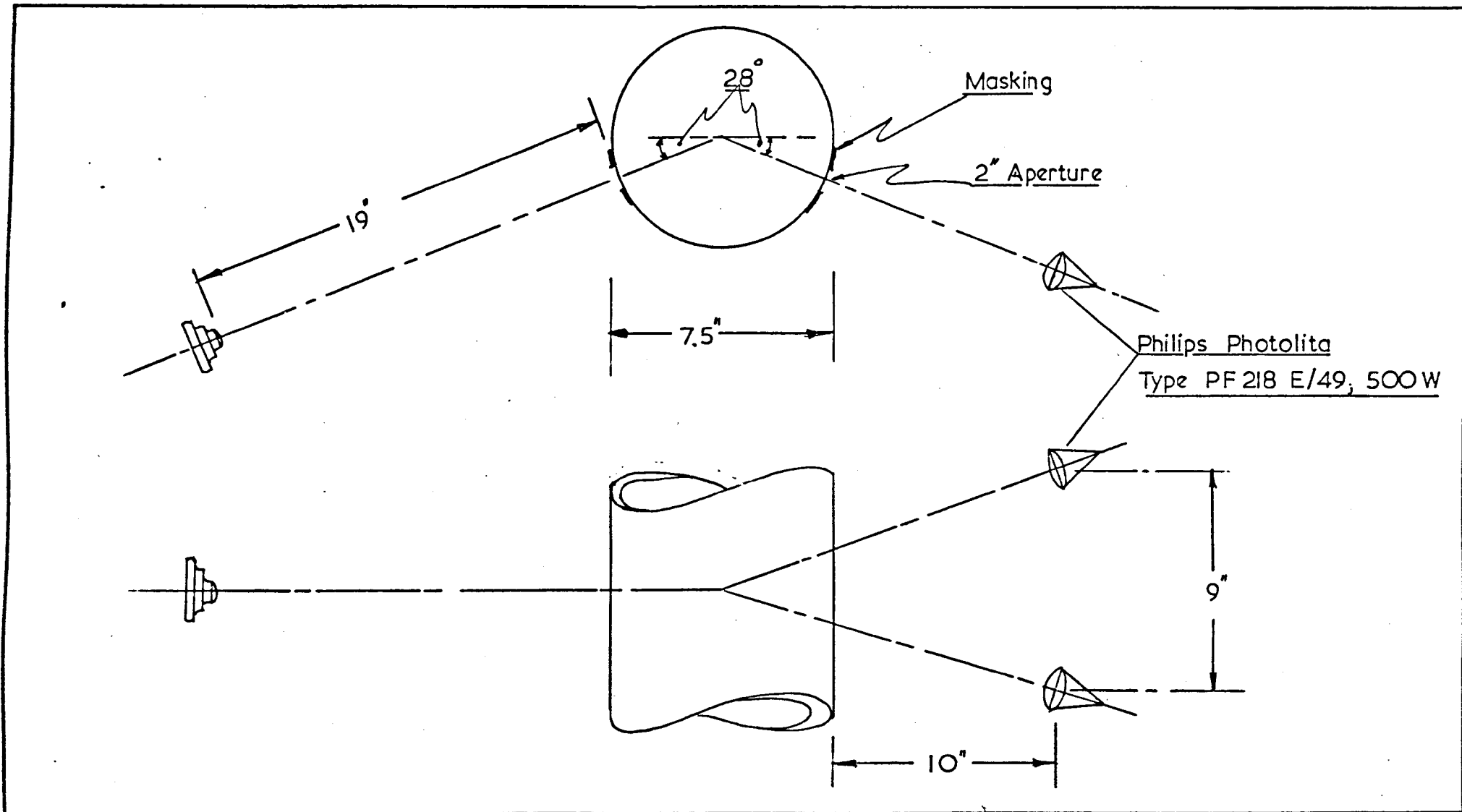
FIG. 8.2 ARRANGEMENT FOR PHOTOGRAPHY

Labels within figure:
- 28°
- Masking
- 2" Aperture
- 19°
- 7.5"
- Philips Photolita Type PF 218 E/49, 500 W
- 9"
- 10"

With the gradual introduction of swirl initially there was no
change in the flow pattern except that a slight twist was imparted
to the flow. As swirl was increased further minute air bubbles
tended to remain longer in the central area of the duct before
floating to the top. At this point polystyrene particles were
introduced through a side tapping near the area under consideration.
These particles began to execute random motion in the central area
of the duct instead of floating to the top like the lighter air-
bubbles. Fig. (8.3a) shows this, though very faintly. Fig. (8.3b)
shows the formation of an axis of polystyrene on further increase
of swirl. Still there was a continuous loss of particles and air
bubbles. With continuous increase of swirl this axis moved upstream
until it covered the entire duct. However observations were confined
to one area of the test section.

At this stage the supply of air was curtailed as the larger
bubbles tended to disturb the polystyrene-axis. The axis was by no
means well defined and its appearance was very irregular. On
further increase of swirl the axis became more permanent though it
oscillated forwards and backwards. There was still an overall loss
of particles indicating that flow reversal had not occurred. Further
increase of swirl triggered an pseudo-resonant state. This was
characterised by large distortion of the particle-axis executing a
'whipping' spiral motion as shown in Fig. (8.3.c). This is not a
vortex breakdown phenomenon as the axis does not degenerate at any
point.

As swirl was increased further some minute air bubbles appeared around the axis. They seemed to be entrained air separating from the water. It was a tussle between the force of attraction of the sub-atmospheric central core and the buoyancy force associated with the air bubbles. Larger bubbles with which a higher buoyancy force is associated still tended to float to the top. Work with polystyrene particles had to be abandoned at this stage as they tended to become sticky with recirculation. Thus the photographs that follow do not contain any polystyrene particles. At this point use of the Nitrobenzene/Olive oil mixture aided observation. The axis is made up of air bubbles and globules of the Nitrobenzene/ Olive Oil tracer agent and the core is made up of only the latter. Fig. (8.3d) shows globules of the tracer agent hovering around the breakdown axis while Fig. (8.3e)shows the core which forms just after the above development.

From this stage onwards the various modes of breakdown began to manifest themselves. Very fine control of speed was necessary and the feed-back control system incorporated to obtain this paid dividends. However this was off-set by the pulsating axial flow from the pump. The effect of a very small increase of swirl is shown in Fig. (8.3.f). The axis gently assumes a spiral motion before breaking up viciously. This in fact was the state just before the occurrence of the well-known spiral mode of vortex breakdown, shown in Fig. (8.3g), described in Chapter 4. It was interesting to observe that when breakdown was imminent the radius of gyration reduced and the breakdown-axis and the geometric axis of the duct were almost coincident.
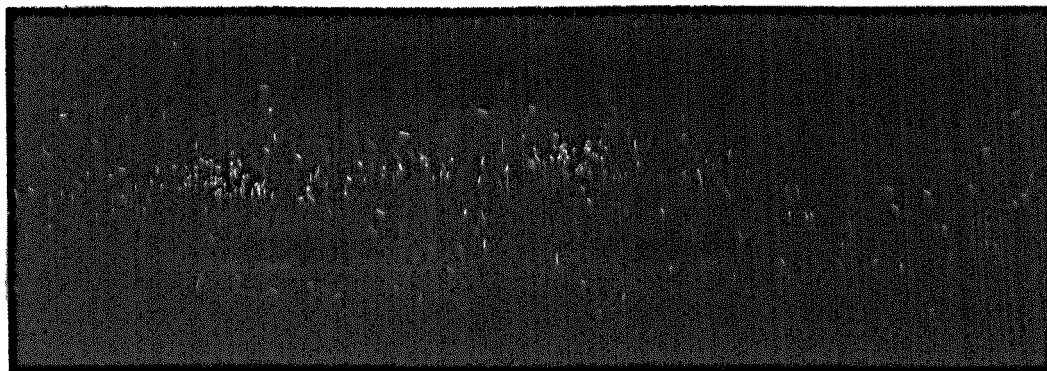
FIG. 8.3 a – Movement of polystyrene particles towards centre of duct

High-speed flash at f.5.6
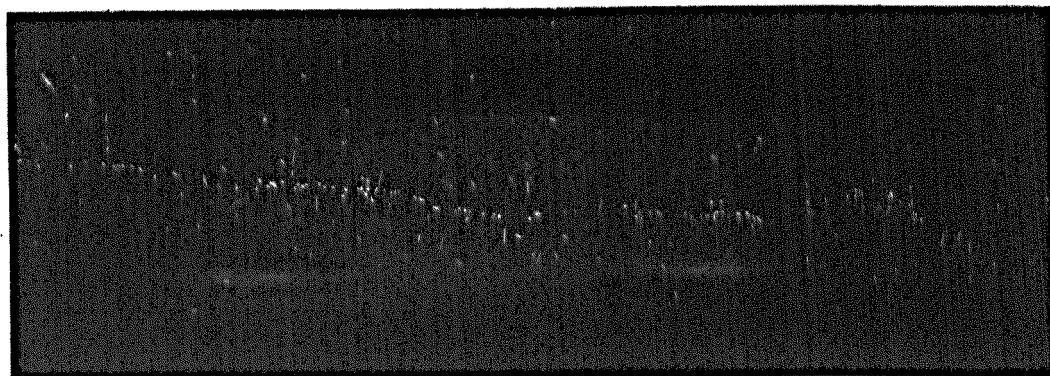
FIG. 8.3 b – Steady well-defined axis of polystyrene almost coincident with axis of duct

High-speed flash at f. 5.6
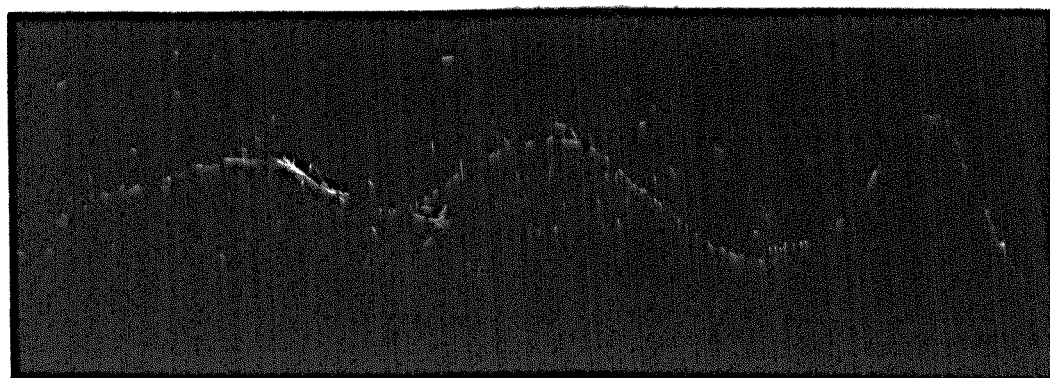
FIG. 8.3 c – Spiral deformation of axis in pseudo – resonant state

High-speed flash at f.8
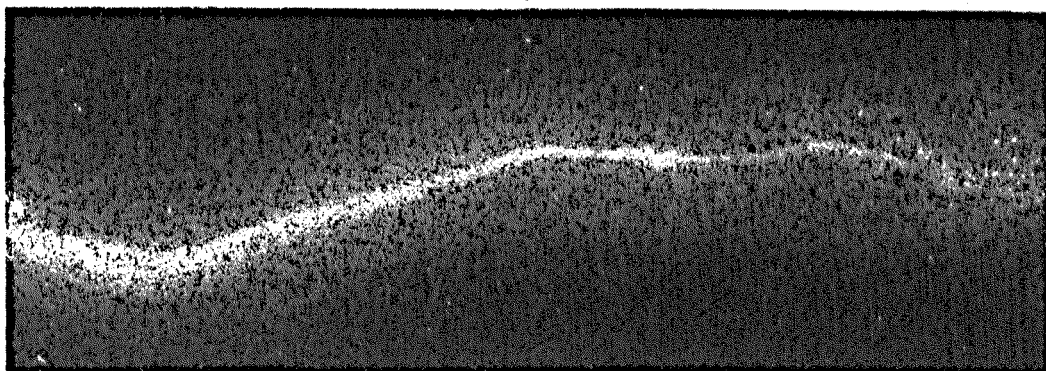
FIG. 8.3 d — Globules of liquid tracer hovering around axis
of air bubbles and globules
High-speed flash at f.11
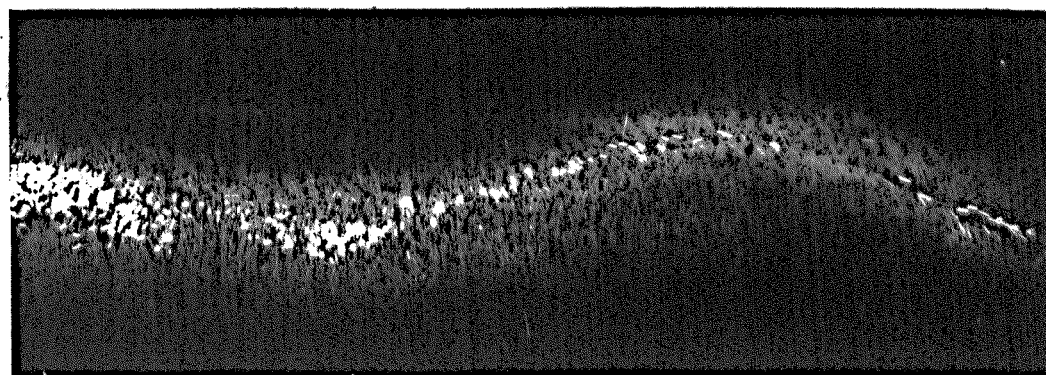
FIG. 8.3 e — Axis of air bubbles and globules encircled by
primary core of globules
Photo-floods: 1/60 th. secs at f.11
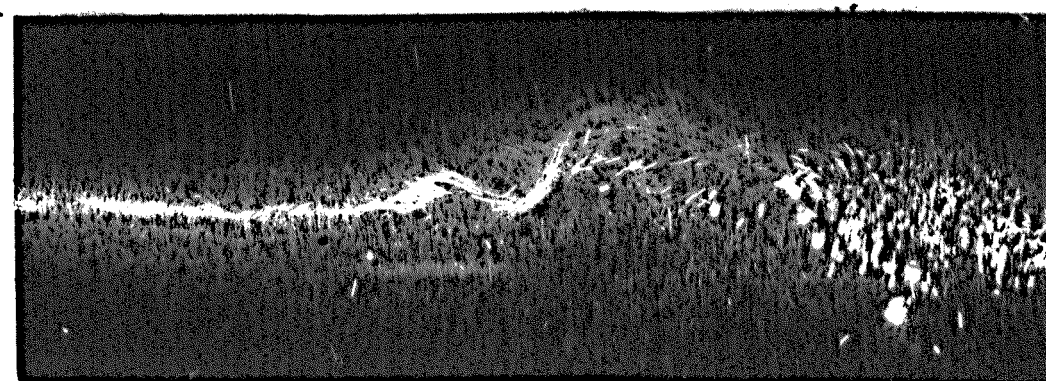
FIG. 8.3 f — Spiral deformation of axis just before
vortex breakdown
Photo-floods: 1/60 th. secs at f.11
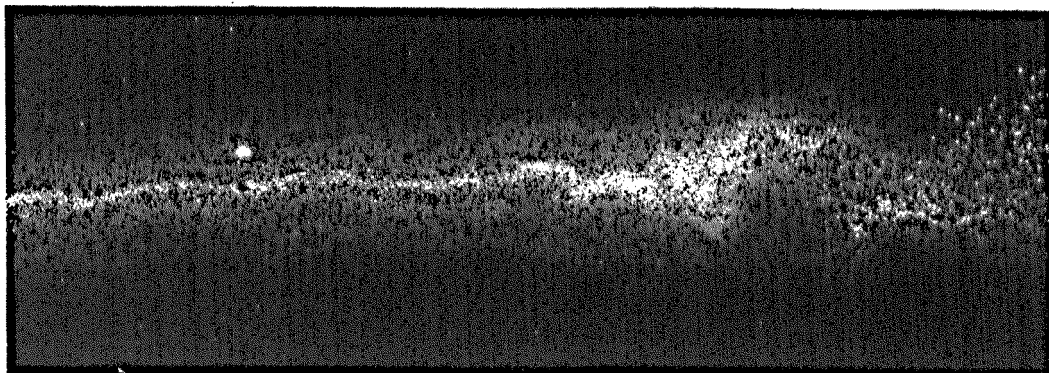
FIG. 8.3 g - The spiral vortex breakdown with upstream
axis straightened and coincident with axis of duct
High-speed flash at f.ll
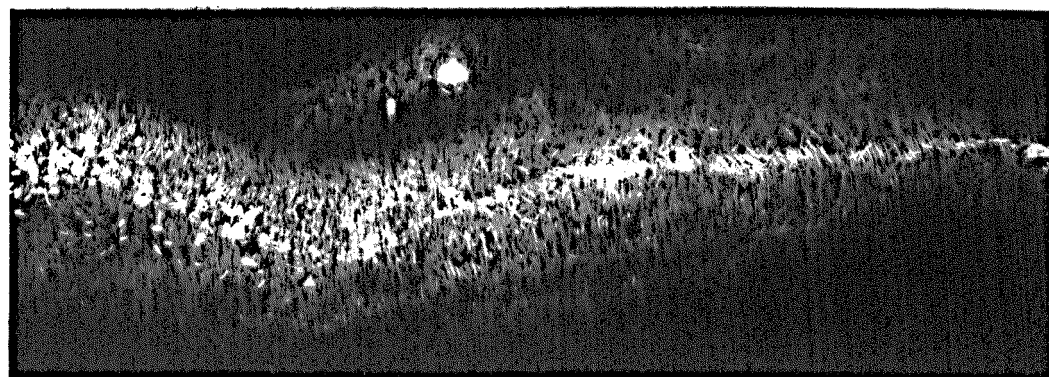
FIG. 8.3 h - The breakdown axis encircled by the primary
core and a secondary core
Photo-floods: 1/30 th. secs at f.8
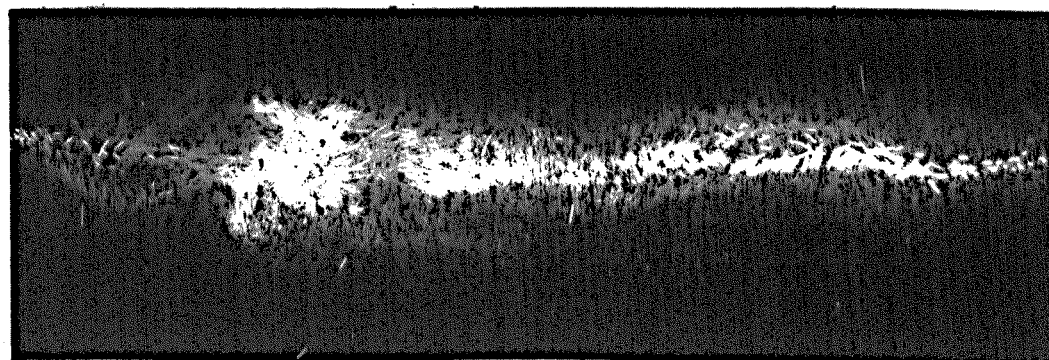
FIG. 8.3 i - Formation of stagnation point associated with
axisymmetric breakdown
Photo floods: 1/60 th. secs at f.ll
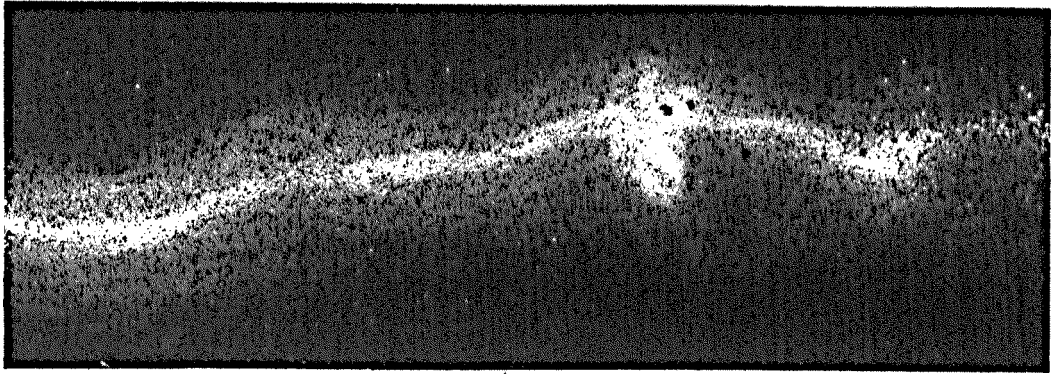
FIG.8.3j The well known feed bubble associated with
axisymmetric breakdown
High-speed flash at f.11
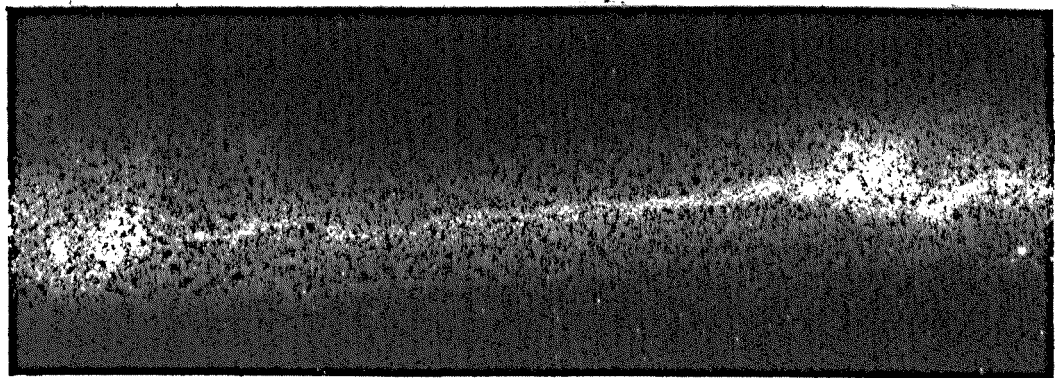
FIG.8.3k Clustering of globules and air bubbles to form
two breakdown regimes
High-speed flash at f.11
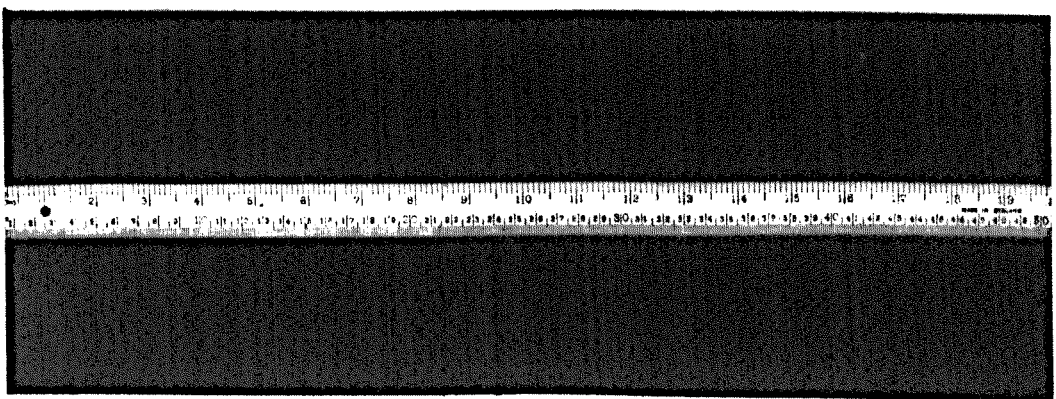
FIG.8.3l Scale of above photographs

On further increase of swirl the breakdown moved upstream and the
system established a much calmer state. With this a secondary core
appeared around the primary core. This mode, shown in Fig. (8.3h),
is similar to the helical breakdown observed by Sarpkaya (1971).
It was not often repeatable and its presence was very irregular.
It consists of the breakdown axis, the primary core and the secondary
core. The sense of rotation of both cores was the same as that of
the bulk flow. Owing to the disturbance caused by the pulsating
flow from the pump it was not possible to identify its occurrence
in relation to the spiral breakdown.

Increasing swirl still further led to the appearance of
a stagnation point. As seen from Fig. (8.3i) the tail is still
present though the leading edge is very blunt. Further increase
of swirl resulted in the appearance of the large feed-bubble
associated with the classical axisymmetric breakdown. The bubble
continuously expanded and contracted and Fig. (8.3j) shows it in
the contracted form. This bubble moved upstream on increasing swirl
allowing the development of another breakdown. Capturing both
breakdowns simultaneously proved extremely difficult. The best
attempt is shown on Fig. (8.3k). This shows two distinct
concentrations of bubbles forming what might be two feed-bubbles.
Owing to its faintness it is not possible to identify clearly the
mode of breakdown. By this time collection of air bubbles on the
walls of the duct obscured clear vision. Added to this,
contamination of the water by the Nitrobenzene/Olive Oil tracer
agent made experimentation extremely difficult. Hence it was decided
to terminate flow visualisation at this point.

The first stage of the flow visualisation experiments
were devoted solely to obtaining a photographic record of the
events associated with vortex breakdown. Having done this,
attention was focussed on quantifying the developments. Following
earlier work it was clear that the developments, in turbulent flow,
were too closely related to identify individual regions of each
mode of the phenomenon. For a fixed flow rate the swirler-speed at
which each phenomenon occurred was recorded. This was repeated
several times and for different flow rates. These curves have been
plotted in Fig. (8.5), with circulation number and Reynolds number
as abscissa and ordinate respectively, to facilitate comparison with
earlier work.

8.5.2 Vortex Breakdown in a diffuser

Unlike that in a pipe, vortex breakdown in a diffuser, in
turbulent flow, caused difficulties. The behaviour could only be
observed up to a point and hence photographic recording was not
possible.

On gradual increase of swirl the primary core, which
had already formed downstream of the diffuser, started its movement
upstream. When it entered the diffuser, a distance of approximately
one-half of a throat diameter, it suddenly disintegrated following
a spiral deformation. On further increase of swirl the core was
not seen until it reappeared at the throat of the diffuser. The
motion from there onwards was as described earlier. Altering the
flow-rate did not affect the situation though replacing the 30°
diffuser by the 10° diffuser did improve it considerably. The

FIG. 8.4 DEVELOPEMENT OF V.B. IN PIPE FLOW

▽ formation of axis of polystyrene

× formation of regular primary core

◉ first sign of axisymmetric v.b.
(feed-bubble formation)

○ distinct formation of first feed-bubble

rotational speed of swirl generator – r.p.m.

manometer reading – Δh cms Hg.

209
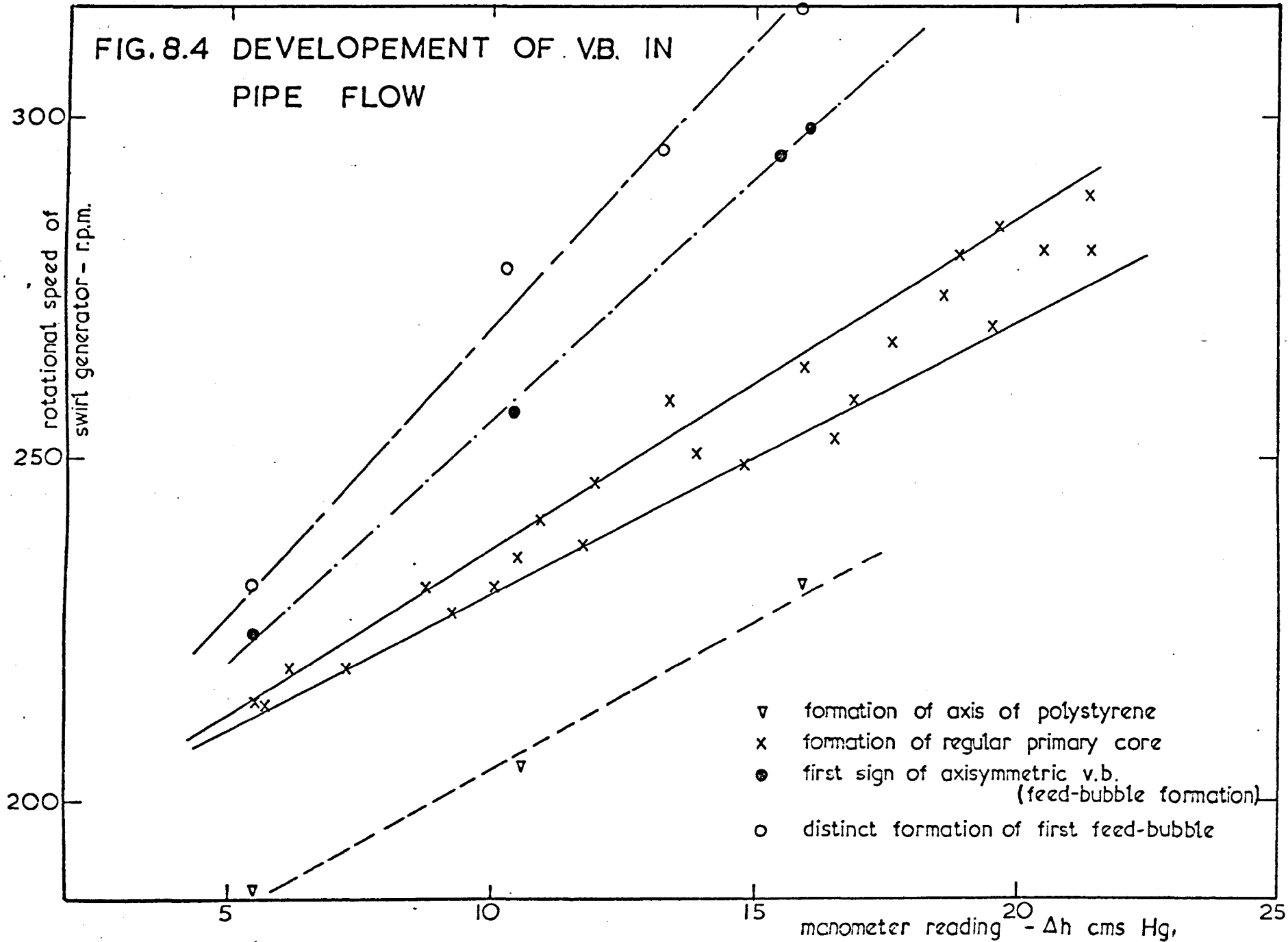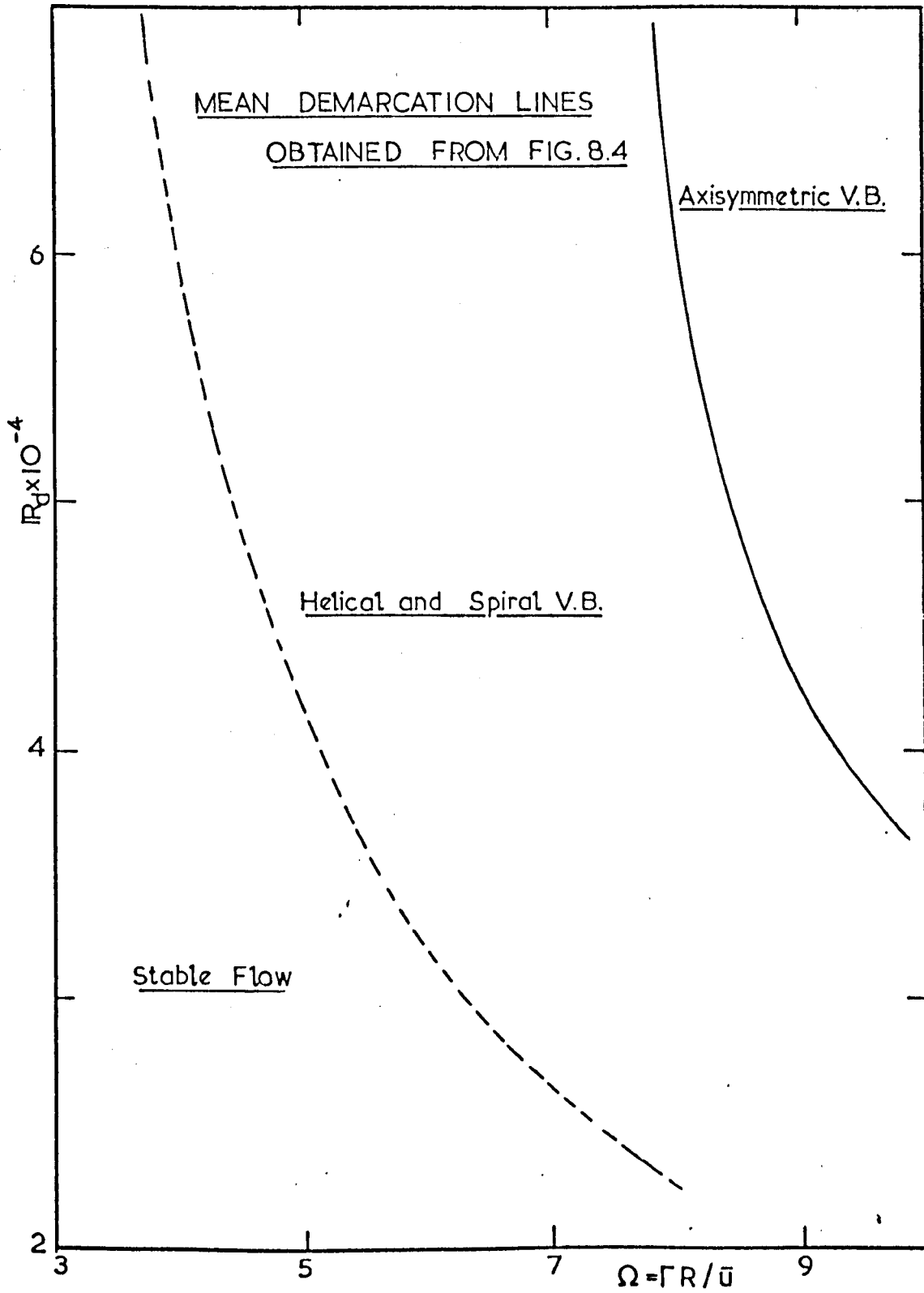
FIG.8.5 FLOW REGIMES IN SWIRLING PIPE FLOW

spiral motion that preceded this disappearance suggests that this could have been caused by the changing radius of the diffuser. This (and his work in the laminar range) would also explain the success Sarpkaya had with his very mild diffuser (3° cone angle).

8.5.3   The Travelling Primary Core-Head

The movement of the primary core was studied for a fixed flow rate. The core exhibited areas of varying density. This was evident as the largest air bubbles tended to move at the head of the travelling core while bubbles of diminishing diameters trailed behind. The head of the core tended to oscillate along the axis with an amplitude of approximately 50 mm. Fig. (8.6) shows the upstream movement of the core as it grows to cover the entire pipe.

8.6   CONCLUSIONS

The primary object of flow visualisation was to determine the various stages leading to the development of vortex breakdown. All conclusions being based on observation studies, no clear demarcation of regions exhibiting the various phenomena was possible. Following early exploratory studies it was possible to divide experimentation into three stages.

The first stage was the photographic recording of the development of the various modes of the vortex breakdown phenomenon. Owing to irregularity of occurrence of these it was not possible to determine the swirl rate at which they occurred for different flow rates. Hence this stage was conducted for a fixed flow rate. Owing to turbulence it was not possible to obtain photographs of the same clarity as those obtained by Sarpkaya in laminar flow.
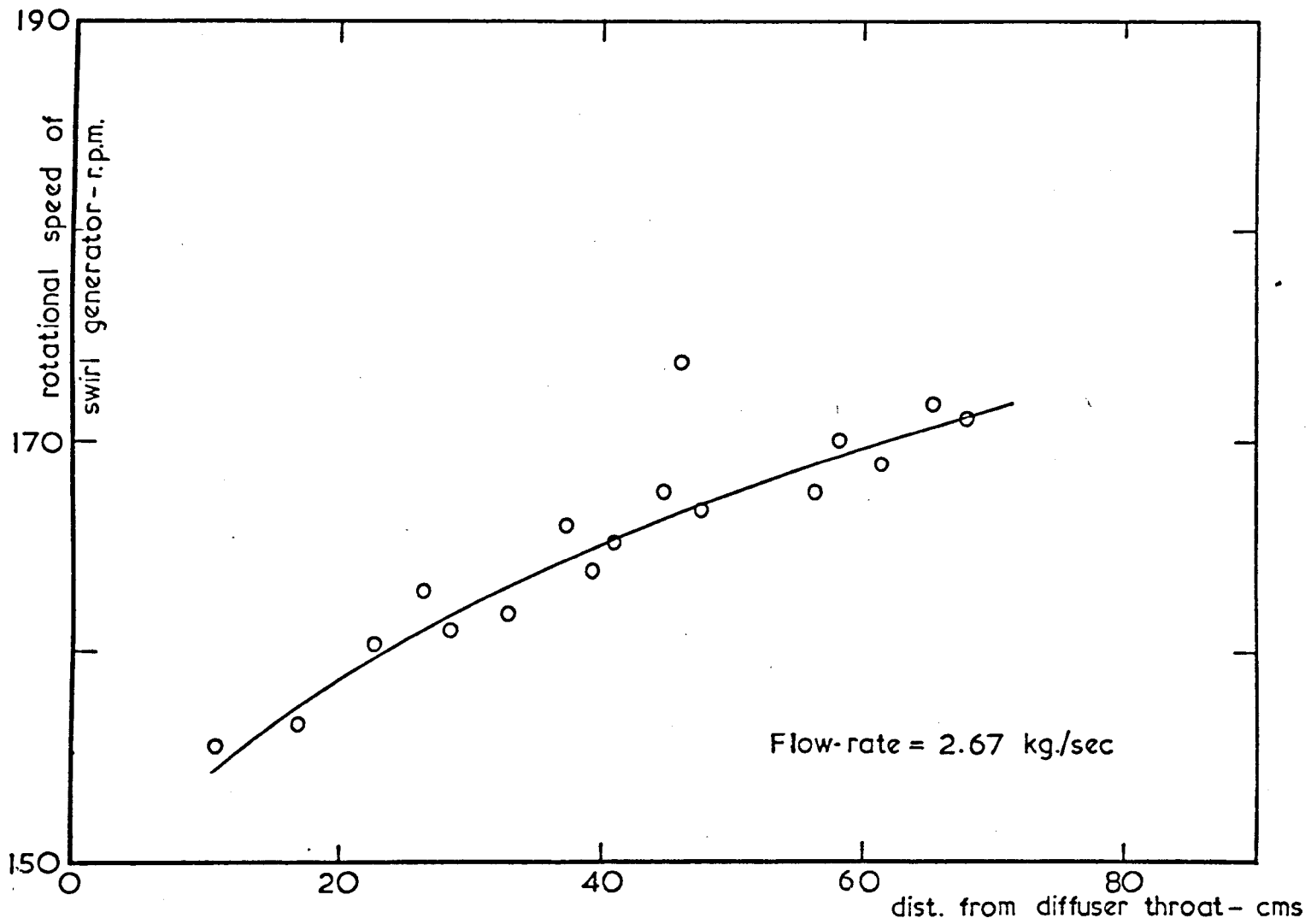
FIG.8.6 THE TRAVELLING PRIMARY CORE-HEAD IN SWIRLING
PIPE FLOW

All three tracer agents, namely Polystyrene particles, Nitrobenzene/Olive Oil mixture and Air bubbles, played useful roles in the flow visualisation. The sequence of development can be seen quite clearly from the series of photographs in Fig. (8.3). Here it is only sufficient to outline briefly the development with increasing swirl.

a. Formation of a very fine axis (low pressure region) near the centre of the duct. This was steady though faint, Fig. (8.3b).

b. This axis began to undergo a periodic spiral deformation without actually degenerating; Fig. (8.3c).

c. The extent of the deformation (in amplitude) decreases while a primary core forms; Fig. (8.3e). The sense of rotation of this core is the same as that of the main flow.

d. The vortex breakdown phenomenon in the spiral mode. Upstream of the breakdown the core straightened and became coincident with the geometric axis of the duct. The sense of rotation of the breakdown is unchanged. Fig. (8.3g)

e. The formation of a secondary core, generally referred to as a breakdown in the helical mode. Once again the axis and the cores undergo deformation. The sense of rotation of both cores are identical. Fig. (8.3h)

f. The formation of the upstream stagnation point just before the axisymmetric breakdown. Fig. (8.3i)

g. The well-known 'feed-bubble' associated with breakdown in
    the axisymmetric mode. This is constantly expanding
    and contracting and Fig. (8.3j) shows it in the latter
    form.

h. Two distinct clusters of bubbles displaying breakdown
    formation. Owing to experimental difficulties it was
    not possible to determine the exact modes.

The sequence of development of the phenomena compares well
with that reported by Sarpkaya who used a mild diffuser (laminar
flow) though no direct comparison is possible. The present work
does not support the view [Jones (1960) and Lambourn and Bryer
(1961)] that the two cores have opposite sense of rotation.

The second stage was a study of the stability of flow
with increasing swirl and axial flow. Owing to experimental
difficulties it was not possible to obtain as much detail as
discussed above for each flow rate. Hence an overall flow map is
presented. Fig. (8.5) is an attempt to standardise the flow map
which may be compared with Fig. (8.7) which is the work of the other
investigators. As far as the present author is aware only Talbot and
Sarpkaya have provided flow maps. Unfortunately it is not possible
to compare their work with the present owing to the various methods
of swirl generation employed. Talbot used a rotating pipe section
to produce swirl and relied solely on viscous action to generate
swirl. He points out that his swirl was not 'fully developed' on
exit from the generator into another pipe. Hence the circulation
number applicable to rotating section was not that associated with
breakdown.
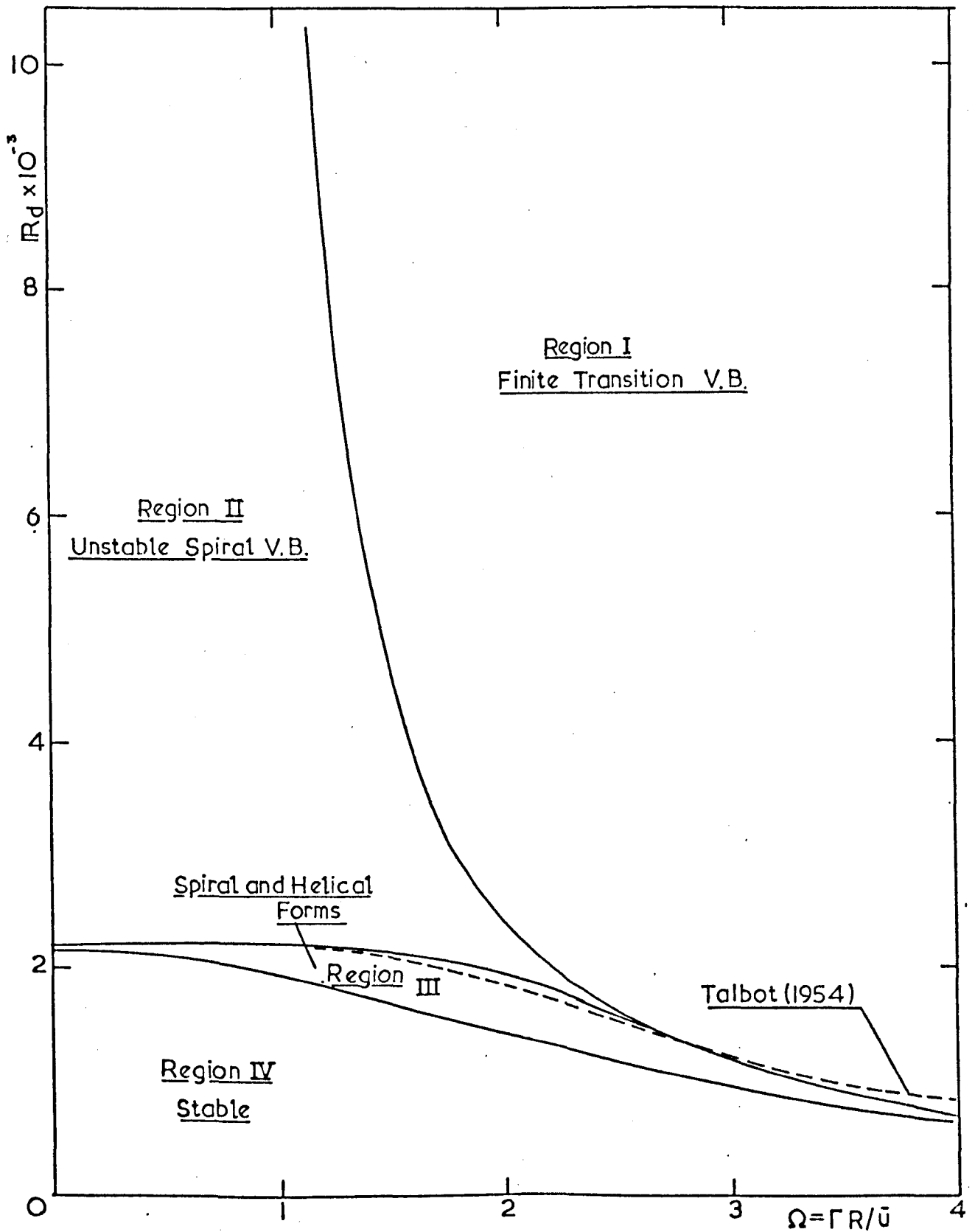
FIG.8.7 VORTEX BREAKDOWN IN A DIFFUSER FROM SARPKAYA (1971)

Sarpkaya used guide vanes to generate swirl in a diffuser. In this project design limitations precluded working in the area of low Reynolds numbers. Swirl was produced by means of a rotating honeycomb. Though it would be elegant to be able to provide a comparison of all the work in the form of a complete breakdown map this is not possible at this early stage owing to the reasons discussed above. Thus Sarpkaya's attempts to compare his work with that of Talbot do not appear to be fully justified.

The trends of the curves in Figs. (8.5) and (8.7) are similar though no curves have been provided by the present author in the low range. It is diffucult to overlook a possible anomaly in Sarpkaya's curves in Fig. (8.7). According to the figure it appears that the flow is unstable even without any swirl above a Reynolds number of 2200; i.e. beyond the laminar range. This is contrary to that observed in practice.

The third stage focussed attention on the upstream movement of the primary core. No comparison can be offered here as this aspect has not been investigated before.

The above discussion has highlighted the difficulties associated with visualisation studies of swirling flow in the turbulent range. The need for very fine control of swirl has also been highlighted, amply justifying the efforts directed towards developing the speed control system for the drive motor. Scope for further work in this area will be discussed in Chapter 10.

CHAPTER NINE

MEASUREMENT OF FLOW IN DIFFUSERS

9.1   INTRODUCTION

From the discussions presented in the previous chapters

it is evident that very little work has been done on flow in diffusers

when flow at entry possesses swirl. Setting out suitable guidelines

for experimental work proved difficult. The fact that all the

requirements, in relation to swirling flow in diffusers, could not

be satisfied was realised and consequently subjective decisions had

to be taken on priority requirements.

Initially, an exploratory study was conducted to establish

some guidelines for further work in relation to the time scale and

the limitations imposed by various factors. The output of the

swirl generator was then analysed to evaluate its performance. On

the strength of this it was decided to restrict flow measurement to

mild swirl and to make an overall assessment on the basis discussed

in Chapter two. This has been supplemented by a detailed analysis

of flow in the 10° diffuser. All experimental work was conducted

at an entry Reynolds number of 5.7×10^4.

9.2   EXPERIMENTAL APPARATUS

The arrangement shown in Fig. (6.2a) was used for all the

experiments with air as the flow medium. The five-hole pressure

probe, with the associated instrumentation, was used for flow

measurement.

9.3   EVALUATION OF FLOW PROPERTIES.

Before launching into any discussion on the constancy
or variation of the various flow properties it is necessary to
consider the contribution of the errors due to experimental work
and that due to analysis. As a result of these errors the
suitability of the kinetic energy (weighting) factor as a measure
of the distortion of the velocity profile could be argued. The
deviation of this factor from unity, for a uniform profile, is
accentuated by the disturbances due to experimental errors.

At any point in the diffuser the two necessary measurements
are the total pressure and the angle of yaw. It was pointed out in
Chapter Seven that any sensing hole in the five-hole probe was
insensitive to a change of $\pm 3^\circ$. Thus it may be concluded that most
of the errors lay in the measurement of the angle of yaw. These
errors may be minimised by resorting to the known tangential
velocity distribution for rigid body rotation which is

$$v = r\omega$$

Also $v = \tilde{V} \sin\psi$ and $u = \tilde{V} \cos\psi$

where $\tilde{V}$ and ψ are experimental values.

The angular velocity ω given by,

$$\omega = v/r = \tilde{V} \sin\psi/r = \text{constant}$$

is determined from regressional analysis. The above equation may
now be transposed to calculate the corrected values of ψ . Thus

$$\psi = \sin^{-1}(\omega r/\tilde{V})$$

Then the corrected axial velocity is

$$u = \tilde{V}\sqrt{1-\sin^2\psi}$$

or $u = F(\tilde{V},r)$ (9.3.1)

and accordingly

the mass flux is $\propto \int F(\tilde{V}, r) r . dr$,

the kinetic energy is $\propto \int F(\tilde{V}, r)^2 r . dr$ and

the angular momentum is $\propto \int F(\tilde{V}, r) r^3 dr$.

The numerical technique employed for the evaluation of the integrals required the function in equal intervals. At this stage it is worth recalling that the indexing provided by the slotted slider-crank mechanism was unequal. Thus it was necessary to use an interpolation technique to evaluate the function at equal intervals.

As the function $F(\tilde{V}, r)$ is the axial velocity it has a non-zero value at the centre-line and a zero value at the wall. However the product of $F(\tilde{V}, r)$ and the radius has zero values at the centre-line and at the wall. The two cases are as shown below.
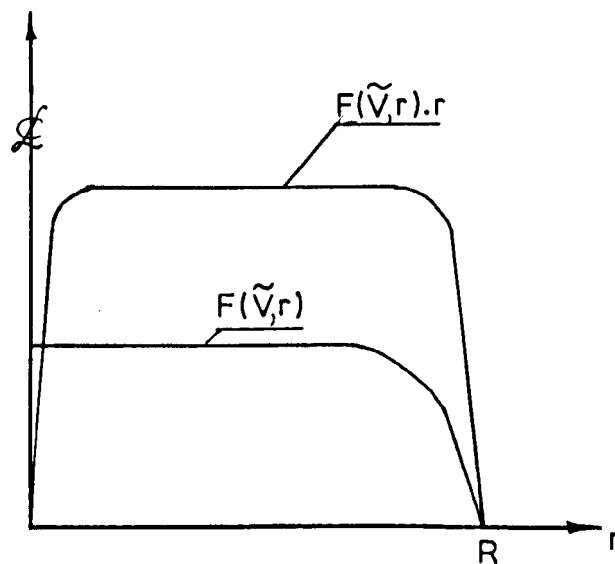
The integrals were first evaluated by interpolating the entire function (product) and then integrating.

Later the function $F(\tilde{V},r)$ was evaluated at equal intervals by
interpolation and then the necessary multiplications were
performed before the final integration. The first method did not
display a good constancy of the known properties but the second
method did show this. The descrepancy was found to be associated
with the technique of interpolation which curve fits three points
at a time to a parabola. The region where the function starts
from zero and rises rapidly to its typical values causes curve
fitting problems owing to the lack of data along the acute gradient.
In the first method, curve fitting has to be conducted through two
such regions while in the later method errors are effectively
halved as only the wall region is involved. It should be pointed
out that the values in the vicinity of the wall are very uncertain
owing to blockage effects.

9.4   PERFORMANCE OF SWIRL GENERATOR

Early studies indicated that the honeycomb swirl generator
was capable of producing a very good 'rigid-body' type vortex. The
mean turbulence was approximately 3% with the swirl generator
stationary. The speed of the swirl generator had to be limited
to approximately 500 r.p.m. as above this speed structural vibration
problems developed. This unfortunate experience seriously limited
the range of experimental work initially envisaged.

Fig. (9.1) shows the relationship between tangential
velocity and swirl generator speed for three typical cases.

FIG. 9.1 VARIATION OF TANGENTIAL VELOCITY WITH SPEED OF SWIRL GENERATOR
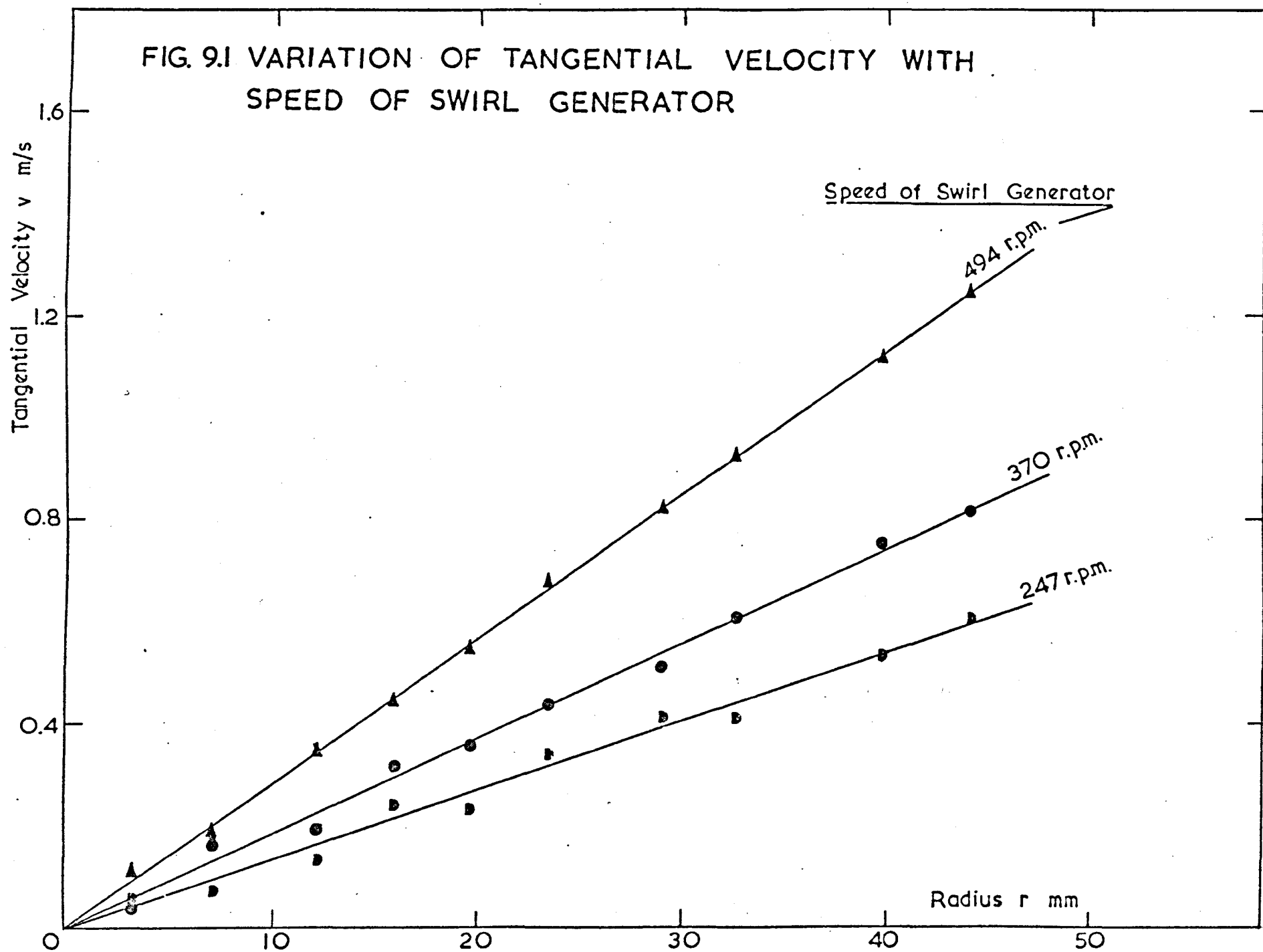
	Speed (R.P.M.)	Tacho. Output (Volts)
Swirl 1	247	16
Swirl 2	370	24
Swirl 3	494	32

There was no measurable decay in the inlet pipe between the generator and the diffuser, hence swirl measurements shown in Fig. (9.1) were made at the entry part of the 10° diffuser. It was not possible to measure the swirl angle at lower speeds, at each radial position, as the change in swirl angle between two points was less than 1^O, thus outside the capabilities of the probe. However such an error does not affect total velocity measurements as the spherical probe is insensitive to such a change. This is reflected clearly in the data points in Fig. (9.2) which corresponds to axial velocity at inlet for the three cases of swirl. On comparison with Fig. (9.1) it is seen that the former displays a higher degree of consistency. This confirms the comment made in the previous section on the causes of errors. From the same figure it can be seen that the errors in angular measurement decrease with increasing swirl.

Fig. (9.3) shows the variation of angular momentum, axial kinetic energy, its weighting factor, mean velocity and mass flux. From the percentage deviation figures (from the mean) shown in parentheses, mass flux and axial kinetic energy are seen to be conserved within the accuracy of experimentation and the method of evaluation. In Chapter two (eqn. 2.4.4) it was shown that the total kinetic energy could be expressed as

$$(\rho/2)\int \tilde{V} u \, dA = \dot{Q} q \chi_* /\rho + \omega \dot{M}/2$$
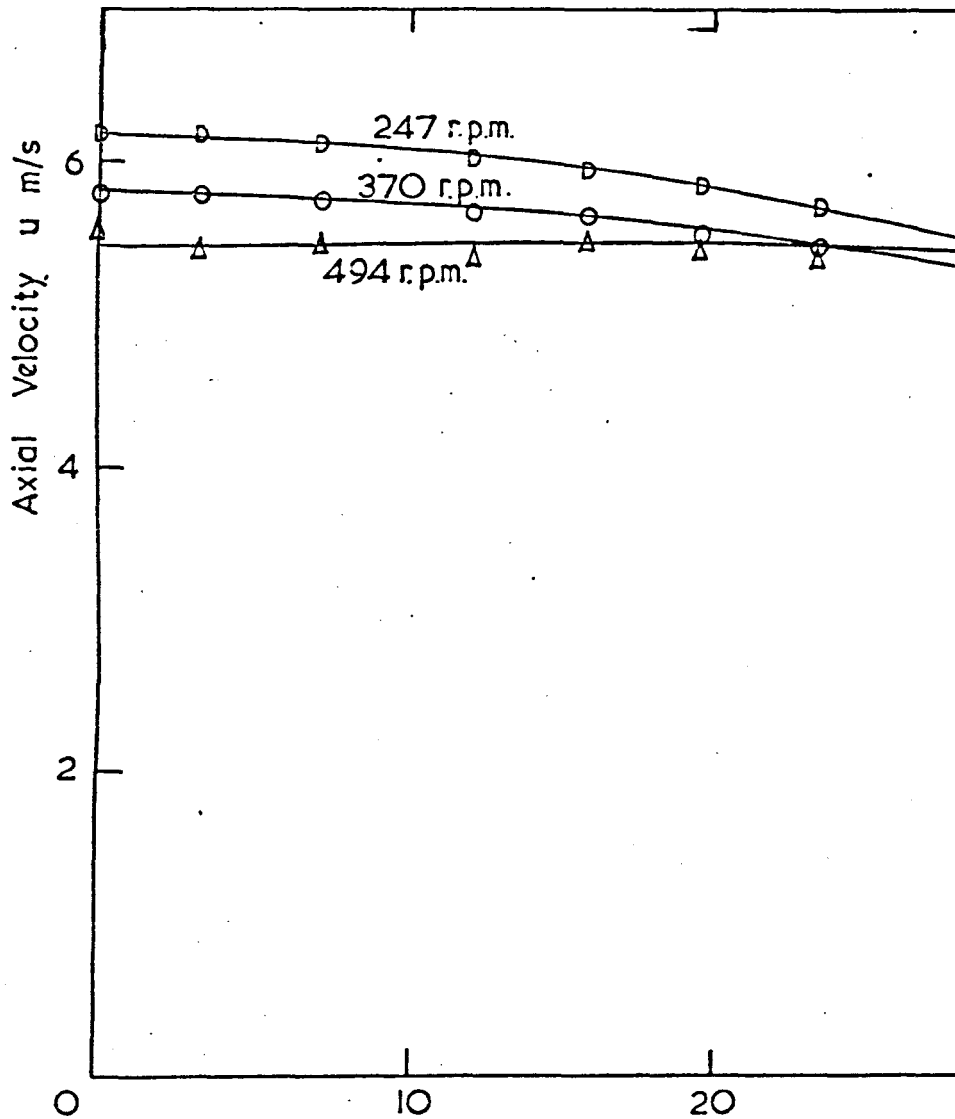
FIG.9.2 VARIATION OF AXIAL VELOCITY

Radius r mm

30   40   50
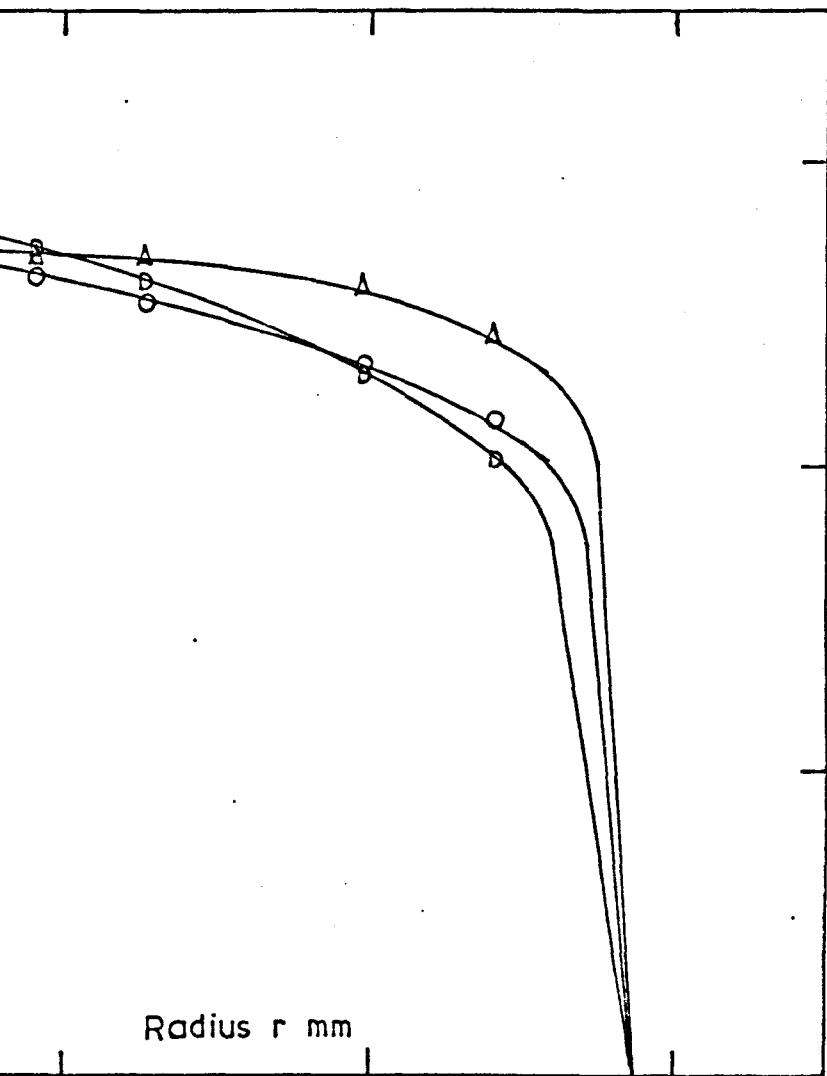
WITH SPEED OF SWIRL GENERATOR

FIG.9.3 VARIATION OF FLOW PROPERTIES WITH INCREASING SWIRL

For the present range of swirl the tangential kinetic
energy (second term) was found to be less than 3% of the total
kinetic energy. The above flow properties, which will be used at
a later stage for evaluating diffuser performance, are tabulated
in Table (9/1).

9.5 FLOW IN THE 10° DIFFUSER

Various researchers have experienced highly unstable flow
in the exit regions of diffusers. In some of the wider angle
diffusers time-variance of flow has been observed. Hence it was
necessary to conduct long time integrations in the time domain,
with the aid of the computing voltmeter, to obtain steady values.
Typically these were of the order of 8-12 minutes for each point.

Flow measurements in the 10° diffuser were made with axial
flow and with swirl 2. Fig. (9.4) shows the axial velocity
distribution associated with the two cases, while Fig. (9.5) shows
the tangential velocity distribution for swirl 2. Considering the
axial velocity distribution curves it can be seen that further
downstream in the diffuser the inflexion associated with
separation is developing. It is very encouraging to see the
tremendous improvement with the introduction of swirl. The tangential
velocity distribution curves shown in Fig. (9.5) display an inflexion
at stations 3 and 4. This feature was also reported by Van
Dewoestine (1969).

The profiles were analysed as outlined in section 9.3 to
obtain the necessary flow properties. These and the observations
are recorded in Tables (9/II) and (9/III) and are also plotted in
Figs (9.6) and (9.7).
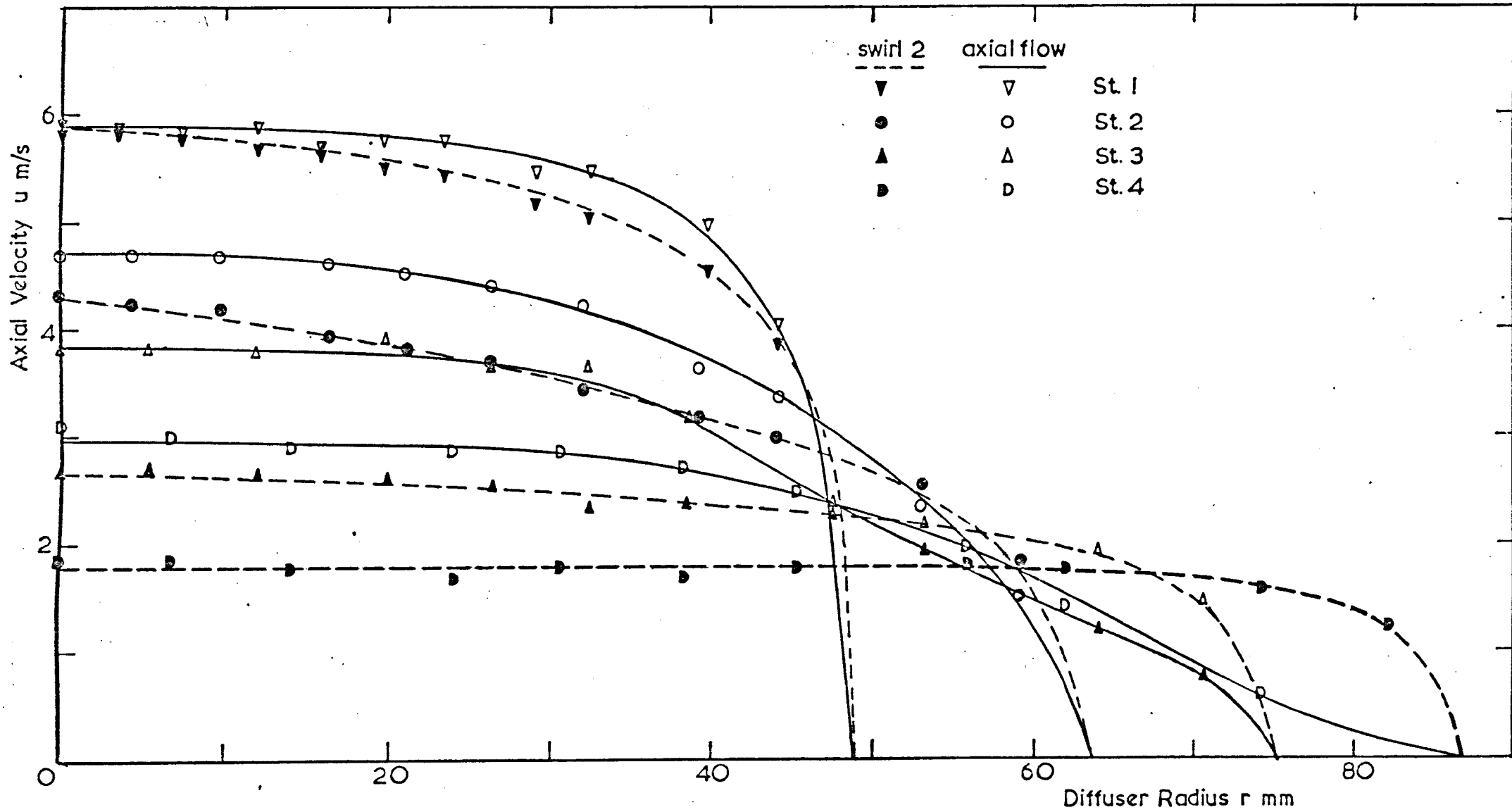
FIG.9.4 AXIAL VELOCITY DISTRIBUTION IN 10 DEGREE DIFFUSER
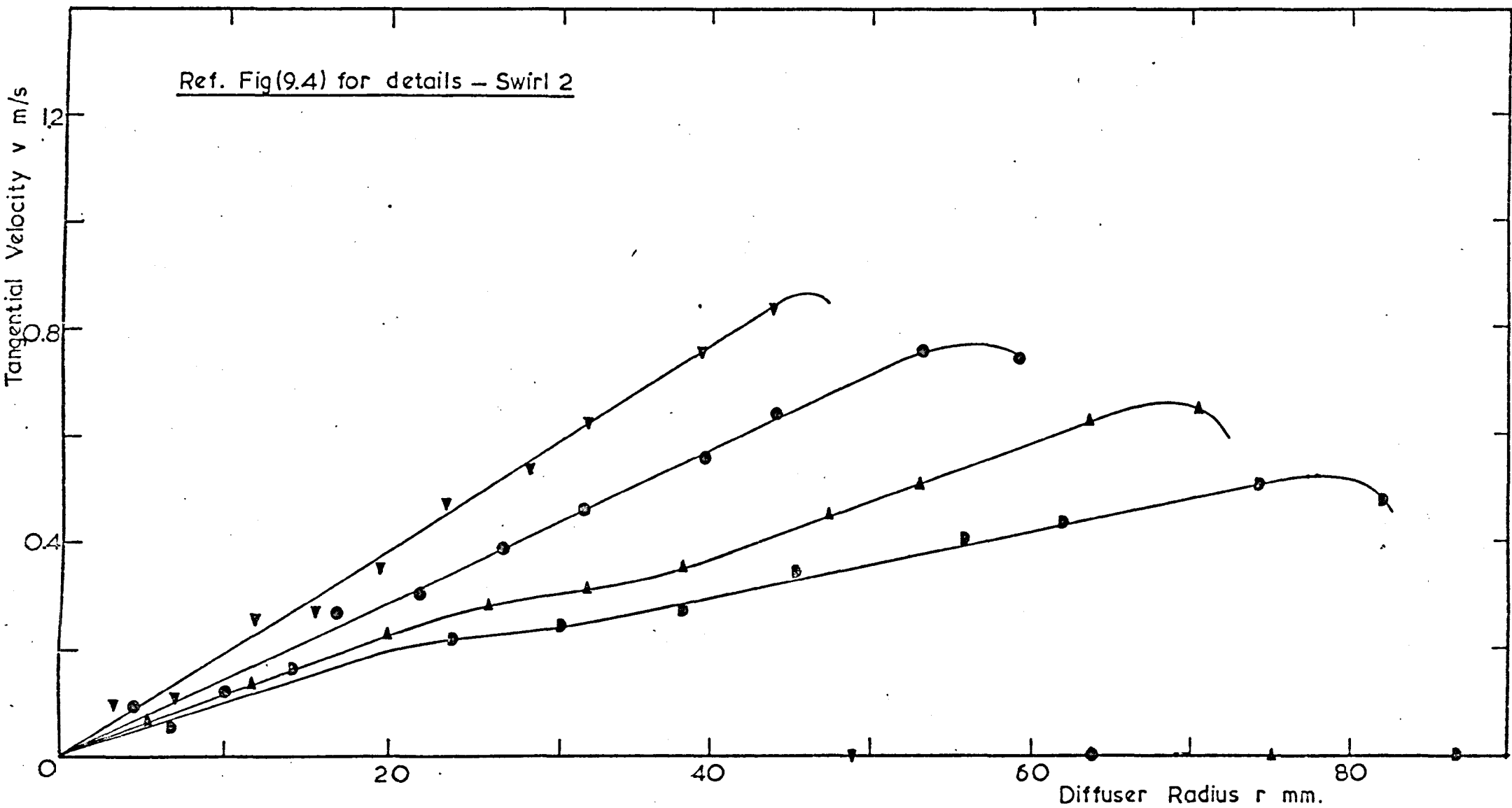
FIG. 9.5 TANGENTIAL VELOCITY DISTRIBUTION IN 10 DEGREE DIFFUSER
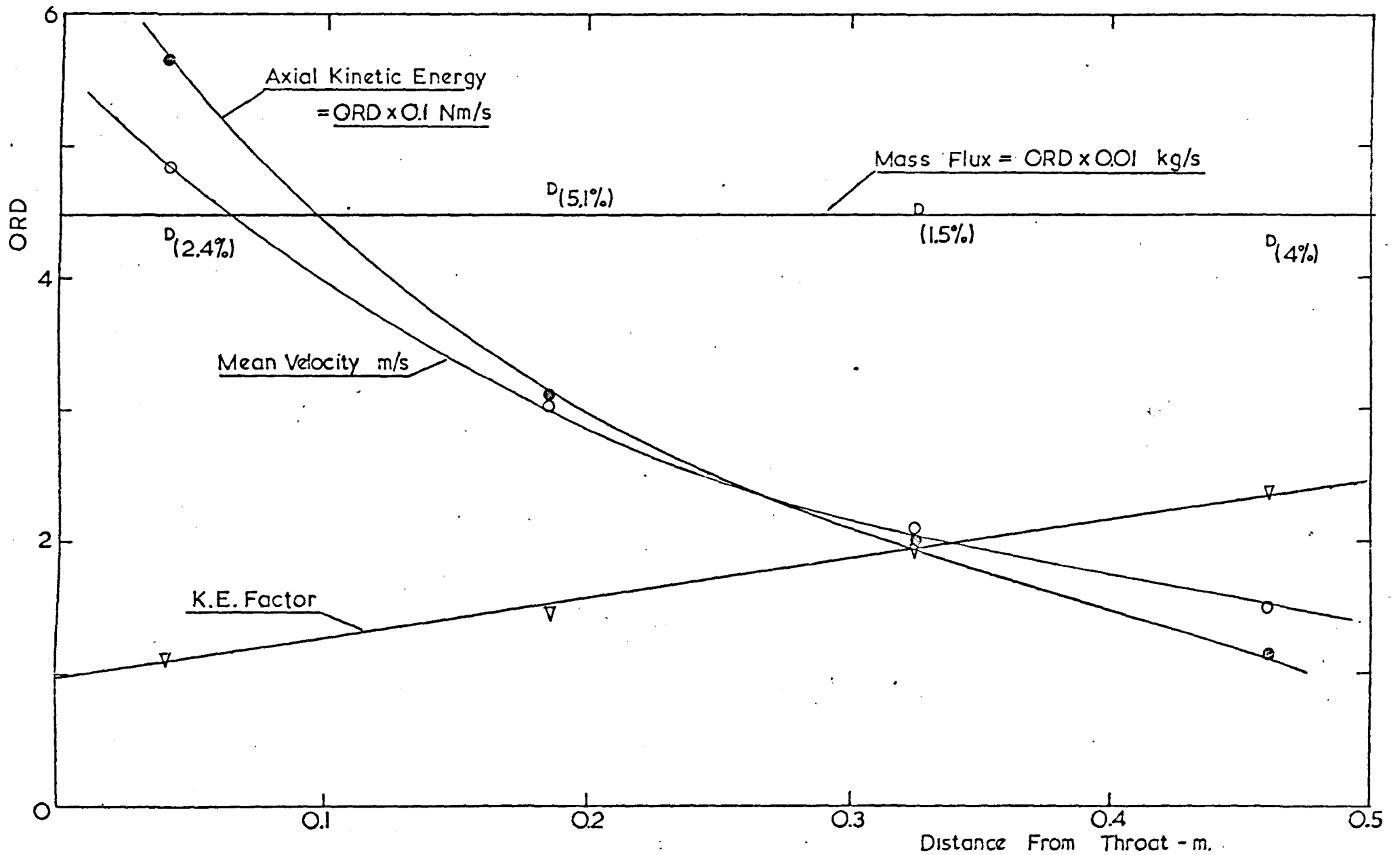
FIG. 9.6 VARIATION OF FLOW PROPERTIES IN 10° DIFFUSER WITH SWIRL 2
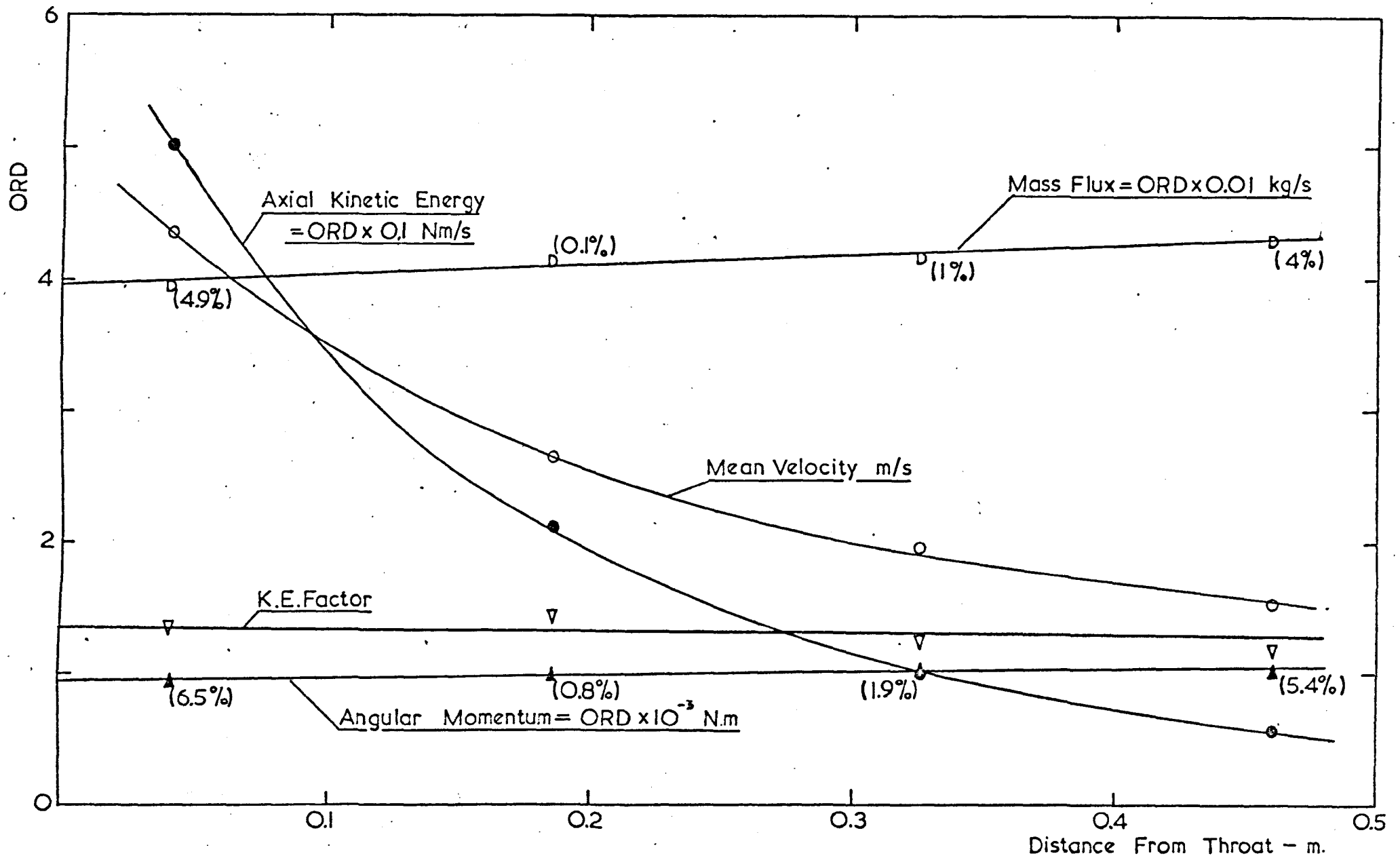
FIG. 9.7 VARIATION OF FLOW PROPERTIES IN 10° DIFFUSER WITH AXIAL FLOW

The figures in parentheses are the percentage deviations of the
respective values from their mean. The significance of the
variation of these properties will be discussed in the ensuing
sections.

9.6   WALL-STATIC PRESSURE MEASUREMENT

Unlike measurements inside the ducts, wall-static pressure
measurements proved very straightforward. The observations too were
very steady excepting in the 25° and 30° diffusers. In these two
the exit pressure fluctuated about 10%. The computing voltmeter took
care of this in about 15 seconds.

Initially, static pressure variation with increasing
swirl was measured in the 10° diffuser, the upstream pipe and the down-
stream pipe. This was repeated with each diffuser in turn. The
observations in the inlet pipe are recorded in Table (9/IV); the
measuring stations correspond to those in Figs (6.2a) and (6.12a).
As seen from the table there is no appreciable variation in the
pipe pressure-drop up to about the third measuring station irrespective
of the diffuser in position. However beyond this the pressure drop
is accentuated. The pipe pressure-drop for axial flow and swirl 3,
are plotted in Fig. (9.8). The deviations associated with the
intermediate swirl cases have been omitted for clarity. It is also
clear from the figure that the greater the divergence angle the
greater is the deviation. This in turn seems to indicate that the
greater the adverse pressure gradient the greater is the effect on
the flow in the pipe. It is also possible that the blend at the
throat has some effect.

The wall-static pressures associated with the diffusers
are plotted in Fig. (9.9).
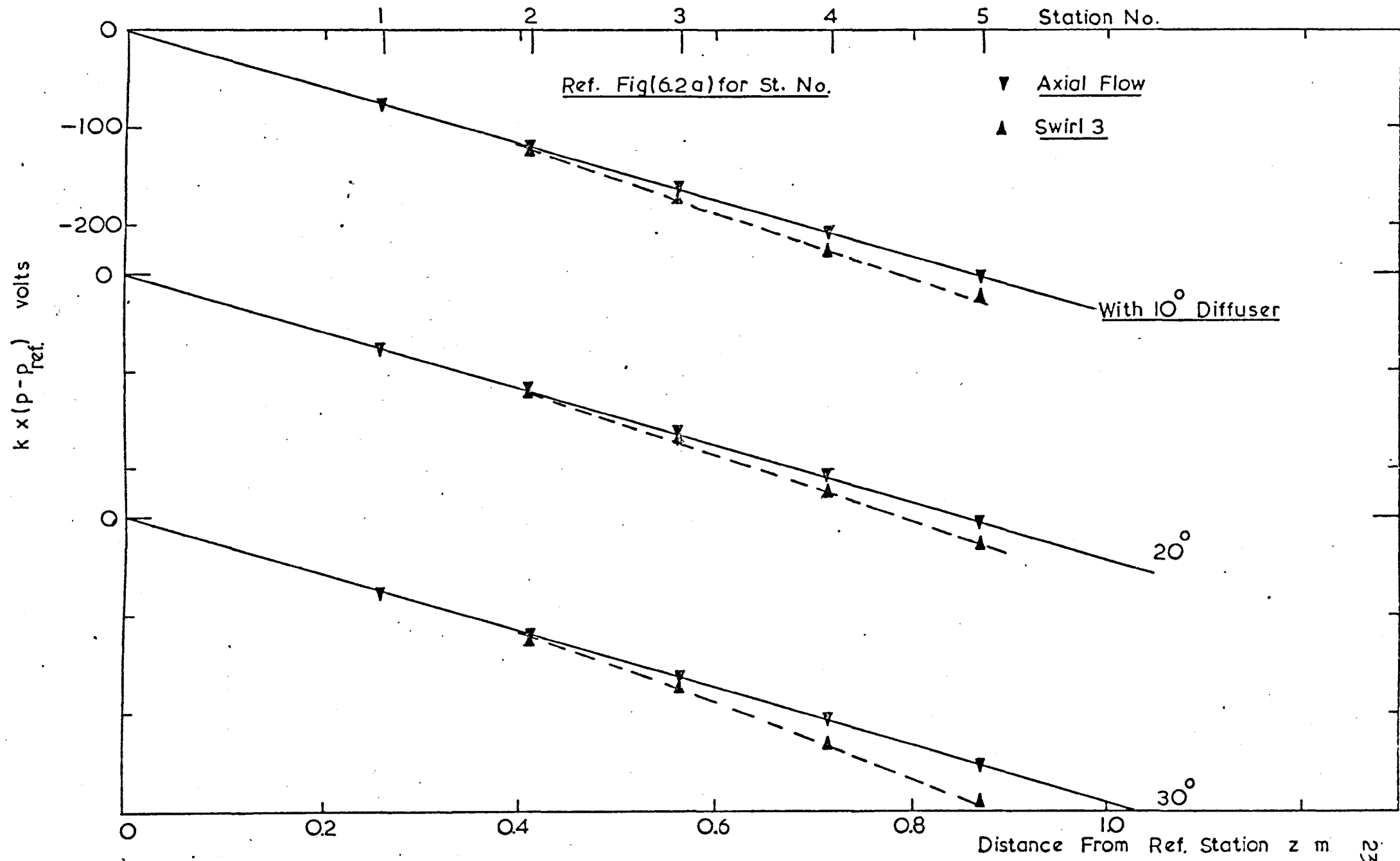
FIG. 9.8 WALL STATIC PRESSURE DROP IN INLET PIPE
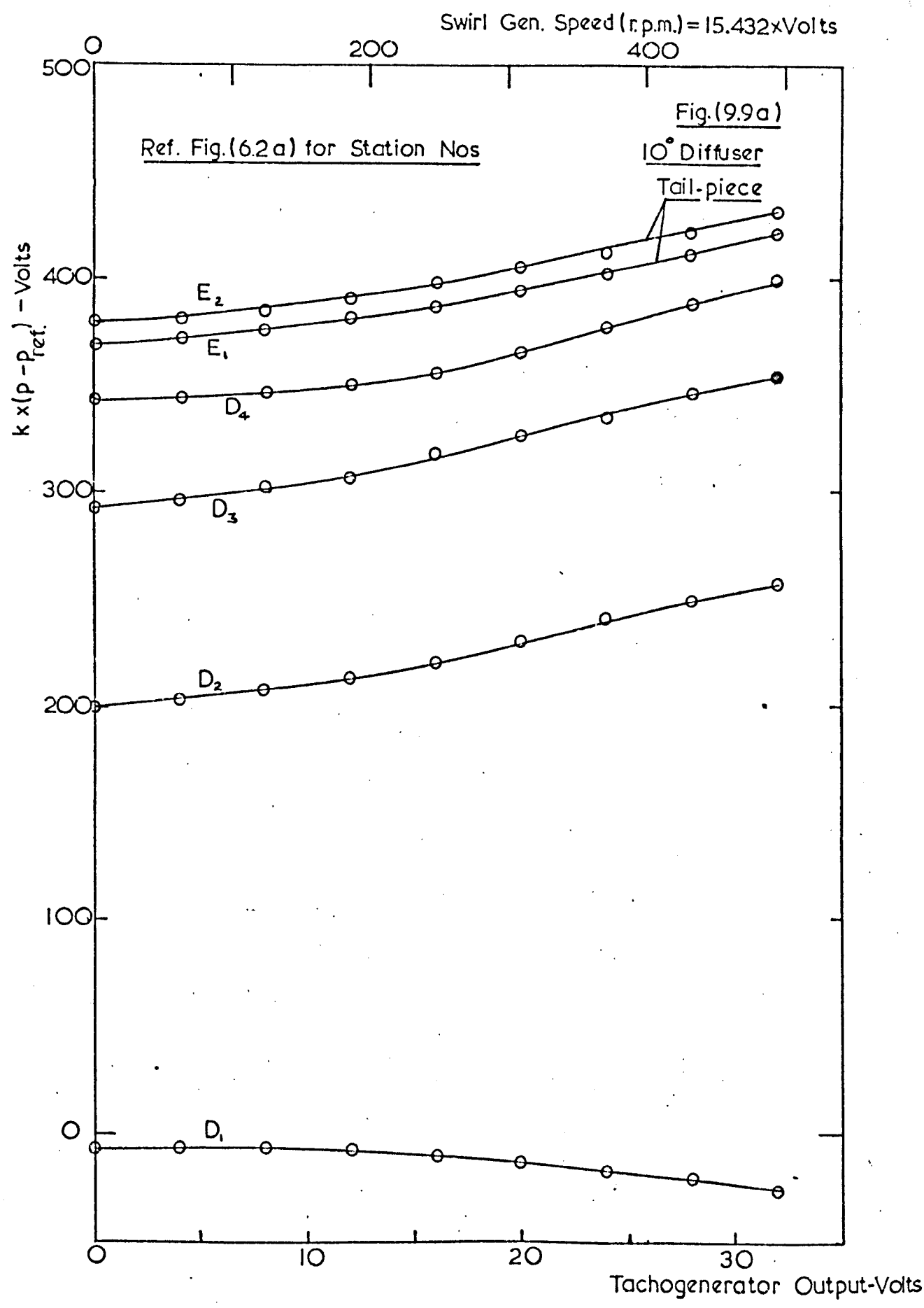
FIG. 9.9 WALL STATIC PRESSURE IN DIFFUSER AND TAIL-PIECE
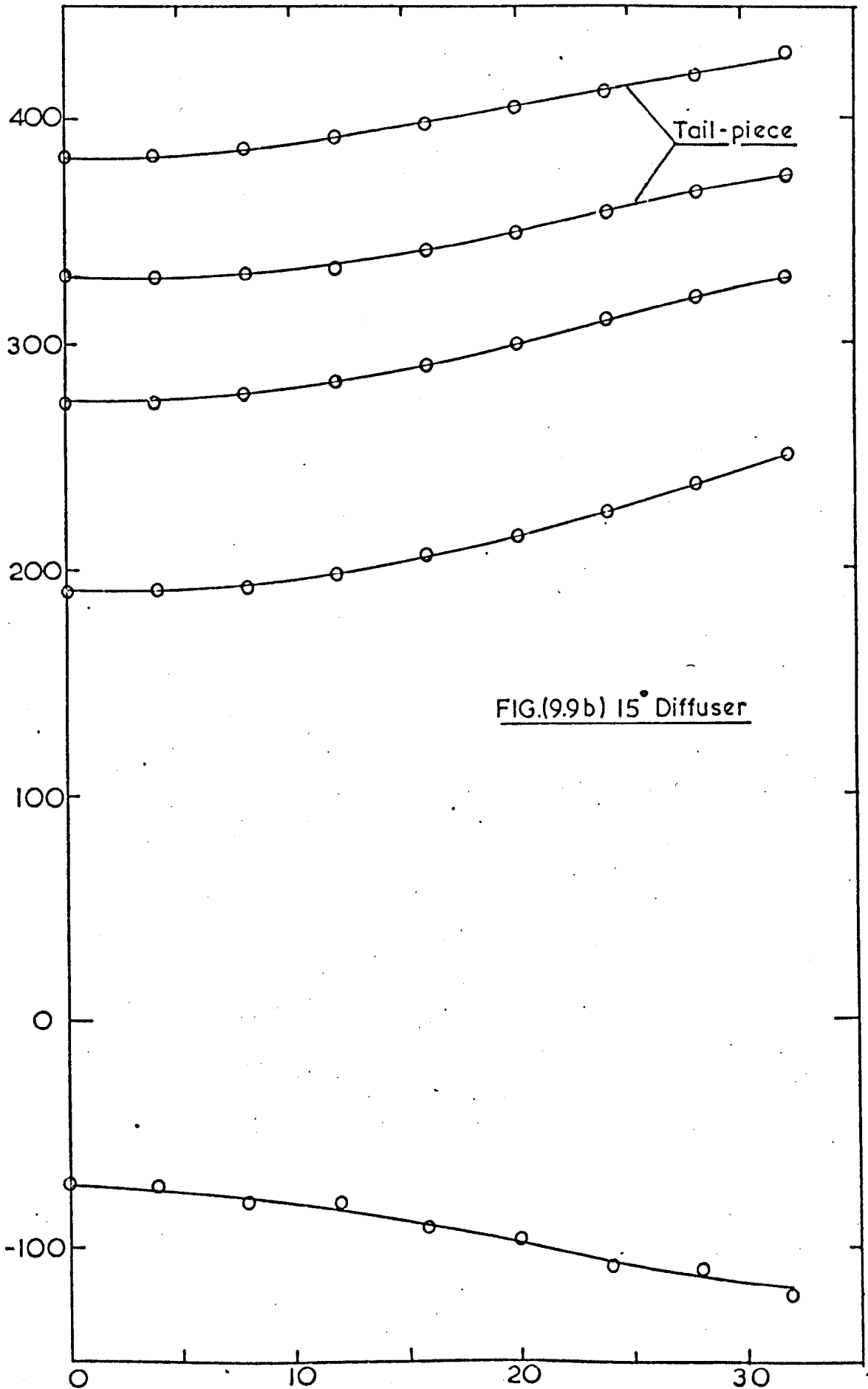
FIG.(9.9 b) 15° Diffuser

FIG.(9.9c) 20° Diffuser

Tail-piece
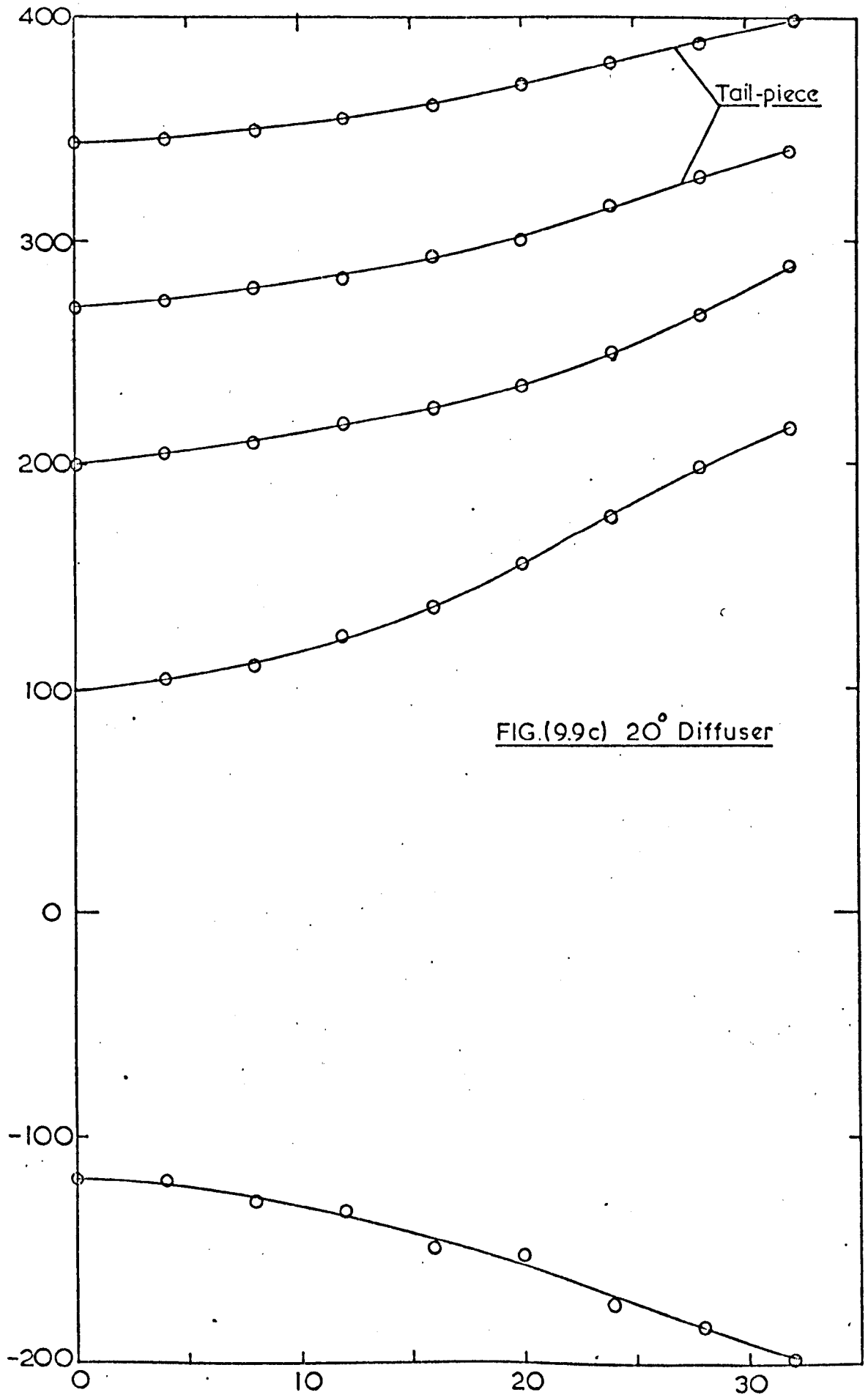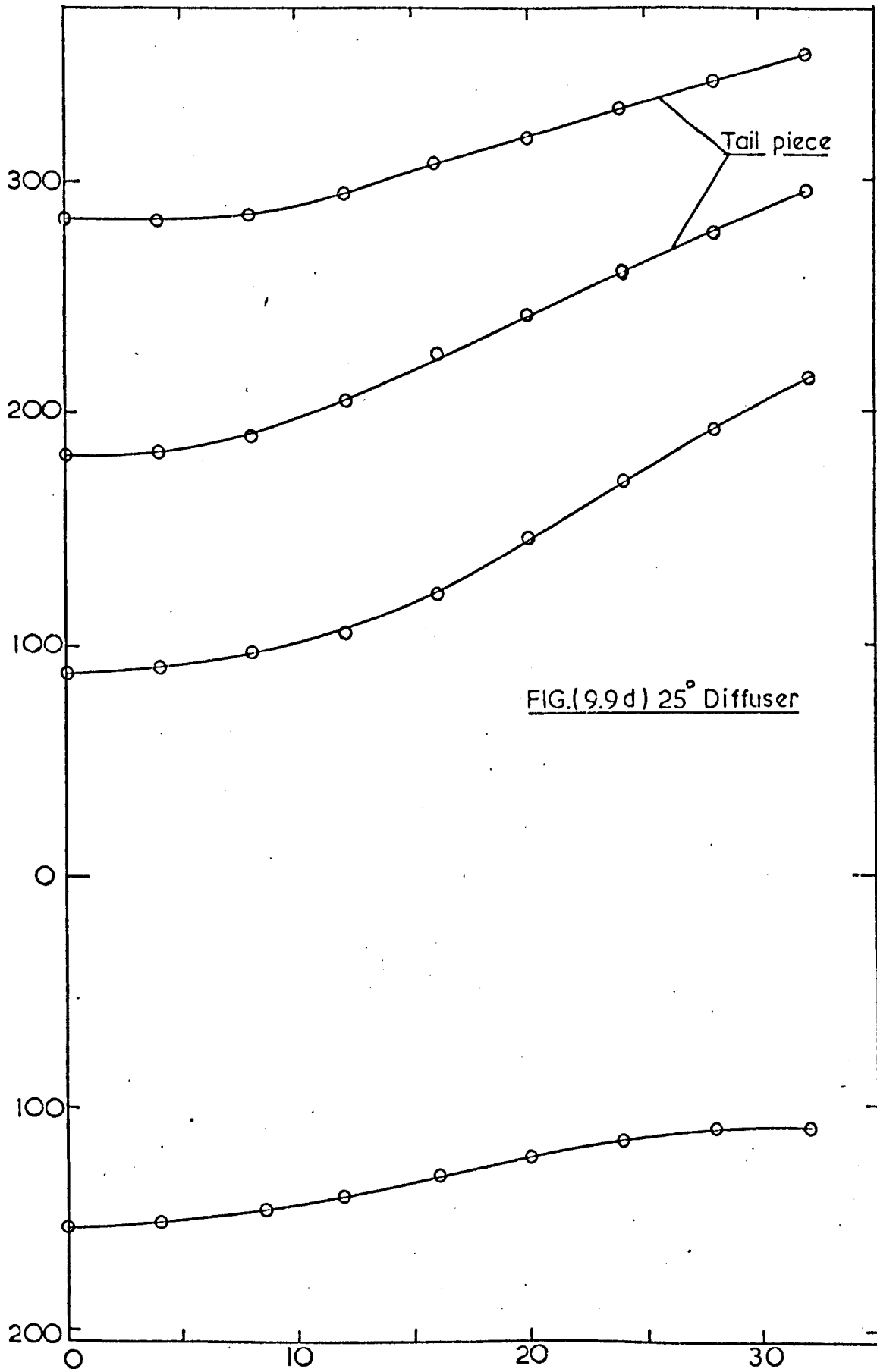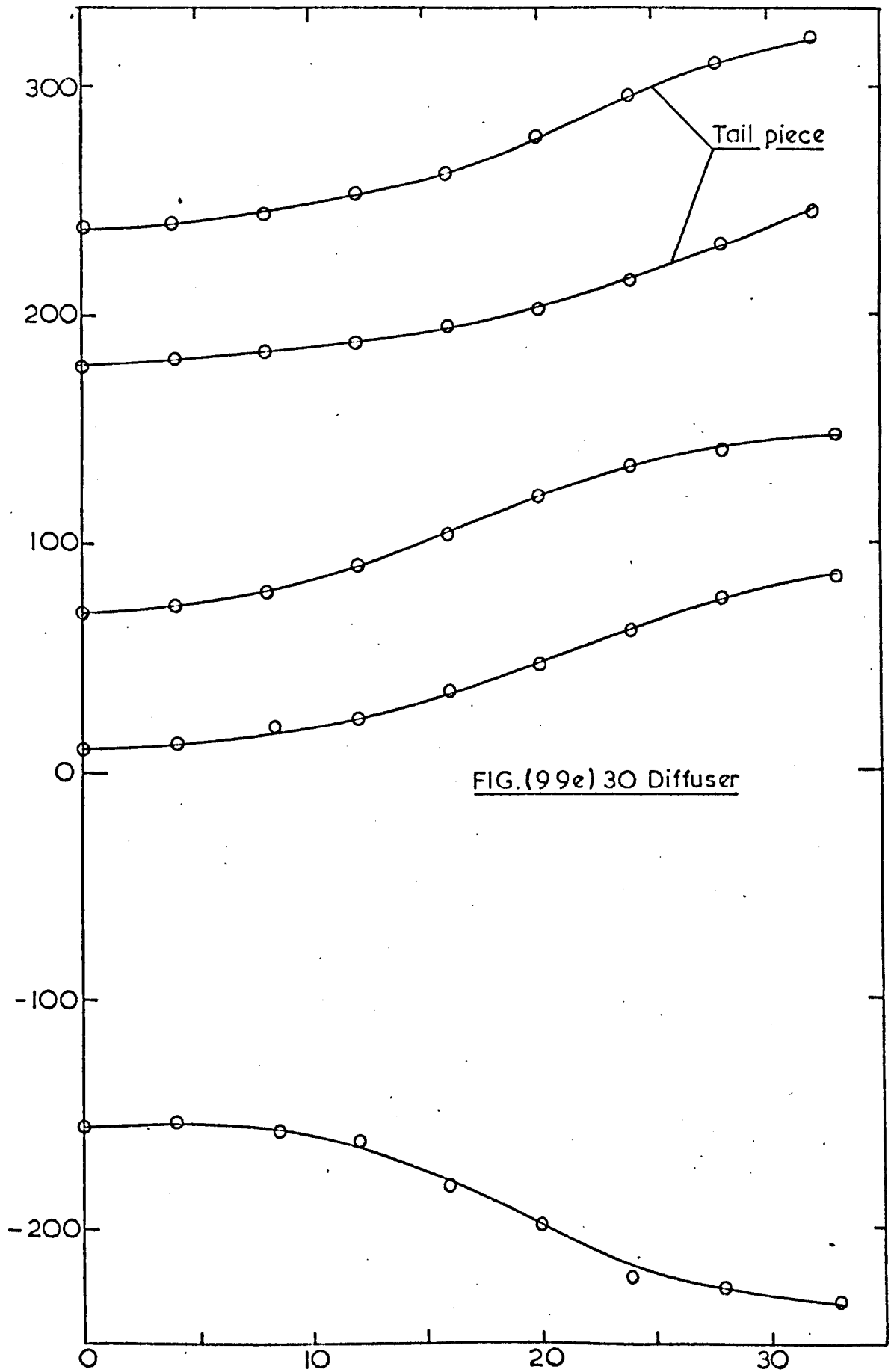
FIG.(9.9 d) 25° Diffuser

FIG.(99e) 30 Diffuser

It can be seen that for the 10° and 15° diffusers there is only a token improvement up to about 125 r.p.m.; beyond this all diffusers exhibit an improvement.

9.7 PRESENTATION OF PERFORMANCE INFORMATION

9.7.1 Basic Assumptions

In Chapter Two, the general expression for the 'overall energy efficiency' for the swirl case [eqn. (2.4.5)] was simplified on the assumption of conservation of angular momentum to obtain eqn. (2.4.6)

$$\eta_D^* = \frac{\dot{Q}(p_{c_{12}} - p_{a_1})/\rho + \dot{M}_1\omega_1(\omega_2/\omega_1 - 1)/2}{\dot{Q}q\chi_{x_1}(1 - AR^{-2}\chi_{x_2}/\chi_{x_1})/\rho - \dot{M}_1\omega_1(\omega_2/\omega_1 - 1)/2}$$

From the previous analysis of the 10° diffuser , Fig. (9.7), it is seen that angular momentum is conserved to within 7% of mean. At least for this case the above assumption is seen to be valid though its logical extension to the higher angles needs to be verified. In axial flow studies it is common practice to use only the inlet kinetic energy as the reference. For convenience the same basis is adopted in the present analysis which yields

$$\eta_{D^*}^* = \frac{\dot{Q}(p_{c_{12}} - p_{a_1})/\rho + \dot{M}_1\omega_1(\omega_2/\omega_1 - 1)/2}{\dot{Q}q_1\chi_{x_1}/\rho + \dot{M}_1\omega/2} \qquad (9.7.1.1)$$

This may be separated to obtain

$$\eta_{D^*}^* = \frac{(p_{c_{12}} - p_{a_1})}{q_1\chi_{x_1} + \rho\omega_1\dot{M}/2\dot{Q}} + \frac{(\omega_2/\omega_1 - 1)}{1 + 2\dot{Q}\chi_{x_1}q/\rho\omega_1\dot{M}_1} \qquad (9.7.1.2)$$

In Chapter Two, a very mild swirl was assumed, which implied that the pressure distribution across a radius was uniform. This resulted in the 'pressure recovery coefficient' [eqn. (2.4.7)]

$$C_p^* = (p_{c_{12}} - p_{a_1})/(q_1\chi_{x_1} + \rho\dot{M}_1\omega_1/2\dot{Q})$$

which is a very convenient basis for comparison of performance.
The validity of this assumption may be verified by substituting
the above equation into eqn. (9.7.1.2)

$$\eta_{D''}^* = C_p^* + \frac{(\omega_2/\omega_1 - 1)}{1 + 2\gamma_{*1}q\dot{Q}/\rho\dot{M}\omega_1}$$ (9.7.1.3)

as swirl decays in the diffuser

$$\omega_2/\omega_1 < 1$$

Thus the performance as evaluated by eqn. (2.4.7) is
always greater than the actual performance.

An estimate of the influence of this additional term may
be made by simplifying the denominator.

The angular momentum is

$$\dot{M} = 2\pi\rho\int_0^R uvr^2 dr$$

Introducing the weighting factor λ_+ and uniform axial velocity
this simplifies to

$$\dot{M} = \pi\rho\omega\lambda_+\bar{u}R^4/2$$

Also $\quad q = \rho\bar{u}^2/2 \quad$ and $\quad \dot{Q} = \rho\pi R^2\bar{u}$

Using these give

$$\frac{2\dot{Q}q\gamma_{*1}}{\rho\omega_1\dot{M}_1} = \frac{2\gamma_{*1}\bar{u}_1^2}{\lambda_{*1}\omega_1^2 R_1^2}$$

$$= . \frac{2\gamma_{*1}\cot^2\hat{\psi}}{\lambda_{+1}}$$

Substituting into eqn. (9.7.1.3) yields

$$\eta_{D''}^* = C_p^* - \frac{1 - \omega_2/\omega_1}{1 + 2\gamma_{*1}\cot^2\hat{\psi}/\lambda_{+1}}$$ (9.7.1.4)

The extreme value of $\overset{\wedge}{\psi}$ shown in the tables is zero and must not be used. A projected value must be used in accordance with the above definition. On inspection of the above equation it is seen that for zero inlet swirl (pure axial flow) the secondary term is zero which reduces the above equation to the axial flow case.

It can be seen from Fig. (9.2), that for the range of swirl considered the axial velocity distribution is reasonably uniform. Consequently the angular momentum factor and the kinetic energy factor will be approximately unity; the latter being evident from Fig. (9.3).

This simplifies eqn. (9.7.1.4.) to

$$\eta_{_{D'}}^{*} = C_{p}^{*} - (1 - \omega_{2}/\omega_{1})/(1 + 2\cot\overset{\wedge}{\psi}) \qquad (9.7.1.5)$$

The table below shows the contribution of the secondary term for various decay numbers for given maximum projected inlet swirl angles.

$\overset{\wedge}{\psi}$ $^{\circ}$ / ω_{2}/ω_{1}	5	10	15	20	25
0.25	0.003	0.012	0.026	0.047	0.074
0.50	0.002	0.008	0.017	0.031	0.049
0.75	0.001	0.004	0.009	0.016	0.025

For the 10° diffuser analysed the decay number ω_{2}/ω_{1} is 0.36 and the projected maximum swirl angle is 12°. These correspond to a value of 0.014. Thus it is clear that the assumption of mild swirl in the present work is justified.

9.7.2   Diffuser Performance

A convenient method for estimating the performance of diffusers with mild swirling flow was derived in Chapter Two. The accompanying assumptions were critically examined in the previous section. Figs. (9.10) are familiar cross plots of Figs. (9.9). These figures themselves are useful in that they indicate the rate of pressure recovery for a given case. The flattening out of the curves of the 10° diffuser compared with the still rising curves of the 30° diffuser are typical examples of this. Design problems arising due to the varying dimensions in a diffuser were discussed in Chapter Six and similar difficulties, with experimental work, were also discussed earlier. Presentation of performance information too is plagued by the same problems. For ready comparison it is necessary to maintain the same scale for all diffusers. Figs (9.10) shows the problem associated with this in that the wide angle diffusers tend to be cramped.

Fig. (9.11 - continuous curves) shows the performance of diffusers with increasing swirl. These curves are based on eqn. (2.2.5) assuming a mean inlet axial kinetic energy. In section (9.4) it was shown that the second term was less than 3% of the total kinetic energy. It can be seen that initially with very mild swirl there is hardly any increase of performance. However this situation is improved rapidly with further increase of swirl. The increase in the wider angle diffusers being noticibly good.

9.8   DISCUSSION AND CONCLUSIONS

The earlier sections in this chapter were concerned with means of improving experimental data and minimising errors resulting from numerical analysis.
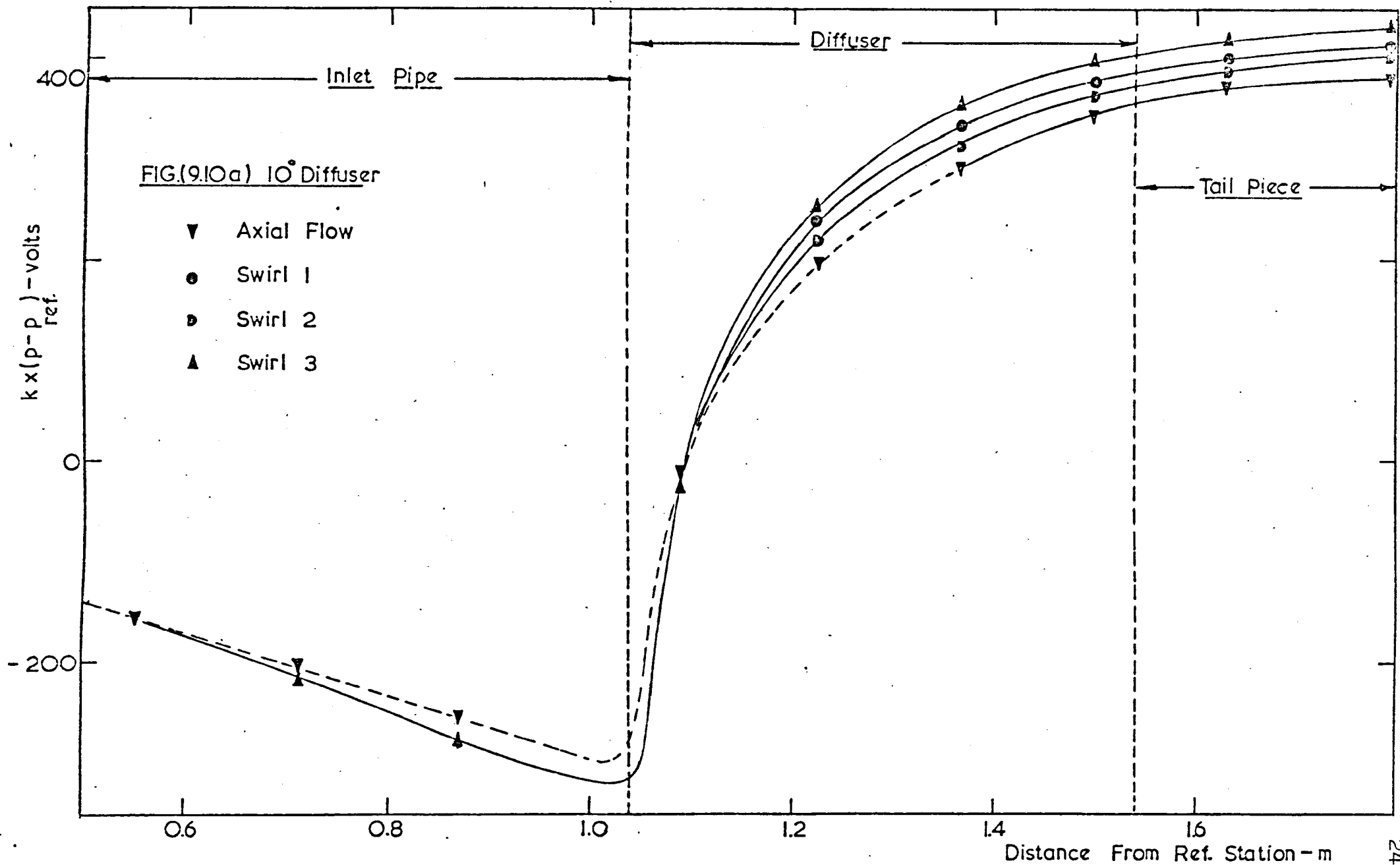
FIG. 9.10 PRESSURE VARIATION IN DIFFUSER — PIPE COMBINATION

FIG.(9.10 b) 15° Diffuser

FIG.(9.10c) 20° Diffuser

FIG.(9.10 d) 25° Diffuser
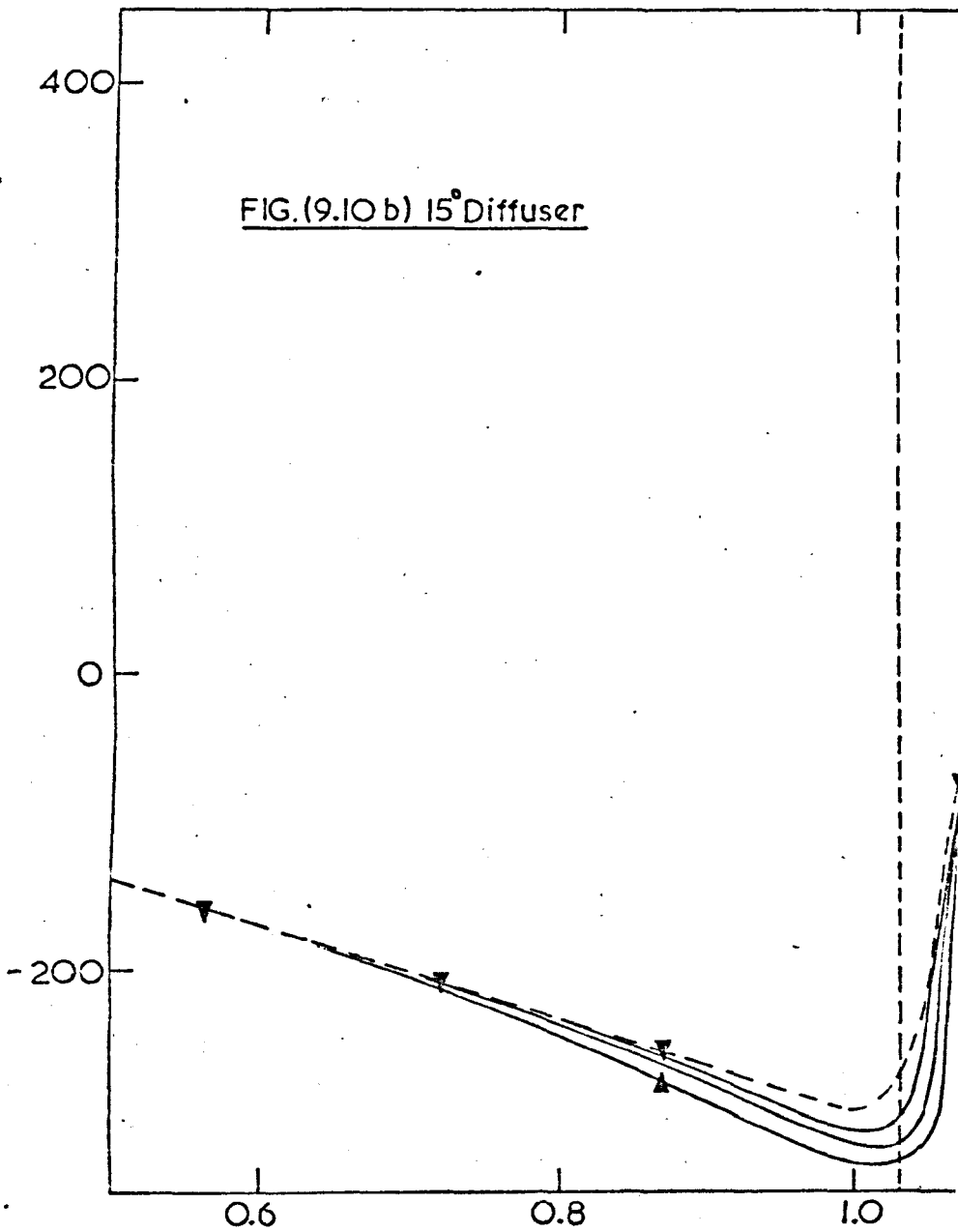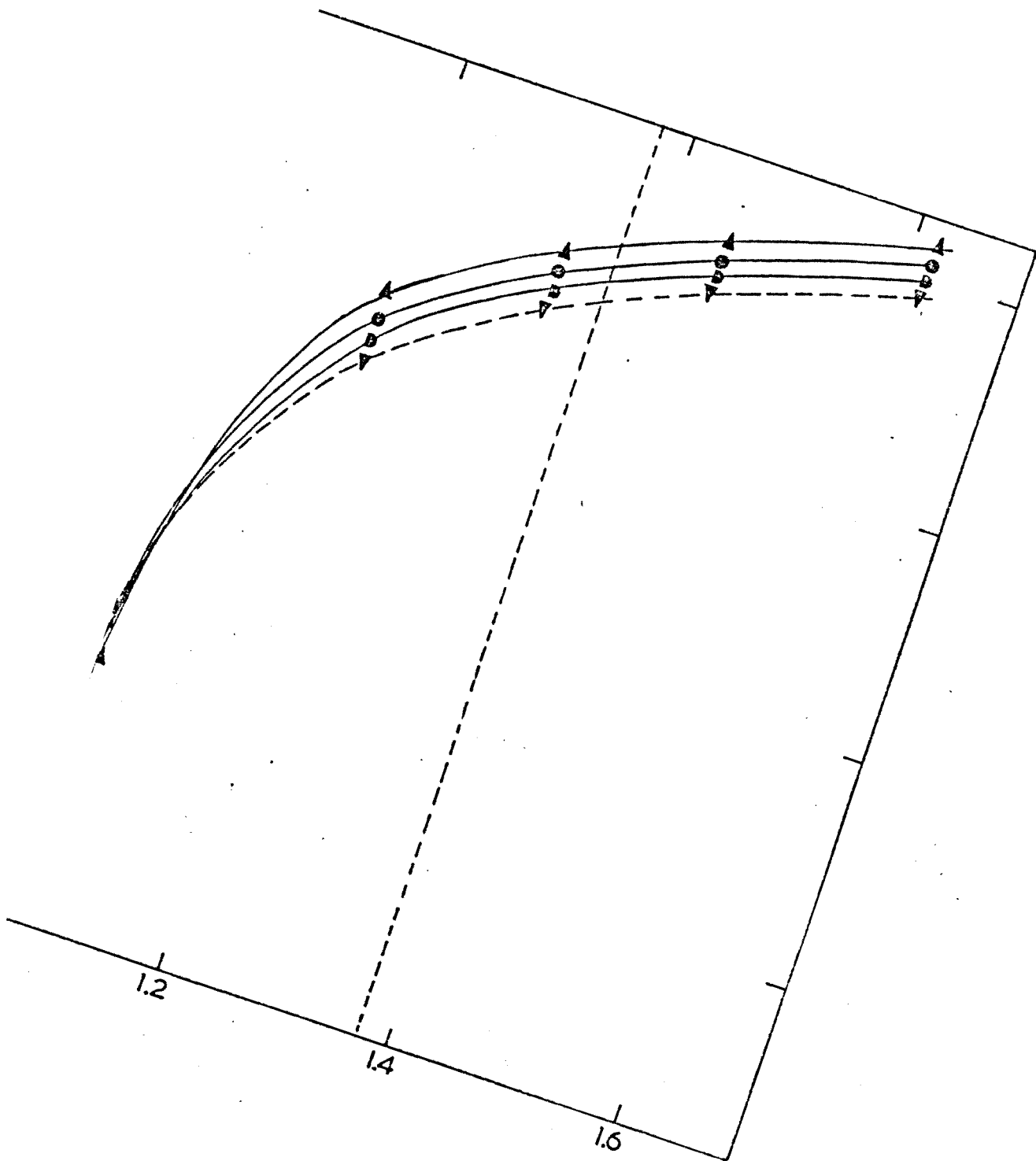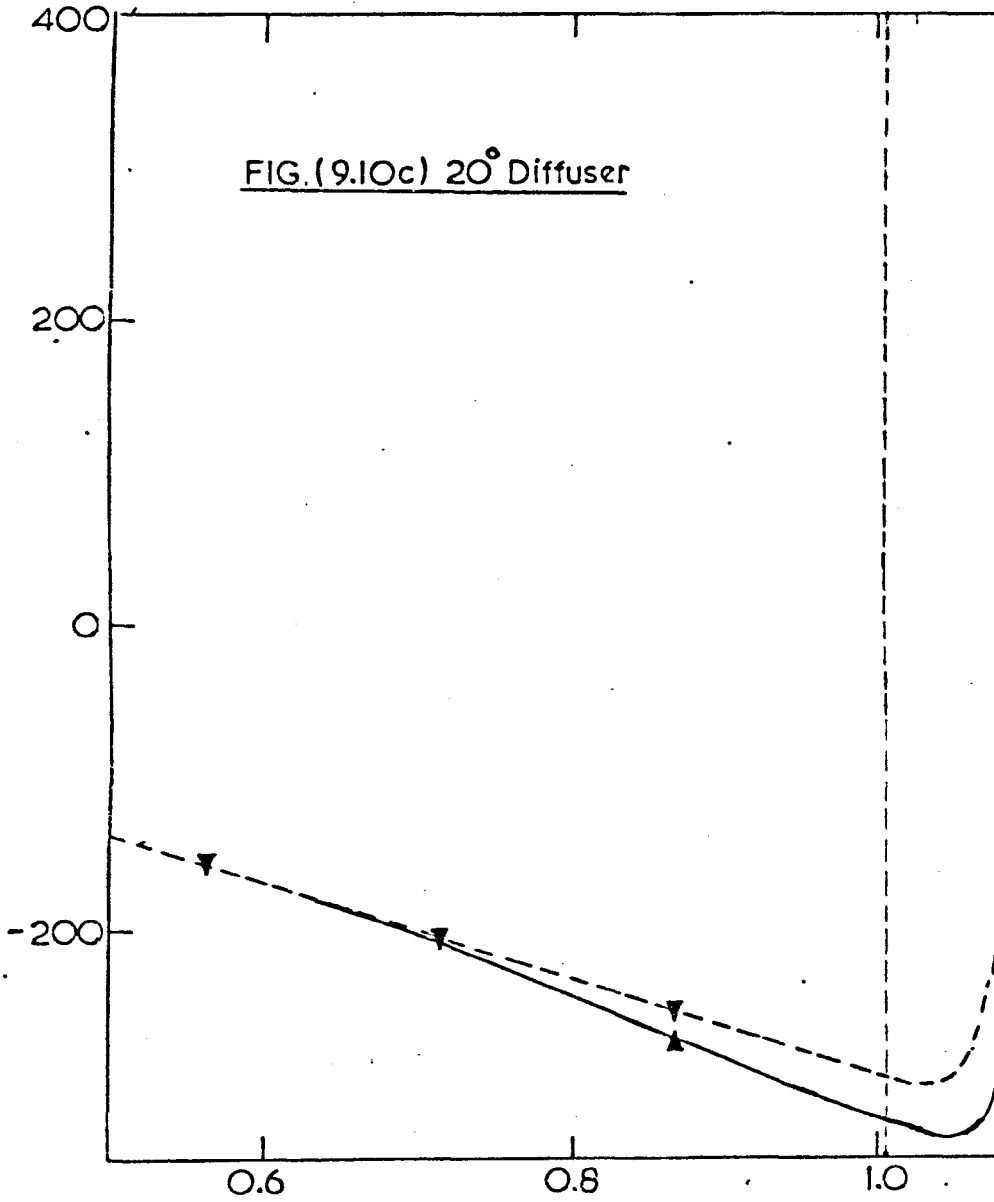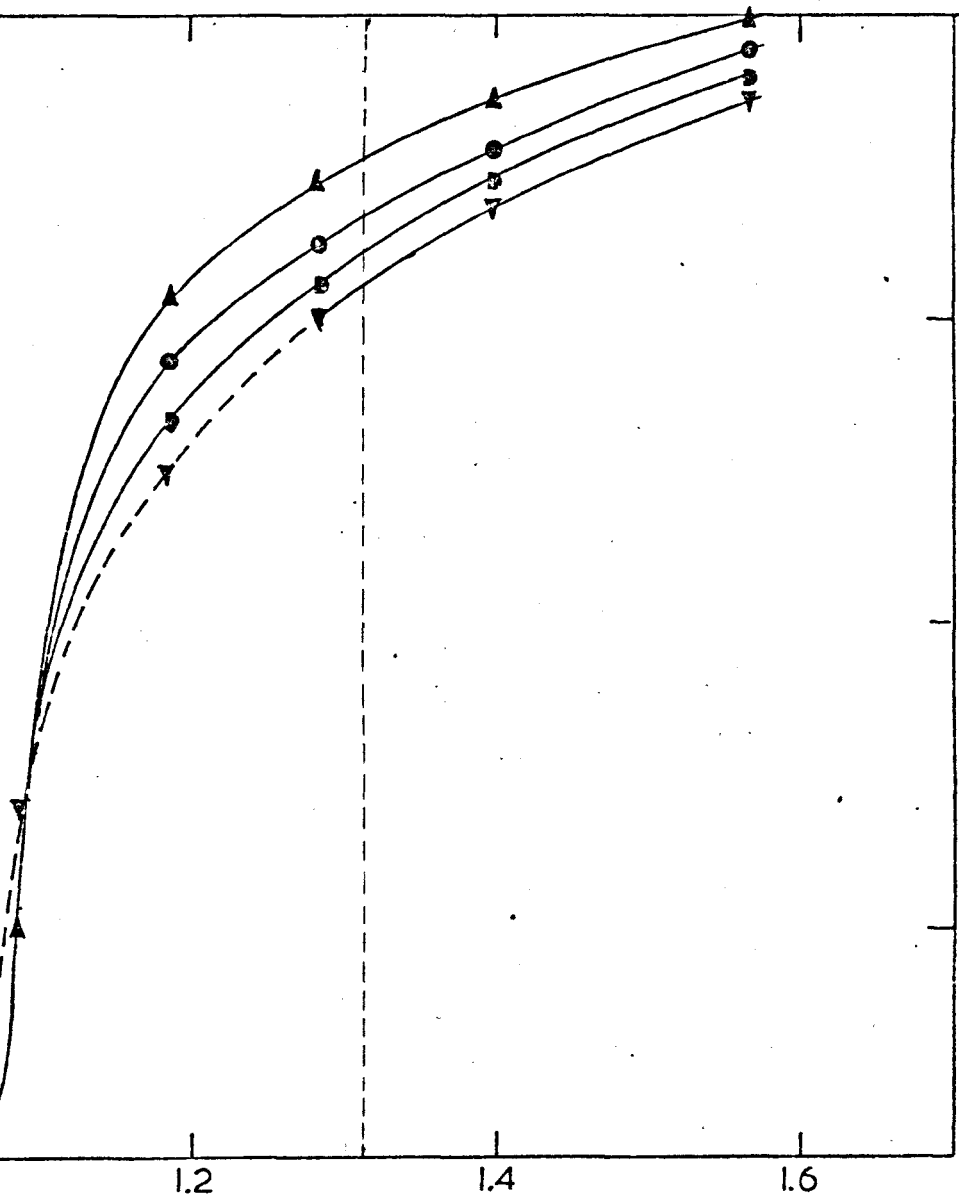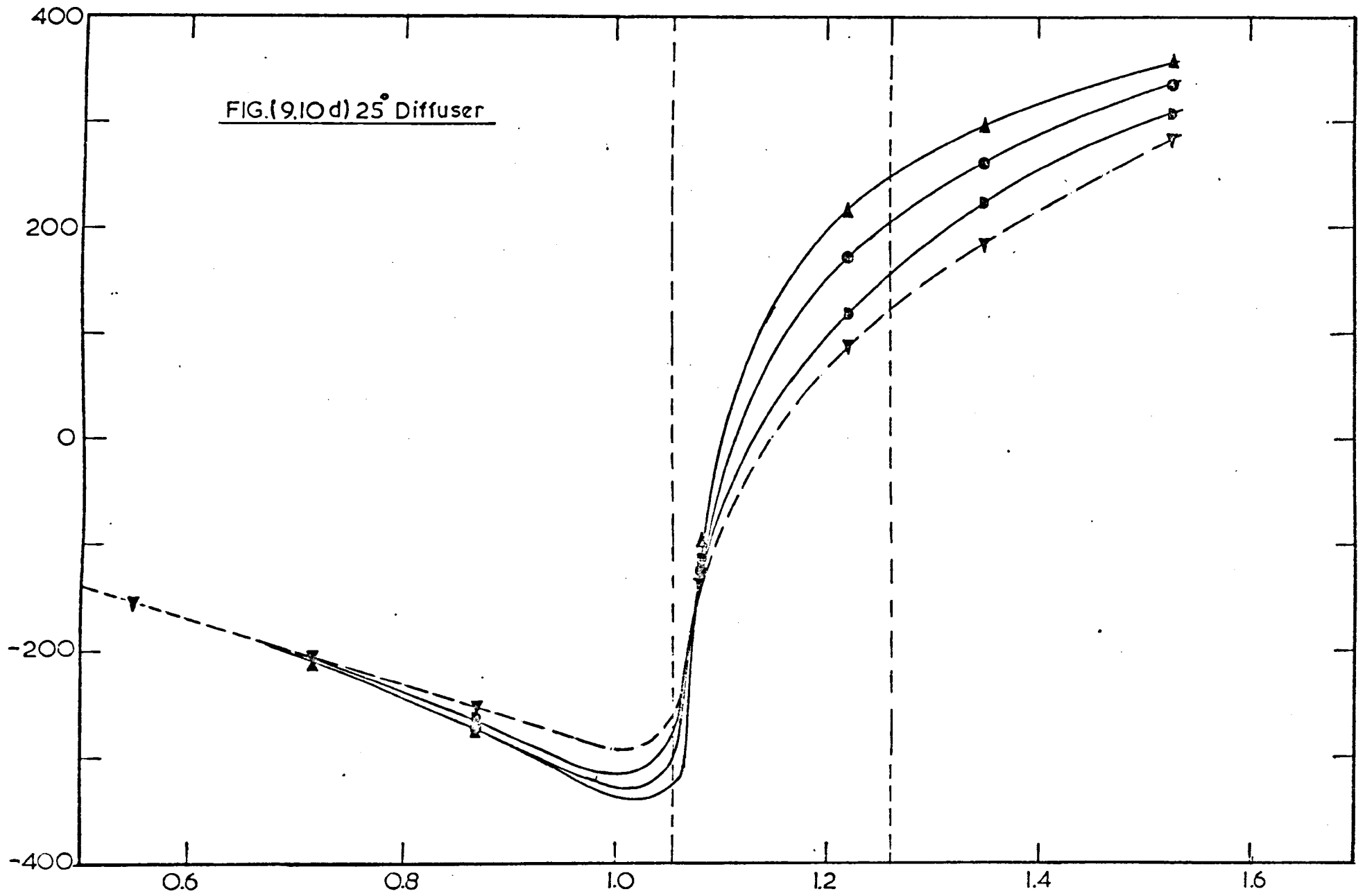
FIG.(9.10 e) 30° Diffuser
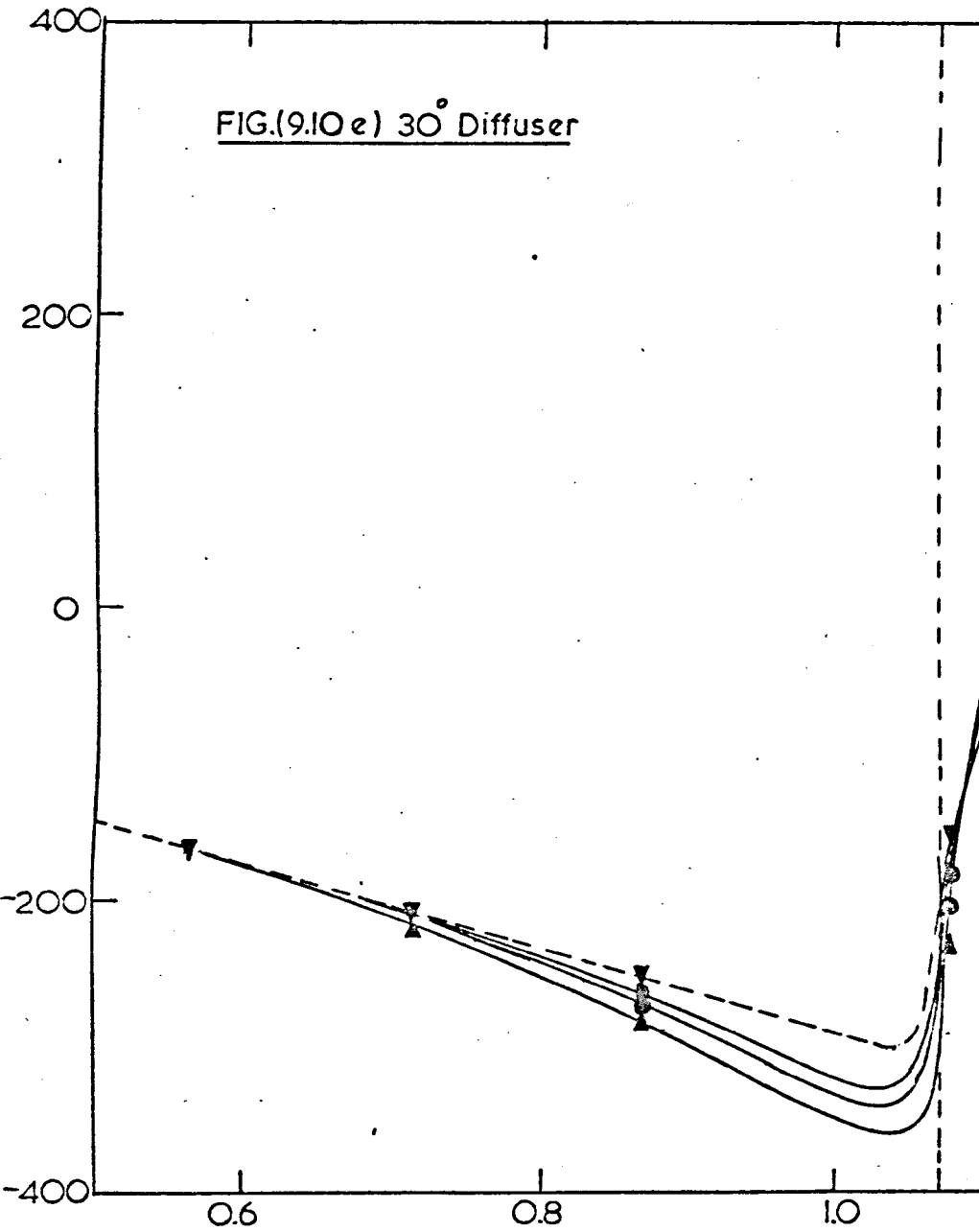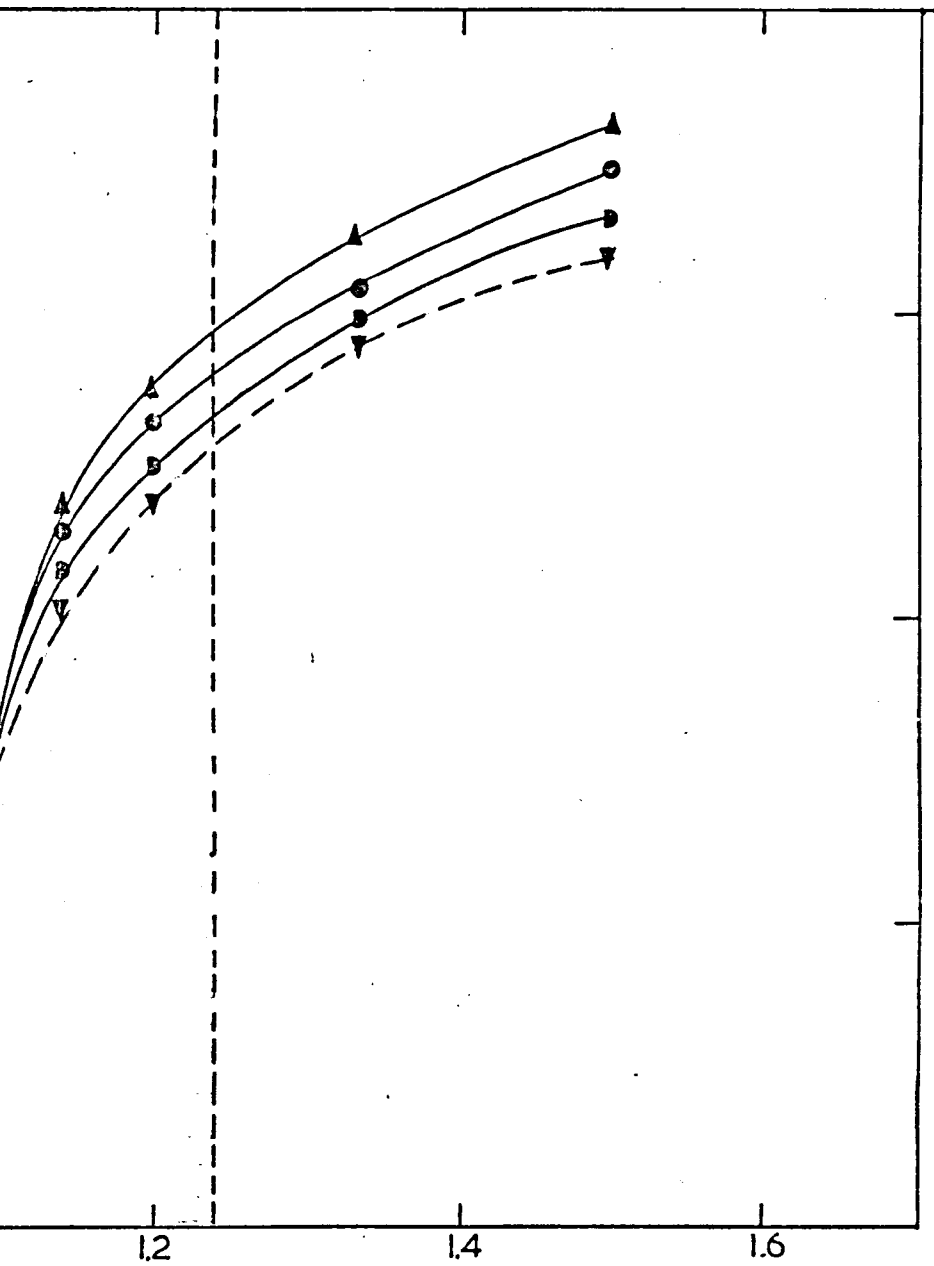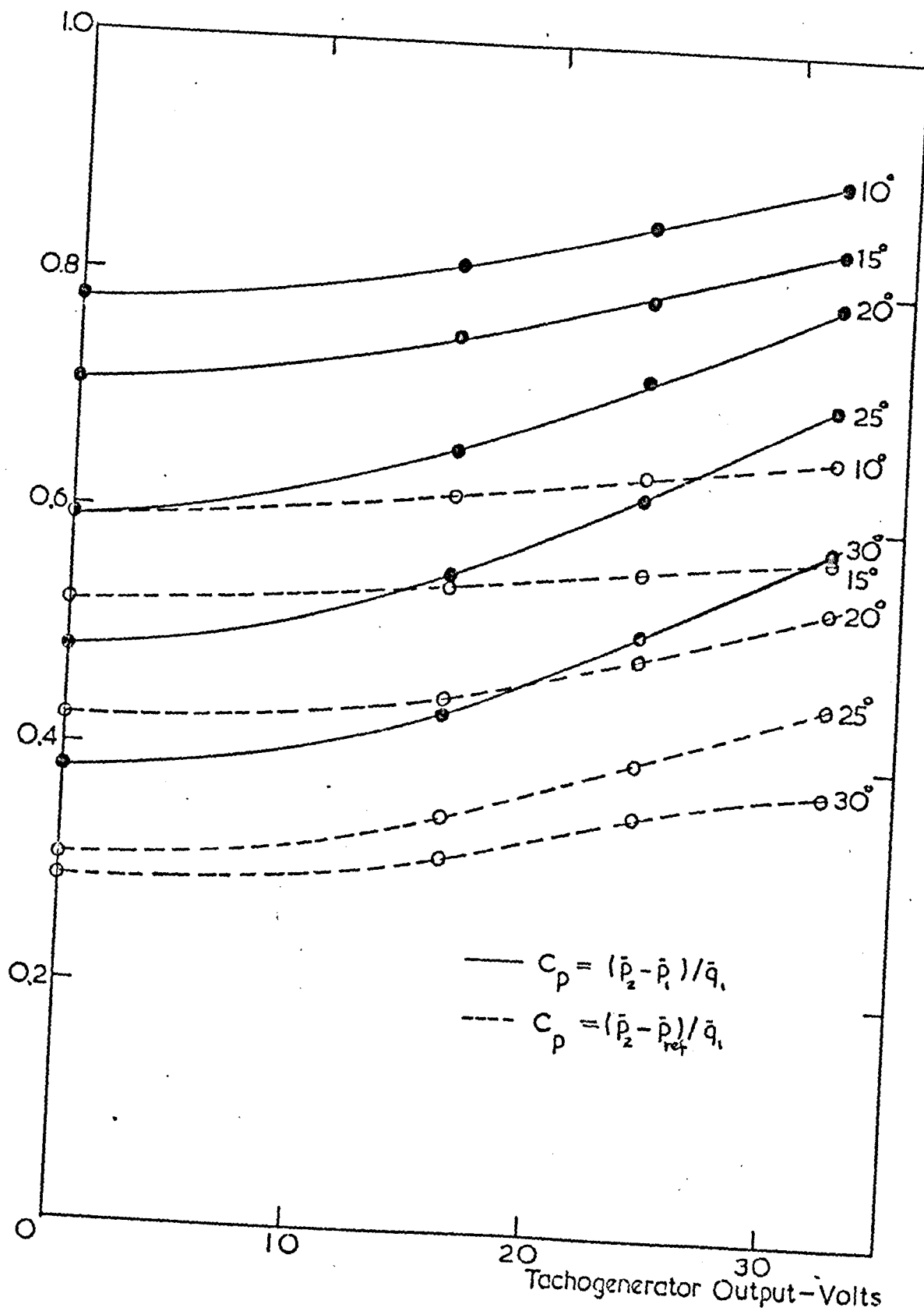
FIG. 9.11 DIFFUSER PERFORMANCE WITH SWIRL

In calibrating the swirl generator velocity measurements were conducted at the inlet station of the 10° diffuser. A study of the decay of swirl in the inlet pipe was not pursued as the variation between two stations was not measurable. Hall (1967) solved the governing equations for swirling pipe flow, numerically, and showed that swirl decayed to $1/3^{rd}$ of its initial value in about 100 radii. The assumption that angular momentum was conserved was verified and confirmed for the 10° diffuser. Area-averaged mass flux is constant to within 6% for both cases of flow in the 10° diffuser. The most significant feature in this analysis is the manner in which separation tendency has been eliminated [Fig. (9.4)] by swirl.

In the analysis of wall static pressure variation along the test section it was seen that the presence of swirl modified the pressure drop in the pipe. As a consequence, two interesting questions develop. The first question is the subjective nature of the curve used to blend the pressure drop in the pipe and the pressure rise in the diffuser. The second question is the applicability of the definition used hitherto to evaluate performance. If the pressure at an upstream station in the inlet pipe is regarded as the reference value (as this is appreciably constant with all the diffusers) instead of the pressure at diffuser inlet then the increase in performance with swirl will be much less. Additional static pressure points are required in the transition area to obtain a better estimate of the wall static pressure variation in this region.

The dashed-line curves in Fig. (9.11) indicate the performance referred to station 2 in the inlet pipe. Comparing these with the continuous lines, it is seen that the useful improvement is much less than that indicated by the conventional definition. The curves as a whole indicate that there is scope for further increase of performance with increase of swirl. The exception is the 30° diffuser, which indicates a drop in performance with further increase of swirl. It is likely that with the high swirl angles at exit, the assumptions of "mild swirl" and that of conservation of angular momentum are invalidated.

Owing to the widely differing conditions of experimentation it is difficult to offer any worthwhile comparison with the limited amount of published data. The author is not aware of any previous work which has cited the modification of the pressure drop in the inlet pipe. Figs. (4.4a) and (4.5c) support Fig. (9.11) in that swirl definitely has a beneficial effect on flow in diffusers. However a much more detailed analysis is required before a quantitative comparison is possible.

CHAPTER TEN

CONCLUDING COMMENTS.

10.1   AIMS AND METHOD OF INVESTIGATION

Various investigators have expressed the view that it may be possible to improve the performance of the conical diffuser by imparting swirl to the fluid at entry. In addition to this, in fluid handling devices such as pumps, turbines, vortex amplifiers etc., swirling flow is an inherent feature and as such diffuser performance data are required in these instances. A research programme was initiated at this establishment, the aim of which was to investigate the performance of diffusers with swirling flow and where necessary contribute to the existing knowledge on performance with axial flow. The current project was established to lay a sound basis for the main programme, and was carried out in three stages. Stage one was seen as one that would survey the present state of the subject as such an exercise had not been conducted previously. Stage two was concerned with formulating an overall strategy to include as much of the forseeable future requirements of the main programme. Stage three was primarily concerned with theoretical and experimental work and had a secondary function of steering future research.

10.2   RESULTS

Each chapter was concluded with a discussion and the results were presented. The associated assumptions and the limitations were included in the discussion. Here it suffices to present the results in a concise form. The discussion that follows is of necessity qualitative in nature.

As a vast number of definitions have been used in the past to define diffuser performance with axial flow it was necessary to review these and determine their inter-relation. On this basis, criteria for presenting performance data with swirling flow were developed. On the basis of "mild swirl" these were simplified to managable forms. This assumption was critically examined and justified.

A new 'AREA-PLOT' method was developed for presenting performance information. The advantage of this method is two-fold. Firstly the new plot permits comparison of performance of plane and conical diffusers and secondly it displays all three geometric variables.

As a contribution to axial flow studies the 'Ross-Fraser' method for predicting boundary layer growth in a diffuser was extended to obviate the need for intermediate wall static pressures. In the two original models flow parameters were grouped so as to obtain linearised semi-empirical relationships governing their growth. These themselves were insufficient to solve completely for all the unknowns. This difficulty was overcome by introducing the continuity equation. However to determine the mass flux accurately it was necessary to express the complete velocity profile in a mathematical form thus eliminating the need to "fair-in". The model was computerised as a closed-form solution. This makes the method much more attractive unlike the previous models which required reference to graphs. The predictions compare very well with Fraser's experimental data. The limitations of the method were discussed in Chapter Three.

An extensive survey of previous experimental and theoretical
work associated with swirling flow and vortex breakdown was conducted,
with particular emphasis on areas not covered previously. This was
considered necessary as it would permit future investigators to
proceed with their work without having to make individual surveys
on each occasion.

The Navier-Stokes equations as applied to laminar swirling
flow were solved. Resort was made to experimental data for obtaining
the constants which appear in the model. The velocity profiles
appear to be very weak functions of radius as the presence of the
boundary layer was ignored. It was seen that towards the exit end
of the diffuser mass flux and angular momentum are conserved. In the
last three sections this is remarkably good though not so for the
first two sections. It was shown that the tangential velocity in a
diffuser or in a pipe may be represented by a family of exponential
curves. The solid-body rotation core in the diffuser was seen to
diverge parallel to the diffuser in the 6° diffuser. The model seems
to admit the possibility of extension to turbulent flows by replacing
the kinematic viscosity by the eddy viscosity.

The characteristics of the spherical pitot probe were
investigated to see if it was possible to use Wright's method of
analysis when the stem was at right angles to it. It was found that
this was not possible, and hence a simplified calibration was used
instead.

The development of the various modes of vortex breakdown
in turbulent flow in a pipe was observed and photographed quite
successfully.

It was observed that vortex breakdown in the pipe was not an instability phenomenon but a reversible transition from one state to another. Regions of stability and instability have been identified in the context of the present work. The sense of rotation of the primary and secondary cores were the same.

It was seen that the honeycomb swirl generator produced a very good solid-body rotation. Swirl was seen completely to eliminate separation tendencies in the 10° diffuser. Within the range considered angular momentum was seen to be conserved in the 10° diffuser. The introduction of swirl modified the pressure drop in the inlet pipe immediately upstream of the diffuser. This invalidates the use of the conventional definition of diffuser performance. Thus it is not possible to quantify the effectiveness of swirl though it is evident that it does improve performance.

10.3   GUIDELINES FOR FUTURE RESEARCH

Research in the field of axial flow in diffusers has been in progress for nearly a century and as yet the associated characteristics of flow are not fully understood. At the very outset it was accepted that a single project would not be able to do more than scratch the surface on the subject of swirling flow in diffusers. Accordingly a purposeful research strategy was formulated with the onus on this project to lay a sound foundation and identify guidelines for future research. As each chapter was self contained the discussion that follows will treat each area in the same manner.

The 'Ross-Fraser' method has several weaknesses when applied to a general flow situation. Now that a closed form solution is available it is necessary to examine critically the range of validity of the empirical relationships used in the model.

As the computerised model is capable of handling higher order
equations there is no need to confine it to linearised equations.
Another area that needs investigation is that of the applicability
of the model to thick inlet boundary layers.

In the theoretical investigation of swirling laminar flow
the tangential velocity function must be further examined to obtain
a better fit for severe swirl and also modified to include the 'no-
slip' condition at the wall. The present investigation indicated
that the 'solid-body' rotation core diverged parallel to the diffuser.
The applicability of this to wider angle diffusers needs further study.
Explicit solution of the governing equations for turbulent swirling
flow does seem difficult at this stage. It would seem worthwhile
investigating the possibility of using an indirect approach by
including the radius-dependent eddy viscosity to take account of
turbulence. The inclusion of even one of the above extensions would
add greatly to the already complex problem and it may well be that an
alternative to the method of solution may have to be sought. It was
shown from the solution of the governing equations that it would be
preferable to use a conical coordinate system. In addition, two
conditions that may be used are that of conservation of mass flux
and of angular momentum.

The experimental rig which is due to be moved must be sited
such that air-suction is free of environmental disturbances. The main
structure should be stiffened and if necessary steps must be taken to
isolate the test area from structural vibration. This may be necessary
for flow visualisation.

Additional static pressure points are necessary in the inlet pipe immediately upstream of the diffuser and also in the diffuser immediately downstream of the throat. Provision has been made to incorporate a data logging system (which has been purchased). Some work is required to fully automate data logging.

It was seen that the method of calibration, of the spherical pitot probe, as proposed by Wright was not directly applicable when the stem is at right angles to the probe-head. Further work is necessary to accommodate high swirl as the method used in the present project is limited to mild swirl.

There is plenty of scope for work in the area of flow visualisation in diffusers. In the present project it was only possible to visualise flow in a pipe. Once regions of stability are established it is necessary to enquire into the effect of vortex breakdown on diffuser performance. As a supplement to this it would be necessary to identify the parameters influencing the movement of the primary core-head.

An analysis of flow in the 10° diffuser was conducted and it was established that angular momentum was conserved. Further work is required to determine if at higher swirl rates and wider angles angular momentum is conserved. The influence of the blend at the throat on the modification of the wall static pressure drop in the pipe should be further investigated. This needs to be followed by a close scrutiny of data to establish an acceptable definition for evaluating performance data with swirling flow.

The above discussion was concerned with possible extensions in particular areas.

The requirements of the main programme are seen from Fig. (1.2).
The test-rig however was designed with wider applications in mind.
Provision has been made to incorporate other forms of swirl
generators and to use non-Newtonian liquids.

Two research projects have been initiated in support of
this programme. One is concerned with the growth of the boundary
layer downstream of a honeycomb. It is hoped that it may be
possible to obtain at least an empirical relationship to predict
the growth of the boundary layer. This would enable the creation
of a known boundary layer in an industrial application thus obviating
the need to measure the velocity profile at inlet to the diffuser.
The other project is concerned with the improvement of jet-pump
performance by swirling the induced flow.

REFERENCES

ACKERET, J. (1958) Grenzschichten in geraden und gekrummten
diffusoren; Boundary Layer Research, IUTAM,
pp. 22-40

ANDRES, K. (1909) GERMAN PUBLICATION V.D.I. p. 76

BENJAMIN, T.B. (1962) Theory of vortex breakdown phenomenon; J. OF
FLUID MECH.; Vol. XIV; p.593

BENJAMIN, T.B. (1965) Significance of the vortex breakdown phenomenon
A.S.M.E.; J. BASIC ENG., Vol. LXXXVIII; pp 518-524

BINNIE, A.M. et.al.(1957) The flow of swirling water through a
convergent-divergent nozzle; J. OF FLUID MECH;
Dec.

BOSSEL, H.H. (1968) Stagnation criterion for vortex flows; A.I.A.A.;
Vol. VI; No. 6; pp 1192-93.

BOSSEL, H.H. (1969) Vortex breakdown flow-field. THE PHYSICS OF
FLUIDS; Vol. XII; No. 3; pp. 498-508

BOSSEL, H.H. (1971) Vortex computation by a method of weighted
residuals using exponentials; JOUR.A.I.A.A.;
Vol. IX; No. 10; pp.2027-34

CHIGIER, N.A. & CHERVINSKY, A. (1967) Experimental investigation of
swirling vortex motion in jets; JOUR.A.S.M.E.,
34 (E); Vol. II; pp.443-451

CLAYTON, B.R. & MASSEY, B.S. (1967) Flow visualisation in water: A
review of techniques; J. SCI. INST.; Vol. XXXI;
pp. 2-11

CRANE, C.M. & BURLEY, C.J. (1974) Numerical studies for viscous
swirling flow through annular diffusers: Pt I &
II; J. OF ENGINEERING MATHEMATICS; Vol. VIII;
No. 3; pp.181-207

CHOW, C.Y. (1969) Swirling flow in tubes of non uniform cross-section;
J. OF FLUID MECH.; Vol. XXXVIII; Pt.4; pp.843-854

COCKRELL, D.J. & MARKLAND, E. (1963) A review of incompressible
diffuser flow; AIRCRAFT ENGINEERING; p. 286; Oct.

COCKRELL, D.J. (1964) Boundary layer effects in diffusers; Ph.D. Thesis;
UNIV. OF NOTTINGHAM

FALKOVICH, S.V. (1967) Spreading of a twisted stream in an infinite
space flooded by the same fluid; PMM; Vol. XXXI;
No. 2; pp.282-288

FALKOVICH, S.V. & KOROBKO, V.I. (1969) Development of a swirling jet in infinite space; IZV. AN SSSR. MEKHANIKA ZHIDKOSTI I GAZA; Vol. IV; No. 3, pp.56-63

FOX R. & KLINE, S.J. (1962) "Flow regimes on curved subsonic diffusers" JOUR. A.S.M.E.; Series D; Vol. 84; No. 3; pp.303-16

FRASER, H.R. (1956) Study of an incompressible turbulent boundary layer in a conical diffuser; Ph.D. Thesis; UNIV. OF ILLINOIS

FRASER, H.R. (1958) The turbulent boundary layer in a conical diffuser; A.S.C.E.; J. OF HYD. DIV.; Paper 1684

FURUYA, Y. et. al. (1966) Loss of flow in conical diffusers with suction at entry; JAP.S.M.E.; Vol. IX; No. 33; p.131

GARTSHORE, I.S. (1962) Recent work in swirling incompressible flow; N.R.C. (CANADA) AERO. REP. LR-343

GORE, R.W. & RANZ, W.E. (1964) Backflows in rotating fluids moving axially through expanding cross-sections; A.I.CHEM.E. JOURNAL; Vol. X; No. 1; p. 83

HALL, M.G. (1966) The structure of concentrated vortex cores; PROGRESS IN AERO SCIENCES; Vol. VII

HALL, M.G. (1967) A numerical method for solving the equation for a vortex core; A.R.C.   R & M. 3467; HMSO(LONDON)

HARVEY, J.K. (1962) Some observations of the vortex breakdown phenomenon; J. OF FLUID MECH.; Vol. XIV; p.585

HOADLEY, D. (1970) Some measurements of swirling flow in an annular diffuser; Rept. W/M (3E); p. 1621; M.E.L. WHETSTONE, ENGLISH ELECTRIC CO. LTD.

JONES, J.P. (1960) The breakdown of vortices in separated flow; U. of SOUTHAMPTON AERO DEPT REPT NO. 140

JONES, J.P. (1964) On the explanation of vortex breakdown; IUTAM SYMP. ON VORTEX MOTION, 1964; ANN ARBOR

KING, M.K. et. al. (1969) Static pressure and velocity profiles in swirling incompressible tube flow; A.I.CH.E. JOURNAL; Vol. XV; No. 6; pp.837-842

KIRKPATRICK, D.L.T. (1964) Experimental investigation of the breakdown of a vortex in a tube; ARC C.P. 821

KLINE, S.J. et. al. (1959) Optimum design of straight walled diffusers; A.S.M.E.; J. OF BASIC ENG.; Vol. LXXXI; pp.321-331

LAMBOURNE, N.C. & BRYER, D.W. (1961) The bursting of leading edge vortices - Some observations and discussion of the phenomenon; ARC R & M 3282

LAMBOURNE, N.C. (1965) The breakdown of certain types of vortex; NAT. PHY. LAB. AERO R & M 1166

LAVAN, Z. et. al. (1969) Separation and flow reversal in swirling flows in circular ducts; THE PHYSICS OF FLUIDS; Vol. XII; No. 9; pp.1747-57

LOITSIANSKI, L.G. (1953) Propagation of a swirling jet in an infinite space filled with the same fluid; PMM; Vol. XVII; No. 1

LONG, R.R. (1953) Steady motion around a symmetrical obstacle moving along the axis of rotating liquid; J. METEOROLOGY; Vol. 10; p.197

LIEPE, F. (1960) Efficiency of slender conical diffusers with swirling flow; MASCHINENBAUTECHNIK; Vol. IV; No. 8; pp.405-412 (Available from B.H.R.A.)

LIEPE, F. (1963) Investigation into the conditions of swirling flow in conical diffusers. MACHINENBAUTECHNIC; Vol. XII; No. 3; pp 137-147 (Available from B.H.R.A.)

LUDWIEG, H. (1964) Explanation of vortex breakdown by the stability theory for spiralling flows; IUTAM SYMP. ON VORTEX MOTION, 1964; ANN ARBOR

McDONALD, A.T. & FOX, R.W. (1966) Incompressible flow in conical diffusers; INT.J.MECH.SCI.; Vol. VIII; No. 2; p.125

McDONALD, A.T. et. al. (1971) Effect of swirling inlet flow on pressure recovery in conical diffusers; JOUR. A.I.A.A.; No. 71-84

MENIS, M. (1960) Effect of vortex decay on pipe flow; M.I.T. GAS TURBINE LAB REP. 61

MOON, I. (1958) Distributed suction boundary layer control on conical diffusers; Res. rept. THE AERO-PHYSICS DEPT. OF MISSISSIPPI STATE COLLEGE

MOORE, C.A. & KLINE, S.J. (1958) Some effects of vanes and of turbulence in two dimensional wide angle diffusers; NACA TN 4080

NEVE, R.S. (1971) An investigation of factors influencing the static and dynamic performance of fluidic vortex amplifiers; Ph.D. Thesis, The City University (London)

NICOLL, W.B. & RAMAPRIAN, B.R. (1970) Performance of conical diffusers with annular injection at inlet; A.S.M.E.; PAPER NO. 70-FE-18

NISSAN, A.H. & BRESSAN, V.P. (1961) Swirling flow in Cylinders; A.I. CHEM.E. JOURNAL; Vol. VII; p. 535

NUTTALL, J.B. (1953) Axial flow in a vortex; NATURE; Vol. CLXXII; P. 582

PATTERSON, G.N. (1938) Modern diffuser design; AIRCRAFT ENGINEERING; Vol. X; p. 267

PECKHAM, D.H. & ATKINSON, S.A. (1967) Preliminary results of low speed wind tunnel tests on a gothic wing of aspect ratio 1.0; ARC C.P. 508

PEDLEY, T.J. (1969) On the stability of viscous flow in a rapidly rotating pipe; J. OF FLUID MECH.; Vol. XXXV; Pt. 1; p. 97

PERERA, E. (1975) THE CITY UNIVERSITY (LONDON), AERO-DEPT. (Ph.D. Thesis to be presented)

PERSH, J. & BAILEY, B.M. (1954) Effect of surface roughness over the downstream region of a 23° conical diffuser; NACA TN 3066

PETERS, H. (1934) Conversion of energy in cross-sectional divergences under different conditions of inflow; NACA TM734

PRANDTLE, L. The mechanics of viscous fluids, in aerodynamic theory; A general review of progress by W.F. DURRAND; Vol. III: p.68

ROSS, D. (1956) A physical approach to turbulent boundary layers. A.S.C.E.; Vol. XXI, pp 1219-1254

ROBERTSON, J.M. & FRASER, H.R. (1960) Separation prediction for conical diffusers; A.S.M.E., J. OF BASIC ENG. pp201-209

SARPKAYA, T. (1971) On stationary and travelling vortex breakdown; J. OF FLUID MECH. Vol. XLV. Pt.73; pp545-559

SARPKAYA, T. (1971a) Vortex breakdown in swirling conical flow; JOUR. A.I.A.A.; Vol. IX; No. 9; pp 1792-1799

SCHLINGER, W.G. et. al. (1953) Temperature gradient in turbulent gas streams: Non uniform flow; IND. ENG. CHEM. Vol 45; p.662

SENOO, Y. & NISHI, M. (1974) Improvement of the performance of conical diffusers by vortex generators; A.S.M.E. J. OF FLUIDS ENG.; pp. 4-10

SO, K.L. (1967) Vortex phenomenon in conical diffuser; JOUR. A.I.A.A.;
        Vol. V; No. 6; p. 1072

SOVRAN, G. & KLOMP, E.D. (1967) Fluid Mechanics of internal flow; ed.
        by G. SOVRAN; ELSEVIER PUBLISHING CO. AMSTERDAM; pp.
        270-319

SPRENGER, H. (1959) Experimental investigation of Straight and
        curved diffusers; Translation available as B.L.L.
        5809.95 T 5134

SQUIRE, H.B. (1960) Analysis of the vortex breakdown phenomenon;
        IMP. COLL. AERO DEPT. REP. NO. 102-ARC 21977.

SRINATH, T. (1968) Effect of flow on the flow regimes and performance
        of annular diffusers with equal inner and outer cones;
        PH.D. THESIS UNIV. OF WATERLOO.

TALBOT, L. (1954) Laminar swirling pipe flow; J. APP. MECH.; Vol. XXI
        No. 1; p.1

VAN DEWOESTINE, R.V. (1969) An experimental investigation of
        boundary layer development and swirling flow in conical
        diffusers; PH.D. THESIS PURDUE UNIV.

VULLERS, H. (1933) ZEITSCHRIFT DES VEREINES DEUTSCHER INGENIEURE;
        Vol. LXXVII; No. 31

WALSH, J.   Numerical Analysis: An introduction; Ch. 8; Published
        by Acadamy Press

WERLE, H. (1960) RESEARCH AERONAUT; No. 79; pp9-26

WILLIAMS, R.T. & HORI, A.M. (1970) Formation of hydraulic jumps in a
        rotating system; J. OF GEOPHY. RES.; Vol. LXXV; No. 5;
        pp. 2813-21

WINTERNITZ, F.A.L. & RAMSAY, W.J. (1957) Effect of inlet boundary
        layer on pressure recovery, energy conversion and losses
        in conical diffusers; J. ROY. AERO. SOC.; Vol. LXI;
        p. 116

WIRASINGHE, N.E.A. (1972) Diffuser performance with swirling flow;
        Part 1: A review of the problem; M.E.D. Res. Memo.
        ML44; THE CITY UNIVERSITY (LONDON)

WIRASINGHE, N.E.A. (1974) Boundary layer growth in conical diffusers;
        M.E.D. Res. Memo. ML67; THE CITY UNIV. (LONDON)

WYGNANSKI, I. (1970) Swirling axisymmetric laminar jet. THE PHYSICS
        OF FLUIDS; Vol. XIII; No. 10; pp 2455-60

YANG, T. (1965) Splitter effect in conical diffusers; ENG-EXPT
            STATION-BULLETIN 103; CLEMSON UNIV. COLL.

YOUSSEF, T.E.A. (1966) Some investigations of the rotating flow
            with a recirculation core in straight pipes;
            A.S.M.E., No. 66 - WA/FE - 36

STATION NO.	AXIAL DISTANCE	DIFFUSER RADIUS	BOUNDARY LAYER THICKNESS	DISPLACEMENT THICKNESS	MOMENTUM THICKNESS	SHAPE PARAMETER	CORE VELOCITY	COEFF. OF SHEAR STRESS
IN	$\alpha = z/R_o$	$\beta = R/R_o$	Y/R_o	δ/R_o	θ/R_o	D	$\mu = U_c/U_{co}$	$C_f \times 10^3$
1	.0	1.000	.1403	.0192	.0135	.310	1.000	3.50
2	.4918	1.0403	.1620	.0248	.0168	.350	.944	2.70
3	.8284	1.0693	.1750	.0323	.0205	.400	.897	2.00
4	1.6535	1.1416	.2015	.0495	.0290	.620	.809	1.40
5	2.7096	1.2340	.2775	.0828	.0426	.800	.739	.80
6	3.4522	1.2990	.3370	.1145	.0515	.925	.704	.58
7	3.8416	1.3333	.3700	.1267	.0561	.975	.686	.52
8	4.5479	1.3947	.4560	.1670	.0647	1.150	.663	.35
9	5.2607	1.4574	.5350	.2020	.0733	1.200	.645	.25
10	6.0990	1.5307	.6275	.2460	.0828	1.300	.622	.16

TABLE 3/I; DIFFUSER BOUNDARY LAYER DATA; FRASER (1958)

BOUNDARY LAYER GROWTH IN A DIFFUSER

INPUT PARAMETERS

THROAT RADS. = 3.03
AREA RATIO= 2.38
LENGTH TO RADS. RATIO= 6.20
CONE ANGLE= 10.000
MOM. THK. REY. NO.= 3000.000

EVALUATED PARAMETERS

AXIAL ST. IN	AXIAL DIST. $a=z/R_o$	WALL RADIUS $\beta=R/R_o$	B/LAY THKNS Y/R_o	MOMTUM THKNS θ/R_o	D FACTOR D	CORE VELY $\mu=u_c/u_{co}$	MOMTUM FACTOR γ_{**}	FRCTON FACTOR $C_f \times 10^3$	AVRAGE VELCTY $\bar{U}/\bar{U}_o$	ENERGY FACTOR γ_*	DSPMNT THKNS δ/R_o	INT.MNT THKNS θ/R_o
1	0.000	1.000	0.140	0.014	0.277	1.000	1.006	3.392	0.966	1.060	0.0174	0.0130
2	0.689	1.060	0.174	0.020	0.394	0.907	1.012	2.727	0.859	1.106	0.0283	0.0199
3	1.379	1.121	0.216	0.028	0.530	0.835	1.022	2.021	0.769	1.184	0.0450	0.0282
4	2.068	1.181	0.264	0.037	0.675	0.779	1.039	1.435	0.692	1.305	0.0678	0.0386
5	2.757	1.241	0.320	0.046	0.814	0.737	1.063	0.984	0.627	1.479	0.0965	0.0483
6	3.446	1.302	0.379	0.055	0.939	0.703	1.094	0.652	0.570	1.709	0.1300	0.0569
7	4.136	1.362	0.443	0.063	1.045	0.676	1.130	0.435	0.521	2.000	0.1671	0.0641
8	4.825	1.422	0.509	0.071	1.132	0.654	1.171	0.235	0.477	2.353	0.2068	0.0699
9	5.514	1.482	0.578	0.079	1.204	0.634	1.214	0.185	0.439	2.770	0.2484	0.0746
10	6.203	1.543	0.649	0.086	1.262	0.616	1.260	0.118	0.406	3.253	0.2913	0.0783

TABLE 3/II; COMPUTED USING PRESENT METHOD

VELOCITY PROFILE INFORMATION

OUTPUT FORMAT—RAD. DIST. FROM WALL (y/R_0)/VELOCITY (u/u_c)

STATION NO. 1
0.0005/0.2134	0.0011/0.3730	0.0016/0.4787	0.0022/0.5307
0.0051/0.6145	0.0081/0.6620	0.0111/0.6932	0.0140/0.7169
0.0193/0.7517	0.0246/0.7807	0.0298/0.8037	0.0351/0.8203
0.0614/0.8833	0.0827/0.9565	0.1140/0.9775	0.1403/1.0000

STATION NO. 2
0.0007/0.1913	0.0013/0.3344	0.0020/0.4202	0.0027/0.4758
0.0064/0.5532	0.0100/0.5242	0.0137/0.6222	0.0174/0.6435
0.0239/0.6746	0.0305/0.7011	0.0370/0.7241	0.0435/0.7443
0.0761/0.8339	0.1088/0.9096	0.1414/0.9680	0.1740/1.0000

STATION NO. 3
0.0008/0.1647	0.0017/0.2870	0.0025/0.3695	0.0034/0.4096
0.0079/0.4752	0.0125/0.5102	0.0170/0.5342	0.0216/0.5525
0.0296/0.5801	0.0377/0.6056	0.0458/0.6304	0.0539/0.6556
0.0943/0.7763	0.1347/0.8782	0.1751/0.9569	0.2155/1.0000

STATION NO. 4
0.0011/0.1378	0.0022/0.2425	0.0032/0.3113	0.0043/0.3451
0.0098/0.3909	0.0154/0.4270	0.0209/0.4470	0.0264/0.4632
0.0364/0.4872	0.0463/0.5084	0.0562/0.5324	0.0661/0.5489
0.1157/0.6153	0.1653/0.8450	0.2149/0.9452	0.2645/1.0000

STATION NO. 5
0.0014/0.1269	0.0028/0.2000	0.0041/0.2578	0.0055/0.2858
0.0121/0.3264	0.0187/0.3510	0.0253/0.3682	0.0320/0.3807
0.0439/0.3998	0.0559/0.4164	0.0679/0.4349	0.0799/0.4716
0.1398/0.5565	0.1997/0.6130	0.2596/0.9339	0.3195/1.0000

STATION NO. 6
0.0018/0.0941	0.0035/0.1644	0.0053/0.2110	0.0070/0.2339
0.0148/0.2606	0.0225/0.2852	0.0302/0.2982	0.0379/0.3683
0.0522/0.3219	0.0664/0.3350	0.0806/0.3554	0.0968/0.3909
0.1663/0.6040	0.2371/0.7844	0.3083/0.9238	0.3794/1.0000

STATION NO. 7
0.0023/0.0974	0.0045/0.1336	0.0068/0.1715	0.0090/0.1901
0.0178/0.2146	0.0267/0.2290	0.0355/0.2392	0.0443/0.2472
0.0609/0.2549	0.0775/0.2660	0.0941/0.2844	0.1107/0.3222
0.1938/0.5592	0.2768/0.7604	0.3599/0.9152	0.4429/1.0000

STATION NO. 8
0.0029/0.0618	0.0058/0.1089	0.0087/0.1387	0.0115/0.1537
0.0214/0.1717	0.0312/0.1824	0.0411/0.1916	0.0509/0.1968
0.0700/0.2033	0.0891/0.2090	0.1082/0.2257	0.1273/0.2654
0.2223/0.5223	0.3183/0.7400	0.4138/0.9081	0.5093/1.0000

STATION NO. 9
0.0037/0.0498	0.0074/0.0870	0.0111/0.1117	0.0143/0.1238
0.0255/0.1376	0.0363/0.1448	0.0470/0.1509	0.0578/0.1557
0.0795/0.1605	0.1012/0.1625	0.1228/0.1779	0.1445/0.2191
0.2528/0.4921	0.3613/0.7236	0.4696/0.9023	0.5780/1.0000

STATION NO. 10
0.0047/0.0398	0.0095/0.0696	0.0142/0.0894	0.0190/0.0991
0.0305/0.1079	0.0419/0.1139	0.0534/0.1184	0.0649/0.1220
0.0892/0.1237	0.1135/0.1245	0.1378/0.1388	0.1622/0.1814
0.2838/0.4676	0.4054/0.7102	0.5271/0.8975	0.6487/1.0000

TABLE 3/III; COMPUTED USING PRESENT METHOD

STATION NUMBER =	1	2	3	4	5	6
NO. OF AXIAL RAD=	1.1420	3.4300	5.7100	8.0000	10.2900	12.5800
WALL RADIUS =	1.0600	1.1800	1.3000	1.4200	1.5400	1.6600
CONSTANT CC(1,I)=	1.2442	1.2645	1.3573	1.3221	1.2772	1.4346
CONSTANT CC(2,I)=	13.3347	6.8160	3.4453	2.6413	2.2054	1.4023
CORE RADIUS =	0.5070	0.4293	0.6039	0.6897	0.7548	0.9466
MAX. TANG. VELY.=	0.4614	0.3353	0.2521	0.2182	0.1926	0.1725
MOM OF MOMENTUM =	0.5601	0.5767	0.5932	0.5528	0.5371	0.5606
MASS FLUX =	3.0420	3.1628	3.2478	3.1498	3.2042	3.1802
TANGENTIAL K.E.=	0.1399	0.0995	0.0755	0.0578	0.0448	0.0400
AXIAL K.E. =	1.3402	1.0142	0.7554	0.4776	0.3579	0.2602
VARI,BLTY OF FIT=	99.2080	98.0033	99.0439	97.4866	99.3861	98.0998

TABLE 5/I. COMPUTED FLOW PROPERTIES OF 6° DIFFUSER

ANGLE OF PITCH = -30.00

-50.	-25.	-20.	-15.	-10.	-5.	0.	5.	10.	15.	20.	25.	30.
287.	294.	301.	306.	309.	308.	311.	304.	295.	288.	282.	271.	254.
200.	208.	215.	215.	218.	220.	216.	212.	209.	204.	193.	186.	179.
307.	298.	286.	272.	259.	246.	224.	213.	202.	184.	169.	160.	155.
294.	306.	309.	312.	323.	320.	315.	316.	312.	305.	295.	241.	284.
174.	180.	198.	210.	225.	230.	252.	267.	275.	291.	295.	302.	309.

ANGLE OF PITCH = -25.00

-50.	-25.	-20.	-15.	-10.	-5.	0.	5.	10.	15.	20.	25.	30.
285.	299.	305.	315.	320.	322.	317.	316.	306.	303.	286.	281.	266.
204.	218.	222.	222.	228.	232.	228.	223.	219.	220.	214.	202.	185.
311.	304.	291.	278.	263.	242.	224.	211.	198.	182.	168.	162.	145.
281.	290.	300.	301.	304.	306.	302.	294.	303.	285.	281.	262.	260.
164.	174.	196.	208.	231.	240.	258.	275.	289.	300.	308.	315.	314.

ANGLE OF PITCH = -20.00

-50.	-25.	-20.	-15.	-10.	-5.	0.	5.	10.	15.	20.	25.	30.
295.	309.	319.	324.	327.	331.	328.	324.	318.	309.	297.	285.	272.
219.	222.	234.	241.	240.	249.	246.	242.	237.	227.	220.	215.	203.
320.	309.	301.	284.	267.	248.	233.	217.	199.	180.	168.	154.	150.
263.	277.	276.	285.	292.	298.	291.	285.	286.	280.	266.	262.	250.
162.	180.	190.	212.	232.	245.	263.	282.	295.	307.	320.	327.	331.

ANGLE OF PITCH = -15.00

-50.	-25.	-20.	-15.	-10.	-5.	0.	5.	10.	15.	20.	25.	30.
303.	314.	327.	330.	333.	335.	331.	331.	323.	314.	305.	290.	284.
233.	240.	248.	255.	259.	262.	261.	261.	253.	246.	243.	235.	226.
324.	314.	300.	285.	271.	247.	233.	218.	203.	189.	177.	173.	168.
252.	254.	258.	260.	267.	274.	269.	267.	262.	259.	256.	243.	238.
169.	182.	194.	211.	229.	246.	265.	284.	297.	314.	325.	330.	334.

ANGLE OF PITCH = -10.00

-50.	-25.	-20.	-15.	-10.	-5.	0.	5.	10.	15.	20.	25.	30.
313.	318.	330.	335.	337.	340.	339.	338.	332.	317.	306.	291.	277.
253.	259.	260.	271.	279.	275.	271.	272.	268.	262.	252.	241.	224.
326.	317.	299.	285.	273.	253.	233.	217.	201.	184.	169.	160.	158.
250.	254.	243.	250.	256.	253.	252.	252.	251.	247.	241.	228.	226.
171.	183.	199.	217.	231.	253.	270.	287.	304.	319.	326.	332.	340.

ANGLE OF PITCH = -5.00

-50.	-25.	-20.	-15.	-10.	-5.	0.	5.	10.	15.	20.	25.	30.
309.	321.	330.	334.	341.	341.	336.	332.	325.	317.	302.	291.	276.
267.	278.	281.	287.	290.	292.	290.	285.	284.	272.	273.	255.	246.
322.	317.	299.	284.	267.	251.	228.	218.	199.	182.	175.	168.	168.
215.	225.	234.	231.	234.	236.	236.	235.	230.	224.	222.	217.	201.
175.	188.	196.	216.	232.	250.	270.	287.	302.	314.	324.	334.	338.

ANGLE OF PITCH = 0.00

-50.	-25.	-20.	-15.	-10.	-5.	0.	5.	10.	15.	20.	25.	30.
306.	316.	325.	335.	336.	337.	335.	331.	325.	315.	302.	285.	277.
272.	286.	294.	296.	301.	306.	298.	298.	295.	285.	273.	261.	255.
320.	310.	299.	276.	265.	252.	229.	211.	200.	184.	177.	169.	165.
197.	206.	206.	205.	213.	226.	217.	215.	218.	210.	212.	200.	196.
173.	188.	197.	214.	228.	244.	267.	285.	295.	309.	319.	326.	332.

ANGLE OF PITCH = 5.00

-50.	-25.	-20.	-15.	-10.	-5.	0.	5.	10.	15.	20.	25.	30.
301.	307.	316.	324.	326.	328.	328.	325.	312.	309.	298.	281.	266.
289.	296.	306.	306.	310.	311.	311.	310.	304.	296.	288.	275.	261.
315.	295.	289.	271.	258.	241.	223.	207.	187.	182.	171.	165.	166.
189.	190.	193.	192.	195.	195.	199.	197.	192.	190.	191.	188.	182.
174.	182.	192.	206.	226.	241.	258.	273.	285.	296.	312.	315.	319.

ANGLE OF PITCH = 10.00

-50.	-25.	-20.	-15.	-10.	-5.	0.	5.	10.	15.	20.	25.	30.
294.	299.	312.	314.	317.	321.	317.	310.	308.	304.	290.	285.	266.
295.	299.	312.	315.	321.	322.	319.	322.	314.	306.	300.	286.	275.
304.	292.	281.	269.	245.	234.	214.	200.	190.	185.	175.	172.	175.
184.	185.	185.	182.	180.	181.	180.	179.	185.	181.	183.	181.	182.
178.	184.	189.	204.	214.	231.	245.	266.	279.	293.	305.	311.	316.

ANGLE OF PITCH = 15.00

-50.	-25.	-20.	-15.	-10.	-5.	0.	5.	10.	15.	20.	25.	30.
285.	289.	300.	311.	314.	315.	306.	306.	301.	296.	282.	273.	260.
298.	307.	318.	329.	329.	330.	331.	325.	322.	313.	307.	293.	285.
296.	280.	272.	265.	240.	228.	212.	200.	191.	185.	182.	185.	188.
181.	178.	183.	173.	177.	177.	177.	178.	182.	181.	184.	184.	183.
177.	182.	189.	205.	215.	226.	246.	258.	274.	290.	297.	303.	305.

ANGLE OF PITCH = 20.00

-50.	-25.	-20.	-15.	-10.	-5.	0.	5.	10.	15.	20.	25.	30.
273.	287.	285.	300.	301.	302.	300.	300.	288.	291.	278.	266.	253.
305.	317.	312.	331.	331.	334.	333.	333.	328.	322.	311.	303.	287.
279.	275.	272.	248.	237.	223.	208.	202.	190.	186.	181.	182.	191.
182.	179.	179.	176.	177.	175.	175.	182.	182.	184.	184.	184.	188.
183.	187.	190.	197.	215.	219.	233.	250.	262.	271.	281.	287.	296.

ANGLE OF PITCH = 25.00

-50.	-25.	-20.	-15.	-10.	-5.	0.	5.	10.	15.	20.	25.	30.
268.	271.	279.	286.	287.	289.	286.	284.	278.	274.	266.	259.	248.
311.	322.	326.	333.	336.	336.	335.	335.	329.	323.	315.	304.	293.
272.	264.	255.	258.	232.	218.	207.	200.	191.	189.	188.	186.	195.
194.	185.	182.	181.	181.	182.	185.	185.	182.	189.	182.	192.	191.
187.	190.	191.	199.	205.	211.	232.	240.	252.	262.	273.	274.	282.

ANGLE OF PITCH = 30.00

-50.	-25.	-20.	-15.	-10.	-5.	0.	5.	10.	15.	20.	25.	30.
262.	266.	269.	273.	277.	277.	277.	274.	272.	265.	258.	246.	238.
322.	326.	328.	333.	337.	342.	339.	337.	332.	322.	317.	303.	296.
262.	256.	244.	233.	225.	215.	205.	199.	194.	191.	190.	193.	196.
203.	198.	193.	191.	194.	192.	194.	195.	195.	195.	197.	197.	201.
189.	192.	196.	201.	206.	215.	223.	233.	239.	249.	258.	261.	269.

TABLE 7/I . PROBE CHARACTERISTIC DATA ; (FIG. 7.4)

TABLE 9/I   FLOW PROPERTIES FOR INCREASING SWIRL

SWIRL 1

RADIUS MM	0.000	5.514	7.181	12.114	15.797	19.644	23.529	29.161	32.628	39.652	44.250	48.750
ANG. OF YAW	0.000	0.414	0.906	1.558	2.057	2.605	3.191	4.190	4.830	6.617	8.587	0.000
AXL VEL M/S	6.193	6.185	6.129	6.014	5.939	5.828	5.698	5.374	5.213	4.615	4.052	0.000
TNG VEL M/S	0.000	0.045	0.097	0.164	0.213	0.265	0.318	0.394	0.440	0.535	0.597	0.000

ANG. MOM. FLUX= 0.5942E-03 N.M   MASS FLUX=0.04030KG/S   OMG= 0.135E 02 RDNS/S
MEAN VEL.= 4.4979M/S   AXL K.E.= 0.5546E 00 N.M/S   K.E. FACTOR= 1.3605

SWIRL 2

RADIUS MM	0.000	5.514	7.181	12.114	15.797	19.644	23.529	29.161	32.628	39.652	44.250	48.750
ANG. OF YAW	0.000	0.611	1.336	2.295	3.007	3.825	4.652	5.994	6.887	9.168	11.089	0.000
AXL VEL M/S	5.601	5.600	5.748	5.642	5.613	5.485	5.398	5.184	5.043	4.586	4.214	0.000
TNG VEL M/S	0.000	0.062	0.134	0.226	0.295	0.367	0.439	0.544	0.609	0.740	0.826	0.000

ANG. MOM. FLUX= 0.9250E-03 N.M   MASS FLUX=0.03930KG/S   OMG= 0.187E 02 RDNS/S
MEAN VEL.= 4.3866M/S   AXL K.E.= 0.5012E 00 N.M/S   K.E. FACTOR= 1.3255

SWIRL 3

RADIUS MM	0.000	5.514	7.181	12.114	15.797	19.644	23.529	29.161	32.628	39.652	44.250	48.750
ANG. OF YAW	0.000	1.003	2.151	3.764	4.859	6.132	7.273	9.059	10.111	12.452	15.001	0.000
AXL VEL M/S	5.559	5.597	5.448	5.248	5.298	5.211	5.254	5.212	5.215	5.118	4.706	0.000
TNG VEL M/S	0.000	0.094	0.205	0.345	0.450	0.560	0.671	0.831	0.930	1.130	1.261	0.000

ANG. MOM. FLUX= 0.1543E-02 N.M   MASS FLUX=0.04027KG/S   OMG= 0.285E 02 RDNS/S
MEAN VEL.= 4.4951M/S   AXL K.E.= 0.5241E 00 N.M/S   K.E. FACTOR= 1.2882

TABLE 9/II   AXIAL FLOW: 10 DEG. DIFFUSER

STATION NO. 1

RADIUS MM	0.000	3.514	7.181	12.114	15.797	19.644	23.529	29.161	32.628	39.652	44.250	48.750
ANG. OF YAW	0.000	0.000	0.000	0.000	0.000	0.000	0.000	0.000	0.000	0.000	0.000	0.000
AXL VEL M/S	5.843	5.826	5.741	5.893	5.690	5.733	5.784	5.488	5.497	4.992	4.023	0.000
TNG VEL M/S	0.000	0.000	0.000	0.000	0.000	0.000	0.000	0.000	0.000	-0.000	0.000	0.000

ANG. MOM. FLUX= 0.0000E 00 N.M   MASS FLUX=0.04349KG/S   OMG= 0.000E 00 RDNS/S
MEAN VEL.= 4.8541M/S   AXL K.E.= 0.5686E 00 N.M/S   K.E. FACTOR= 1.1097

STATION NO. 2

RADIUS MM	0.000	4.589	9.922	16.689	21.711	26.929	32.166	39.696	44.293	53.507	59.460	63.960
ANG. OF YAW	0.000	0.000	0.000	0.000	0.000	0.000	0.000	0.000	0.000	0.000	0.000	0.000
AXL VEL M/S	4.698	4.698	4.646	4.593	4.517	4.474	4.202	3.516	3.373	2.344	1.502	0.000
TNG VEL M/S	0.000	0.000	0.000	0.000	0.000	0.000	0.000	0.000	0.000	0.000	0.000	0.000

ANG. MOM. FLUX= 0.0000E 00 N.M   MASS FLUX=0.04694KG/S   OMG= 0.000E 00 RDNS/S
MEAN VEL.= 3.0435M/S   AXL K.E.= 0.3145E 00 N.M/S   K.E. FACTOR= 1.4466

STATION NO. 3

RADIUS MM	0.000	5.581	12.049	20.228	26.274	32.533	38.786	47.728	53.153	63.944	70.850	75.350
ANG. OF YAW	0.000	0.000	0.000	0.000	0.000	0.000	0.000	0.000	0.000	0.000	0.000	0.000
AXL VEL M/S	3.623	3.836	3.836	3.949	3.666	3.679	3.179	2.406	1.931	1.213	0.767	0.000
TNG VEL M/S	0.000	0.000	0.000	0.000	0.000	0.000	0.000	0.000	0.000	0.000	0.000	0.000

ANG. MOM. FLUX= 0.0000E 00 N.M   MASS FLUX=0.04531KG/S   OMG= 0.000E 00 RDNS/S
MEAN VEL.= 2.1170M/S   AXL K.E.= 0.1984E 00 N.M/S   K.E. FACTOR= 1.9535

STATION NO. 4

RADIUS MM	0.000	6.601	14.235	23.856	30.942	38.252	45.527	55.871	62.110	74.428	82.240	86.740
ANG. OF YAW	0.000	0.000	0.000	0.000	0.000	0.000	0.000	0.000	0.000	0.000	0.000	0.000
AXL VEL M/S	3.137	2.988	2.916	2.859	2.865	2.736	2.493	1.981	1.279	0.572	0.256	0.000
TNG VEL M/S	0.000	0.000	0.000	0.000	0.000	0.000	0.000	0.000	0.000	0.000	0.000	0.000

ANG. MOM. FLUX= 0.0000E 00 N.M   MASS FLUX=0.04285KG/S   OMG= 0.000E 00 RDNS/S
MEAN VEL.= 1.5106M/S   AXL K.E.= 0.1161E 00 N.M/S   K.E. FACTOR= 2.3750

TABLE 9/III — SWIRLING FLOW: 10 DEG. DIFFUSER

STATION NO. 1

RADIUS MM	0.000	3.314	7.181	12.114	15.797	19.644	23.529	29.161	32.628	39.652	44.250	48.750
ANG. OF YAW	0.000	0.600	1.300	2.300	3.000	3.800	4.650	6.000	6.900	9.200	11.100	0.000
AXL VEL M/S	5.801	5.800	5.748	5.642	5.613	5.485	5.398	5.184	5.043	4.586	4.214	0.000
TNG VEL M/S	0.000	0.001	0.130	0.227	0.294	0.364	0.439	0.545	0.610	0.743	0.827	0.000

ANG. MOM. FLUX= 0.9250E-03 N.M   MASS FLUX=0.03930KG/S   OMG= 0.000E 00 RDNS/S
MEAN VEL.= 4.3865M/S   AXL K.E.= 0.5012E 00 N.M/S   K.E. FACTOR= 1.3255

STATION NO. 2

RADIUS MM	0.000	4.589	9.922	16.689	21.711	26.929	32.166	39.696	44.293	53.507	59.460	63.960
ANG. OF YAW	0.000	1.237	1.632	2.423	4.546	6.100	7.626	10.001	12.012	16.946	21.073	0.000
AXL VEL M/S	4.306	4.259	4.212	3.946	3.811	3.659	3.443	3.176	3.017	2.560	1.939	0.000
TNG VEL M/S	0.000	0.092	0.120	0.167	0.303	0.391	0.461	0.560	0.642	0.780	0.747	0.000

ANG. MOM. FLUX= 0.9810E-03 N.M   MASS FLUX=0.04171KG/S   OMG= 0.000E 00 RDNS/S
MEAN VEL.= 2.7043M/S   AXL K.E.= 0.2152E 00 N.M/S   K.E. FACTOR= 1.4109

STATION NO. 3

RADIUS MM	0.000	5.581	12.049	20.228	26.274	32.533	38.786	47.728	53.153	63.944	70.850	75.350
ANG. OF YAW	0.000	1.400	2.900	5.100	6.400	7.800	8.400	11.000	12.900	17.900	23.200	0.000
AXL VEL M/S	2.699	2.744	2.684	2.629	2.527	2.289	2.352	2.281	2.212	1.937	1.493	0.000
TNG VEL M/S	0.000	0.067	0.136	0.235	0.283	0.314	0.347	0.443	0.507	0.626	0.640	0.000

ANG. MOM. FLUX= 0.1008E-02 N.M   MASS FLUX=0.04171KG/S   OMG= 0.000E 00 RDNS/S
MEAN VEL.= 1.9488M/S   AXL K.E.= 0.1008E 00 N.M/S   K.E. FACTOR= 1.2721

STATION NO. 4

RADIUS MM	0.000	6.601	14.235	23.856	30.942	38.252	45.527	55.871	62.110	74.428	82.240	86.740
ANG. OF YAW	0.000	1.800	5.300	7.300	8.000	9.000	11.600	13.300	13.800	17.800	21.500	0.000
AXL VEL M/S	1.850	1.804	1.750	1.680	1.787	1.673	1.752	1.800	1.782	1.582	1.217	0.000
TNG VEL M/S	0.000	0.059	0.162	0.215	0.251	0.265	0.360	0.426	0.438	0.508	0.479	0.000

ANG. MOM. FLUX= 0.1042E-02 N.M   MASS FLUX=0.04295KG/S   OMG= 0.000E 00 RDNS/S
MEAN VEL.= 1.5142M/S   AXL K.E.= 0.5831E-01 N.M/S   K.E. FACTOR= 1.1843

TABLE 9/IV   WALL STATIC PRESSURE DISTRIBUTION IN PIPE (VOLTS)

$$PRESS.(N/M^2)=0.01962 \times VOLTS$$

AXIAL	SWIRL 1
SWIRL 3	SWIRL 2

STATION	1	2	3		4		5	
DIFFUSER								
10	-79	-120	-166	-165	-208	-212	-252	-259
			-166	-166	-224	-218	-275	-267
15	-79	-120	-167	-166	-208	-211	-253	-259
			-168	-167	-224	-217	-278	-268
20	-79	-120	-166	-167	-207	-213	-251	-261
			-166	-168	-225	-219	-280	-270
25	-79	-120	-166	-166	-209	-216	-252	-262
			-169	-167	-230	-223	-285	-273
30	-79	-120	-165	-167	-209	-216	-252	-265
			-168	-166	-234	-225	-292	-277

APPENDIX 3/A

THE MODIFIED AITKEN - DELTA PROCESS

The AITKEN - DELTA process and its modified form are discussed below.

Consider the general case of an iterative process which may be represented as

$$u_i \longrightarrow \boxed{\text{operation}} \longrightarrow Z_i = f(u_i) = u_{i+1}$$
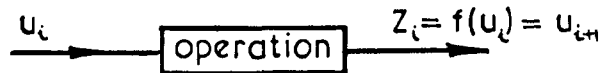
For each successive operation u_{i+1} is made the input.

If the process is convergent, then,

$$\mathcal{L}_{i \to \infty} (u_i - Z_i) = 0$$

Only a convergent process is of interest here and hence the discussion will be confined to this case. The iterative process, while being convergent, may be either monotonic or oscillatory. The two cases may be graphically represented as in Figure (3.8).

The straight-forward 'Aitken-Delta' process predicts the true solution as

$$M_{pred} = (u_1 u_3 - u_2^2)/(u_1 - 2 u_2 + u_3)$$

(The proof of this may be found in any standard text on numerical analysis.).

Owing to the symmetry of the above expression, (i.e. U_1 and U_3 may be interchanged without altering the result), if the equation is "severly non-linear" the process would diverge.

The present problem does suffer from a "severe non-linearity" in character, and in addition to this there is a need to solve a quartic equation (using Bairstow's process).

Depending on the starting value U_1, the calculated value Z_1 (or u_2) may be unsatisfactory for further progress. This is because, as pointed out earlier, the quartic equation may not yield a positive root. Then a smaller value of Z_1 is used until the quartic equation yields an acceptable solution.

The purpose of the Aitken-Delta process is to speed-up the rate of convergence. Because of the presence of the previously mentioned sub-iterative the general 'Aitken-Delta' process needs to be modified before it can be usefully employed.

Before using the process it is first necessary to observe the evaluated approximate roots. (i.e. if monotonic or oscillatory.)

Then test for convergence,

we have
$$u_{i+1} = f(u_i)$$

If M is a solution then $M = f(M)$

thus
$$u_i = M + \epsilon_i$$

and
$$M + \epsilon_{i+1} = f(M + \epsilon_i)$$
$$= f(M) + \epsilon_i f'(M) + \text{h.o.t.}$$

thus convergence if $|f'(M)| < 1$

The process requires three values of U to evaluate the predicted solution. The first value is the starting value U_1, but the calculated Z (or U_2) may not be suitable for evaluating U_3. Thus a fraction (λ) of U_2 is used to obtain U_3

Now
$$x_1 = u_1$$
$$x_2 = u_1 + \lambda(u_2 - u_1) \tag{3/A.1}$$
$$x_3 = f(x_2)$$

for a solution

$$M = f(M) \quad \text{and} \quad u_1 = M + \epsilon_1 \tag{3/A.2}$$

this yields $\quad u_2 = f(M + \epsilon_1) \simeq M + \epsilon_1 f'(M)$

using equation (3/A.1), yields

$$u_2 = (1 - \lambda) u_1 + \lambda [M + \epsilon_1 f'(M)] \qquad (3/A.3)$$

Also $\quad u_3 = M + \epsilon_3 = f(M + \epsilon_2) \simeq f(M) + \epsilon_2 f'(M)$

i.e. $\quad u_3 = M + \epsilon_2 f'(M) = [1 - \lambda + \lambda f'(M)] \epsilon_1 f'(M) + M \qquad (3/A.4)$

using equations (3/A.2, .3, .4,) and eliminating ϵ_1 and f'(M)

yields

$$M = [\lambda u_1 (u_3 - u_2) - u_2 (u_2 - u_1)] / [u_1 - (1 + \lambda) u_2 + \lambda u_3] \qquad (3/A.5)$$

where λ is given by the expression

$$u_{i+1} = u_i + \lambda (u_{i+1} - u_i)$$

and is less than unity as a new value smaller than the previous one

is sought. Obviously when $\lambda = 1$ both values are identical.

Thus equation (3/A.5) may be used repeatedly on the basis

of figure (3.9) to obtain an acceptable value.

APPENDIX 3/B

BAIRSTOW'S PROCESS

Consider the quartic equation

$$q_4 x^4 + q_3 x^3 + q_2 x^2 + q_1 x + q_0 = 0 \qquad (3/B.1)$$

as a solution consider the approximate quadratic factor

$$x^2 - px - l \qquad (3/B.2)$$

dividing equation (3/B.1) by (3/B.2) yields the other quadratic.

Now find $\qquad q_s = a_s + p q_{s+1} + l q_{s+2}$

for $s = 4,3,2,1$ with $q_5 = q_6 = 0$

Also find $\qquad T_s = q_{s+2} + p T_{s+1} + l T_{s+2}$

for $s = 2,1,0$ · with $\quad T_4 = T_3 = 0$

Then the increments of p and l are

$$dp = (T_1 q_0 - T_0 q_1)/G$$

$$dl = (M q_1 - T_0 q_0)/G$$

where $\qquad M = l T_1 + p T_0$

$$G = T_0^2 + M T_1$$

Now test $\quad |dp| \leqslant \epsilon_1 \quad$ and $\quad |dl| \leqslant \epsilon_2$

when converged the factors are

$$(x^2 - px - l) \qquad \text{and} \qquad (q_4 x^2 + q_3 x + q_2)$$

and the roots are

$$x_{1,2} = +(p/2) \pm \sqrt{(p/2)^2 + l}$$

$$x_{3,4} = -(q_3/2q_4) \pm \sqrt{(q_3/2q_4)^2 + q_2/q_4}$$

APPENDIX 3/C

COMPUTER PROGRAMME

3/C.1   The entire model is in the form of a computer programme
requiring only one data card of input information. Explanatory
comments have been included in the programme explaining the
various stages of operations. The flow diagram displays the
master segment in skeleton form. A list of the programme is
given in Wirasinghe (1964).

3/C.2   Principal Computer Notations

NSTAT   - no. of stations used (inclusive of initial station)

ARR   - area ratio

THTRN   - momentum thickness Reynolds no.

BLTR   - thickness of boundary layer (N-D)*

THTR   - momentum thickness (N-D)

RO   - throat radius

SUBL   - thickness of laminar sub-layer

RMU   - core velocity

GP2   - exponent (G + 2)

ALPHA   - axial distance (N - D)

BETA   - duct radius (N - D)

D   - shape parameter

THKM   - momentum thickness integrated from velocity profile

* (N-D)   - non-dimensional

3/C.3   Input information

e.g.   NSTAT   = 10

        ARR   = 2.75

THTRN   = 3000

BLTR   = .1403

THTR   = .0135

RO   = 3.03

CONANG   = 10

3/C.4   <u>Output information</u>

See tables 3/II and 3/III.

APPENDIX 5/A

This appendix outlines the procedure used in fitting the exponential function

$$ v = [1 - \exp(-C_2 r^2)] C_1 / 2\pi r $$

to the data from So (1967). The numerical procedure which was used is described in Walsh. This technique requires initial values of C_1 and C_2. The above equation cannot be easily solved for the constants. A good estimate was necessary to prevent divergence in the fitting process as a result of ill-conditioned data. The initial values are calculated by fitting a straight line to the first three data points which represent the forced vortex in the core. Once the best estimate of the constant has been made, these values are used in the subsequent downstream stations.

To determine the core radius (i.e. radius corresponding to peak velocity) the throat radius is used as the starting value for the first station. Once again the current value is used for the subsequent stations. The function being non-linear, double-precision arithmetic had to be used to speed-up convergence.

APPENDIX 5/B

This appendix contains additional information on the solution of the mathematical model reported in Chapter 5. Equation (5.3.4.1) is

$$v = (1 - G)C_i/2\pi r$$

where $\quad G = \exp(-\beta) \quad$ and $\quad \beta = (r/k_i r_c)^2 = [r/k_i(\phi z + k_2)]^2$

To evaluate the partial differentials the following are required

$$[\beta]_z = 2k_i\phi\beta^{3/2}/r \qquad \text{and} \qquad [\beta]_r = 2\beta/r$$

also $\qquad [G]_z = -G[\beta]_z \qquad$ and $\qquad [G]_r = -G[\beta]_r$

The following expressions are obtained using the above

$$[v]_z = C_i k_i\phi\beta^{3/2}G/\pi r^2$$

$$[v]_r = C_i[G(2\beta+1) - 1]/2\pi r^2$$

$$[v]_{zz} = C_i k_i^2\phi^2\beta G(3 - 2\beta)/\pi r^3$$

$$[v]_{rr} = -C_i[G(2\beta^2 + \beta + 1) - 1]/\pi r^3$$

from which, ψ, p and q are obtained following lengthy manipulation to give

$$\psi = [v]_{rr} + [v]_r/r + [v]_{zz} - v/r^2$$

$$= 2C_i k_i^2\phi^2\beta^2 G(k_3 - \beta)/\pi r^3$$

$$p = [v]_r + v/r = C_i\beta G/\pi r^2$$

$$q = [v]_z = -C_i k_i\phi\beta^{3/2}G/\pi r^2$$

where $\quad k = (3k_i^2\beta^2 - 2)/2k_i^2\phi^2$

and using these, the following are obtained

$$L(r,z) = p/q$$

$$M(r,z) = -(v/q)[[\psi]_z - [q]_z\psi/q]$$

$$N(r,z) = [p/q]_z - 1/r = [L]_z - 1/r$$

The necessary partial differentials may be obtained using

previously evaluated functions to give

$$[\psi]_z = -4C_i k_i^3 \phi \beta^{5/2} G [\beta^2 - (3 + k_3)\beta + 2k_3]/\pi r^4$$

$$[q]_z = C_i k_i^2 \phi^2 \beta^2 G (3 - 2\beta)/\pi r^3$$

$$[p]_z = 2C_i k_i \phi \beta^{3/2} G (\beta - 1)/\pi r^3$$

and making the appropriate substitutions yields

$$L(r,z) = 1/k\phi\beta^{1/2}$$

$$M(r,z) = 2k_i^2 \phi^2 \nu \beta (3\beta - k_3)/r$$

$$N(r) = -2/r$$

APPENDIX 6/A

If the system shown in Fig. (6.11) is dismantled then reassembling is likely to cause difficulty owing to the "tight" design limits. To obtain the full range the following procedure must be adhered to:

1. Using the scale on the radius-wheel (Fig. (6.9)) set the radius to the maximum value required; in this case 45 mm. (Note that this corresponds to a maximum linear traverse of 90 mm. which is the traverse required at the exit of the diffuser).

2. Set the crank radius to $\theta = 0^o$ position (i.e. giving maximum extension of probe) and move the 'arm' until the connector (Fig. (6.11)) almost touches the probe carrier. Clamp the probe to the connector and also clamp the 'arm' to the crank at A.

3. To test the suitability of the positioning of the probe retract the probe gradually. The probe may need re-positioning if it runs against a limit stop; (Fig. (6.8)).

4. Set the crank to $\theta = 180^o$. Adjust the slider P until the recess on its under-side lines up against the 'traverse-lock' and clamp it to the 'arm'.

5. Now clamp the slider Q to the arm at a suitable point ensuring that it does not slip out of the slide at maximum extension.

APPENDIX   6/B

The method of operation of the relay circuit shown on
Fig. (6.13) is as follows.

1.   Press start switch and release; the relay C is energised
      and held and the actuator is activated.

2.   The withdrawing plunger operates the micro-switch MS/1
      to energise A, operates MS/2 to start the drive motor.
      Now the indexing commences.

3.   When the withdrawing plunger operates MS/3, C is
      de-energised and D is energised; the actuator is then
      de-activated.   The plunger now sits on the periphery
      of the radius - wheel until it drops into the next slot.

4.   When the plunger drops into the slot MS/2 is released,
      B is released and the supply to the drive motor is cut-
      off.   MS/1 is also released during this operation.
      If the system stalls it can be easily released by manually
      retracting the plunger.

APPENDIX 7/A

SPHERICAL COORDINATE TRANSFORMATION

Let OC be of unit length
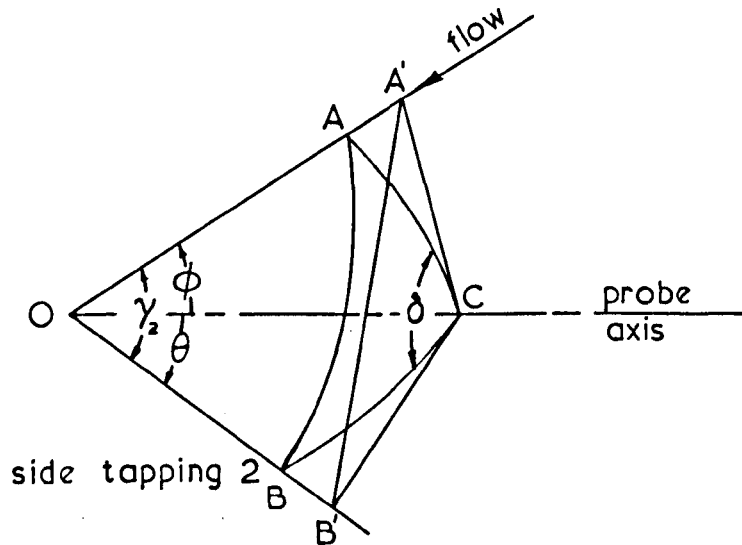
from Δ^s OA'B' and CA'B' (for common side A'B')

$$(OA')^2 + (OB')^2 - 2OA' \cos \gamma_2 = (CA')^2 + (CB')^2 - 2CA'.CB'.\cos \delta$$

but $OB' = \sec \theta$; $OA' = \sec \phi$; $B'C = \tan \theta$; $A'C = \tan \phi$

substituting

$$\sec^2 \phi + \sec^2 \theta - 2 \sec \phi . \sec \theta . \cos \gamma_2 = \tan^2 \phi + \tan^2 \theta - 2 \tan \theta \tan \phi . \cos \delta$$

from which

$$\cos \gamma_2 = \cos \phi . \cos \theta + \sin \theta . \sin \phi . \cos \delta$$

also for the other points

$$\gamma_4 ; \quad \theta = -\theta : \cos \gamma_4 = \cos \phi . \cos \theta - \sin \theta . \sin \phi . \cos \delta$$

$$\gamma_1 ; \quad \delta = (90 - \delta) : \cos \gamma_1 = \cos \phi \cos \theta + \sin \theta \sin \phi \sin \delta$$

$$\gamma_3 ; \quad \delta = (90 + \delta) : \cos \gamma_3 = \cos \phi \cos \theta - \sin \theta \sin \phi \sin \delta$$

APPENDIX 7/B

RELATIONSHIP BETWEEN SPHERICAL AND RECTANGULAR

COORDINATE SYSTEMS
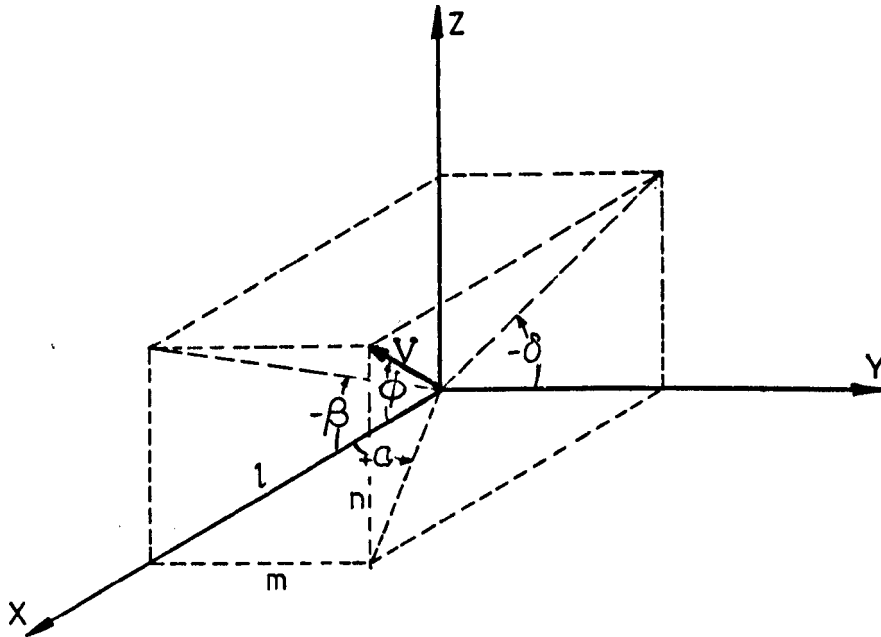
Consider the unit vector $\vec{V} = (l, m, n)$

and since $m = l \cdot \tan a$ and $n = l \cdot \tan \beta$

$$l = (1, l \tan a, l \tan \beta) \qquad (7/B.1)$$

Also $l = \cos\phi$ and $n = m \tan \delta$

but $\sin^2\phi = m^2 + n^2 = m^2 \sec^2\delta$

$$\therefore m = \pm \sin\phi \cdot \cos\delta$$

$$n = \pm \sin\phi \cdot \sin\delta$$

Thus $l = (\cos\phi, \pm \sin\phi \cos\delta, \pm \sin\phi \sin\delta)$ $\qquad (7/B.2)$

From (7/B.1) and (7/B.2)

$$l \tan a = \sin\phi \cdot \cos\delta$$

$$l \tan \beta = \sin\phi \cdot \sin\delta$$

from which $\tan\delta = \tan\beta / \tan a$

and $\tan^2\phi = \tan^2 a + \tan^2\beta$

APPENDIX   7/C

LEAST SQUARE FIT APPLIED TO SURFACE SMOOTHING

It is assumed that the variation of the function with respect to yaw (α) and pitch (β) can be represented by polynomials.

Consider a general β , suppose

$$V_{ij} = a_1 + a_2\alpha_i + a_3\alpha_i^2 - - - - - + a_k\alpha_i^{n-1} \qquad (7/C.1)$$

where i and j are the indices associated with yaw and pitch

respectively and n is the degree of the polynomial

representing the variation of the function with respect

to the yaw angle. N and M are the limiting values of i

and j respectively.

Using the method of least square, the coefficients of equation

(7/C.1) are given by

$$\begin{bmatrix} a_1 \\ a_2 \\ \vdots \\ \vdots \\ \vdots \\ a_n \end{bmatrix}_j = (\underline{A}^T \underline{A})^{-1} \cdot \underline{A}^T \begin{bmatrix} V_{1j} \\ V_{2j} \\ \vdots \\ \vdots \\ \vdots \\ V_{Nj} \end{bmatrix} \qquad (7/C.2)$$

where

$$\underline{A} = \begin{bmatrix} 1 & \alpha_1 & \alpha_1^2 - - - - - - - - - \alpha_1^{n-1} \\ 1 & \alpha_2 & \alpha_2^2 - - - - - - - - \alpha_2^{n-1} \\ \vdots & \vdots & \vdots \\ \vdots & \vdots & \vdots \\ 1 & \alpha_N & \alpha_N^2 - - - - - - - - \alpha_N^{n-1} \end{bmatrix}$$

If the above procedure is applied to all the j values then

$$\underline{a} = \begin{bmatrix} a_1 \\ a_2 \\ \vdots \\ \vdots \\ a_n \end{bmatrix}_j$$

Now considering the variation of a w.r.t. β,

let

$$a_j = \underline{a}_1 + \underline{a}_2\beta_j^2 - - - - - - + \underline{a}_m\beta_j^{m-1} \qquad (7/C.3)$$

where m is the degree of the polynomial.

Then, as before

$$\begin{bmatrix} a_{11} \\ a_{21} \\ \vdots \\ \vdots \\ a_{m1} \end{bmatrix} = (\underline{B}^T\underline{B})^{-1}\underline{B}^T \begin{bmatrix} a_{11} \\ a_{12} \\ \vdots \\ \vdots \\ a_{1M} \end{bmatrix}$$

and similarly for j = 2, 3 --- m.

where

$$\underline{B} = \begin{bmatrix} 1 & \beta_1 & \beta_1^2 - - - - - - - \beta_1^{m-1} \\ 1 & \beta_2 & \beta_2^2 - - - - - - - \beta_2^{m-1} \\ \vdots & \vdots & \vdots \qquad\qquad \vdots \\ \vdots & \vdots & \vdots \qquad\qquad \vdots \\ 1 & \beta_M & \beta_M^2 - - - - - - - \beta_M^{m-1} \end{bmatrix}$$

But

$$V_{ij} = (1 \quad a_i \quad a_i^2 - - - - - - - a_i^{n-1}) \begin{bmatrix} a_1 \\ a_2 \\ \vdots \\ a_n \end{bmatrix}$$

$$v_{ij} = (1 \quad a_i \quad a_i^2 \text{-------} a_i^{n-1}) \, [\underline{a}_1 \quad \underline{a}_2 \text{------} \underline{a}_m] \begin{bmatrix} 1 \\ \beta_j \\ \beta_j^2 \\ \vdots \\ \beta_j^{m-1} \end{bmatrix}$$

The matrix $\underline{a}$ is given by

$$\begin{bmatrix} a_{11} & a_{12} \text{------} a_{1n} \\ a_{21} & a_{22} \text{------} a_{2n} \\ \vdots & \vdots & \vdots \\ a_{m1} & a_{m2} \text{------} a_{mn} \end{bmatrix} = (\underline{B}^T \underline{B})^{-1}. \underline{B}^T \begin{bmatrix} a_{11} & a_{12} \text{------} a_{n1} \\ a_{12} & a_{22} \text{------} a_{n2} \\ \vdots & \vdots & \vdots \\ a_{1M} & a_{2M} \text{----} a_{nM} \end{bmatrix}$$

i.e.
$$\underline{a} = (\underline{B}^T \underline{B})^{-1} \underline{B}^T \, \underline{a}^T \qquad\qquad (7/C.4)$$

Using equation (7/C.2) to eliminate a from equation (7/C.4) yields

$$\underline{a} = (\underline{B}^T \underline{B})^{-1} \underline{B}^T \begin{bmatrix} V_{11} & V_{21} \text{------} V_{N1} \\ V_{12} & V_{22} \text{------} V_{N2} \\ \vdots & \vdots & \vdots \\ V_{1M} & V_{2M} \text{----} V_{NM} \end{bmatrix} \underline{A}(\underline{A}^T \underline{A})^{-1}$$

and finally

$$\underline{v}_{ij} = (1 \quad a_i \quad a_i^2 \text{-----} a_i^{n-1}).(\underline{A}^T \underline{A})^{-1}. \underline{A}. \underline{V}. \underline{B}.(\underline{B}^T \underline{B})^{-1} \begin{bmatrix} 1 \\ \beta_j \\ \beta_j^2 \\ \vdots \\ \beta_j^{m-1} \end{bmatrix}$$

where $\underline{v}$ and $\underline{V}$ are the calculated and experimental values of the function respectively,

or

$$\underline{v}_{ij} = \underline{\alpha}^T . \underline{M} . \underline{\beta}$$

where M is calculated from experimental information.

Now it is possible to obtain a smooth set of values for v_{ij} . However, as always there are unacceptable "rogue" points in the raw data. The test for their existence is as follows:

Let v and v^* be the experimental and fitted values of the population, then the variance is given by

$$S = \sum_{i=1}^{N} \sum_{j=1}^{M} (v_{ij} - v_{ij}^*)^2$$

and the standard deviation is

$$\sigma = \sqrt{S/(N \times M - n \times m)}$$

If at any point $|(v_{ij} - v_{ij}^*)| > 2\sigma$ then that point is a 'rogue' point.

This 'rogue' point is replaced by a new point estimated on the following basis;

Consider c to be a 'rogue' point. It may be replaced by an estimate based on the points surrounding it provided suitable weightings are introduced.

From Taylor's series the value at any point is

$$v(x,y) = v_c + h(\partial v_c/\partial x + \partial v_c/\partial y) + [h^2/2!](\partial^2 v_c/\partial x^2 + 2\partial^2 v_c/\partial x \partial y$$

$$+ \partial^2 v_c/\partial y^2) + \text{----}$$

$$= v_c \exp(hD_x + hD_y)$$

where $D_x = \dfrac{\partial}{\partial x}$ and $D_y = \dfrac{\partial}{\partial y}$
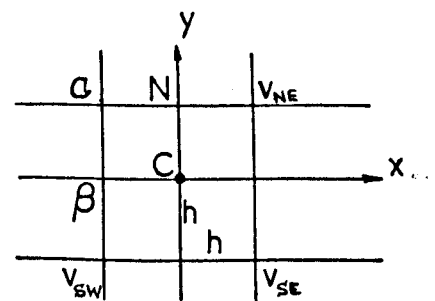
From the figure

$$v_{sw} + v_{ne} = [\exp(-hD_x - hD_y) + \exp(hD_x + hD_y)] \; v_c$$

$$= 2v_c \cdot \text{Cosh.}(h.(D_x + D_y))$$

Considering all the nodes surrounding c with their respective

weightings and replacing hD_x and hD_y by θ and ϕ yields

$$v_c \left\{ \alpha \, [2 \, \text{Cosh} \, (\theta + \phi) + 2 \, \text{Cosh} \, (\theta - \phi)] + \beta \, [2 \, \text{Cosh} \, \theta + 2 \, \text{Cosh} \, \phi] \right\} = v_c$$

i.e. $4\alpha \, \text{Cosh} \, \theta \, \text{Cosh} \, \phi + 2\beta \, (\text{Cosh} \, \theta + \text{Cosh} \, \phi) = 1$

expanding in series form

$$4\alpha \, [1 + \theta/2! + \text{-----}] \, [1 + \phi/2! + \text{------}] + 2\beta \, [2 + (\theta + \phi)/2 + \text{-----}] = 1$$

from which

$$\alpha = -1/4 \quad \text{and} \quad \beta = 1/2$$

Thus

$$v_c = \tfrac{1}{2} \, [v_n + v_s + v_e + v_w] - \tfrac{1}{4} \, [v_{ne} + v_{se} + v_{sw} + v_{nw}]$$

Similarly it could be shown that for an end point

$$\alpha = 1/2 \; ; \quad \beta = -1/2 \quad \text{and} \quad \gamma = 1$$

and that

$$v_c = \tfrac{1}{2}(v_n + v_s) - \tfrac{1}{2}(v_{ne} + v_{se}) + v_e$$